Trinity College Dublin
Coláiste na Tríonóide, Baile Átha Cliath
The University of Dublin

Investigation of Phosphorescent Materials for Photovoltaic Device Applications

By

Moacir Gomes de Oliveira, BSc Eng, MBA

A thesis submitted for the Degree of Doctor of Philosophy in Engineering to the University of Dublin, Trinity College Dublin

Department of Civil, Structural and Environmental Engineering
The University of Dublin
Ireland

2019

Declaration

I declare that this thesis has not been submitted as an exercise for a degree at this or any other university and it is entirely my own work.

I agree to deposit this thesis in the University's open access institutional repository or allow the Library to do so on my behalf, subject to Irish Copyright Legislation and Trinity College Library conditions of use and acknowledgement.

_____

Moacir Gomes de Oliveira BSc. Eng, MBA

March 2019

Abstract

Phosphorescence is used in photovoltaic devices by embedding phosphorescence species within a transparent host polymer to absorb ultraviolet solar radiation followed by a slow emission of visible light. Phosphorescent material has come to the fore in luminescent applications as well light emitting and harvesting applications. Utilising long persistent phosphorescent energy converters in PV devices is just one avenue for improving the efficiency of the PV device under light and dark conditions. Combining these technologies in a passive approach can enhance the photovoltaic efficiency and effective energy transfer. The energy transfer from long persistent phosphors to the photovoltaic device has been investigated both to increase the fundamental understanding of the mechanisms and also with a view towards viable device applications.

Concentration dependence of the spectroscopy and photoluminescence spectra of luminescent layers as well as quantum efficiency and photoluminescence decay has been investigated across the range of ultraviolet to visible light. It shows that a highly concentrated phosphorescent layer on top of the photovoltaic device is unable to satisfactorily enhance the photovoltaic efficiency under illumination. However, under dark conditions the efficiency can be significantly improved. During photoluminescence, the energy transfer from the luminescent layer is shown to increase the PV device power output and to also power a LED light for more than 5 minutes.

Acknowledgements

I always was fascinated by these technologies since I was a little boy… then I embraced engineering as career, and I found the best girlfriend to marry … this is our first baby.

The knowledge that I have now is imperfect; but then I shall know as fully as I am aware of that imperfection.

Doing a PhD is 'minha culpa', is not a solo endeavour, it is a commemoration of what I have become.

"Choose a job you love, and you will never have to work a day in your life" – Confucius

Beware of the man who works hard to learn something, learns it, and finds himself no wiser than before, Bokonon tells us. He is full of murderous resentment of people who are ignorant without having come by their ignorance the hard way. – Kurt Vonnegut, Cat's Cradle

"An expert is a man who has made all the mistakes, which can be made, in a very narrow field" –Niels Bohr

I am grateful to my God Almighty for giving me the strengths every day to undertake this research project and to persevere and complete it successfully.

This research project has been funded by CAPES (Coordenação de Aperfeiçoamento de Pessoal de Nível Superior) Science Without Boarders - Brazilian Program - process: 9384-13-8.

My wife Carina for standing beside me, continued support and encouragement always.

My Supervisor Dr. Sarah McCormack throughout the course of this research project.

All the Trinity staff for their kind help and co-operation throughout my study period.

I acknowledge valuable discussions with many colleagues including Dr. Karsten Fleischer, Dr Manuel Ruether, Prof. Louise Bradley, Dr. Gavin McManus and Prof. Joe McDonagh.

I would like to express my deep gratitude and appreciation to Dr. Toby Meyer and Dr. Andreas Meyer, Dr Frederic Oswald and the other team members of Solaronix S.A. for the support and technical assistance.

Last but not the least, I would also gratefully acknowledge the help provided by Dr Alex Siemiarczuk at Horiba Scientific, Mr Brian Corbett at Tyndall UCC, Dr Jan Goldschmidt at Fraunhofer ISE, and to those who could not be mentioned here but played an important role during this project.

I would like to place on record my deepest gratitude to my great friend Ms Ingrid Toner for her constant support, encouragement and help with this thesis.

Finally, I extend my deepest thanks to my family for their patience and understanding.

Table of Contents

List of Figures

List of Tables

List of Acronyms

AFM	Atomic Force Microscopy
AM1.5	Air Mass 1.5
Arc	Anti-Reflection Coating
A-Si	Amorphous Silicon
ASTM	American Society for Testing and Materials
APCE	Absorbed Photon to Current Efficiency
B_2o_3	Boron Oxide
$BaAl_xO_y$	Barium Aluminate
BN	Boron Nitride
CB	Conduction Band
CdS	Cadmium Sulphide
CdSe	Cadmium Selenide
CdTe	Cadmium Telluride
CiGs	Copper Indium Gallium Selenide
Co2	Carbon Dioxide
CPC	Compound Parabolic Concentrator
CRT	Cathode Ray Tube
Cu	Copper
DC	Down-Conversion
DS	Down-Shifting
DSC	Differential Scanning Calorimetry
Dy	Dysprosium
Eds	Energy Dispersive Spectroscopy
Eg	Band Gap Energy
EQE	External Quantum Efficiency
Eu	Europium
Fe	Iron
FF	Fill Factor
FOB	Fibre Optic Bundle

FRET	Förster Resonant Energy Transfer
FTIR	Fourier Transform Infrared Spectroscopy
GaAs	Gallium Arsenide
GaInP	Gallium Indium Phosphide
H_2O	Water
HOMO	Highest Occupied Molecular Orbital
HRTEM	High Resolution Transmission Electron Microscopy
IQE	Internal Quantum Efficiency
IQY	Internal Quantum Yield
Isc	Short-Circuit Current
LDPE	Low Density Polyethylene
LDS	Luminescent Down Shifting
LED	Light Emitting Diode
LSC	Luminescent Solar Concentrator
LUMO	Lowest Unoccupied Molecular Orbital
Mc-Si	Multicrystalline Silicon
MgF_2	Magnesium Fluoride
MgTe	Magnesium Telluride
Nd	Neodymium
Ni	Nickel
NIR	Near Infra-Red
PL	Photoluminescence
PMMA	Polymethylmethacrylate
IPCE	Incident Photon to Current Efficiency
PV	Photovoltaic
PXRD	Powder X - Ray Diffraction
QD	Quantum Dot
QE	Quantum Efficiency
QY	Quantum Yield
RE	Rare Earth

RET	Renewable Energy Technology
SEM	Scanning Electron Microscopy
Si	Silicon
SrxAlyOz	Strontium Aluminate
SrxMgSiyOz	Strontium Magnesium Silicate
TB	Terbium
TEM	Transmission Electron Microscopy
TGA	Thermo-Gravimetric Analysis
TiO_2	Titanium Dioxide
TIR	Total Internal Reflection
Tl	Thermoluminescence
UC	Up-Conversion
UV	Ultraviolet
UV–Vis	Ultraviolet-Visible
VB	Valence Band
Voc	Open-Circuit Voltage
WP	Watt Peak
Xe	Xenon
XRD	X-Ray Diffraction
Y_2O_3	Yttrium Oxide
$Y3Al_5O_{12}$	Yttrium Aluminate
Zn_2SiO_4	Zinc Silicate
ZnO	Zinc Oxide
ZnS	Zinc Sulphide

Nomenclature

		Unit
a	Absorbance	arbitrary unity (a.u.)
G	Solar Irradiance	W/m2
I	Current through load	A
Id	Current through diode	A
Ipv	Current generated by PV	A
Ish	Current through the shunt resistor	A
Rs	Equivalent circuit series resistance	Ω
Rsh	Equivalent circuit shunt resistance	Ω
U	Voltage applied to the load	V
Ush	Shunt voltage	V
Io	Reverse saturation current	V
k	Boltzmann's constant (1.3806488×10−23)	$J.K^{-1}$
q	Elementary charge = (1.602176565×10−19)	C
Tp-n	Junction absolute temperature	K
Impp	Current at maximum power	A
Isc	Short circuit current	A
Uoc	Open circuit voltage	V
Umpp	Voltage at maximum power	V
I_{mpp}	Current at maximum power	A
I_{sc}	Short circuit current	A
U_{oc}	Open circuit voltage	V
U_{mpp}	Voltage at maximum power	V
I_{mpp}	Current at maximum power	A
I_{sc}	Short circuit current	A
U_{oc}	Open circuit voltage	V
K	Conductivity	W/m-K
Ta	Ambient temperature	°C

U_{mpp}	Voltage at maximum power	V
Ema	Mean annual solar radiation	kWh/m2
Ep	Estimated peak energy delivered	kWh
kWp	Nominal peak energy	kW
Pmax	Maximum power	W
Tc	Temperature of the PV cell	K
Tstc	Temperature of STC, 25 °C	K
Wp	Peak energy of a single module	W
η	Efficiency of system	
ϒ	Power temperature coefficient	$°C^{-1}$
α	Absorptance	arbitrary unity(a.u.)
T	Transmittance	arbitrary unity(a.u.)
Ψ	Azimuth angle	°

CHAPTER 1

INTRODUCTION

1.1 Introduction

With the agreement reached at the 21st annual Conference of the Parties (COP) in Paris and recently updated in COP24 in Poland, to limit global average temperature rise to well below 2°C ("COP24," 2018, Eurostat, 2015), substantial cuts to greenhouse gas (GHG) emissions are required. Photovoltaics (PV) technologies are being considered as an indispensable alternative to reduce these gas emissions. As almost 60% of GHG are derived from the energy sector (UNFCCC, n.d.), it is important that we move to renewable sources such as PV for our energy supply. Photovoltaics convert solar energy directly into electricity and integrating PV into buildings is now widely recognised as the most cost-effective form of grid-connected PV power generation in industrialised countries. This project addresses these issues and demonstrates the use of phosphorescent phosphors in order to enhance PV efficiencies in the UV-Visible spectral range and therefore improve overall solar PV device efficiencies.

A significant amount of research has been conducted in the field of photovoltaic technology devices which helps to reach innovative solutions by understanding the fundamentals involved. However, significantly less research has been carried out in the field of phosphorescent materials and integration with PV devices as a passive and purely optical approach that can provide a solution for the enhancement of the poor UV spectral response of PV. There are many types of losses for PV device materials such as the sub band-gap (Eph<Eg) photons, which are energy photons that are not absorbed by PV material, and higher energy (Eph - Eg) photons, which can also cause heating and degradation of the PV device.

Hence, PV devices still need improvements and one solution can be applying a passive approach such as Down Conversion (DC) or Down-Shifting (DS) mechanisms (Kennedy et al., 2010; Liu et al., 2006). This has the features which can overcome some of the losses, (and

improve the poor spectral response in UV and visible range), to the wavelengths where the PV devices exhibit a better response as illustrated in Figure 1.1. This approach can be applied without changing the electronic interface of the PV device, and can be optimised by process application or materials. The materials required in these mechanisms, DC and DS, may be divided into two major classifications: host and luminescent materials.

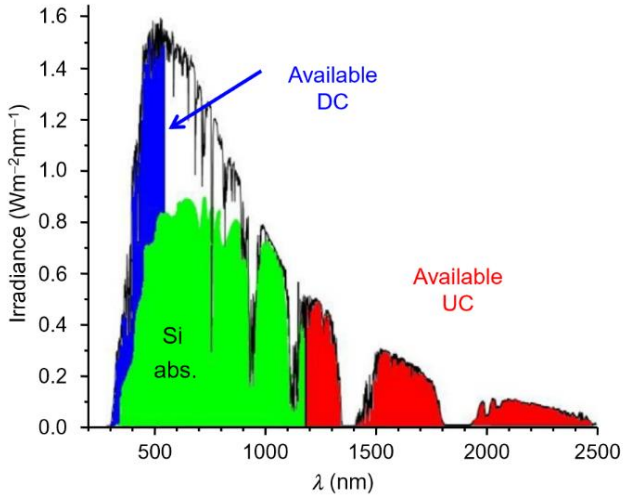

Figure 1.1. Air-Mass 1.5 G (AM1.5G) solar irradiance spectrums along with fractions absorbed by a thick silicon wafer,(about 48%) available for down-conversion (DC, about 16% up to 500 nm) and up conversion (UC, about 17%, in the 1.2–2.5 mm range) (Bünzli and Pecharsky, 2013).

This research project has investigated these two main materials for the application in the Luminescent Down-Conversion (DC) layers by applying a range of rare-earth-doped inorganic phosphorescent phosphors as luminescent material and a host material using a Polysiloxanes silicon. This research recognises the benefits of long persistent phosphors selected as preferable luminescent material for this research application because of the multi-capabilities such as down-conversion, light scattering, and light storage, and will be applied to test the performance of various types of PV devices, including a multi-junction a-Si.

1.2 Research Objectives

The aim of this research is to investigate Long Persistent Phosphors (LPP) species for PV device technologies as a passive approach, to assess its suitability to enhance PV device performance. In particular, it will be studied for various types of PV device technologies including the “First

Generation" and "Third Generation" of PV devices such as Dye-Sensitized Solar Cell (DSSC) and thin-film PVs. The fabrication and performance of the luminescent layers, which will be used as a passive approach, with a transparent polymer host matrix, will be investigated as a device application for the enhancement of the power output of the PV device.

To successfully answer this research question, this thesis addresses the following objectives:

1) To present a comprehensive literature review of energy converters to enhance the PV device technologies.
    - Investigate the research surrounding PV devices and LPP phosphor technologies and identify methods to combine both technologies.
    - To identify ideal PV device technologies and the gaps in the present devices which still need improvements in terms of optical and physical properties.
    - To identify the potential of energy converters amongst the range of luminescent applications for PV device technologies and its requirements and to identify an ideal mechanism which describes the application of LPP phosphors.
    - To investigate different species of LPP phosphors such as $Sr_{2.90}Eu_{0.03}Dy_{0.07}Al_4SiO_{11}$, $Sr_{3.84}Eu_{0.06}Dy_{0.10}Al_{14}O_{25}$, $Sr_{0.95}Eu_{0.02}Dy_{0.03}Al_2O_4$ and SrAl2O4:$Eu2^+$, Dy^{3+} by comprehensively reviewing the physical and chemical properties literature to date.

2) To synthesise and develop production methods for fabrication of the luminescent layers
    - To identify transparent polymeric matrices for use as a host material for luminescent applications.
    - Investigation of the curing process, stability and degradation of potential host material by analysing the total transmission.
    - To identify the reproducibility and replicability of the method for the fabrication of the luminescent layers.
    - To study the optical properties of the luminescent layer including: transmission, absorptance, emission, excitation, reflectance, quantum efficiency and photoluminescence decay of the LPPs in the host matrix.

- To undertake concentration dependence studies of luminescent layers.
- To fabricate an optimized and novel luminescent layer for PV device applications.

3) To experimentally characterize the performance of the energy converters with various types of PV device technologies.

- Electrical characterization of the PV devices with and without the luminescent layers attached to the top or at the rear surfaces of the PV device, under standard test conditions.
- Electrical characterization of the PV devices with and without the luminescent layers attached to its surfaces, after exposure to illumination, under dark test conditions.
- To investigate if the photon energy converted from the luminescent layer, after exposure to illumination can be used to power a PV device in the dark condition, through photoluminescence, "afterglow in the dark".
- To calculate the amount of energy converted from the luminescent device to the PV device in terms of electrical power.
- To conceptually investigate if the amount of electrical power generated by the PV device with the luminescent device under the dark condition, can be enough to power a LED light and thereby provide a real-world application.

1.3 Thesis Outline

This thesis is structured into 9 chapters, in order to address each of the above objectives. The following is a summary of each of these chapters:

Chapter 2: Literature Review

Chapter 2 contains an extensive literature review which has been conducted to highlight the current available PV technologies, phosphorescent species and energy conversion mechanisms. It highlights gaps in the current PV device technologies and the phosphorescent technologies, forming the motivation for the investigation of this research topic.

Chapter 3: Materials and Experimental Methods

This chapter lists the materials which were used in this project including its chemical and physical properties. It also outlines the experimental methods used in this research, to fabricate the LPP species, and to characterize the physical and optical properties of the fabricated luminescent layers. This chapter also presents the new method that was developed to measure the quantum efficiency of the luminescent layers. The final sections of this chapter describe the electrical characterization techniques and used to measure the PV device under illumination and dark conditions.

Chapter 4: Phosphorescent Species, Synthesis and Characterisation

This chapter is the experimental analysis of the synthesis of a long persistent phosphor to investigate its formation and physical properties. Its aim was to reproduce the phosphor developed by Professor Matsuzawa in 1996 which is the $SrAl_2O_4$: Eu^{+2}, Dy^{3+} (Strontium Aluminate, Dysprosium and Europium doped) (Matsuzawa et al., 1996). This chapter discusses the results of the synthesis of the phosphorescent phosphor and the potential to improve its optical properties, and the gaps, which lead to a different approach instead of the synthesis.

Chapter 5: Host Materials and Luminescent Layer, Synthesis and Characterizations

This chapter consists of the experimental investigation of the host polymer matrices; with different types, including resins, polymers and silicone to identify the ideal host polymer materials to fabricate the luminescent layers. It also describes the method developed for the fabrication of the host material, including the characterization, analysis of the stability, and degradation of the host layer. It also presents the index of refraction of the host material and other optical properties of the host, and a thickness measurement of the layers and particles dispersion into the layer by 3D image. The final section describes the method that was used to fabricate the luminescent layer of various concentration ratios.

Chapter 6: Optical Characterizations of The Luminescent Layers

Chapter 6 presents the results of the optical characterization of the six different species of LPP phosphors which were used in the fabrication of the luminescent layers. The characterization

results include; transmission, absorptance, reflectance, emission, internal and external photoluminescence quantum efficiency, and phosphorescence lifetime.

Chapter 7: Luminescent Layers Applications and PV Devices Electrical Characterization Under Illumination.

Chapter 7 presents the application of the luminescent layers attached on the top and at the rear surface of the various PV devices. It presents the results of the electrical characterization of the various PV device technologies used to test the fabricated luminescent layer or down-converter device, LDC, under Standard Test Conditions, STCs.

Chapter 8: Determination of Energy Output of LDC Layers Attached to The PV Device in The Photoluminescence Decay.

Chapter 8 presents a novel Luminescent Down Converter, LDC layer, which was used to empower a PV device and a LED light, under dark conditions for more than 5 minutes. It also presents the results of the electrical characterization of the various PV devices with LDC layers, under dark conditions. The amount of energy converted from the LDC layer into the PV devices was calculated in terms of the electrical power output of the PV devices which were characterized together.

Chapter 9: Conclusions and Recommendations

The key conclusions derived from this research project are presented in Chapter 9. This chapter includes a conclusion related to the PV device attached to the LDC layers under illumination and dark conditions, the usage of the LDC layer as an energy storage device, and its potential for further applications. The conclusions refer to the objectives outlined in this section. Future research recommendations are also outlined in Chapter 9.

1.4 Research Project Flow Chart

A flow chart of the research project is illustrated in figure 1.2 followed by the identification of gaps in the research which are the basis for this thesis. They are outlined below

1. Investigation of long persistent phosphorescent materials and characterizations.

2. Investigation of PV devices and luminescent materials for the enhancement of the PV devices performance.
3. Investigation of the polymer Polysiloxane, which may be ultra-transparent in the UV spectral range, and materials that may be used as host materials for luminescent applications.

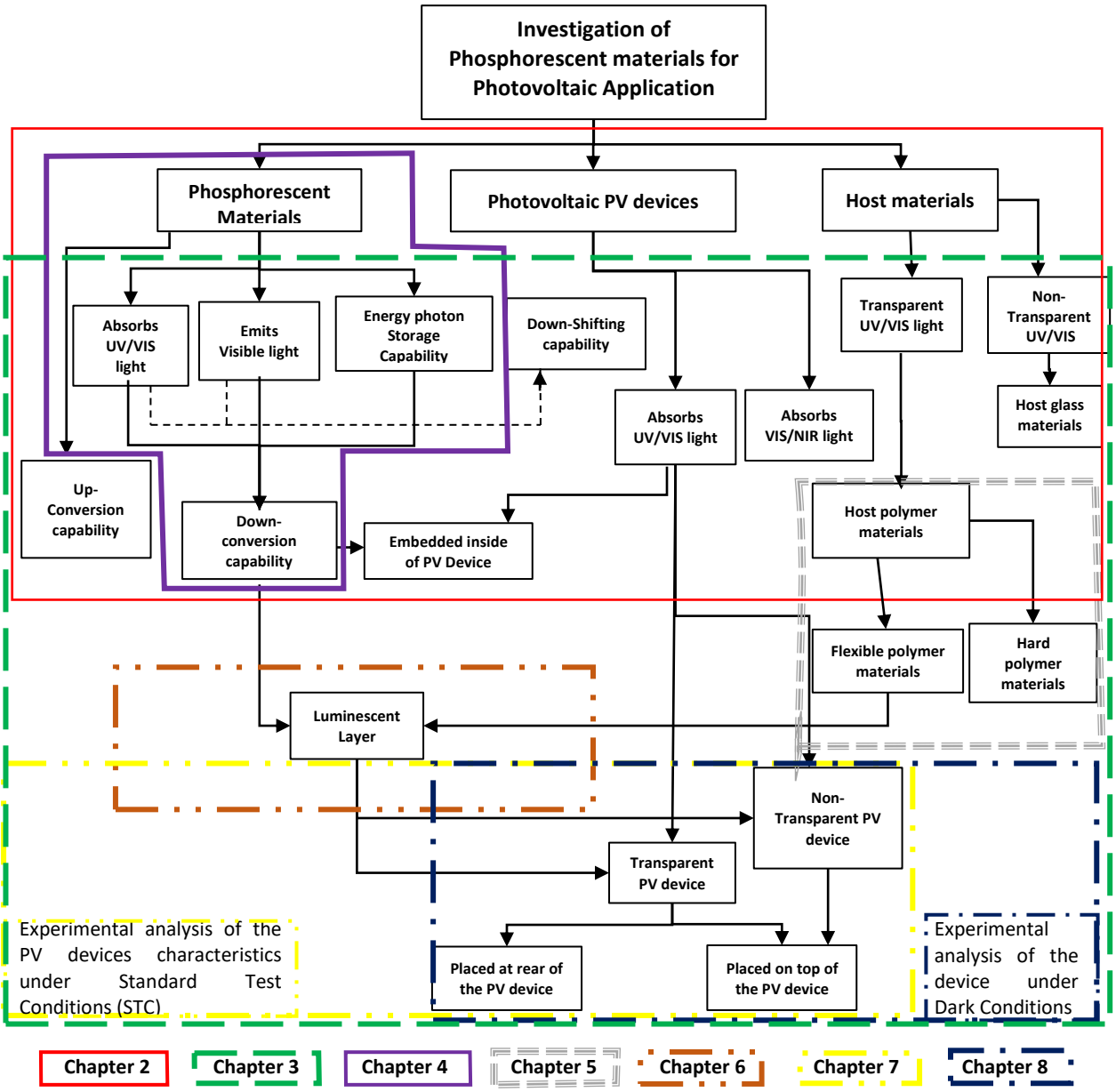

Gaps in the Research

For Phosphorescent	PV Devices	Host Material
•Non standards methods found for synthesis or characterization, neither optical nor physical properties of the LPP. •Non-standards reference for LPP for PLQY.	•To date experimental studies are limited to small LPP phosphor concentration ratio with the PVs, and normally applied as a non-passive approach, inside of the PV device. •The characterization of the PV devices are carried out with luminescent materials only, and not compared to the PV device itself without it.	•To date host polymer materials applied for luminescent materials are not ultra-transparent in the UV spectra range.

Figure 1.2. Flow chart of this research project and the gaps identified in the research Literature Review.

CHAPTER 2

LITERATURE REVIEW

2.1 Introduction

An extensive literature review was conducted in order to gain knowledge of the research topic in the field of PV devices and phosphorescent species technologies, to create a firm foundation for advancing knowledge. This chapter is divided into four primary sections: (1) Photovoltaic device technologies, from first generation to third generation PV technologies and the selection of PV devices for this project; (2) Different types of luminescent materials used to enhance the PV device performance; (3) A comprehensive literature review into the luminescent phenomena, exploring the differences between fluorescent and phosphorescent phosphors and a review of phosphorescent mechanisms and (4) a review of different types of host materials which can be used to dispense the phosphorescent species. The literature review presents and discusses each of these topics relevant to this research project.

Chris Hart has defined the literature review as "the use of ideas in the literature to justify the particular approach to the topic, the selection of methods, and demonstration that this research contributes something new" (Hart, 1998).

2.2 Photovoltaic Devices Technologies

2.2.1 Silicon Photovoltaic Devices

The photovoltaic effect was first discovered by Alexandre Edmond Becquerel in 1839 during instrumental experiments, showing a strong relationship between light and the electronic properties of light absorbing materials (Petrova-Koch, 2009). The photovoltaic work principle is described as follows: "In this effect (i) absorption of light generates electron–hole pairs in a semiconductor material and (ii) the charge carriers are separated and extracted into an external circuit, generating electricity in it"(Bünzli and Pecharsky, 2013). Albert Einstein won a Nobel Prize in physics in 1905 for describing the nature of light and the photoelectric effect,

on which photovoltaic technology is based. The first photovoltaic module was built by Bell Laboratories in 1954, and since then it has been constantly evolving, as shown in Figure 2.1.

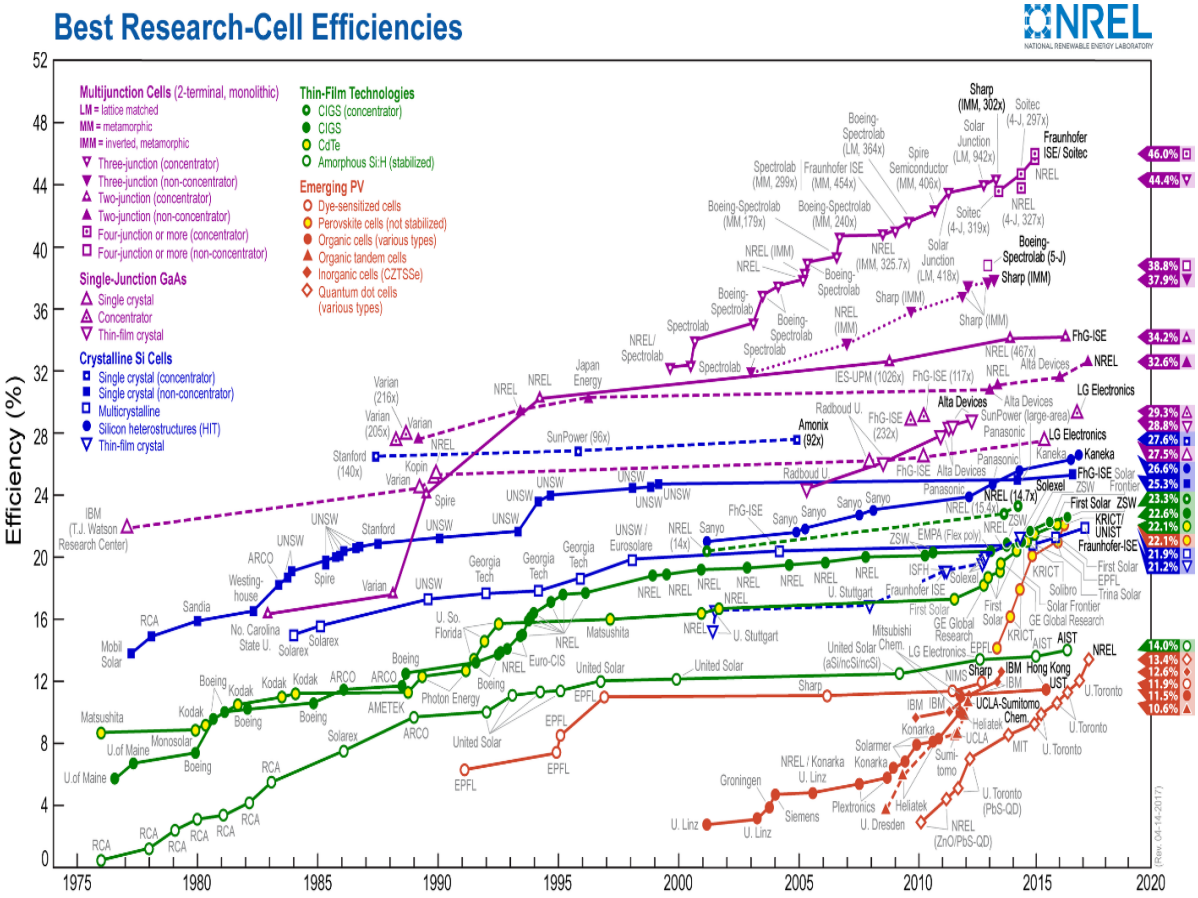

Figure 2.1. Evolution of the conversion efficiencies for various PV technologies and materials with their developers (Source: The National Renewable Energy Laboratory, NREL, 2018).

The fundamental spectral losses that limit the theoretical maximum efficiency of these devices is caused by the material properties (Green, 1982). For example, one of the most widespread semiconductor materials used for PV is silicon, and it absorbs at most only about 48% of the total solar emission spectrum, and not all that absorbed light is converted into electrical power (Bünzli and Pecharsky, 2013). Today's most common PV manufactured devices use a single junction, to create an electric field within a semiconductor, and exhibit a significantly lower efficiency, η (%), ranging from 6% from Amorphous, a-Si, to 25.3% for silicon, c-Si, (NREL, 2018). There is potential to increase these values by making better usage of the wavelength light, where it shows poor response (Green, 1982; Tahhan et al., 2015).

There are many strategies towards improving PV efficiency, such as stacking two or more different PV devices, with different band gaps. Such devices exist and are called multi-junction PVs or tandem cells and they have a higher efficiency because they can convert more of the energy spectrum of light to electricity. Figure 2.2 illustrates the schematic diagrams of silicon and a multi-junction PV device, which is a stack of a single sequence of p-i-n cells. A-Si type thin film PV devices are commonly found in calculators and have a high response to visible light.

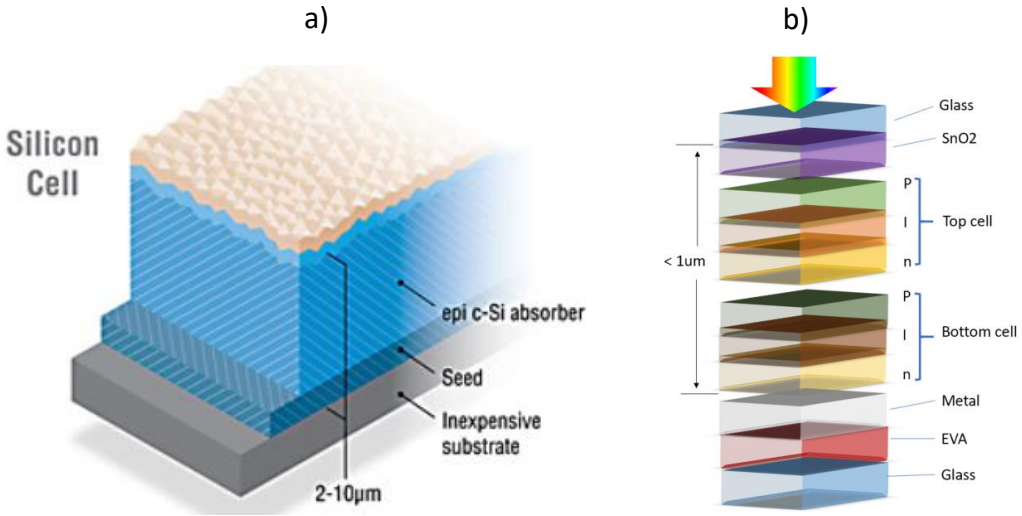

Figure 2.2. (A) Schematic diagram of the silicon PV device (NREL, 2016). (B) Schematic illustration of an a-Si/a-Si multi-junction structure PV device (PV) (Marsrock Science Technology, n.d).

Apart from material property losses that contribute to lower power conversion, many other losses contribute to reducing the power efficiency, for example; reflection losses, lattice thermalisation, recombination, junction, and contact voltage losses. The overall theoretical limit efficiency of silicon-based PV devices is: $\eta \approx 31\%$, also known as the Shockley-Queisser, (SQ), limit (Shockley and Queisser, 1961). Efficiency limits for PV devices can be theoretically higher than that, considering thermodynamic effects with carrier multiplication, which is the phenomenon wherein the absorption of a single photon leads to the excitation of multiple electrons. For instance, in a PV device illuminated by the Sun's unconcentrated black-body radiation, the theoretical maximum efficiency is 43%, whereas for a PV device illuminated by the Sun's fully concentrated black-body radiation , the efficiency limit is 85% (Brendel et al., 1996). These detailed balance limit of efficiency analyses are still used to study the limitations of the PV materials and performance such as transparency losses arising from sub-bandgap

($(E_{ph}<E_g)$ photons, (which are energy photons that are not absorbed by PV material) and some higher energy (E_{ph} - E_g) photons, (which are lost via non-radiative relaxation of the excited electrons to the conduction band, and can also cause heating and degradation of the PV device) (Klampaftis et al., 2009). The best experimental PV devices fabricated in laboratories are shown in Figure 2.1, which describes the recent achievements of PV conversion efficiencies and gives some examples of these efficiency results including: ɳ≈ 27.6 for wafer-based crystalline silicon (c-Si), under concentrator, η≈ 21.2% for Thin-film (c-Si) and η≈ 37.9% Multijunction PV with three-junction (non-concentrator).

Many experts describe that one method toward improving the light absorbed-to-electricity conversion yield is to concentrate the solar light on the photovoltaic devices, hence reaching higher surface power density, and consequently better conversion (French et al., 2011). At present, the most efficient model is the tandem PV device (such as the GaInP/GaAs PV device), with an efficiency of 46% conversion efficiency under illumination equivalent to 508 suns (Green et al., 2018). Alternatively, a spectral-splitting module comprising a pair of two-cell stacks (GaInP/GaAs and GaInAsP/GaInAs) reached a photovoltaic efficiency of approximately 38.5% under 20-sun irradiation. In this design, a dichroic reflector is used to split the light beam into two sub-beams which are focused on the two different device stacks (Green et al., 2012).

Many strategies towards improving PV efficiency such as re-engineering its design, (which is considered more complex and expensive than just by applying a luminescent layer such as phosphorescent materials attached into the surface of the PV device), are known as passive approaches (Goetzberger et al., 2008; Richards, 2006a; Stanley et al., 2016). As illustrated in Figure 1.1, light conversion mechanisms such as down-conversion (DC) or down-shifting (DS) have the capacity to shift the wavelengths of incoming solar UV photons to higher values where the external quantum efficiency of the PV device is also higher. Up-Conversion (UC) is the conversion of two or more low energy photons into a high energy photon. By applying these mechanisms to PV devices, it is possible to maximize the amount of photons with sufficient energy to be absorbed by the PV device, which results in a higher electrical power output.

2.2.2 Emerging PVs Devices

The new era of PV devices also called “third-generation solar cells” explore low cost material processes, and have a realistic energy-conversion efficiency that can be applied to many applications (Conibeer, 2007; Green, 2006, Girtan, 2017). These emerging PV technologies, shown in Figure 2.1, were initiated by Brian O'Regan and Michael Grätzel (1991) with Dye-sensitized Solar Cells (DSSC), and are the evolution of new branches of PVs such as Perovskite Cells (PSC), Organic cells (OPVs) and Quantum dot Cells technologies. These emerging PVs have been one of the hottest topics in solar energy presenting all the advances and many new attractive features, like low cost devices and production processes, and physical flexibility (Jacoby, 2016; Leow, 2014). However, there is a need for higher efficiency, as can be observed when comparing the efficiencies of other types of PV technologies, (see Figure 2.1), and also better chemical stability, in order to become comparable to the commercial silicon PV technologies, which currently claim about 90% of the solar-cell market (Jacoby, 2016).

2.2.3 Dye-sensitized Cells (DSSCs)

A typical DSSC consists of a dyed nanocrystalline TiO_2 electrode based on a transparent conducting oxide (TCO) substrate, a platinum (Pt) counter electrode, and an electrolyte solution containing an I_3^-/I^- redox couple between the electrodes (Chergui et al., 2011; Grätzel, 2003, Girtan, 2014), as shown in Figure 2.3. The main operating principle of DSSCs is as follows: under light illumination, the dye adsorbed on the TiO_2 film are excited and the photo-generated electrons in the dyes are injected into the conduction band of TiO_2, and then transported through the film to the TCO substrate. In the meantime, the dyes are regenerated by the reduction of oxidized dyes by I^- ions from the electrolyte. The I^- ions are then further regenerated at the counter electrode via the reduction of I_3^- ions. The regenerative processes in DSSCs allow the generation of electricity from solar light without any permanent chemical transformation (Zhang et al., 2014).

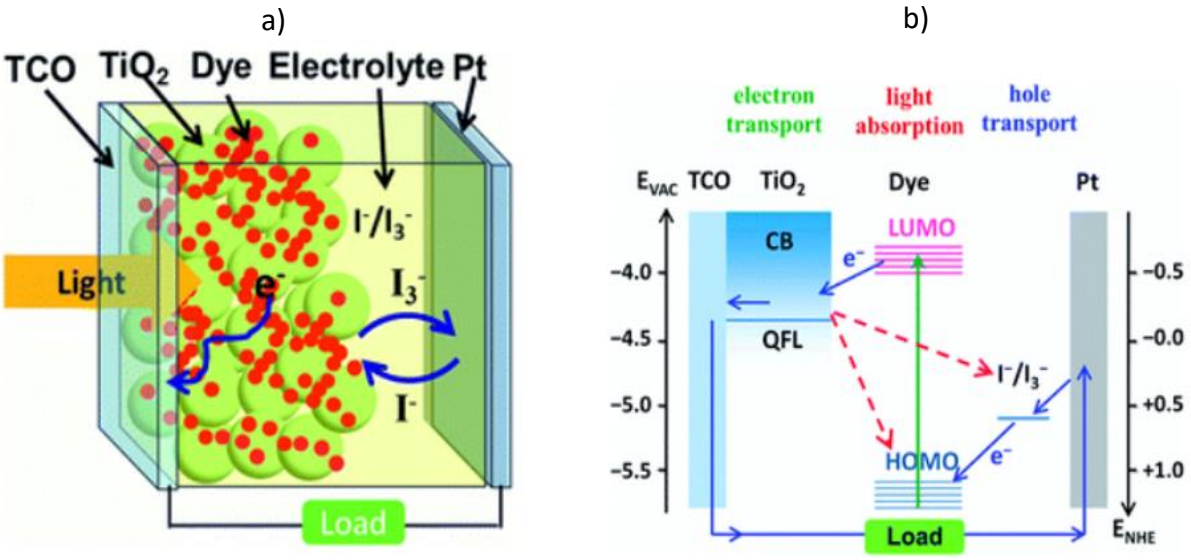

Figure 2.3. (a) Schematic representation of the principle of the dye-sensitized PV device. (b) The completed circuit through the external load (Zhang et al., 2014).

The addition of luminescent layers to DSSCs could improve this emerging technology by leading to a higher efficiency and long-term stability of the dyes sensitivities as this device has a poor absorbance in the UV range <450nm. Using a luminescent layer that can shift the ultraviolet light and re-emit at longer wavelength >400-700, it could reduce the spectral losses resulting from inefficient use of ultraviolet photons before or after they reach the PV device. The long-term stability is expected as this layer absorbs, blocks or traps the high-energy photons and UV, which can result in an optimised PV device.

It was reported by Slooff et al., (2006), that in a DSSC with a near-infrared sensitizer, the photovoltaic performance was significantly enhanced using a reflective luminescent down-shifting (R-LDS) layer to increase the light-harvesting efficiency at the wavelength region (400–550 nm) where the sensitizer dye has weak absorption. The group reported a relative enhancement greater than 200% in incident photons converted to current efficiency (IPCE) near 500 nm, and 40–54% in J_{SC} using a red phosphor CaAlSiN3:Eu2+ as the LDS material, thus attaining 5.0 and 4.8% overall efficiencies of power conversion for the R-LDS layer coated on the counter electrode (front illumination) and working electrode (back illumination) respectively, (see Figure 2.4). In another case involving DSSC and LDS materials, an improvement was reported of the efficiency of dye-sensitized solar cells by 23.3% (Liu et al., 2006).

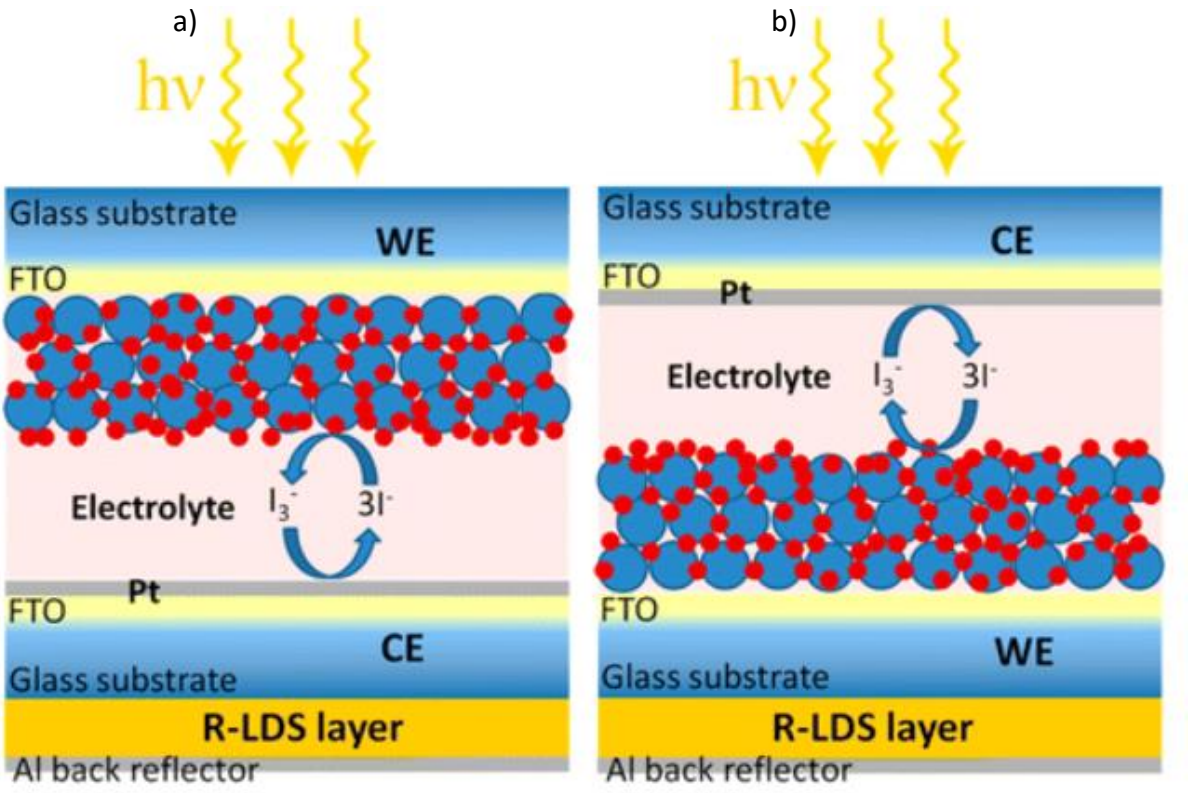

Figure 2.4. Schematic demonstration of two DSSC structures containing the R-LDS layer. (a) the R-LDS layer is placed on the counter electrode (CE) side and incident light illuminated from the working electrode (WE) side (front illumination); (b) the R-LDS layer is placed on the WE side and the incident light illuminated from the CE side (back illumination) (Slooff et al., 2006).

Dye-sensitized solar cells (DSSCs) are an example of an inexpensive device that is suitable for this project application because of its physical properties, such as being made of transparent glass, and having a strong response in the visible spectral range, which matches with the LPP emission range. By applying this type of transparent PV device, it will be possible to test the phosphorescent materials at the rear surface of the PV device. This DSSC PV device is selected and it will be applied in this research in the attempt to improve its power conversion efficiency by applying the fabricated luminescent layer on the top and at the rear surface, as this device is considered transparent.

2.2.4 Perovskite-Based Solar Cells (PSCs)

This is another example of a PV device that could benefit from a passive approach containing phosphorescent materials. It consists of luminescent materials because of its physical structure, which can also be made of transparent glass substrate (Bagher, 2014). This type of

device is based on organic or inorganic perovskite-structured semiconductors and was initially seen as “silicon-like” and introduced as a type of DSSC device, but today studies indicate that they have a unique working mechanism depending on the material’s properties. The latest achievement marks the first time that a PSCs device has overtaken the multi-crystalline Silicon PV device with an efficiency higher than 28.0% and is greater than multi-crystalline PV 22.3% (NREL, 2018). PSCs have broken the all-time efficiency record in a short period of time. By charting this history (NREL, 2018), an improvement in efficiency can be seen rising from 13% in 2013 to 28.0%, four years later.

In the PSCs, the absorption of incident photons results in an instantaneous generation of free charges (Collavini et al., 2015). Figure 2.5 shows the schematic representation of the principle of the perovskite PV device, with light passing through the transparent electrode (green) of a perovskite solar cell onto a layer of a photosensitive perovskite material (blue), stimulating excitations called electron-hole pairs (e^-/h^+).

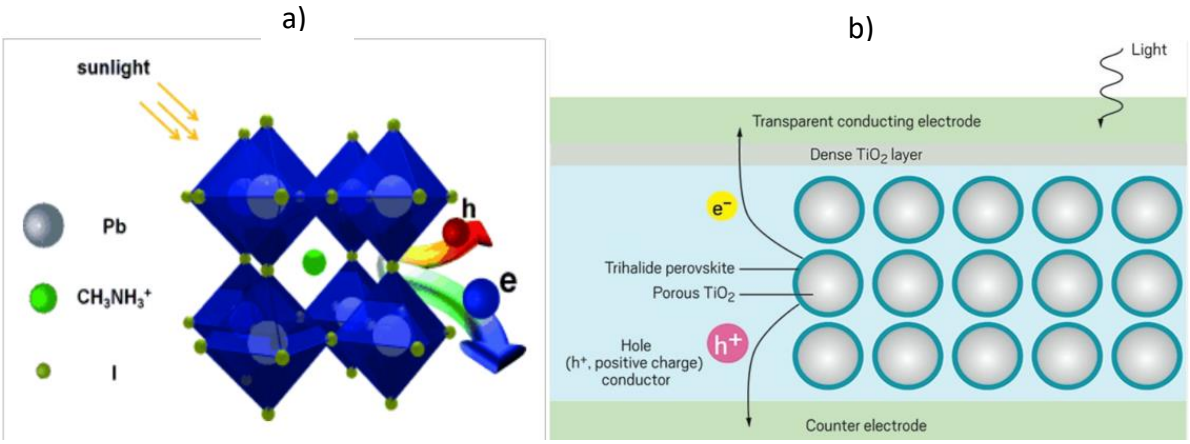

Figure 2.5. (a) The schematic representation of the principle of the perovskite PV device. (b) The charged particles separate and diffuse through the charge-conducting layers to their respective electrodes, thereby generating an electric current (Jacoby, 2016).

The efficiency of the Perovskite PVs with a poor UV response can be improved by altering the incident light spectrum with a luminescence layer device. More recently, a laboratory experiment produced CH3NH3PbBr3 perovskite with the CH3NH2/PbBr2: 6/1 M ratio and 7.0 %wt. perovskite concentration in Polyvinyl Alcohol (PVA) lead to the highest efficiency recorded, it increased by about 45%, compared to an uncoated PV device, (Mirershadi and Ahmadi-Kandjani, 2015).

However, these devices, PSC and DSSC, are still considered very unstable compared to Silicon PV devices due to dissolution of the perovskite/dye in the liquid electrolyte. Amongst alternative PSC PV device structures, a carbon-based perovskite solar cell, as illustrated in Figure 2.6, appears to be an ideal candidate for this research project due to the stability reported by several research groups and also the device structure is composed of more stable materials such as TiO_2, ZrO_2, carbon black and graphite powders (Hashmi et al., 2017; Hu et al., 2014).

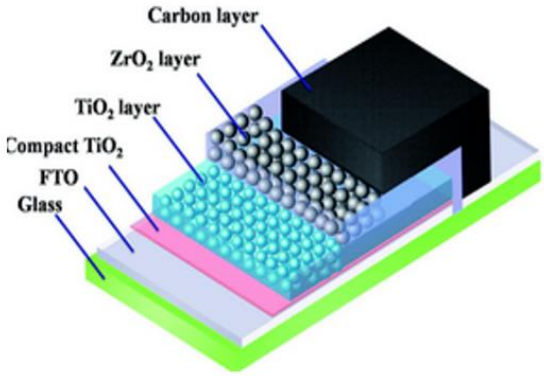

Figure 2.6. The schematic structure of a typical mesoscopic perovskite PV device with carbon counter electrode (Hu et al., 2014).

In addition, these devices have demonstrated that a hysteresis effect may occur due to the small current that arises as a result of a potential step charging certain capacitances within a cell. Thus, these are considered an undesirable effect for the LPP phosphor applications, but it is worth testing this type of PV device in the experimental sections.

On account of the selection of the PV device for this project application there are many different technologies, as observed in the Figure 2.1, that their efficiency may be improved by applying luminescent layers on its surfaces. This research project will explore the three potential PV candidates which are a-Si multijunction, DSSC and a Perovskite PV device in order to test the fabricated luminescent layer. It is clear how these PVs have different mechanisms, physical structures and exhibit different performance across the spectrum. However, the selection of the a-Si PV is due to the fact of it being a silicon-based device, with a wider absorbance in the visible spectra range which can respond well with the application of the phosphorescent species, no hysteresis effects, and is more stable compared to DSSC and PSC.

The selection of the DSSC and perovskite PV devices are motivated because of being transparent devices fabricated without reflective coating at the rear interface which may allow applications of the luminescent layers at the rear surface. Using the luminescent layer at the rear of the PV device it may work as a reflective coating as well as a down-convertor layer.

In the schematic shown in Figure 2.7, it illustrates the applications of the luminescent layers attached to the PV device surfaces to enhance the PV device performance, and the working principle of this passive approach is described as follows: (i) long persistent phosphors are embedded inside of a host transparent polymer used to fabricate the layer; (ii) the application of the layers can be attached on the top as well as at the rear surface of the PV device depending of the internal mechanism of the PV device. Using a transparent PV device such as Dye-sensitized Solar Cells (DSSC) and Perovskite that does not contain an internal reflective coating or metal conductive layer at the rear, it may allow the energy photon pass through the PV device, reaching the luminescent layer at the rear surface. Apart from the PV devices structure, the spectrum response of the PV device that matches with the phosphorescent emission is another important parameter influencing the selection of the ideal PV device, thus increasing the likelihood that the non-silicon-based PV devices will be better suited to testing the phosphorescent approach focussed on in this research.

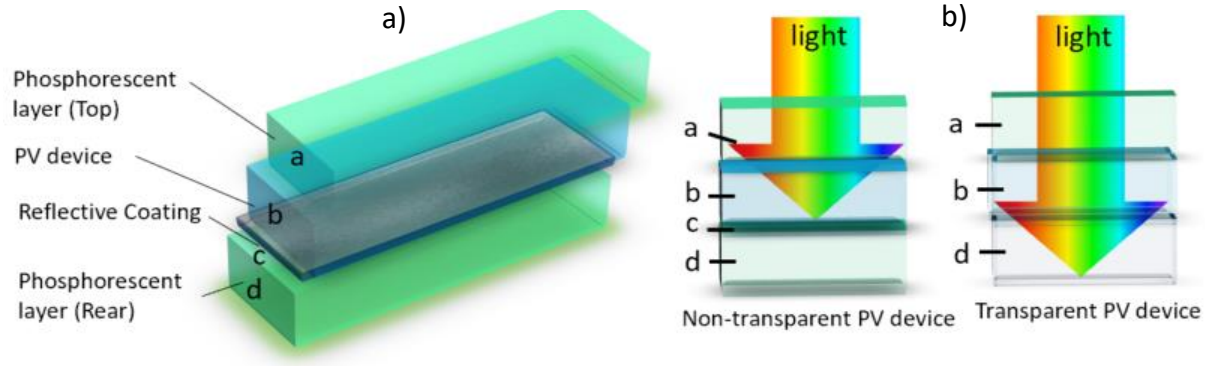

Figure 2.7. (a) Schematic of phosphorescent layers attached at the top and rear surfaces of a PV device. (B) schematic diagrams showing two possible configurations using a non-transparent PV device (containing a reflective coating and metal contact) which does not allow the transmission of light through the PV device, and a transparent PV device. The transparent PV device allows a non-absorbed energy photon to pass through the PV device structure before it reaches the rear phosphorescent layer (LDC), LDC may act as a reflective coating as well as a light emitting device.

2.3 Luminescence Materials for Light Conversion Mechanisms

Currently, the advanced optical materials e.g., phosphors, quantum dots, organic dyes, are used as luminescent materials to fabricate a luminescent layer for light conversion mechanisms, (or also known as Luminescent Solar Concentrators (LSCs)) to enhance the PV devices performance. These mechanisms have been investigated by many experts and applied as a passive approach on different types of PV devices technologies (Richards, 2006a, H. Sun et al., 2014; Sun et al., 2013; Wang et al., 2014). These layers are produced by certain types of host materials, which are usually transparent polymers and luminescent materials such as fluorescent or phosphorescent materials.

The working principle of the luminescent layer, is that the incident energy photons are absorbed by the luminescent particles and re-emitted at shorter or longer wavelengths, with a fraction of photons whose emission angle is larger than the critical angle, trapped in the waveguide through total internal reflection and redirected to the PV device for collection (Leow, 2014). Examples of these applications are silicon-based and dye-sensitized PV devices which benefit from the Down-Conversion (DC) and Up-Conversion (UC) capabilities of lanthanide ions to harvest UV and NIR (Near-infrared) solar light and to boost the overall quantum efficiency of these next-generation devices (Feldmann et al., 2003).

These types of luminescent mechanisms have been applied also in PV devices to concentrate light from the larger surface area of the concentrator onto a smaller PV area, thus increasing the power output of the PV devices. A schematic of conventional LSC design with a side-mounted PV device is shown in Figure 2.8, and the working mechanism of this LSC is described as follows: (I) with a magnified view of dye molecules embedded in the flexible acrylic layer (inset); innovative LSC design with front-facing PV devices (II). Where a, acrylic layer; b, luminescent layer; c, PV cell; d, incident photon absorbed by luminescent dye; e, photon emitted by luminescent dye, wave-guided and absorbed by PV device; f, incident photon absorbed by luminescent dye and re-emitted at angle within escape cone; g, dye molecule excited by photon, light is downshifted and re-emitted isotopically; h, downshifted photon is

re-emitted into the waveguide; i, dye molecule; and j, direct sunlight absorbed by front-facing PV device (Leow, 2014).

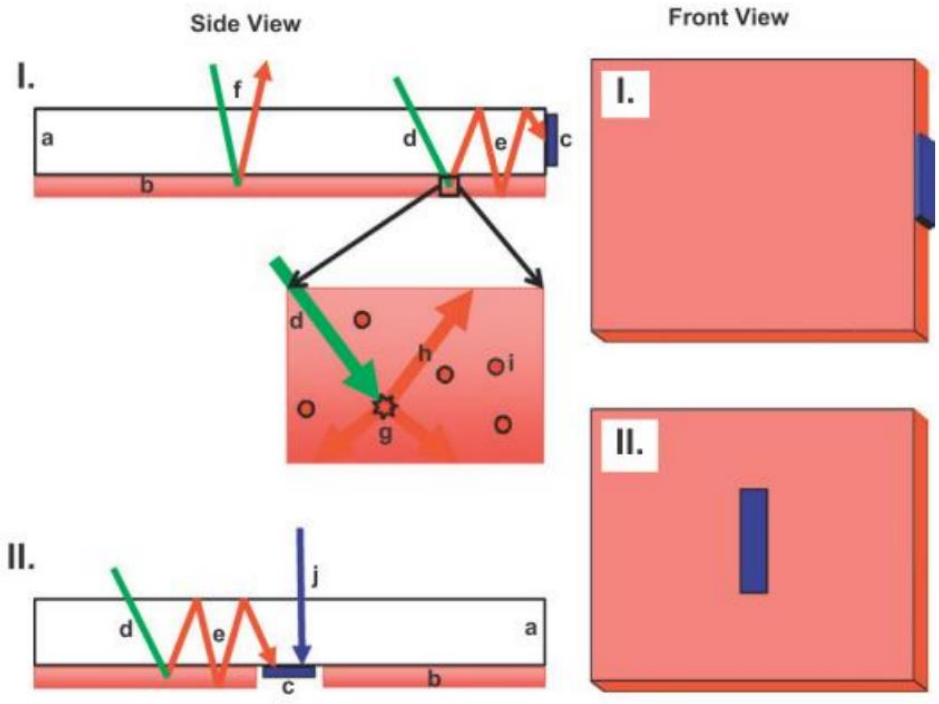

Figure 2.8. Schematic of luminescent layer side-mounted PV cells (Leow, 2014).

Many scholars from different disciplines are studying these possibilities to enhance the PV devices by Light Conversion Mechanisms (Shalav et al., 2003, 2007; Trupke et al., 2002b). Pairs of lanthanide ions (Yb^3/Er^3 or Yb^3 /$Tm^{3)}$ involving a sensitizer and a luminescent ion provide efficient up-conversion mechanism systems (Auzel, 2004). Silicon based PV devices, up-converting systems which use the sole Er^3 ion are described as more suited to this mechanism (Marques-Hueso et al., 2011). Some transition metal ions, quantum dots (QDs) (de Wild et al., 2011), and organic dyes are also useful for up-conversion (Cheng et al., 2012; Schulze et al., 2012) or down-conversion (Strumpel et al., 2007). Trupke et al., (2006) show, from theoretical calculations, that adding an up-conversion layer to semiconductor multi-junction PV devices could increase the absolute external quantum efficiency (EQE) from about 40% to 50% under AM1.5G illumination. Thus, there are many different types of luminescent mechanisms that can be used to enhance the PV device and depending on its internal structure it can be classified, for example; as Down-shifting (DS), Down-conversion (DC) or Up-Conversion.

2.3.1 Down-Shifting (DS)

Luminescent Down-shifting (LDS) of the incident of the solar spectrum was initially proposed by Hovel et al., (1979) in order to overcome the low spectral response and AM0 in the blue region of the solar spectrum for several types of solar cells. This mechanism uses luminescent materials in an optical application that exhibit a stokes shift, absorbing short wavelength radiation and emitting longer wavelengths, to improve the poor spectral response (SR) of PV devices to short-wavelength light (Kennedy et al., 2010; Klampaftis et al., 2009; Stanley et al., 2016). Nowadays, Klampaftis et al., (2009) describe this as one of the most powerful approaches to achieve a more efficient utilization of the short wavelength of the solar spectrum, considering it is a passive approach that involves applying a luminescent species in a layer prior to the device, thus eliminating the need to interfere with the active material of a PV device. Figure 2.10 shows a schematic illustration of the down-shifting concept using a luminescent layer to enhance the PV device.

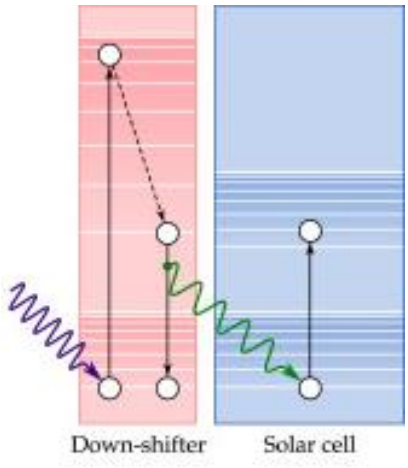

Figure 2.9. Schematic illustration of the energy down-shifting concept (de la Mora et al., 2017).

The passive approach is normally made by doping highly transparent polymers, for example, polymethyl methacrylate (PMMA) or polyvinyl acetate (PVA)) with luminescent dyes, semiconductor quantum dots, or silicon nanocrystals (Hind Ahmed et al., 2014), Stanley et al., 2016). The LDS layer absorbs photons, typically in the 300–500 nm range, and re-emits them at a longer wavelength where the photovoltaic device exhibits a significantly better response (Klampaftis et al., 2009, Kennedy et al., 2010). Additionally, this type of mechanism can be

placed in front of the devices, allowing down-shifted photons to reach the devices, and is then capable of minimizing the losses at the top or at the rear of the cell surface (Stanley et al., 2016).

Using a passive mechanism which can collect direct and diffuse solar radiation, can improve the power conversion efficiency of the PV devices and helps to protect the PV material from degradation by using a transparent host material on the top surface of the panel or module. A passive layer on the rear of the PV panel can help it to overcome some problems such as poor absorption by applying a luminescent layer as a reflector, and heat that is caused by high energy photons on the conductor band of the PV material (Klampaftis et al., 2009).

It is considered that, each type of PV device technology differs by the type of semiconductor material used for its fabrication, (which makes them perform differently under the same sunlight conditions), because each semiconductor absorbs at specific wavelength ranges as shown in Figure 2.7 and converts solar radiation into electricity.

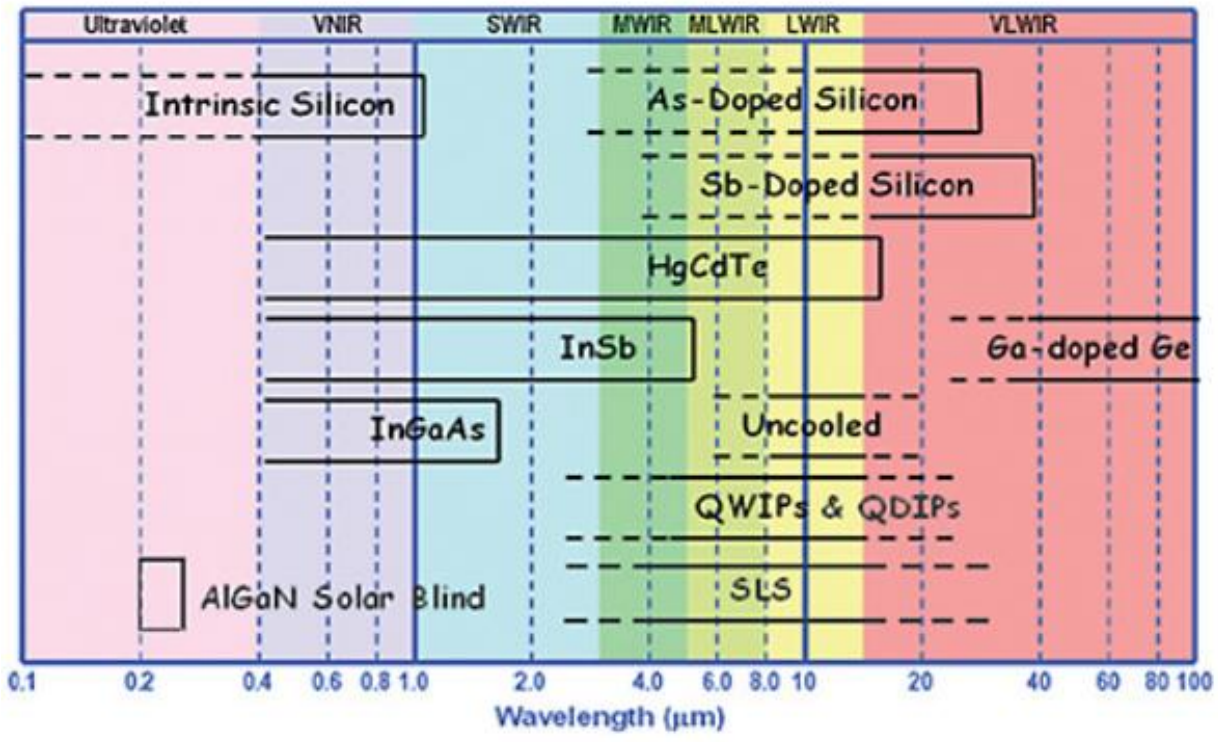

Figure 2.10. PV materials for UV-visible-infrared detection (Technologies et al., 2010).

The conversion efficiency of various PV devices is presented in Table 2.1 and Figure 2.11 shows representative EQEs for these devices, at short wavelength, the region where, for example, LDS is most relevant. The wavelength-dependent response of a PV device can be described by its external quantum efficiency (EQE), i.e. it is defined as the percentage or ratio of the number of electron–hole pairs generated to the number of photons incident on the front surface of the cell (Klampaftis et al., 2009).

Type	Label	V_{oc} (V)	J_{sc} (mA/cm^2)	FF (%)	η (%)
Crystalline silicon					
Monocrystalline Si	m-Si	0.696	42.0	83.6	24.4
Multicrystalline Si	p-Si	0.650	37.4	76.2	18.5
Thin film transfer Si	t-Si	0.650	37.8	77.6	19.1
III-V-cell					
GaAs	GaAs	1.122	29.7	86.5	28.8
Thin film chalcogenide					
CIGS	CIGS	0.705	35.5	77.9	19.5
CdTe	CdTe	0.845	25.9	75.5	16.5
Amorphous silicon					
Amorphous silicon	a-Si	0.859	17.5	63.0	9.5
Dye sensitized solar cell					
Dye sensitized solar cell	DSSC	0.736	20.9	72.2	11.1
Organic solar cell					
DTDCTP:C70	Org.	0.950	12.1	56.0	6.4

Table 2.1. An overview of the different type of PV devices and their characteristics: open circuit voltage, Voc, short circuit current density, Jsc, fill factor, FF, and power conversion efficiency η, under standard test conditions.

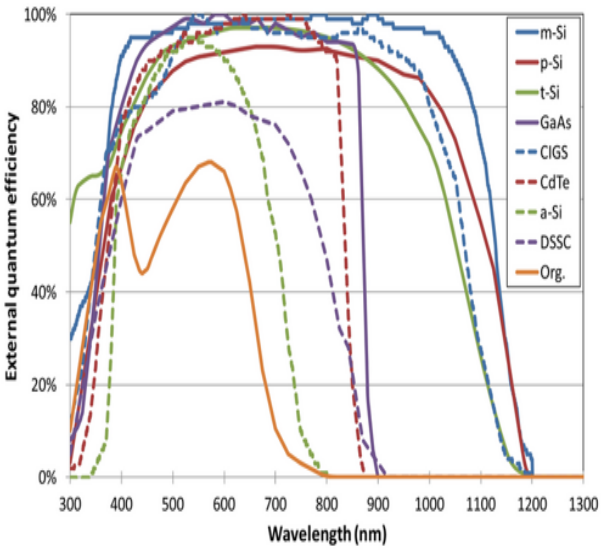

Figure 2.11. The external quantum efficiency of these PV devices considered (Minnaert and Veelaert, 2014).

As can be observed, all the PV device technologies have a poor response at shorter wavelengths < 400nm. This behaviour may be caused by the technical processing difficulties in the design or imperfect properties of the PV semiconductor materials (Klampaftis et al., 2009). One solution to improve the PV device efficiency without changing the semiconductor properties is by applying a passive approach mechanism such as LDS. Accordingly, two types of material are incorporated to fabricate a down-shifting layer; host matrix and luminescent species (Klampfatis et al., 2009).

Host materials: For a suitable host material, the following factors must be considered, high transmittance in the UV and visible spectral range, low scattering, adequate resistance to heat

and humidity variation, compatibility with luminescent species, prolonged photostability over an extended period of time of the PV, UV resistance and low cost. Examples of materials used in this mechanism that have been reviewed by many scholars (French et al., 2011, 2011; Maruyama et al., 2000; Richard, G. Jones, 1995; Richards and McIntosh, 2007; Slooff et al., 2006) include:

- Poly-methyl methacrylate (PMMA)
- Poly-vinyl acetate (PVA)
- Inorganic crystalline materials (Al2O3, CaF2)
- Glass
- Organic Molecule Silicates

The solar spectrum considered for PV devices can be divided into UV (UV-A: 320-400 nm; UV-B: 280-320 nm; UV-C: 200-280 nm), visible light (400-750nm) and infrared (750nm – 1mm-) regions. For a PV device, indoor characterization is described at one sun illumination or 1000 W/ m^2, and outdoor solar spectrum at Air Mass 1.5 global (AM 1.5G) illumination for the top surface of the device within the range from 280 nm to 4000 nm, see Figure 2.12.

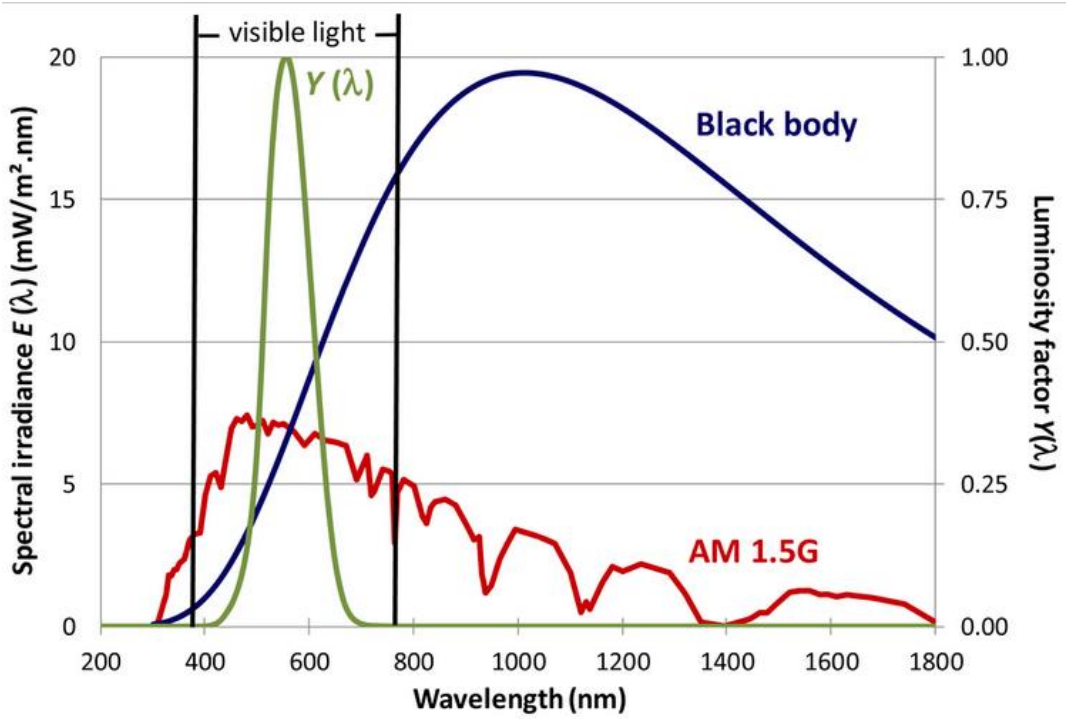

Figure 2.12. The solar spectral irradiance E(λ) spectrum AM 1.5G and black body on temperature T = 2856 K, (Minnaert and Veelaert, 2014).

Luminescent materials: According to Klampaftis et al., (2009) the selection of these materials must also consider various factors such as: (i) unity LQE; (ii) a wide absorption band in the region where the EQE of the cell is low; (iii) a high absorption coefficient; (iv) a narrow emission band, coinciding with the peak of the cell EQE; (v) good separation between the absorption and emission bands in order to minimize losses due to re-absorption; and (vi) low cost. Most common luminescent materials used for such applications are:

- **Quantum dots:**(Kennedy et al., 2010; Leow, 2014; NREL, 2010; H. Sun et al., 2014; Švrček et al., 2004, Richards and McIntosh, 2007).
- **Organic dyes:** (Galluzzi and Scafé, 1984; Sark et al., n.d.; Slooff et al., 2006).
- **Rare-earth ions:**(Bünzli and Pecharsky, 2013; CAO et al., 2011; Jin et al., 1997; Katsuya Kawano et al., 1997; Katsuyasu Kawano et al., 1997; Marchionna et al., 2006).

2.3.2 Down Conversion (DC)

This is another light conversion mechanism that has been widely used to enhance the performance of PV devices (CAO et al., 2011; Liu et al., 2006; Richards, 2006b; Spitzer et al., 2013). Down-conversion, was first reported by D.L. Dexter and it was described as the feasibility to obtain higher quantum efficiencies by creating multiple photons through converting a single photon into two low energy photons (Dexter, 1957). This mechanism involved the simultaneous energy transfer from a donor to two acceptors, each accepting half the energy of the excited donor. The practical evidence was first published in 1974 (Piper et al., 1974; Sommerdijk et al., 1974) where experiments found quantum yields above 100% for YF_3:Pr^{3+}.

Recently, a multipurpose device offering both light scattering and light down-converting properties was developed using LLP ($SrAl_2O_4$: Eu, Dy) on top of TiO_2 layers and applied in CdS, QDSCs PV devices, resulting in a “power conversion efficiency of 1.24%, 26.5% higher than that of the cells without $SrAl_2O_4$: Eu, Dy”(H. Sun et al., 2014a). In both cases, it was found that the enhanced PV device efficiency mainly resulted from the improved light scattering and the contribution from light down-converting from the LPP (Sun et al., 2013, X.-Y. Sun et al., 2014).

Another investigation was carried out as a non-passive approach, which is inside the PV device, using CdSe quantum dot-sensitized PV devices based on an efficient bifunctional structured layer composed of long afterglow $SrAl_2O_4$: Eu, Dy phosphors placed on top of a transparent layer of nanocrystal TiO_2, see Figure 2.13. The results show that a high-power conversion efficiency of 1.22% is achieved for the cell with $SrAl_2O_4$: Eu, Dy at one sun illumination, with an increase of 48%, compared to the device without LPP (SrAl2O4: Eu, Dy) 0.82%. After one sun illumination for 1 min and subsequent turning off of the light source, the cell with $SrAl_2O_4$: Eu, Dy still shows an efficiency of 0.04% under dark conditions due to the irradiation by the long persistent light from SrAl2O4: Eu, Dy. Some researchers described the possibility of fulfilling the operation of solar cells even in the dark (H. Sun et al., 2014a). It has been found that down-conversion and downshifting materials are usually doped into thin layers inside of the PV devices (Hosseini et al., 2013; Richards, 2006b; Spitzer et al., 2013).

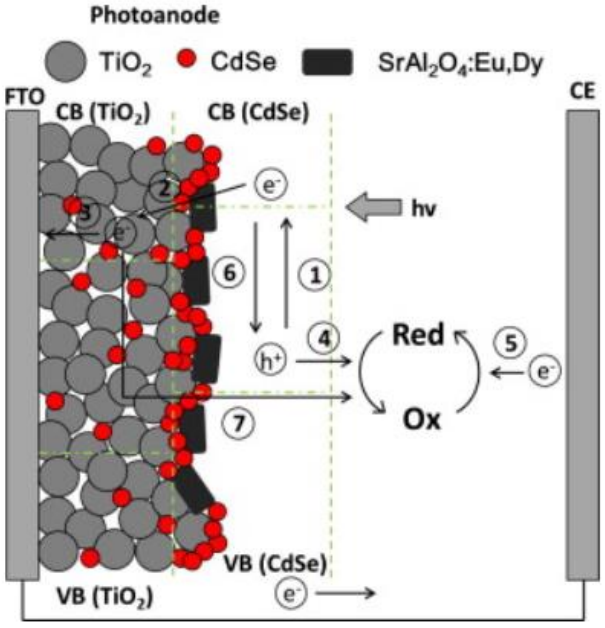

Figure 2.13. Schematic diagram of the structure and working mechanism of CdSe QDSSCs with P25/$SrAl_2O_4$:Eu,Dy/CdSe electrode (H. Sun et al., 2014a).

Several different mechanisms of the down-conversion for PV devices by including LPP has been proposed by Wegh et al., 1999, see Figure 2.15, and are described as follows: Arrows connecting different ions and dashed arrows indicate energy transfer between ions. (a) Quantum cutting on one ion via cascade emission. Processes (b to d) occur on two types of

ions. As a first step the ion (I) is excited into a high energy level. From the high energy level energy transfer will excite the high energy level of the second ion of the species (II). Subsequently two photons will be emitted by two ions (II), after a second energy transfer step (b), or by both ion (I) and (II) (c). Down-conversion can also occur via the emission of a photon by ion I, followed by energy transfer to an ion of the species (II) (d).

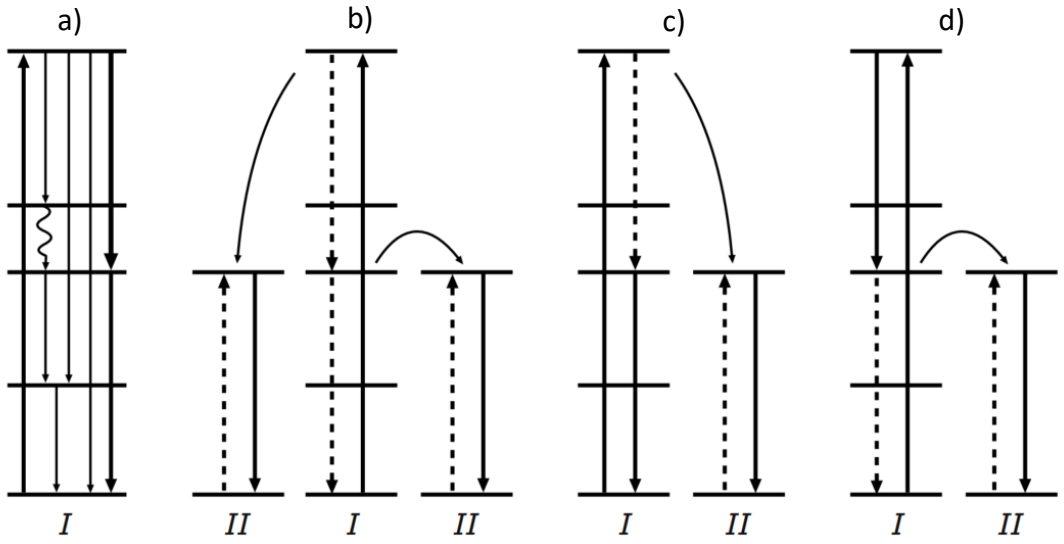

Figure 2.14. Schematic representation of several different down-conversion mechanisms. Solid vertical arrows indicate radiative transitions (Wegh et al., 1999).

Thus, this schematic d, describes the mechanism of the down-conversion of the LPP phosphors which has been proposed in this research project, to the fabricate the luminescent layers. The down-conversion process (illustrated above) occurs via the emission of a photon by ion I, followed by energy transfer to an ion of the species (II).

2.3.3 UP-Conversion (UC)

This mechanism is described as the absorption of two photons with lower energy, for example deep-red or IR, followed by the emission of one photon with higher energy in the visible spectra (Feldmann et al., 2003). According to Shalav “UC research has been dominated by applications requiring the UC of NIR to visible light and has also been restricted mainly to the UC of monochromatic light” (Shalav et al., 2005). One example of this would be that the dominant photovoltaic devices on the market are made of Silicon (Si) and only absorb NIR light

with energies greater than the band gap of 1.12 eV corresponding to wavelengths (λ) shorter than 1100 nm and could benefit from the UC of sub-band-gap NIR light (λ>1100nm) to visible/NIR light (λ<1100nm) (Shalav et al., 2005). Researchers have determined the upper limit of the photovoltaic conversion efficiency of a single junction PV device coupled to an ideal UC device is 47.6%, when considering the sun is modelled as a 6000 K blackbody and 50.7% under the standard air-mass, as AM1.5,(Trupke et al., 2002). The application of NaYF4:Er^{3+} phosphors applied as up-converting for enhanced near-infrared silicon PV devices is present in Figure 2.16 and described as follows: Energy relaxation from one Er^{3+} ion (the sensitizer) can result in energy transfer to a neighbouring Er^{3+} ion (activator) giving rise to higher energy photons. Solid lines represent photon absorption (up) and emission (down), dotted lines represent energy transfer, wavy lines represent phonon emission. For the two step process, photons with energies greater than the band gap of silicon are emitted. (Shalav et al., 2005).

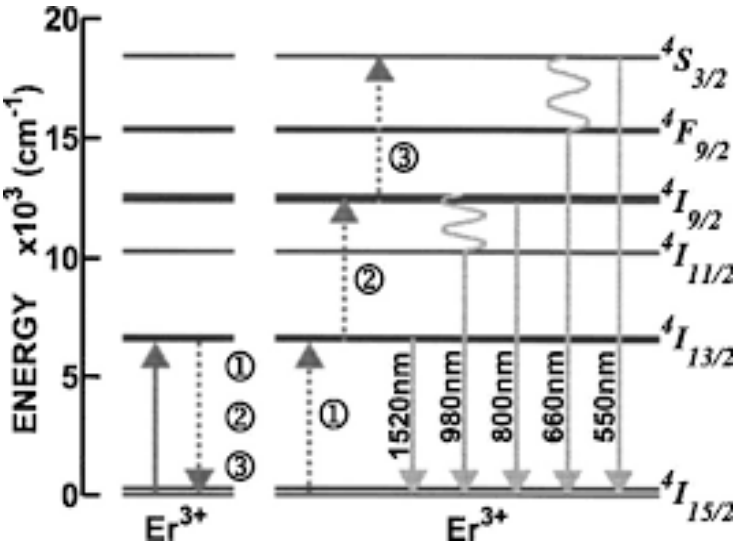

Figure 2.15. Three-step UC process between two erbium Er^{3+} ions (Shalav et al., 2005)

Thus, the down-conversion of the LPP phosphors was discussed and was proposed in this investigation to fabricate the luminescent layers, and subsequently attached on the top or at the rear of the selected PV devices. Based on these emerging fields and possibilities, this research focuses on applying the long persistent phosphors species, with potential to enhance the efficiency of PV devices. The researcher believes that adopting luminescent down-conversion mechanisms as a passive approach could improve the PV device performance. In

order to enhance this mechanism, an investigation into several types of LPP phosphors species were conducted to help identify the ideal LPP species to produce LDC layers for PV devices.

2.4 Luminescent Phenomena

2.4.1 Fundamental of Luminescence

Luminescent phenomena have been known since approximately the tenth century in China and Japan as well as since the end of the middle ages in Europe (Harvey, 1957). The Stone of Bologna ($BaSO_4$) as presented in Table 2.2 (Feldmann et al., 2003), was the first luminescent material that was found in nature in the early 16th century, which attracted Galilei's interest (Feldmann et al., 2003). In the 18th century the applications of these luminescent materials for devices including cathode-ray tubes, fluorescent lamps, and X-ray intensifying screens started. Today, luminescent materials are applied in a wide variety of applications, this includes displays such as TVs, smartphones, laptops, watches, computer monitors and sunbeds (Feldmann et al., 2003; Höppe, 2009).

Table 2.2. Early milestones in the discovery of luminescent material and devices (Feldmann et al., 2003).

Year	Kind of discovery	Excitation source	Type of luminescent material	Emission color
~1600	Stone of Bologna	sunlight	$BaSO_4$ (BaS)	yellow
1858	Geißler's tube	gas-discharge (Hg)		UV
1859	Becquerel	gas-discharge (Hg)	ZnS	yellow-white
1895	X-rays (by Röntgen)		none (photographic plate)	
1896	X-ray intensifier (by Pupin)	X-ray	$CaWO_4$	blue
1896	Fluorescent lamp (by Edison)	gas-discharge (Hg)	$CaWO_4$	blue
1897	Braun's tube	cathode-ray	$CaWO_4$	blue
1916	Neon discharge lamp (by Claude)	gas-discharge (Ne)	none	red
1925	Black-and-white television	cathode-ray	$ZnS:Ag^+$; $(Zn,Cd)S:Ag^+$	blue; yellow
1937	Neon discharge lamp (by Claude)	gas-discharge (Ne)	$CaWO_4$; $Zn_2SiO_4:Mn^{2+}$	blue; green
1938	Fluorescent lamp	gas-discharge (Hg)	$MgWO_4$; $(Zn,Be)_2SiO_4:Mn^{2+}$	blue-green; green-red
1941	Radar screen	cathode-ray	$(Zn,Cd)S:Cu^+,Al^{3+}$	green
1946	Insect lamps	gas-discharge (Hg)	$CaWO_4$	blue
1960	Color television	cathode-ray	$ZnS:Ag^+$; $(Zn,Cd)S:Cu^+,Al^{3+}$; $(Zn,Cd)S:Ag^+$	blue; green; red
1960	Laser (by Maiman)	gas-discharge (Hg)	$Al_2O_3:Cr^{3+}$	red
1972	Computed tomography (by Houndsfield)	X-ray	$NaI:Tl^+$	green
1972	Rare-earth phosphors	gas-discharge (Hg)	$Sr_3(PO_4)_5Cl:Eu^{3+}$; $LaPO_4:Ce^{3+},Tb^{3+}$; $Y_2O_3:Eu^{3+}$	blue; green; red

The Luminescence phenomenon is the emission of light from any substance, occurring from electronically excited states and can be divided into two phenomena: phosphorescence and

fluorescence (Lakowicz, 2011). Depending on the type of excitation sources, luminescence is broadly classified as: Photoluminescence, Cathodoluminescence, Electroluminescence, Chemiluminescence, and Triboluminescence as classified in the flowchart in Figure 2.16 (O'Hara et al., 2005).

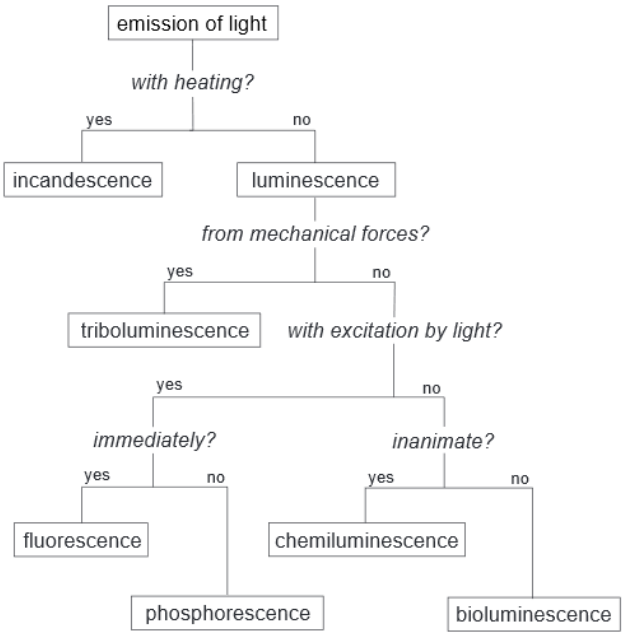

Figure 2.16. Possible luminescent fates for an atom or molecule after excitation source (O'Hara et al., 2005).

The luminescent mechanism showing the Energy Diagram was proposed by Professor Aleksander Jabłoński (shown in Figure 2.17), and includes the ground state (S_0), as well as first (S_1) and second (S_2) excited singlet energy states. Positioned to the right of the singlet states are the vibrational energy levels of the excited triplet (T_1) state, the so-called "forbidden transitions". The sequence of excitation and relaxation events dictated by the process are listed above. Once the electron arrives at an excited state vibrational energy level, it will slowly relax to the lowest vibrational level of the first excited state. From this level, the electron can behave as fluorescence or phosphorescence depending on the internal conversion (IC). Phosphorescence life times are usually longer than the life time of excited states and depend on the trap depth and trapping/de-trapping rates. Fluorescence, on the other hand, is based on the two-level electron transition mechanisms, a ground state and an excited state. The decay time of fluorescence depends on the transition strength between the two states.

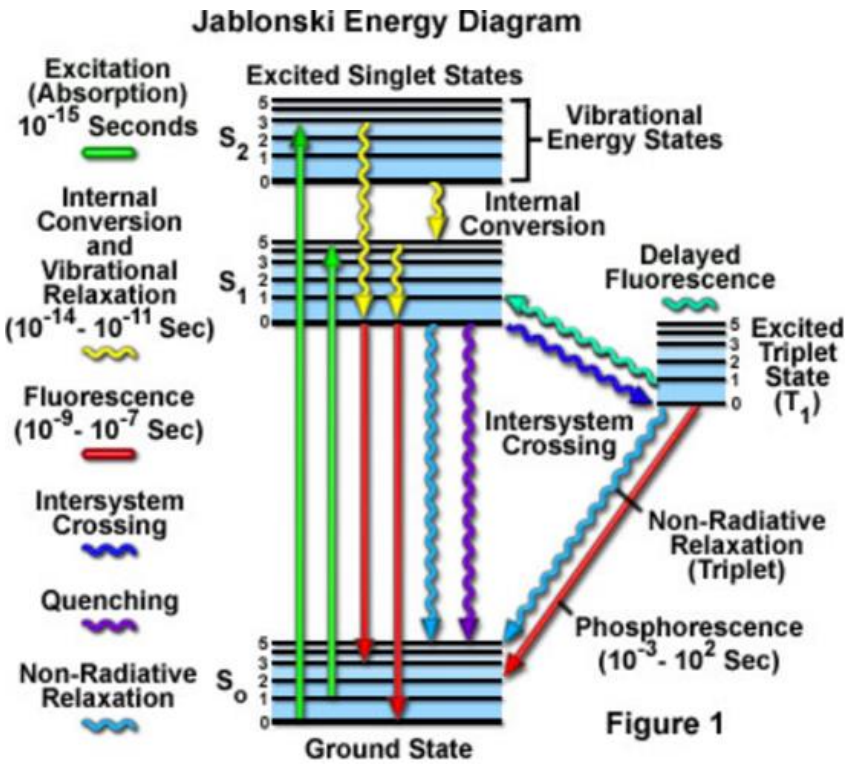

Figure 2.17. Jabłoński Diagram (Johnson and Davidson, 2012)

2.4.2 Phosphorescence Phenomena

The phenomena of phosphorescence was first discovered by the alchemist Henning Brand in 1669 (Goodman et al., 1983). The word Phosphorus (*Greek* Φωσφόρος Phōsphoros) comes from the Greek dictionary and means "bringer of light". In 1866 a French chemist Théodore Sidot, observed that ZnS crystals or compounds grown by a sublimation method exhibited phosphorescence. His compound is still used in a variety of visual applications (Bol et al., 2002). The main difference between phosphorescence and fluorescence is that the duration of the fluorophore stays in an excited state. The probability of a fluorescent transition is very high, and the average lifetime of the electron in the excited state is only 10^{-5}–10^{-8} second, whereas phosphorescence may have a lifetime from 10^{-4} second to hours (Valeur and Berberan-Santos, 2013). The phenomena of phosphorescence is also described as "If the molecules pass, between absorption and emission, through a stable or unstable intermediate state", there is phosphorescence (Valeur and Berberan-Santos, 2013). The emission of fluorescence takes place probably when the absorption of light raises a molecule from the ground state to one of the upper electronically excited states. It is considered that almost all complex molecules after

excitation rapidly drop back to the lowest vibrational level of the first excited state, and it is from here therefore that they return to the ground state. Since atoms return to their ground state by the fastest mechanism, fluorescence is only observed if it is a more efficient means of relaxation than the combination of internal conversion and vibrational relaxation. There is a quantitative expression for the analysis of the efficiency of fluorescence which is the fluorescent quantum yield, fΦ, which is the fraction of excited molecules returning to the ground state by fluorescence (Valeur and Berberan-Santos, 2013).

Phosphorescence can be classified according to its persistence: Very Short Persistent Phosphorescence (VSPP) has a lifetime of the same order of magnitude as the lifetime of the excited state, i.e. in the order of milliseconds, and it is associated with very shallow traps (Luitel, 2010). Short Persistent Phosphorescence (SPP) lasts for seconds and generally becomes noticeable to the human eye (Luitel, 2010). Most phosphors show short persistent phosphorescence after they are exposed to UV, visible light, plasma beam, electron beam or X-rays. Persistent Phosphorescence (PP) that lasts for minutes is due to the deep traps in the materials. Long Persistent Phosphorescence (LPP) or long afterglow lasts for tens of minutes or hours (Luitel, 2010).

LPP phosphors such as Strontium aluminate co-doped with divalent Europium trivalent dysprosium ions ($SrAl_2O_4$:Eu^{2+}, Dy^{3+}). The LPP was successfully produced by Matsuzawa et al., (1996), and it shows a green emission and demonstrated long persistence that can last for up to 15 hours under sunlight excitation. Figure 2.18 represents a simple luminescence diagram where, the exciting radiation is absorbed by the activator ion (A), raising it to the excited state (A*). The excited state either returns to the ground state by the emission of the radiation, called luminescence or non-radiative light, returns to the ground state by transferring energy to excite the vibrations of the host lattice, i.e. to heat the host lattice. For example, in the case of Ruby (Al_2O_3: Cr^{3+}); Al_2O_3 is a host and Cr^{3+} is an activator or luminescent centre. The excitation energy is absorbed by Cr^{3+} and excited to the (Cr^{3+})* transient state and it radiates to the red region of the spectrum producing a red colour in the dark (Luitel, 2010).

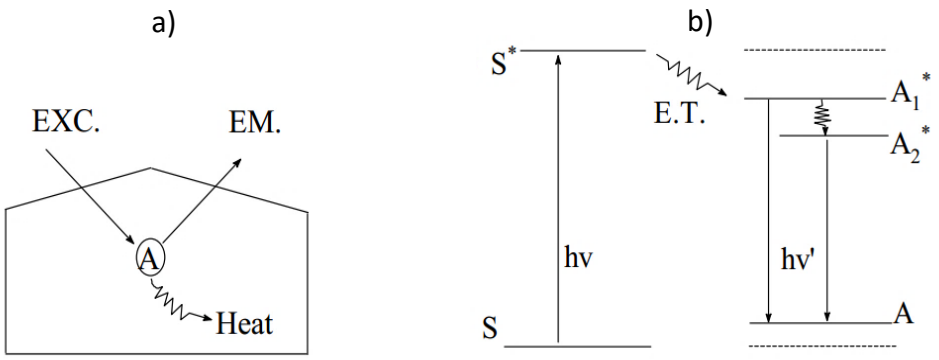

Figure 2.18. (a) Luminescent ion A in the host lattice, EXC: excitation, EM: emission, Heat: non radiative return to ground state and (b) Schematic energy level diagram of the luminescent ion A in the host lattice (Luitel, 2010).

The most prominent and selected example used as a reference in this research is the phosphor Strontium Aluminate co-doped with divalent Europium, and trivalent Dysprosium ions ($SrAl_2O_4$: Eu^{2+}, Dy^{3+}). This long persistent phosphorescence mechanism of the inorganic phosphors activated by rare earth ions is presented in Figure 2.19. It was proposed that in $SrAl_2O_4$: Eu^{2+}, Dy^{3+} phosphor, the UV excitation of Eu^{2+} cations from the ground state (4f7) to an excited state ($4f^6\ 5d^1$) (Eu^{2+} (4f7) + hv→Eu^{2+}* ($4f^6\ 5d^1$)), generates a hole in the f orbital in the vicinity of the valence band (VB). This transition is followed by an electron capture from the CB leading to the reduction Eu^{2+}* + e^- →Eu^+. Thus, the hole created in the VB migrates through it and gets captured by a Dy^{3+} cation located at a suitable depth to form a Dy^{4+} cation, Dy^{3+} + h + →Dy^{4+}. It is supposed that the return to the ground state of Eu^{2+} with light emission is triggered by the thermo-activated promotion of an electron from the VB to the first unoccupied levels of Dy^{4+}, followed by the migration of a trapped hole to a photo generated Eu^+ cation.

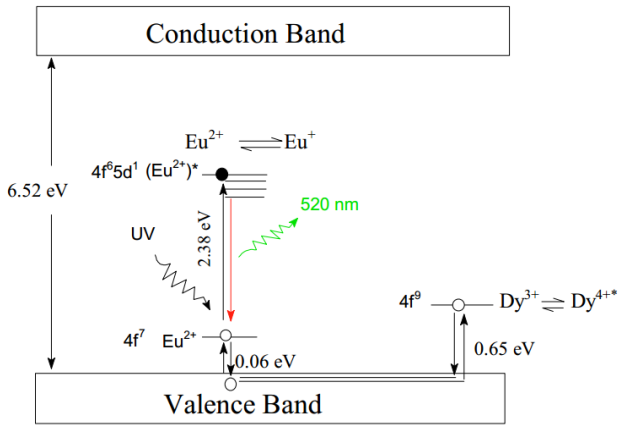

Figure 2.19. Energy level diagram of the SrAl2O4:Eu2+ phosphor and its co-doped derivatives showing energy traps in Matsuzawa's model (Luitel, 2010).

There are some factors that determine the emission wavelengths in different host lattices of the phosphors, hence the emission spectra (and excitation spectra) can be tuned to required specifications. In cases, where at least one of the electronic states is involved in the chemical bonding, the coupling to the lattice must be considered. This situation is encountered in many transition metal ions, for the s^2 ions, and for rare-earth ions showing d $\rightarrow$ f emission, as illustrated in Figure 2.7 for Eu^{2+}. Other rare-earth ions showing d$\rightarrow$ f emission are Ce^{3+}, Pr^{3+}, Nd^{3+} and Er^{3+}, albeit for the last three ions only in the UV. The energy difference between the d- and f-electrons is modified by the covalence of the Eu^{2+} ligand bond and the crystal field strength. An increase in the covalence of the Eu^{2+} ligand bond results in a lower energy difference of the 4f-5d energy separation. This elementary treatment considers the shift of the centre of gravity of the d-electron level, that is, if any splitting is not yet considered. The crystal field interaction splits the d-level, depending on symmetry and crystal field strength, e.g., for Eu^{2+}, emission and can be obtained by extending from the UV part of the optical spectrum to the red part (Ronda, 2007). Some other examples of long energy transfer are $CaAl_2O_4$: Ce^{3+}/Tb^{3+} and $CaAl_2O_4$:Ce^{3+}/Mn^{2+} where at least 10 hours of long persistent afterglow of Ce^{3+} has been successfully transferred to yield 10 hours of green Tb^{3+}, and yellow Mn^{2+} afterglow. Similarly, in $Sr_4Al_{14}O_{25}$: $Eu^{2+}/Dy^{3+}/Cr^{3+}$, the Eu^{2+} blue-green long persistent afterglow has been transferred into Cr^{3+} red afterglow (Luitel, 2010).

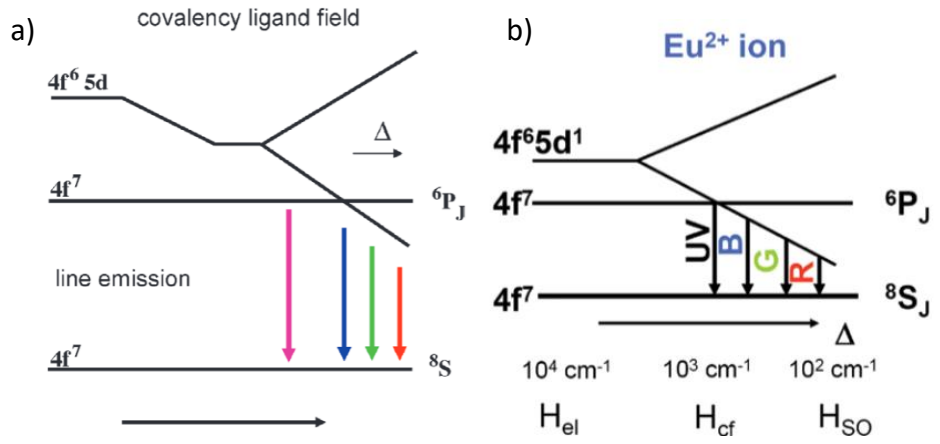

Figure 2.20. a) Energy separation of the 4f ^{7} and 4f ^{6} 5d ^{1} bands as a function of covalence and ligand field strength. The arrows indicate different emission colours. b) The effect of crystal field strength on the energy levels and emission colour of the Eu $^{2+}$ ion in a solid state (Luitel, 2010).

Both phosphors are easily accessible by choosing appropriate host lattices, and for this reason broad-band emitters can in general be tuned within a large spectral range and can be adapted to the application needs. Therefore, in the case of donor-acceptor pair luminescence, both the donors and the acceptors and the magnitude of the band gap strongly influence the spectral position of the emission colour to be obtained (Ronda, 2007).

Some researchers (e.g. Shanker et al., 2015) argue that long persistent phosphor results from intrinsic traps or intentionally induced traps or from both, which can be divided into two groups: electron traps that capture electrons below the conduction band and hole traps that capture holes above the valence band. Some traps appear as defects in the host material, F centres and V (vacancy) centres in crystals and are typical of these types of defects. These centres are usually generated by charge compensation requirements to maintain the neutrality of a host. An example of defect trapping centres occurs in $SrAl_2O_4:Eu^{2+}$ phosphor. Stoichiometric $SrAl_2O_4:Eu^{2+}$ phosphor does not evince any persistent afterglow. If Dy^{3+} is co-doped into $SrAl_2O_4$: Eu^{2+} phosphor, very long persistent afterglow is observed. The traps may be created also intrinsically through the introduction of specific dopants. Defect related traps are easy to produce in host materials that have complicated crystal structures. Ionic size difference can also produce traps by creating dislocation and other strain related defects. Another way of producing defects is through the non-stoichiometric composition host or the addition of some fluxes such as Boron Oxide (B_2O_3). In many co-doped trapping centres, with

the optical excitation, the dynamics of excited ions can be such as to create meta-stable states which properly belong to dopant ions in modified valance states, for example, $(Dy^{4+})^*$ in $SrAl_2O_4:Eu^{2+}/Dy^{3+}$ and $(Tm^{2+})^*$ in CaS: Eu^{2+}/Tm^{3+} phosphors. These meta-stable states can also act as trap centres since their electronic structures differ from those of normal dopant ions. The excited electrons or holes do not modify the bonding situation of the dopants, they are just represented by $(Dy^{4+})^*$ or $(T_m{}^{2+})^*$ where $(Dy^{4+})^* = Dy^{3+} + h +$ and $(Tm^{2+})^* = Tm^{3+} + e^-$. The electrons and holes are created in such a way that they are loosely bonded and can be easily detached thermally (Luitel, 2010).

Other researchers (Suriyamurthy and Panigrahi, 2008) argue that, the LPP luminescence occurs due to the thermally stimulated recombination of trapped charge carriers, which are created by UV or visible light irradiation. These carriers are trapped in the metastable traps. Due to the thermal energy available at room temperature these charge carriers are slowly released from the traps, subsequently releasing energy as they undergo recombination near a luminescence centre. The energy released is then transferred to a dopant ion e.g., Eu, which in turn gets excited and emits green light. The observed delay in LPP emission is due to the time that the trapped electrons spend in meta-stable states before returning to the luminescence centres.

Considering the different mechanisms of phosphorescent materials and their growth as presented in the literature, it is considered that the phosphorescence mechanism is still not fully established and there are still open questions concerning the theoretical aspects. For instance, the efficiency of phosphorescent materials is not yet well determined. Only in case of excitation with high-energy radiation (e.g., cathode rays), can the maximum energy efficiency be calculated precisely, using a surprisingly simple treatment. In contrast, loss processes can still not be predicted well in a quantitative manner (Feldmann et al., 2003).

2.4.3 Quantum Efficiency of Phosphors

Quantum Efficiency (QE) is an important parameter used to define the efficiency of phosphors material and consequently the phosphorescent application. The phosphorescent materials are configured at physical limits in terms of absorption of exciting radiation and the quantum efficiency with which phosphorescence is generated. Quantum efficiency is the number of photons generated divided by the number of photons absorbed (Ronda, 2008). The phosphorescence quantum efficiency (Φp) is determined in relation to the radiative rate constant (k_r) for phosphorescence and the non-radiative rate constant; (see equation 2.1 below).

$$\boldsymbol{Knr}: \Phi\mathrm{p} = \frac{\boldsymbol{k_r}}{(\boldsymbol{k_r} + \boldsymbol{k_{nr}})} \qquad \text{Equation 2.1}$$

Thus, high Φ_p can be attainable either by reducing k_{nr} or increasing k_r. For the case of k_{nr}, the well-known band gap (energy gap) law predicts that $\ln(k_{nr})$ is inversely proportional to the emission energy. This implies that higher Φp can be observed for higher energy phosphorescence. However, due to additional non-radiative transition processes, such as an energy transfer involving thermal activation, the Φp does not strictly obey the band gap law. k_r is strongly related to spin–orbit coupling in the excited states since k_r has a mathematical formalism including transition probability between singlet ground state and triplet excited state. In a widely recognized expression for this spin–orbit coupling effect, the perturbation theory is applied to draw a relationship that k_r is proportional to the square of the phosphorescence emission energy but inversely proportional to the energy difference between two perturbing excited states. Thus, in order to describe Φ_p, it is necessary to consider the nature of the ground state and involved excited states and the relevant photophysical interactions among them (You and Young Park, 2009).

It has been observed that the QE of phosphorescent materials has been receiving much attention in order to quantify and improve their quantum efficiency (Guanming et al., 2007; Höppe, 2009; Secula, 2010; Shanker et al., 2015; You and Young Park, 2009). Higher quantum efficiency has been reported along with phosphorescence optical characteristics such as being

capable of staying in an excited state and emitting visible light for many hours as reported in the literature (Guanming et al., 2007; Luitel, 2010; Matsuzawa et al., 1996; Wang et al., 2014). However, when applying these phosphorescent materials in host matrices such as polymers there are reports that it may change its properties, for instance, it has been observed that it has higher emissions than when applied in solution, this is because there are many deactivation processes that compete with emission, such as non-radiative decay and quenching processes (Lakowicz, 2011). Thus, in order to develop a luminescent layer, it is important to measure its optical properties as a final device, not only as bulk materials or LPP phosphors species.

Table 2.3 summarises the various LPP phosphor species reported in the literature, which are considered suitable luminescent candidates for this project's requirements. These requirements are: 1) a long persistent phosphorescence, 2) a wide absorption in the UV range, 3) emission in the visible range, 4) high luminescent quantum efficiency, and 5) long photostability which could last for many years to enhance the performance of the PV device technology. It must also be taken into consideration that many of these phosphorescent materials are alkaline doped Eu^{2+} earth aluminates and have been reported to have good chemical stability, high quantum yield, wide absorption spectra, and show the visible light spectra emissions with centred peaks and wide band gaps of approximately 6 eV (Dutczak, 2013). Accordingly, Luitel (2010) claims that long persistent phosphors appear to have a high quantum yield (QY) greater than 90% and a wide range of excitation. The table also indicates LPP phosphors which are available from chemical suppliers.

Table 2.3. The physical and optical properties of various reported phosphorescent materials.

Phosphors	Emission Peak (nm)	Colour	Absorption (nm)	Time Excitation (Min)	Quantum Yield (%)	Persistent Time /h	Availability	Reference
Sr4Al14O25:Eu2+, Dy3+	490	Blue-Green	250-450	20	+90	+20	yes	(Luitel, 2010) (Chang and Mao, 2004) (Georgobiani et al., 2009)
(Sr, Ca) MgSi2O7: Eu2+, Dy3+	490	Blue-Green	330	20	+80	+20	Yes	(Liu et al., 2005)(Luitel, 2010)
SrAl2O4:Eu2+, Dy3+	520	Green	200-450	5	90	+12	yes.	(Georgobiani et al., 2009, p. 2; Guanming et al., 2007; Liu et al., 2005; Matsuzawa et al., 1996; Shafia et al., 2014, p. 2)
CaAl2O4:Ce3+, Nd3+	420	Dark Blue	340	20	NA	+12	NA	(Luitel, 2010)
CaAl2O4:Tb3+, Ce3+	543	Green			NA	+10	NA	(Jia et al., 2002; Luitel, 2010)

Based on the presented literature of the LPP phosphors, it can be observed that these values reported in the table above cannot be verified as they were all synthesised and characterised in different conditions. Thus, without a standard test condition such as what was developed to measure the PV characteristics under standard test conditions (STC), these phosphors cannot be applied as a standard reference. Consequently, it will be important to investigate first of all, a method which is able to measure the Photoluminescent Quantum Yield, PLQY, of the LPP phosphors with high accuracy to determine its optical characteristics, before applying these materials to the PV device.

As a result, some LPP phosphor species were acquired from chemical suppliers for this characterization process and listed in Table 3.2. Furthermore, the ideal host materials for LPP phosphor needs to be investigated and used to disperse the LPP species or powders to fabricate the luminescent layers before carrying out the optical characterization process proposed.

2.5 Host Materials

This section provides an overview of the different types of optical materials widely used as host material. The important optical properties which make these materials suitable for optical application in PV devices such as polymers, will be discussed here. Polymers are substances made up of recurring structural units, each of which can be regarded as being derived from a specific compound called a monomer. The number of monomeric units usually is large and variable depending on the desired structure, considering that each polymer is characteristically a mixture of molecules with different molecular weights (Roberts and Caserio, 1977). The concept of polymers being mixtures of molecules with long chains of atoms connected to one another was proposed by H. Staudinger (Roberts and Caserio, 1977). Polymeric materials can exhibit high transparency in the visible region of the spectrum, adequate resistance to heat and humidity variations, and high mechanical strength (Klampaftis et al., 2009). Many types of organic and inorganic polymer are being used in optical systems such as lasers. Some of them can reach up to terahertz (THz; 100GHz - 10THz/ wavelengths 3mm - 30µm) transparencies with relatively low reflectivity. For example, Polymethylpentene (PMP) or TPX® and Polyethylene (PE) have uniform stable transmissions about 80-90%, starting from ~200 µm and reaching up to 1000µm, making them an alternative to inorganic materials such as silicon, crystal quartz, and sapphire (Tydex, 2016). Examples of the common types of polymers and their structures are shown in Table 2.4.

Polymethylpentene (TPX): This appears to be a good candidate for this application because it is one of the lightest of all known polymers. It is optically transparent in the UV, visible, and THz ranges. The index of refraction is ~1.46 and is relatively independent of wavelength. TPX has been observed to have excellent heat resistance and is highly resistant to most organic and inorganic commercial chemicals (Tydex, 2016).

Acrylics: Acrylic acid is the common name for 2-propenoic acid: CH_2=$CHCO_2H$. Acrylic fibers such as Orlon are made by polymerizing a derivative of acrylic acid known as acrylonitrile. One of the most important acrylic polymers is Poly Methyl MethAcrylate (PMMA) (Chemed, 2004). Some acrylic acids have high transmittance because there is no free electron. PMMA plastics

or PMMAs have similar transmission profiles, admitting light from 250 nm through 700nm, as can be seen in Figure 2.21.

Table 2.4. Host Materials (Chemed, 2004)

Structure	Chemical Name	Trade name or Common Name
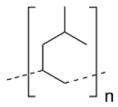	Poly(4-methyl-1-pentene)	PMP/TPX
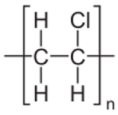	Poly vinyl chloride	PVC
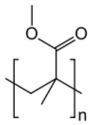	Poly(methyl methacrylate)	Acrylic/PMMA/Plexiglas/Lucite
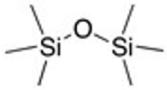	Polysiloxanes	Silicone/ Solaris Silicone

Polysiloxanes (Solaris Silicon/silicone): Unlike most other polymers Polysiloxanes are the most prominent class of inorganic silicon-containing polymers, and have gained much interest within the last decades due to their interesting chemical and physical properties (Rieger et al., 2016). This product is also called silicone and is based on siloxane Si-O linkage found in glass and quartz, and it is an immensely versatile material used in numerous applications (Richard, G. Jones, 1995; Zeigler and Fearon, 1990). Polysiloxane is thus undeniably an ideal type of host material for PV device applications, considering its general properties. It has been described as having an ultra-transparent property, which allows maximum transmission of light, and low viscosity which allows easy flow in and around complex shapes. The hydrolytic stability and refractive index is 1.41 nm (Smooth-on, 2015). Another important characteristic of this material is its flexibility, it is possible to shape the fabricated layers in so many different ways without damaging it. It has been used for this research and further information can be found in Appendix A.

The materials with desirable physical and optical characteristics such as high transmission, which are shown in Figure 2.21, could be used as host matrices for the fabrication of a luminescent device. The graph shows the transmittance, measured in percentage, from various transparent materials from 200-700nm, that can be used as a host material. As can be observed from this graph, quartz glass has a transmittance above 90% across all spectral ranges, and the others reach 90% in the visible range only. As the phosphorescence material absorbs mostly in the UV spectral range by using a host material with a low transmittance in UV, this material could reduce the amount of light that reaches the layer.

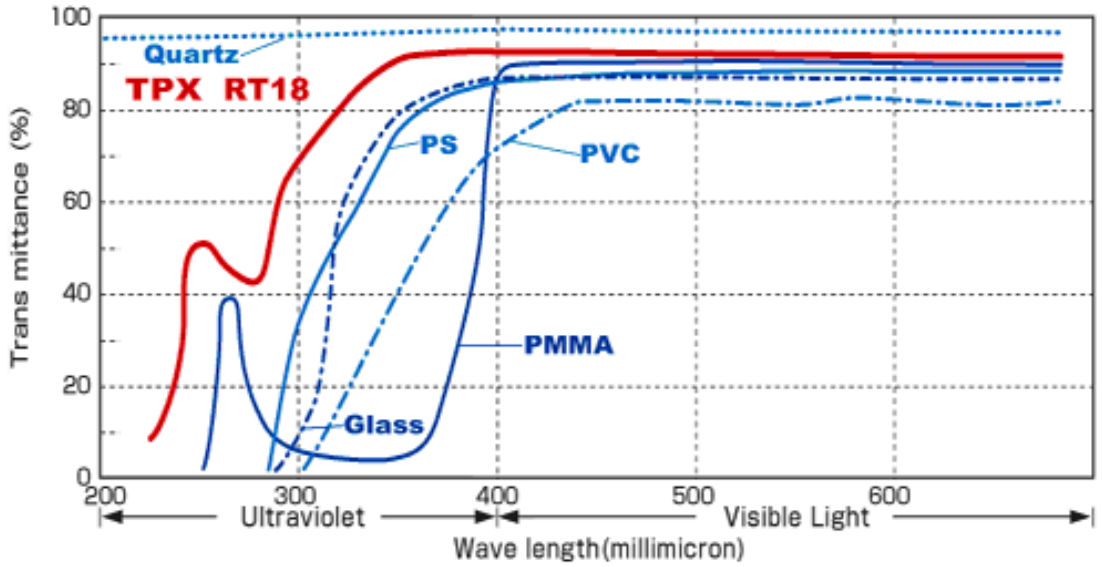

Figure 2.21. Transparent Polymers which have light transmission properties in the UV range. Source: ("TPX® Characteristics - Polymers - Research Materials - Goodfellow," n.d.)

However, by applying an ultra-high transmittance material such as quartz glass and flexible host material properties as are present in Polysiloxane, this could be a major advance in terms of phosphorescent layer fabrication and application because it will help to maintain the phosphorescence integrity of the phosphor species. For a successful application of rare-earth ions phosphorescent species, it is important to identify a highly transparent polymer in the UV range to allow the phosphorescent species to absorb the ultraviolet light and emit it in the visible range; in order to better to improve the performance of the PV device. By doing that, two important facts need to be considered which are the mechanical degradation and chemical stability. Deteriorative reactions can occur during processing or application, when polymers are subjected to heat, oxygen, or mechanical stress. However, Solaris silicon is

considered to be a new type of polymer technology which has been developed for inorganic use, with optimized degradation processes, including the improvement of the curing process.

This research project has identified some polymer materials (such as Polysiloxane silicon), which have the potential to become commercially viable and provide an energy efficient conversion for many PV device applications. A major advantage of using this polymer matrix is that the characterization process of the luminescent layer can be done before it is applied to the PV device, and it can also be used in many applications to test the PV device performance.

In order to assess the workability of the Polysiloxanes Solaris silicon, preliminary experiments will be undertaken to verify the total transmittance of this product, as it is not available in the literature. Thus, at the moment, there are no transmittance spectra for Solaris Silicon to carry out the comparison with the above Figure 2.21. In order to take account of the results of the study and to carry out a detailed evaluation of the transmittance of Solaris silicon, a fabricated layer is required. The experimental sections will present and discuss the findings of this evaluation, which will enable us to judge whether or not this polymer is a suitable candidate for LDC.

2.6 Conclusion

In this chapter, various types of PV device technologies and luminescent mechanisms used to enhance the PV devices performance, have been described. The literature review on PV devices performance and the possible opportunities for improvement, have been presented. The selection of three different types of PV technologies for further investigation was made, namely, a silicon-based a-Si, a Dye-Sensitized Solar Cell (DSSC) and a Perovskite PV device. Thus, the aim of this research is to investigate the potential of Long Persistent Phosphor (LPP) materials applied as a luminescent down-conversion to improve the PV device performance under light and dark conditions.

A significant amount of research has been conducted in the field of Photovoltaic technology devices which helps to define new innovation by understanding the fundamentals involved

(NREl, 2016). However, significantly less research has been carried out in the field of phosphorescent and luminescent integrated PV devices, which is a passive and purely optical approach that can provide a solution for the enhancement of the poor spectral response of the PV. There are many types of losses for PV device materials, such as the sub band-gap (Eph<Eg) photons, which are energy photons that are not absorbed by PV material and higher energy (Eph - Eg) photons, (they can also cause heating and degradation of the PV device).

The PV devices still need improvements and one solution is by applying a passive approach such as down converter. This has the features which can overcome some of the losses, and improve the poor spectral response surrounding UV and visible range where it's low, to the wavelengths where the PV devices exhibit a better response. This approach can be applied without changing the electronic interference of the PV device, and can be optimised by process application or materials. The Luminescent Down-converter (LDC) materials may be divided into two major classifications: host and luminescent materials.

This research project aims to investigate the main materials for the application in the Luminescent Down-Conversion (LDC) layers by applying a range of rare-earth-doped inorganic phosphorescent species as luminescent material and a host material to disperse the luminescent materials. The selection of rare-earth-doped inorganic phosphorescent species as luminescent material goes even beyond the LDC application requirements which are: good luminescent quantum efficiency (LQE), high absorbance coefficients, excellent chemical and thermal stability, photostability and long emission lifetime. The selection of the Polysiloxanes as a host material for this kind of application have not yet been published.

Initial test results of this silicon material have shown great potential and it could fulfil almost all the required specifications for this application such as high-transmittance, low absorbance coefficient, low scattering, UV-resistance, exhibited prolonged photostability, and easy to process. The decision to use these selected materials is motivated by the usage of new, improved and emerging materials that have been produced over the last few decades, which show new possibilities for luminescent applications due to a wide range of properties which can benefit the PV devices, thus enhancing their efficiency.

CHAPTER 3

MATERIALS AND EXPERIMENTAL METHODS

3.1 Introduction

Descriptions of the materials and experimental methods investigated during this research project are presented in this chapter.

- Optical spectroscopy techniques: Analysis of the transmission, reflectance, scatter, absorbance and absorption of various chemical materials, which involve the use of UV/Vis/NIR of the investigated materials.
- The Spectrofluorometer techniques used to investigate the emission, excitation, and phosphorescent lifetime.
- A new method to measure the photoluminescent quantum yield, LPQY, of long persistent phosphors, LPP, dispersed in a host matrix is proposed.
- The Confocal Microscope used to measure the thickness and 3D mapping of the inside and outside of the luminescent layer is presented.
- Fourier Transform-Infrared Spectroscopy (FTIR) analytical technique was used to obtain an infrared spectrum of the host material.
- Differential scanning calorimetry (DSC) and Thermogravimetric analysis (TGA) technique.
- Electrical characterisation of the PV devices: under standard test conductions and under dark conditions.

3.2 Materials and Characteristics

Table 3.1. presents the materials that were used in this research project, along with their relevant physical and chemical properties and their specific use in this work.

Materials	Properties	Application	Supplier
Fluorescein ($C_{20}H_{12}O_5$)	Composition Dye content, 95%, mp 320 °C. absorption λmax 496 nm	Employed as quantum yield standard, Chapter 3.	Sigma-Aldrich
Aluminium Oxide (Al_2O_3)	Form powder mfr. no. CAMAG 507-C-I impurities <0.03% Fe2O3 <0.03% SiO2 <0.4% Na2O particle size 50-300 mesh pore size 58 Å pore size surface area, 155 m2/g pH, 7.0±0.5 (in H2O) mp 2040 °C, Anion traces chloride (Cl-): ≤0.03 (mval/g)	Materials used for the synthesis of the phosphorescent phosphors: SrAl2O4: Eu+2; Dy3+ (Strontium Aluminate, Dysprosium and Europium Doped), used in the application-Chapter 4.	Sigma-Aldrich,
Boron Trioxide (B_2O_3)	Assay 99.98% trace metals basis, mp 450 °C, density 2.46 g/mL at 25 °C.		
Europium (III) Oxide (Eu_2O_3), 99.99%	Assay 99.99% trace metals basis, form powder, density 7.42 g/mL at 25 °C.		
Strontium Carbonate ($SrCO_3$), 99.9+% Metals Basis	Melting point: 1497°C, Density 3.7 g/mL at 25 °C, Form Powder, Specific Gravity 3.7, colour white, Stability: Stable		
Dysprosium (III) Oxide (Dy_2O_3), 99.99+%.	Assay ≥99.99% trace metals basis, form powder, density 7.81 g/mL at 25 °C.		
Ethanol	Linear Formula CH3CH2OH Molecular Weight 46.07		
Crystic 2446 Polyester Resin	Viscosity at 25°C (Rhéomat 37,35 sec-1) Specific gravity 1.1 Volatile content Aspect Blue thixo Stability in dark at 20°C 3 moths "Gel time at 25°C with 100 parts of min 14-17 Resin and 2 parts Catalyst M"	Materials used for fabrication of host materials and luminescent application-Chapter 5.	Glassfibre & Resin
Synolite 0328-A-1 Resin	Viscosity, 23°C 360 - 620 mPa.s 2013 Colour, APHA max. 70 - 2017 Solids content, IR 61.5 - 64.5 % 2033 Refractive index, 23°C 1.545 - 1.547 - 2150 Appearance clear - 2265 Colour blue - Water content Max. 1000 ppm 2350 Acid value, as such 12 - 18 mg KOH/g 2401 Gel time from 25 to 35°C 19 - 23 minutes 2625 Cure time from 25°C to peak 42 - 57 minutes 2625 Peak temperature 40 - 50 °C 2625		Glassfibre & Resin
Crystal Clear-202	Mix Ratio; 100A:90B by weight Mixed Viscosity, cps; 600 (ASTM D-2393) Specific Gravity, g/cc; 1.036 (ASTM D-1475) Specific Volume, cu. in./lb.; 26.7 (ASTM D-1475) Colour; Clear Shore D Hardness; 80 (ASTM D-2240) Heat Deflection Temp; 120°F/50°C (ASTM D-648)		Smooth-On

Polysiloxane/ Solaris Silicon	Mix Ratio by Volume 1A:1B Mix Ratio by Weight 1A:1B Specific Gravity 0.99 g/cc Specific Volume 28.1 cu. in./lb. Pot Life 240 minutes Cure Time 24 hours Colour Clear Shore Hardness 15 A Tensile Strength 180 psi 100% Modulus 25 psi Elongation @ Break 290 % Shrinkage <.001 in. / in. Useful Temperature (min) -149 °F Useful Temperature (max) 400 °F Dielectric Strength 366 volts/mil Dielectric Constant, 100Hz 2.78 Dissipation Factor, 100Hz 0.00 Volume Resistivity 3.16E+15 ohm/cm Thermal Conductivity 0.18 W/M*K Refractive Index 1.41 nm Mixed Viscosity 1,200 cps		Smooth-On
LED Broadcom HLMP-D150	LED Colour Red, Package Type 5mm (T-1 3/4) Mounting Type Through Hole, Forward Voltage 1.6 V Luminous Intensity 3 mcd Number of Pins 2 Viewing Angle 65 ° Lens Shape Round, Dominant Wavelength 637 nm, Dimensions 5 x 9.19mm, LED Material AlGaAs Lens Colour Red	Used for Afterglow measurement and application, Chapter 8	RS Radionics
Electrolytic Capacitor	Chang Saim 47uF 10V 105°C Electrolytic Radial Capacitor		RS Radionics

Table 3.2. Summarized phosphor species, used in the fabrication of the luminescent layers. The phosphor species were assigned with a sample identification, ID, which will be used in the presentation of results.

Supply	Samples (ID)	Empirical Formula (Hill Notation)	Molecular Weight (g/mol)	Particle size	Fluorescence	Supplier
Sigma-Aldrich (PN-756547) (long persistent blue phosphor)	Ph1	$Sr_{2.90}Eu_{0.03}Dy_{0.07}Al_4SiO_{11}$ (Strontium silicate aluminate, Europium and Dysprosium doped)	582.04	300 mesh	λ_{em} Blue (UV excitation source)	Sigma-Aldrich
Sigma-Aldrich (PN-756520) (long persistent blue-green phosphor)	Ph2	$Sr_{3.84}Eu_{0.06}Dy_{0.10}Al_{14}O_{25}$ (Strontium aluminate, Europium and Dysprosium doped)	1139.55	~180 mesh	λ_{em} Blue-Green	Sigma-Aldrich
Sigma-Aldrich (PN-756539) (Green)	Ph3	$Sr_{0.95}Eu_{0.02}Dy_{0.03}Al_2O_4$ (Strontium aluminate, europium and dysprosium doped)	209.11	230 mesh	λ_{em} Green	Sigma-Aldrich
ZhongbanChem (PN-DYY-6C) (Orange)	Ph4	$SrAl_2O_4$, Eu^{2+}, Dy^3	NA	5~65µm	λ_{em} Orange	Dalian Zhongbang Chemical Industry
ZhongbanChem (PN-DPY-6C) (Salman)	Ph5	$SrAl_2O_4$, Eu^{2+}, Dy^3	NA	5~65µm	λ_{em} Salmon	Dalian Zhongbang Chemical Industry
ZhongbanChem (PN-TPY-6C) (Yellow)	Ph6	$SrAl_2O_4$, Eu^{2+}, Dy^3	NA	45~65µm	λ_{em} Yellow	Dalian Zhongbang Chemical Industry
NIMS β-SiALON Green (Standard Green) *	PhNIMS-G (Reference)	$Si_{3\sim5.99}Al_{0.01\sim3}O_{0.01\sim3}N_{5\sim7.99}$: $Eu_{0.001\sim}$ 0.1	NA	21µm	λ_{em} Green	Yuji LED / NIMS
NIMS α-SiALON orange (Standard Orange) *	PhNIMS-O (Reference)	$Ca_{0.25\sim}2Si_{0.01\sim}11.49Al_{0.51\sim}11.99O_{0.01\sim}11.49N_{4.51}$:$Eu_{0.001\sim}$0.1	NA	14µm	λ_{em} Orange	Yuji LED / NIMS
NIMS-NSR CASN-Red (Standard Red) *	PhNIMS-R (Reference)	$Ca_{0.8\sim}1.2Al_{0.8\sim}1.2Si_{0.8\sim}1.2N_{2.4\sim}3.6$:$Eu_{0.001\sim}$0.15	NA	17µm	λ_{em} Red	Yuji LED / NIMS

* Some additional properties are provided (see Table 3.3 and Stability details, Appendix B).

Table 3.3. Optical properties of the standard reference phosphors from Japan's National Institute for Materials Science (NIMS).

		Excitation wavelength	
NIMS sample	**Measurements**	**405nm**	**455nm**
NIMS β-SiALON Green (Standard Green)	Absorption /%	76	65
	Internal Quantum Efficiency /%	82 ± 3	83 ± 3
	External Quantum Efficiency /%	62	54
NIMS α-SiALON orange (Standard Orange)	Absorption /%	81	77
	Internal Quantum Efficiency /%	79 ± 3	79 ± 3
	External Quantum Efficiency /%	64	61
NIMS-NSR CASN-Red (Standard Red)	Absorption /%	80	77
	Internal Quantum Efficiency /%	90 ± 3	92 ± 3
	External Quantum Efficiency /%	72	71

3.3 Characterization Techniques

The characterization techniques described in this chapter, were used in the experimental sections to characterize the materials that were applied throughout this research project. This section will discuss the most used standard techniques. It then explores the new method developed to characterise the PLQY of the fabricated layers.

3.3.1 Spectroscopic Characterisation

The steady state spectroscopic techniques were carried out with the UV/Vis/NIR Spectrophotometer throughout this study, to characterise the optical properties of the materials used thought this research. Two different instruments were used, one for solids and one for liquids.

3.3.1.1 UV/Vis/NIR Spectrophotometry Solids

The Spectrophotometer Perkin Elmer Lambda 650, UV/Vis/NIR with integrating sphere 150 mm, (see Figure 3.1) was used. This spectrophotometer covers a wide range of wavelengths from 190 to 900nm in the UV/Vis/NIR region, with resolution ≤0.17nm and stray light at 220nm

≤0.0001 %T. With the aid of this instrument it was possible to measure transmittance, reflectance and light scatter of the solid sample at room temperature.

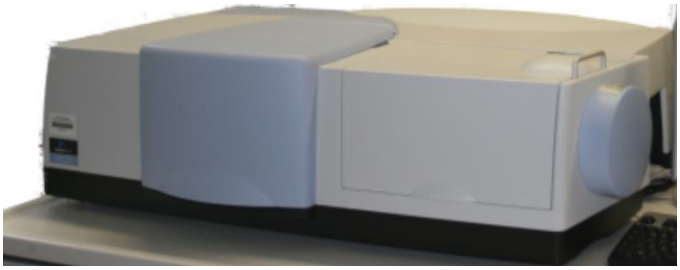

Figure 3.1. The Perkin Elmer Lambda 650, UV/Vis/NIR spectrophotometer with integrating sphere 150 mm, Trinity College Dublin.

A schematic diagram of the Perkin Elmer Lambda 650, UV/Vis/NIR spectrophotometer with integrating sphere 150 mm, is shown in Figure 3.2. A broadband UV/Vis/NIR light source is passed through a double grating monochromator. This results in a narrow band radiation which is divided by the beam-splitter into a Reference beam and a Sample beam. The beams travel through the sample in the transmittance port, and the integrating sphere collects all the light which has passed through the samples. This process allows the spectrophotometer to measure the amount of light transmitted by the sample relative to that transmitted by the reference sample. Depending on the measurement required, the samples can be placed in different ports with the sample holder, as shown in the pictures.

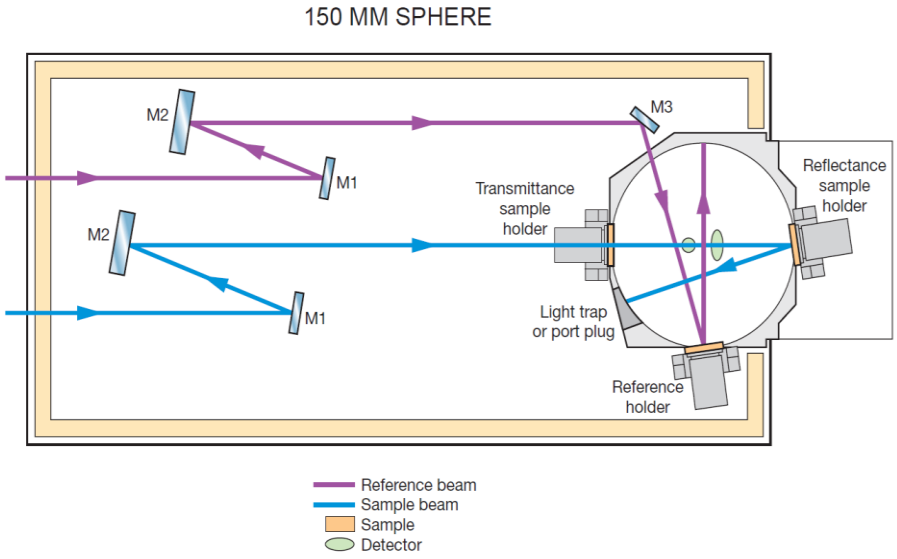

Figure 3.2. Schematic of a Perkin Elmer Lambda 650, UV/Vis/NIR spectrophotometer with an integrating sphere of 150 mm, (Application and Use of Integration Sphere, Perkin Elmer, 2004).

The two most used ports for the measurements were the Transmission and Reflectance ports. The sample is placed in the transmittance port of the sphere if transmittance is being measured, and behind it if reflectance is being measured. The sphere's internal surface is coated with a spectral polymer, which offers levels of diffuse reflectance approaching 100%. The sample is placed against the sphere, and the beam transmitted or reflected by the sample, is reflected onto the internal reflective surface of the sphere before reaching the detectors inside the sphere, as explained in Figure 3.3.

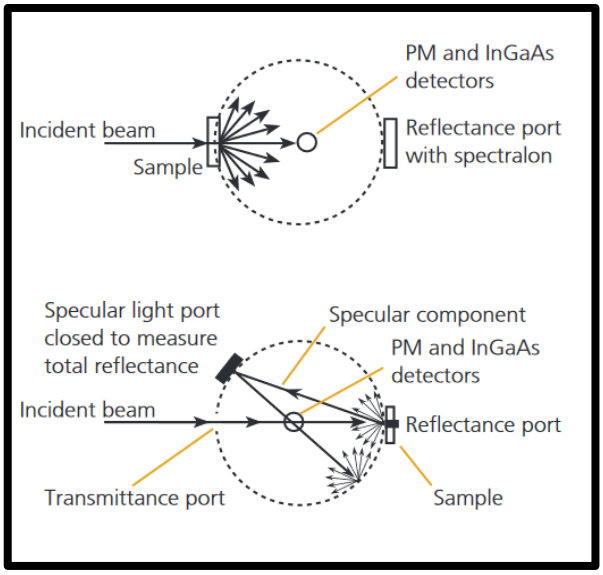

Figure 3.3. Diagrams of an integrating sphere: Transmission (top), Reflexion (bottom). Source: (Catherine Tams and Enjalbert, 2009).

The solid samples such as the phosphorescent species, host matrix, and luminescent layers, have various optical phenomena involved such as transmittance, reflectance, scattering, diffusion and absorptance, Figure 3.4. The total transmittance (i.e. direct transmittance plus diffuse transmittance, including any deviation of the beam), can only be measured using this integrating sphere.

To measure the reflectance, there are two kinds of reflectance considered for these fabricated layers; Specular and Diffuse. Specular reflectance refers to the part of the incident beam reflected at the same angle as the angle of incidence. Diffuse or scattered reflectance refers to the part of the incident beam reflected in all directions; apart from the host material or blank layers, the luminescent layers are concentrated with phosphorescent species that produce the

diffuse reflectance. Specular reflectance was important in verifying whether the layers can be used as reflectors at the rear of the PV devices.

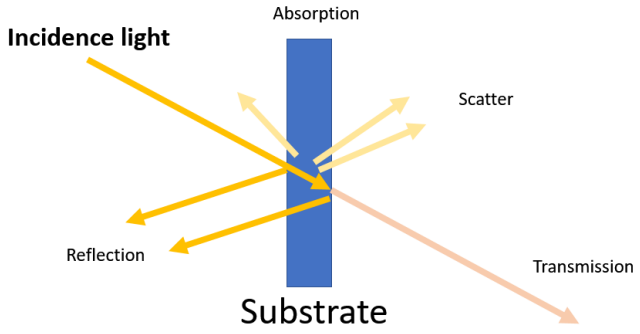

Figure 3.4. Interactions of light with a solid.

These measurements were used to calculate the absorption for luminescent layers as a percentage of the incident beam absorbed by the layers (i.e. that part of the beam which is neither reflected nor transmitted), and they were calculated from the measurements taken for reflectance and transmittance, using Equation 3.1.

Accordingly, the term absorptance differs from absorbance, as it takes into consideration the reflectance or index of refraction, as expressed by the absorptance equation:

$$I_o = I_R + I_T + I_A \qquad \text{Equation 3.1}$$

where the irradiance initial (I_0) = the reflected irradiance (I_R) + transmitted irradiance (I_T) + Irradiance absorbed (I_A). The energy conservation law is given by dividing the equation by I_0, resulting in T + R + A = 1, Transmission + Reflectance + Absorptance = 1.

3.3.1.2 UV/Vis/NIR Spectrophotometry Liquids

For the measurements of liquid samples, the Lambda 35 UV/VIS Spectrophotometer from PerkinElmer was used, (see Figure 3.5), which has variable bandwidths (Range: 190 nm - 1100 nm and Bandwidth: 0.5 nm - 4nm). The absorbance spectroscopy is the analytical technique based on measuring the amount of light absorbed by a sample at a given wavelength. Spectrophotometry, particularly in the visible and UV portions of the electromagnetic

spectrum, is one of the most versatile and widely used techniques in chemistry. The wavelength region generally used is from 200 to about 1000nm, and the absorbing medium is at room temperature.

Figure 3.5. Perkin Elmer UV-VIS Lambda 35- Trinity College Dublin.

The Beer-Lambert-Bouguer law, generally called the Beer-Lambert law, may be written for a single absorber in solution, and it is the linear relationship between absorbance and the concentration of an absorbing species. Using a clear liquid sample, a standard spectroscope measures direct transmittance as a percentage (%T); this represents the percentage of the incident beam of light transmitted by the sample (Swinehart, 1962). Experimental measurements are usually made in terms of transmittance (T), which is defined as:

The transmittance (T) measured is that which is the ratio between the reference (incident) and sample (transmitted) light as follows:

$$T = \frac{I}{I_o} \qquad \text{Equation 3.2}$$

Where **I** is the light intensity after it passes through the sample, and I_0 is the initial light intensity. The absorbance is the amount of radiation absorbed by a material and it can be calculated from the percentage transmittance (%T) data using the following equation:

$$A = 2 - \log_{10} \%T \qquad \text{Equation 3.3}$$

The relationship between absorbance and transmission can be explained as following; if all the light passes through a material without any absorbance, then absorbance is zero, and percent

transmittance is 100%. If all the light is absorbed, then percent transmittance is zero, and absorbance is infinite. Absorbance is widely used to measure the concentration in liquid solutions in accordance with the Beer-Lambert law using a standard spectroscope measuring direct transmittance as a percentage (%T) (Catherine Tams and Enjalbert, 2009).

A schematic diagram of the Perkin Elmer UV-VIS Lambda 35 is shown in Figure 3.6. The Lambda 35 UV/Vis Spectrometer features an all-reflecting optical system. The monochromator is a holographic concave grating with 1053 lines/mm in the center. Two radiation sources, a deuterium lamp and a halogen lamp, cover the working wavelength range of the spectrometer.

For operation in the visible (Vis) range, mirror M1 reflects the radiation from the halogen lamp onto source mirror M2. At the same time M1 blocks the radiation from the deuterium lamp. For operation in the ultraviolet (UV) range, mirror M1 is raised to permit radiation from the deuterium lamp to strike source mirror M2. Source change is automatic during monochromator slewing. Radiation from the source lamp is reflected from source mirror M2 through an optical filter on the filter wheel assembly. A stepping motor drives the filter wheel to create synchronization with the monochromator. Depending on the wavelength being produced, the appropriate optical filter is located in the beam path to prefilter the radiation before it enters the monochromator. Filter change is automatic during monochromator slewing. From the optical filter, the radiation passes through the entrance slit (Slit 1) of the monochromator. The radiation is dispersed at the grating to produce a spectrum. The rotational position of the grating effectively selects a segment of the spectrum, reflecting this segment through the exit slit (Slit 2) to mirror M3. The exit slit restricts the spectrum segment to a near-monochromatic radiation beam. From mirror M3, the radiation is reflected onto a beam splitter which allows 50% of the radiation to pass onto plane mirror M4, which reflects 50% of the radiation onto plane mirror M5. Mirror M4 focuses the radiation beam in the sample cell. The beam then passes through a convex lens onto the photodiode detector. Mirror M5 focuses the radiation beam in the reference cell. The beam then passes through a convex lens onto the photodiode detector (Perkin Elmer Lambda 25.35,45 User's Guide)

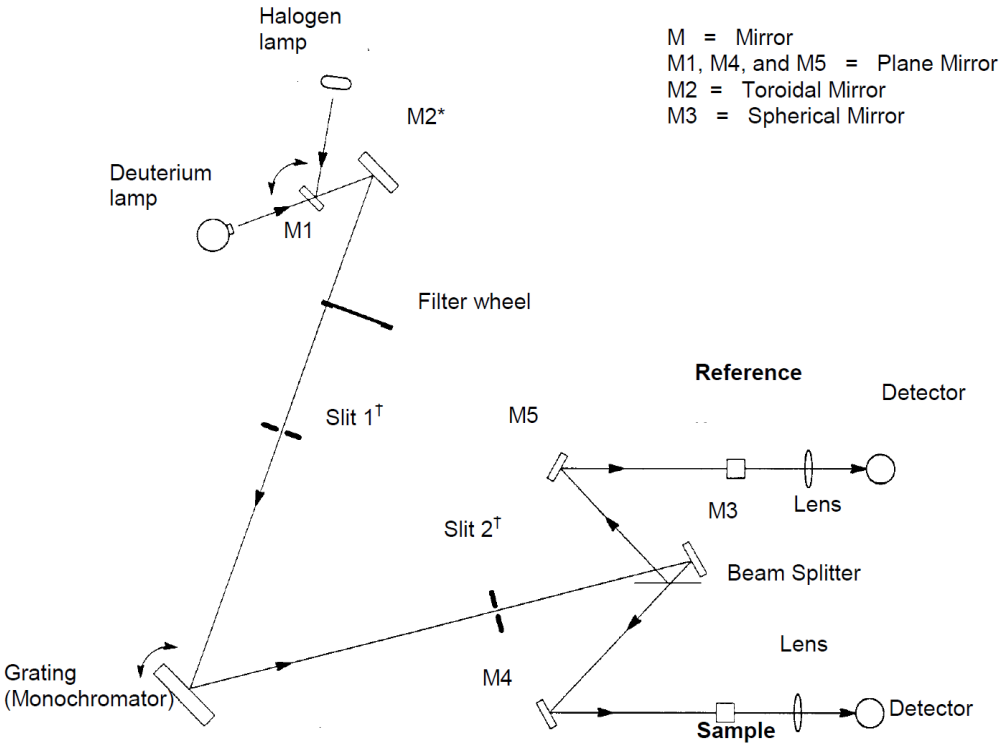

Figure 3.6. Schematic of Perkin Elmer UV-VIS Lambda 35 (Lambda 25, 35, 45, User's Guide, Perkin Elmer, 2000).

3.3.2 Spectrofluorometric Characterization

The measurements of the emission, excitation, phosphorescent lifetime decay and photoluminescent quantum efficiency of the luminescent materials were carried out with the spectrofluorometer. The mainly used instrument was a Horiba FluoroMax-4 (shown in Figure 3.7). In addition, a more updated and calibrated version of this instrument was used, Horiba spectrofluorometer FluoroMax +, combined with a new model integrating sphere to develop a new method to measure the PLQY of the luminescent layers at Horiba scientific, Edison- USA.

This instrument is composed of the following configuration: A 150-W xenon, continuous output, ozone-free lamp. Optics were all-reflective, in order to focus at all wavelengths and to provide a precise imaging for microsamples with dispersion of 4.25mm^{-1}. The Monochromator has a Single-grating excitation and emission spectrometers (standard). Monochromators are of f/3.5 Czerny-Turner design with classically-ruled gratings and all-reflective optics, using 1200- grooves/mm gratings: resolution 0.3 nm, maximum scan speed 80 nm, s^{-1} Accuracy ±0.5

nm, step size 0.0625–100 nm, and the scan measurement range from 0 to 950nm. The excitation has an optical range from 220 to 600 nm. The emission optical range is from 290 to 850 nm. The detector is a calibrated photodiode with excitation reference correction from 200 to 980nm. The emission detector is an R928P for high sensitivity in photon counting mode (200 to 850 nm). High voltage = 950 V, linearity to 2 × 106 counts s^{-1}, <1000 dark counts s^{-1}.

Phosphorimeter has the following components; a light source, and a UV xenon flash tube. The flash rate is 0.05–25Hz. The lifetime range is down to 10µs. The flash duration is 3µs at full-width half-maximum. The Low-intensity tail extends >30µs. The Delay after flash 50µs to 10s, in increments of 1µs. The number of Flashes per data point 1–999. The Sample window 10µs to 10s, in increments of 1µs.

This instrument also has a Time-Correlated Single-Photon Counting (TCSPC) function with the following components; a light source, interchangeable Nanoblend's, peak wavelengths between 265 nm–785 nm, a lifetime range from 200ps to 0.1ms, and a minimum resolution of 55ps/channel.

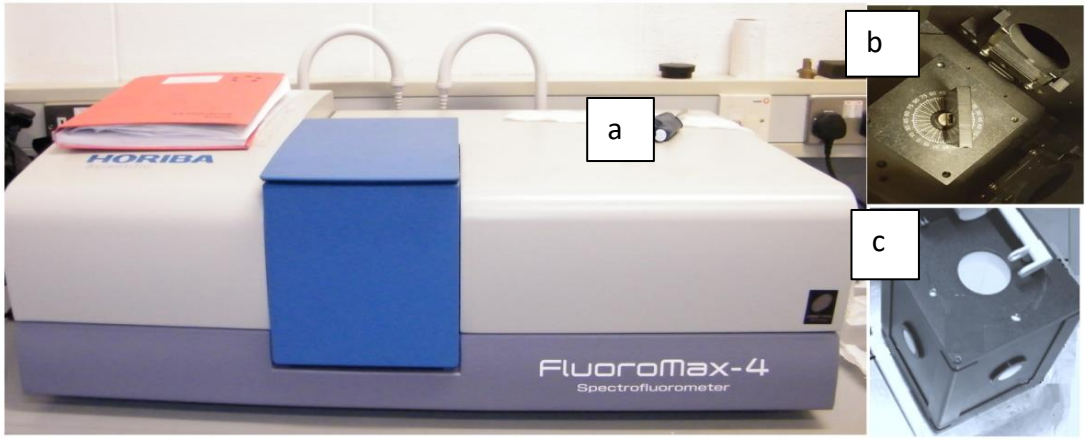

Figure 3.7. a) Spectrofluorometer Horiba Fluoromax-4, b) J1933 Solid Sample Holder, c) Integrating sphere, Trinity College Dublin.

Emission and Excitation Measurements

The emission and excitation spectroscopy use the phenomenon created after manipulation of the sample to an excited state; the transition to the ground state results in the emission of

light, using the spectrofluorometer as a measurement tool, it is possible to measure the fluorescence properties of the luminescence material.

The emission scan shows the spectral distribution of light emitted by the sample. During an emission scan, the excitation monochromator remains at a fixed wavelength, while the emission monochromator scans a selected region.

The excitation scan shows the spectral distribution of light absorbed by the sample. To acquire an excitation scan, the excitation monochromator scans a selected spectral region, while the emission monochromator remains at a fixed wavelength. The schematic of this instrument is shown in Figure 3.8.

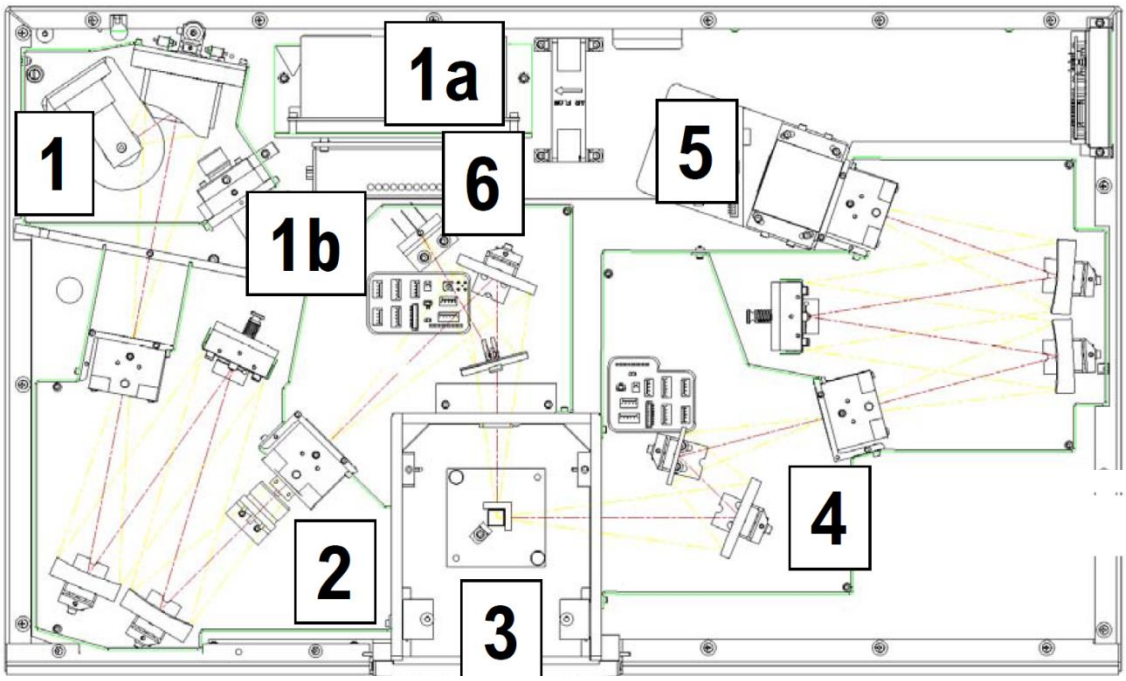

Figure 3.8. Schematic of the Horiba spectrofluorometer instrument with optical layout, 1- xenon arc-lamp and lamp housing, 1a xenon-lamp power supply, 1b xenon flash lamp, 2 excitation monochromator, 3 sample compartment, 4 emission monochromator, 5 signal detector (photomultiplier tube and housing), 6 reference detector (photodiode and current-acquisition module), (Horiba user's manual, Fluoromax -4, 2012).

These optical characterisations of the samples were performed in many experiments within this project, alongside the analysis of the layers. Many luminescent samples were characterized containing different concentration ratios of the luminescent species. In order to measure the spectrum effect of sample layers, a broadband excitation source, with light-dispersing elements, and a detector (all of which are the hardware part of this instrument)

were used. The sample is irradiated with radiation from the excitation source. When this radiation induces a transition to an excited state (S≥1) in the material (S=0 or ground state), this may lead to the emission of light from the sample layer. The detector is used to measure either the intensity of the emitted light or the intensity of the residual light from the excitation source.

3.3.3 Phosphorescent Lifetime

The phosphorescence lifetime measurements were conducted in a time domain through the analysis of the luminescence decay of the phosphorescent sample layers, where the sample signal is monitored as a function of time, while both the excitation and emission spectrometers remain at fixed wavelengths. The spectrofluorometer was used in these measurements, which combines fluorometers with a high intensity light source for excitation. In the phosphorescent materials, optical excitation energy is stored in the lattice by the trapping of photo excited charge carriers. This analytical technique is based on the detection of photons emitted by particles excited by the return of the triplet excited state to the ground state.

Using this technique, the Time-correlated single-photon counting (TCSPC), the arriving photons are timed after the excitation. Gradually a decay curve is built up and the sample's fluorescent lifetime is calculated. This is a measure of a sample lifetime since it gives a direct measurement, observing the decay kinetics in real time. It combines single-photon sensitivity and digital counting, most importantly enabling complex kinetics of long and short-lived components to be analysed simultaneously from a single measurement. This technique was used in conjunction with kinetics analysis, through fitting its phosphorescence-decay curve; fitting which involves choosing the analytical model. For the phosphorescent phosphor, its lifetime is usually expressed by an empirical Equation 3.4 (Berberan-Santos et al., 2005).

$$I = I_o + \alpha_1 \, exp\left(-\frac{t}{\tau_1}\right) \qquad \text{Equation 3.4}$$

where **I** is the phosphorescent intensity (counts), $\mathbf{I_0}$, $\boldsymbol{\alpha_1}$ the constants (amplitude in counts), **t** the time (ms) and τ_1 is decay times for the single exponential component.

The analytical model was analysed using the computer aid, OriginPro 2015/2018 and the values of I_0, α_1, and τ_1 were obtained.

3.3.4 Photoluminescence Quantum Yield (PLQY)

It was important to determine the unity of the photoluminescence (PL) quantum yield (PLQY) of the potential phosphorescent species applied in this work, through the fabricated luminescent layers. This unit value gives a very elementary information or unit in percentage, which yields the energy efficiency to be expected for each phosphor.

The PL Quantum Yield (QY) measurement is taken when a fluorophore of the phosphorescent of the fluorescent compound absorbs a photon of light, and an electron is raised from the Ground (G) state to the Excited (E) state by generating an energetically excited state, G→E. This effect depends on the type of fluorophore species and its surroundings, which will result in deactivation or discharging of this absorbed energy and returning it to the ground state, E→G. The deactivation processes can occur by the emission of a photon, the internal conversion vibrational relaxation (which is a non-radiative loss of energy to the surroundings), or the intersystem crossing to the triplet state, (as shown Figure 2.17).

The external radiative or PLQY, η, is defined by Equation 3.5, which is the fluorescence quantum yield, i.e. the number of photons emitted as a fraction of the number of photons absorbed (de Mello et al., 1997).

$$\eta = \frac{number\ of\ photons\ emitted}{number\ of\ photons\ absorbed} \qquad \text{Equation 3.5}$$

Using a the spectrofluorometer, two different methods were tested to measure PLQY of the luminescent layers, the first being the Comparison method, and the second the Direct Method, which requires the use of the integrating sphere, (FitzGerald, 2008). However, neither of these two methods appeared to be suitable for the luminescent layers, prepared with LPP phosphors, (see Table 3.2), and accordingly, a new method was developed. It is the

combination of both methods, and consistent results can be obtained. The most important reason why these two methods were incompatible can be explained as follows:

Comparison method

In the case of the Comparative method, in order to determine the quantum yield of an unknown (Q_R) it is necessary to compare it to the spectrum of a known standard reference by applying the following equation:

$$Q_F = Q_R \frac{I_F}{I_r} \frac{A_R}{A_F} \qquad \text{Equation 3.6}$$

Where Q_F is the quantum yield of the unknown fluorescent sample, Q_R is the quantum yield of the reference standard, I_F and I_R are the integrated fluorescence intensities for the unknown and the reference, respectively, and A_F and A_R are the absorbance values of the unknown and reference, respectively.

The Comparative method requires the use of a reference standard, a sample with known emission and absorbance properties close to that of the sample of interest and has a known PLQY value. The absorbance and fluorescence of the reference standard are measured and then the same is measured for the sample under study.

Two different attempts were made to use this method by applying fluorescein as a standard reference. With the first attempt, in order to apply the fluorescein to the host polymer, it needed to be dissolved in a solvent which is not viable with the type of host polymer matrix applied to this work. On the second occasion, fluorescein was dissolved in different types of solvents at a very low concentration and measured in a glass curvet. However, unfortunately this attempt result was incompatible when compared with a solid luminescent layer. The measurements of the quantum yield of a highly refractive sample (such as luminescent layers dropped with phosphorescent samples) are problematic owing to difficulties in determining the angular distribution of the emission, reflectivity, and absorptance. Accordingly, a new method was required to examine the PLQY of the phosphorescent species, which was dispersed in a transparent host matrix.

Direct Method

The second method, Direct method, was tested using the spectrofluorometer with an integrating sphere, and by applying standard reference phosphors from the National Institute for Materials Science (NIMS), (see Table 3.2). These standard references were acquired because they were the only phosphor standards available, had shared some similarities in physical and optical properties (such as emission, excitation, photostability), and also had been fully characterized by this method. Nevertheless, these standard references unfortunately show a very short lifetime decay as they are all fluorescent phosphors, but can still be used to validate the method. Prior to testing the reference standards from NIMS, they were dispersed in a host matrix to prepare the luminescent layers, using the standard method, as described in Chapter 5.

After all the layers are prepared, they were measured by applying the Direct method, using the integrating sphere, where sample layers are placed on the inside of the sphere and then fluorescence is measured. A measurement was done of the fluorescence emission (E_c) and the scatter (L_c) of the sample and also the emission and scatter of a blank (L_a and E_a). From these two spectral measurements (sample and blank), the PLQY were calculated using the following Equation:

$$\Phi = \frac{E_c - (1 - A) \times E_b}{L_a \times A} = \frac{E_c - E_a}{L_a - L_c} \qquad \text{Equation 3.7}$$

Where E_b is the integrated luminescence from the sample caused by indirect luminescence from the sphere and A is the absorbance of the sample at the excitation wavelength.

During this measurement care was taken that slit settings were kept constant for these four measurements. It was vital that between each measurement the sample or reference was not moved in any way. To prevent saturation of the instrument detector when measuring the very intense scattered excitation peaks, it is necessary to use a suitable Neutral-Density filter, (see Figure 3.9). The precise transmission value of the filter must be measured for the system settings, (e.g. excitation, wavelength and bandpass), and used for the specific PLQY analysis.

The measured transmission value is then used in the PLQY calculation, to compensate for the use of the filter in the scatter spectra. Spectra recorded on the spectrofluorometer must be correct for the spectrometer response. An additional correct factor for the integrating sphere is applied within the analysis, and the background subtraction method is equal to an empty sphere.

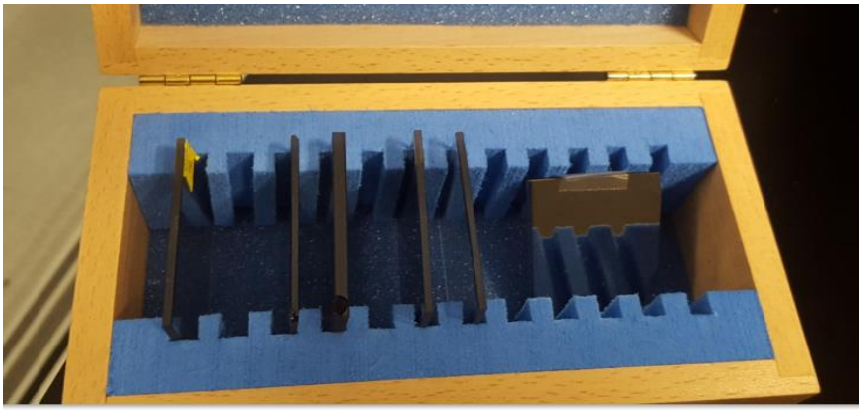

Figure 3.9. Neutral-density filter (ND filter) used for PLQY measurements.

As a result of this method for the measurement of the LPQY of luminescent layers, after more than three respective measurements for the standard and sample layers, it was observed that the error associated with the PLQY measurements was around 10% only for the standard reference luminescent layers. However, for the phosphorescent sample layers, the error associated with the PLQY was much higher and totally inconsistent.

As an example, the luminescent layers fabricated with the phosphorescent phosphor Ph3 (see Table 3.2, at 0.1%wt concentration, were measured six times consecutively, and the PLQY were -0.03, -6.28), 0.04, 4.5, 1.07 and 74.6%. Similar inconsistencies were found in the sample layers with a higher concentration ratio, (1-100%wt), also.

Due to this inconsistency, the Direct Method was demonstrated to be incomplete and indicates an insufficient measure between the fluorescent and phosphorescent phosphor species, which may be caused by the LPP effect of the phosphorescent samples.

In order to compare different phosphorescent species and develop luminescent layers to enhance the PV device efficiency, it is vital to have an accurate measurement unit value of the PLQY of the luminescent layers. This will help to identify the best phosphorescent species, and also define the properties of the mechanism such as down-shifting or down-conversion, where the difference between these two mechanisms is indicated by their units of the PLQY (de la Mora et al., 2017).

New Method - Mixed Methods to measure the PLQY of LLP

In order to remedy this situation, the researcher not only thoroughly examined the available literature, but also through contacted experts in the luminescent field, in order to establish a working method. Amongst these contacts was Dr. Alex Siemiarczuk from Horiba scientific, who demonstrated interest in helping this investigation and offered his luminescent laboratories at Horiba, Edison-USA as a host institution to conduct this investigation, (where a more updated and calibrated spectrofluorometer with an integrating sphere is installed, see Figure 3.10).

Figure 3.10. a) Horiba Spectrofluorometer Fluoromax + with Integrating sphere, b) Integrating sphere, c) Integrating sphere unassembled, Horiba USA.

The Mixed Methods is more specific in that it includes the mixing of Direct and Comparative PLQY methods for one strand of data collection to measure the LPQY value of LPP phosphor, after a constant energetically excited state is reached.

The new method to measure the LPP phosphor of the luminescent layers takes similar steps as the Direct Method, the only difference being that the PLQY measurements are taken only after all the fluorophores of the LPP species absorb enough energy photons of light, and the electrons are raised from the Ground (G) state to the highest Excited (E) state of the luminescent layer by generating a constant energetically excited state, G→cE.

In order for the LPP to be able to reach a constant energetically excited state, it needs to be excited for approximately 5 minutes, unlike those of fluorescent phosphors, which take less than a second. A similar pattern occurs during the deactivation or discharging of this absorbed energy and its return to the ground state, E→G. The deactivation processes can occur by the emission of a photon, internal conversion vibrational relaxation (which is non-radiative loss of energy to the surroundings), and intersystem crossing to the triplet state, which in the case of the LPP species, takes hours to occur. It is believed that this delay caused the inconsistency in the PLQY results, because the measurements could be taken between different levels of energy, resulting in different PLQY unit values, as demonstrated earlier.

After testing the new method, the Comparative Method was applied to validate this new approach using a known reference standard. The same reference standard from NIMS was used to compare these samples, in powder or luminescent layers. The results show that the PLQY measurements of both reference and LPP phosphors were very consistent and reliable in both cases, (i.e. powder and luminescent layers). Thus, the new method applied to measure the PLQY of the luminescent layers prepared with the standards reference and long persistent phosphors, displayed very high consistency, and accuracy with calculated uncertainty up to 0.05%, (Table 6.2 shows these PLQY results).

Using this method and importing this PLQY spectrum measurements, (which is Internal Quantum Efficiency (IQE)), into the Origin pro software, it was possible to calculate the External Quantum Efficiency (EQE) from the EQE of the luminescent layer as described below.

Figure 3.11 shows the Photoluminescent spectra of the blank and sample luminescent layers, measured from 375 to 700nm. For this sample, both excitation and emission wavelengths were kept fixed at 375 and 520nm, at room temperature.

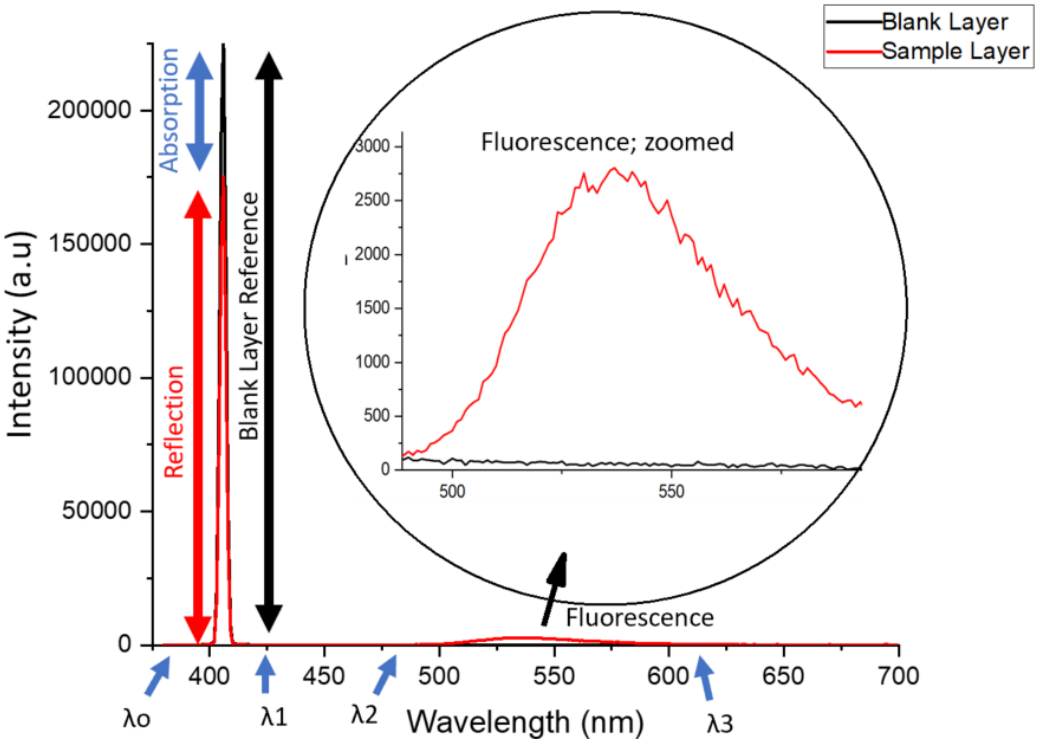

Figure 3.11. Photoluminescent spectra of the blank and sample luminescent layers from 375 to 700nm, measured at fixed wavelength 375, excitation and emission 520nm. Insert; zoomed fluorescence.

External Quantum Efficiency (EQE) is defined as the proportion of the total number of photons emitted by the phosphor (fluorescence) versus the number of excited photons that are emitted by the excitation light source.

The IQE and IQE were calculated using Equations 3.13 and 3.14, as follows:

$$Fluorescence \qquad S_1 = F_1 - B_1 \qquad \text{Equation 3.8}$$

If subtract the fluorescence is F_1 before the excitation interval to cancel out the excitation area, then we get:

$$A_1 = \int_{\lambda 2}^{\lambda 3} S_1(\lambda) d\lambda \qquad \text{Equation 3.9}$$

$$Excitation \qquad S_2 = B_2 - F_2 \qquad \text{Equation 3.10}$$

Then if subtracting the excitation is B_2 before the fluorescence F2 interval to cancel out the fluorescence area, then we get:

$$A_2 = \int_{\lambda 0}^{\lambda 1} S_2(\lambda) d\lambda \qquad \text{Equation 3.11}$$

A_2 gives the area for the excitation curve S_2 (λ) between λ=2 and λ3, before the fluorescence wavelength:

$$S_3 = \int_{\lambda 0}^{\lambda 1} B(\lambda) d\lambda \qquad \text{Equation 3.12}$$

Then for S_3 integrated for Blank from λ_0 to λ_1

Rearranging the terms, it will be possible to obtain both Equations:

$$IQE = \frac{S_1}{S_2} \qquad \text{Equation 3.13}$$

$$EQE = \frac{S_1}{S_3} \qquad \text{Equation 3.14}$$

3.3.5 Confocal Microscope

The Confocal Laser Scanning Microscopy (CLSM, Leica TCS SP8) was used to record phosphorescent dispersion in the luminescent layers by painting the outside of the luminescent layer with known fluorescent material to map the internal and external area of the fabricated luminescent layer. CLSM has many advantages over conventional optical microscopy such as controllable depth of the excitation field, and elimination of out-of-focus light. Images and fluorescence can be recorded simultaneously, and the ability to collect serial optical sections from thick specimens is possible. This is because the laser is moved across the sample in a raster, x-y pattern, and by moving the focus vertically, z, multiple slices can be used to build up a full three-dimensional image, (see Figure 3.12).

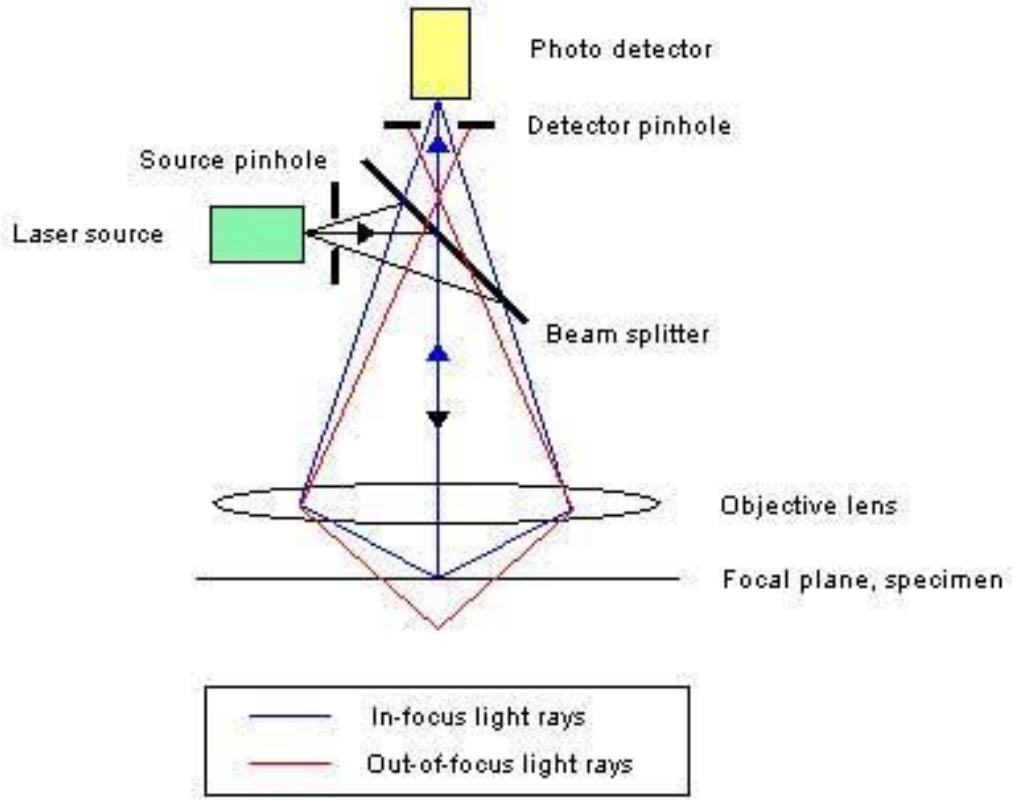

Figure 3.12. Light pathway in a confocal microscope configuration, www.ntnu.edu

The works principle of the Confocal instrument can be described as a beam of laser light focused by an objective lens, onto a fluorescent specimen. The fluorescent energy from the sample is then collected through the same objective and recorded by a photo detector. The optical system is designed so that the laser's focal point in the sample is imaged exactly on the face of the photodetector. This means that fluorescence coming from the point of laser focus will be focused on the photo detector, and fluorescence coming from any other points will be out of focus on the photo detector. By inserting a small aperture, pinhole, in front of the photo detector, the gathered fluorescence can be limited to a region very close to the focal point.
Using this instrument and this method we were able to investigate four main parameters considered: The thickness of the luminescent layer, the position of the phosphor species inside the host matrix, the space distribution of the phosphors, and the particle size of the phosphorescent species. Therefore, using a confocal instrument it was possible to map the internal and external areas of the luminescent layer which helps to better understand details such as formation inside and outside.

3.3.6 Infrared Spectroscopy Analysis

A Fourier Transform Infrared (FT-IR) spectrometer was used for the analysis of the host polymer layers. The use of this spectroscopic techniques for the analysis of the host polymer layer, enabled the generation of spectral images. This FTIR technique allows the detection of traces and the deformation of polymers on the produced layers that could be verified by a wide spectra range. The instrument applied in this analysis was a Perkin Elmer Spectrum 100 FTIR/ATR, (see Figure 3.13). This instrument can operate in ratio, single-beam, or interferogram mode. It has an optical system that allows measurement over a total range of 7800 to 370cm^{-1}, with a best resolution of 0.5 cm$^{-1.}$ These regions comprise a molecular fingerprint of the structure of the host polymer sample analysed. (PerkinElmer user's manual, Spectrum 100 series, 2005).

Figure 3.13. Perkin Elmer Spectrum 100 FTIR/ATR, Trinity College Dublin.

Although the spectral profile allows chemical identification, the combination with microscopy permits the examination of complex structures of the samples. This instrument was used to collect the data spectra range 4000–500 cm^{-1} (2500–20,000 nm), to analyse instability, degradation and polymerization molecules through identification of basic structural components. The instrument was connected to a computer that is used to control and analyse the spectra data collection.

3.3.7 Differential Scanning Calorimetry and Thermogravimetric Analysis

The Differential Thermal Analyzer (DTA) and Thermogravimetry (TG) were applied for simultaneous thermogravimetric and differential thermal analytic measurements on the synthesis of the phosphorescent phosphor. The differential scanning calorimetry is a thermal transition technique which was used to study the behaviour of a phosphorescent species when exposed to heat. The thermal gravimetric analysis (TGA), measures the amount of weight change of a material, either as a function of increasing temperature, or isothermally as a function of time, in an atmosphere of nitrogen, helium, air, other gas, or in a vacuum, (Figure 3.14 below shows the schematic diagram). The instrument applied in this analysis was a Seiko SSC/5200.

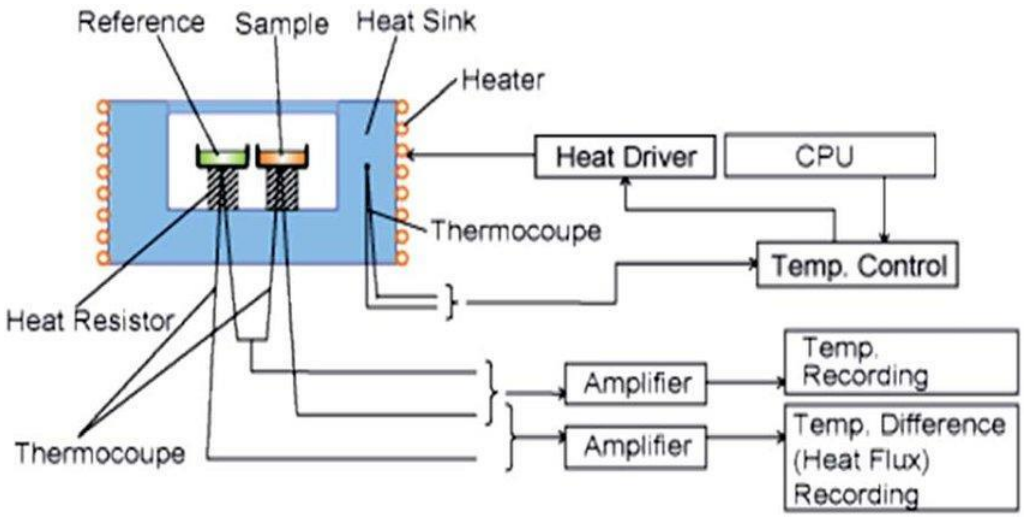

Figure 3.14. Schematic diagram of a DSC system, ("DSC: Hitachi High-Technologies GLOBAL," n.d.)

The work principle of a DSC is aimed to maintain the sample and a reference material at the same temperature, through the controlled temperature programme. Any difference in the independent supplier feed of power to the sample and reference is then recorded against the programmed temperature (Brown, 2001).

3.3.8 Electrical Characterization

The methods by which the electrical characterizations of the PV devices attached to the luminescent layers, (discussed in Chapters 7 and 8), is described in this section. The electrical characterisation was carried out by measuring the I-V characteristics of the PV devices attached to the fabricated luminescent layers. All the PV devices were characterized under standard test conditions (STCs), however, a non STC approach was applied to characterize the PV devices with the LDC layers, after exposure to illumination, under dark conditions. These standard conditions refer to a module temperature of 25°C, 1000 W/m^2 irradiance and an AM1.5 solar spectrum (Leboeuf and Ossenbrink, 1991). The evaluation of the PV devices performance under dark conditions was based on a set of indicators that take into consideration ambient temperature but not a standard irradiance spectrum as there were no standard conditions, such as on the assessment of energy storage into the luminescent layers and the amount of time which it takes for that energy be converted into electrical power by the PV device.

Three different types of PV technologies were used in this study; a dye-sensitized solar cell (DSSCs), a Monolithic Perovskite Solar Cell (MPC), and a silicon-based mini module of amorphous silicon (a-Si). The PV devices were tested with the fabricated luminescent layers on different positions depending on their architecture, on top of non-transparent PV devices, and on top and at the rear of the transparent PV devices (which do not contain a reflective coating or metal layer), as shown in the schematic, Figure 3.15, (see below).

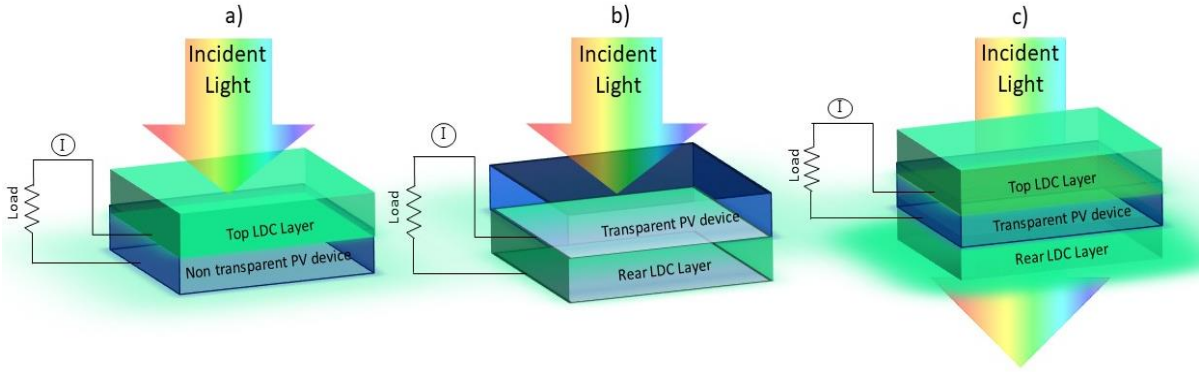

Figure 3.15. (a) Schematic design of the luminescent down-converter Layers attached to the PV devices in different positions. (a) Top application on a non-transparent PV device. (b) Rear application at the rear of a transparent PV device. Both top and rear applications to a transparent PV device.

Figure 3.16 shows the equivalent circuit configurations for PV device characterization with an arbitrary active load, which is applied by the source meter.

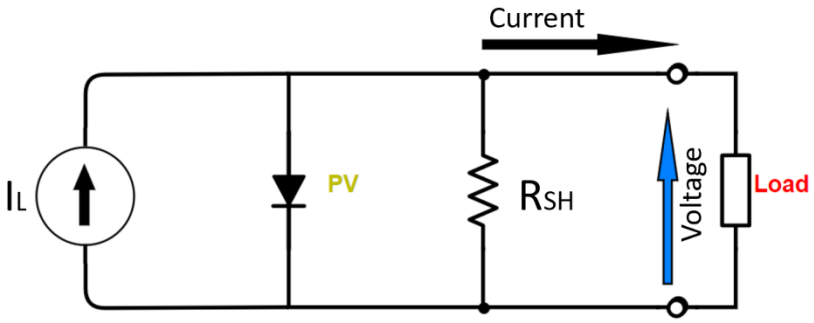

Figure 3.16. Equivalent circuit diagram of a PV device including, I_L the light generated current, R_{sh} shunt resistance, active load and the voltage, across the PV device terminals.

The most common way of representing the I-V characteristic of the PV device which is the combination of current, I, and voltage, V, is a set of graphical curves used to define its operation within an electrical circuit. The I-V curves show the relationship between the current flowing through the PV device and applied voltage across its terminals. The equation for the PV device in the presence of a shunt resistance, is defined as follows;

$$I = I_L - I_o \, exp\left[\frac{qV}{nkT}\right] - \frac{V}{R_{SH}} \qquad \text{Equation 3.15}$$

where: I is the PV device output current, I_L is the light generated current, I_o is the saturation current of the diode, q charge constant (1.6x10^{-19} coulombs), V is the voltage across the device terminals, n is the ideality factor, k is a constant(1.38x10^{-23}J/K), T is the temperature and R_{SH} is the PV shunt resistance.

In the case of the DSSC PV device, the equivalent circuit characterization is defined slightly differently, according to some researchers (Han and Koide, 2006, Chergui et al., 2011; Halme et al., 2010; Han and Koide, 2006; Que et al., 2016; Yang et al., 2012; Zhang et al., 2014). The series resistance of DSSC is the sum of the internal resistance elements related to the charge transfer process at the Pt counter electrode, R_1, TCO substrate resistance, R_h, Nernstian diffusion in the electrolyte, R2. The equivalent circuit of DSSC I-V characteristics is constructed as shown in Figure 3.17.

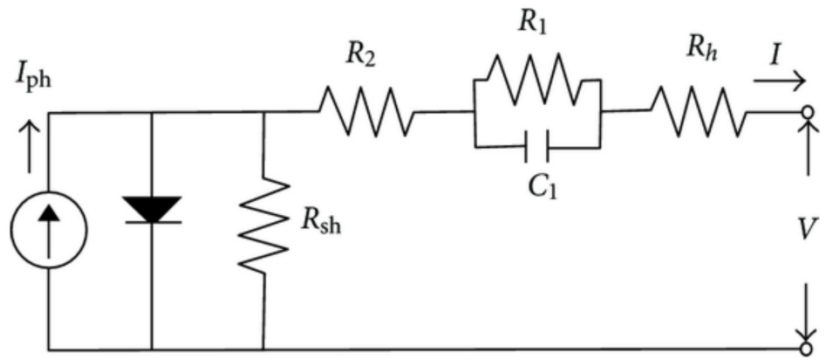

Figure 3.17. Equivalent circuit diagram of a DSSC PV based on I-V characteristics of the device. The sum of R_1, R_2, and R_h corresponds closely to the series resistance of DSSCs. C_1 is capacitance elements (Yang et al., 2012).

In this case, the diode equation can be written as:

$$I = I_{ph} - I_o \left\{exp\left[\frac{q(V + IR_s}{nkT}\right] - 1\right\} - \frac{V + IR_s}{R_{SH}} \qquad \text{Equation 3.16}$$

where I_{ph} is the ideal photocurrent, I_o is the reverse saturation current, n is the ideality factor whose value is between 1 and 2 for the DSSC, R_S is the series resistance which is the sum of R_1, R_2, and R_h, and R_{SH} is the shunt resistance.

As can be observed, the difference between these two types of PV configurations is that a DSSC PV device has a capacitance in its configuration. The capacitance effect describes the fundamental mechanism whereby photogenerated carriers store free energy and produce a voltage and current in the external circuit, as this type of PV is composed of two plates which maintain carriers with different values of electrochemical potential. Excitation is a charging of the electrochemical capacitor. Charge separation relies on a good connectivity into each of the macroscopic plates (Bisquert, 2003). A schematic diagram of a DSSC solar cell is shown in Figure 2.3.

During the I-V measurement, the value of the current can be described as the short-current (I_{sc}), which is the current passing through the PV device when the voltage across the device is zero. The open-circuit voltage, V_{OC}, is the maximum voltage available from a PV device, and this occurs at zero current. The open-circuit voltage corresponds to the amount of forward

bias on the PV device, due to the bias of the PV device junction with the light-generated current. These two and many other important parameters are shown in Figure 3.18 below.

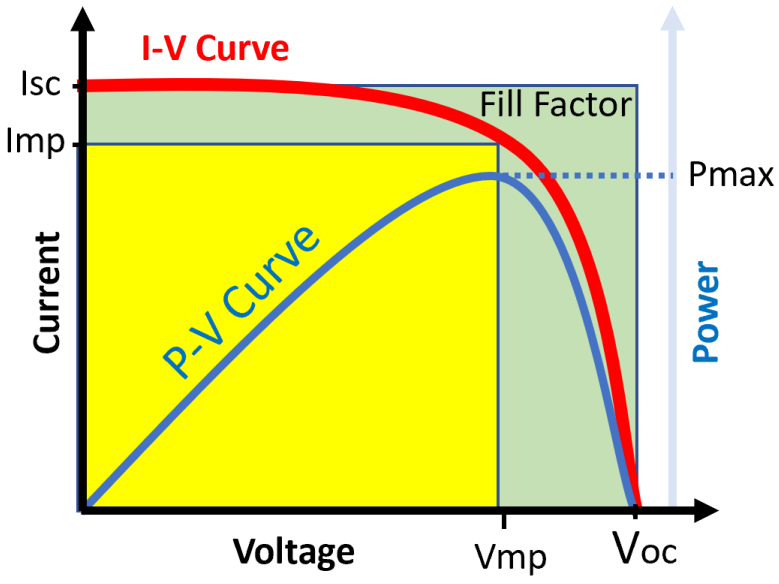

Figure 3.18. The important characterization parameters of the PV device for the I-V characterisation, the output current, Isc, (red line), and power, (blue line), as a function of voltage, Voc. Also shown is the maximum power point (Vmp, Imp), and Fill Factor ("PVEducation," n.d.).

The Isc and the Voc are the maximum current and voltage respectively from a PV device. However, at these operating points, the power from the PV device is zero. The "Fill Factor", (FF), is a parameter which, in conjunction with Voc and Isc, determines the maximum power from a PV device. The FF is defined as the ratio of the maximum power from the PV device to the product of Voc and Isc, so that:

$$FF = \frac{P_{Mp}}{V_{oc} \times I_{sc}} = \frac{P_{Mp} \times P_{Mp}}{V_{oc} \times I_{sc}} \qquad \text{Equation 3.17}$$

The FF is a measure of the squareness of the PV device which is limited by the largest rectangle, (green). Thus, FF is the area of yellow divided by an area of green rectangles.

The efficiency, η, is the most important parameter by which to compare the performance of one PV device to another and determine the cost during a project application, which means the higher the efficiency, the less the number of PV devices required, thus less cost. The efficiency of a PV device is determined as being the fraction of incident power which is converted to electricity and is defined as:

$$\eta = \frac{V_{oc} \times I_{sc} \times FF}{P_{in}}$$ Equation 3.18

Where; P_{in} is taken as the product of the irradiance of the incident light (W/m^2), with the surface area of the PV device, the input power for efficiency calculations is 1 kW/m^2 or 100 mW/cm^2.

Current- Voltage Measurements

The Current-voltage measurements were carried out on different occasions using both Standard Test Conditions. When the PV device was assessed under light conditions, and non-standard procedures (in the dark), was when the PV device was assessed after exposure to light. The STC procedures for the PV device prescribe that the power output of the device is rated at standard testing conditions. For instance, using a light source to power a PV device which does not have a similar spectrum match to the sun (such as a solar simulator spectrum), will result in poor spectrum distribution, subsequently it's unknown how this device would perform under standard conditions. In addition to solar irradiance, other important parameters to be considered include temperature. Temperature is one of the most important factors which can affect the performance of the PV device, as can be observed in I-V Equation 3.15. Consequently, measuring the I-V under a classified solar simulator at different temperatures will result in many uncertainties because temperature is a very influential factor on the overall conversion efficiency of the PV device.

For example, it was found that all result data of the I-V characterization from the DSSC and monolithic perovskite PV devices, which were acquired from Solaronix S.A, resulted in much more inconsistency. These devices do warm up when exposed to the light source. This can affect the Fill factor as well as the efficiency of the PV device. DSSC are very sensitive to temperature changes as they incorporate semiconductor materials. The semiconductor's band gap tends to decrease with increasing temperatures, because when temperature increases, the amplitude of atomic vibrations increase, leading to larger interatomic spacing. This leads to an increase in the short-circuit current and a decrease in the open-circuit potential, (as shown in Figure 3.19).

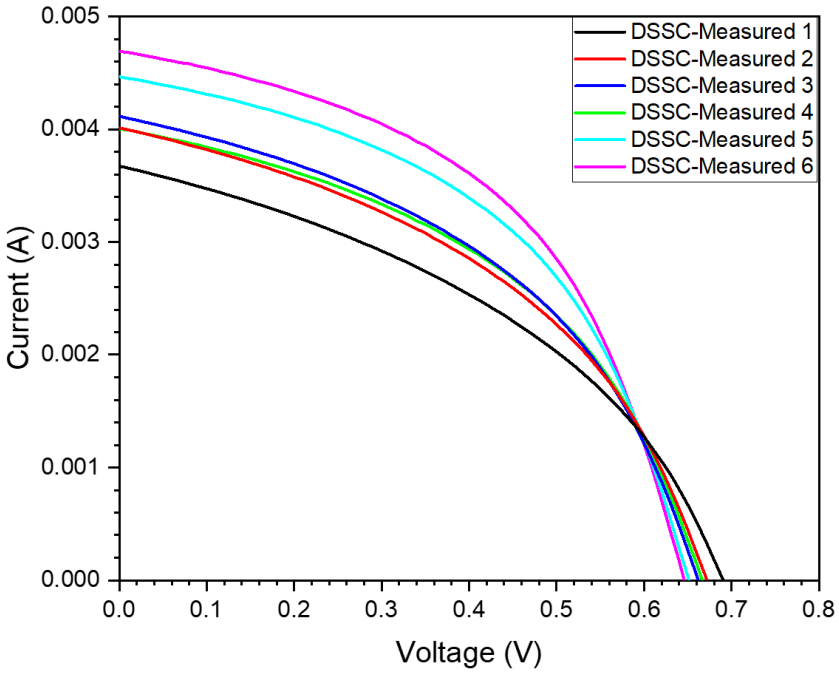

Figure 3.19. The effect of temperature on PV device temperature during multiple I-V measurements.

The measurements were taken under a solar simulator, LOT LS0308, illumination 100mW/cm^2, at Tyndall National Institute, Ireland. However, without a standard probe station chucks, and no calibrated temperature sensor to maintain the STC during the measurements, a scissor lifting jack platform was used instead, as can be observed in Figure 3.20.

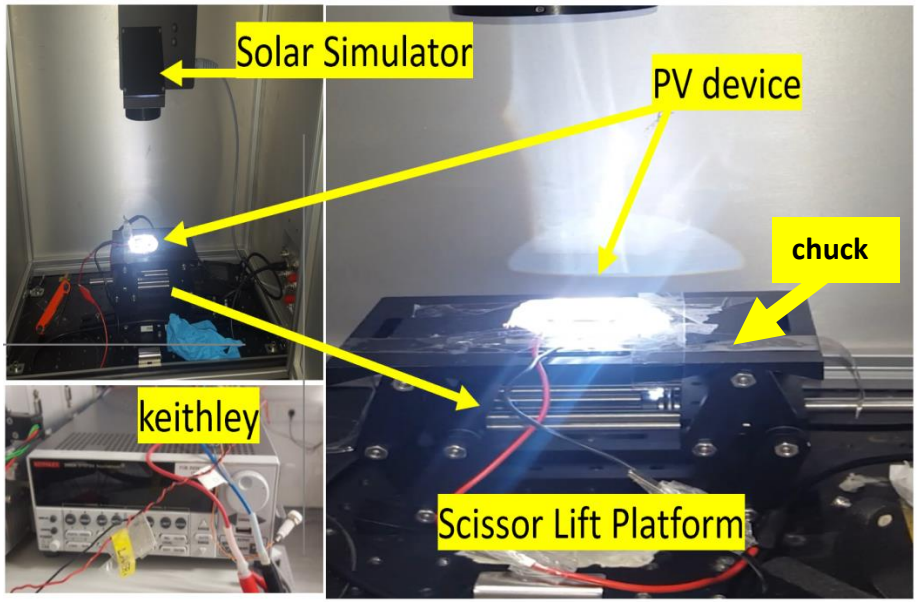

Figure 3.20. Photos of the experimental setup used without a standard probe station chuck or a calibrated temperature sensor, solar simulator Class: ABB, Tyndall National Institute, Ireland.

As observed, initially, the incident light slowly warms up the PV device during the measurements, (measurements from 1 to 6). In this phase, Isc and Voc are drifting significantly and the slopes of the curves near the Isc and open circuit potential are changing. The I-V characteristic appears to overlap between 2-3 measurements, when the PV temperature started to show signs of stabilizing. However, by the end of the measurements section, (measured tests 5-6), it was still not fully stabilized due to the temperature increase, which resulted in a larger FF. The cause of this variation in measurement can be attributed to the material properties of DSSC and the variation of test conditions, including temperature and illumination. Poor agreement is obtained for most of the extracted parameters during the data analysis. These results, in agreement with other results reported ("Dye Sensitized Solar Cells DSSC-DSC," n.d., Chergui et al., 2011, Cotfas et al., 2018), emphasise the performance of this type of PV device, under different temperature conditions.

Thus, following I-V measurements of these PV devices with luminescent layers attached on the top or at the rear surfaces, it was not possible to justify the effect of the addition of the luminescent layer. Consequently, time and resources were lost because of lack of monitored temperature during the measurements. These results will not be included or discussed any further here, since the effects of the luminescent layers on the PV efficiency is unclear.
The results of the I-V measurements of the PV devices with and without the layer are expected to be a small on difference, which can be obscured by temperature and illumination variations, even after several consecutive measurements were taken, such as fixed voltage, current, or efficiency over time, to establish the average of these values.

To overcome this situation, new PV devices were acquired, and the characterization process occurred in a more stable condition, under the STC, at Solaronix S.A PV lab characterisation (Switzerland), in order to avoid any situation likely to cause conflict during the characterization of the PV device with luminescent layers. All measurements were taken after the PV devices showed a consistent I-V result or after the third consecutive measurement. Figures 3.21 and 3.22 below show the set up used at Solaronix, along with the Solar simulator spectrum. These characterisation results are presented in Chapter 7.

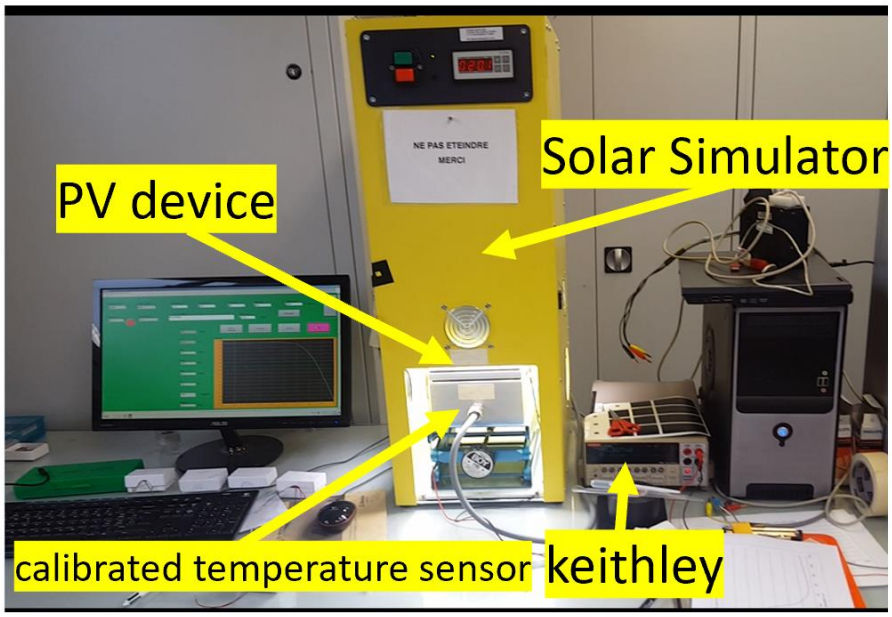

Figure 3.21. Photo of the experimental setup used with a standard probe station chuck and a calibrated temperature sensor, and classified solar simulator, Solaronix S.A, Switzerland.

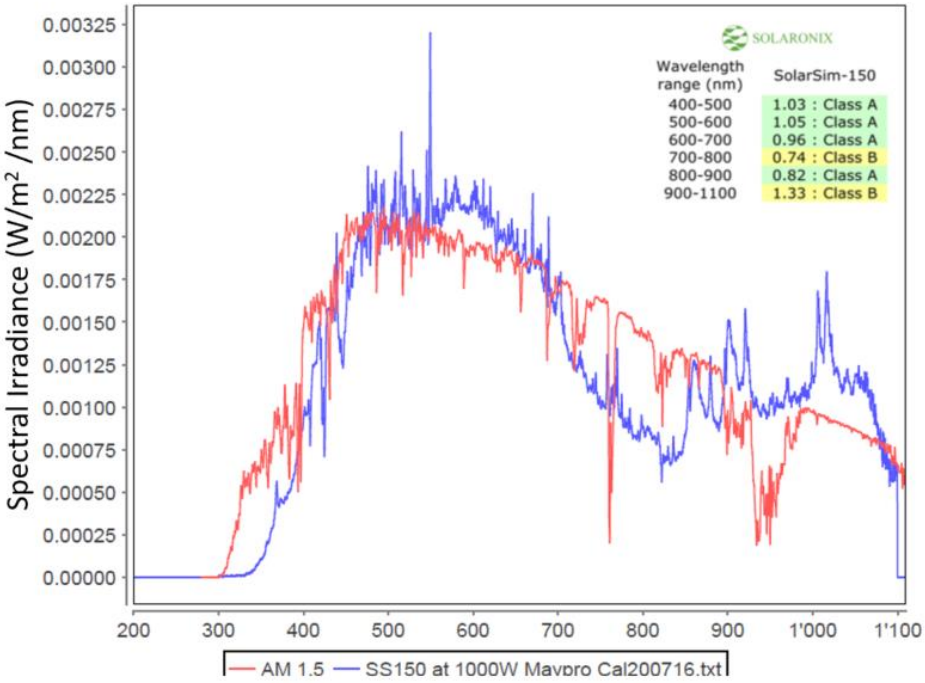

Figure 3.22. Spectrum of the solar simulator used and spectrum of the standard sunlight (AM1.5), with its classification, by Solaronix S.A.

In addition to that, another higher quality and classified solar simulator (AM1.5G) was used to measure the performance of some of the PV devices with the luminescent layers. This set up

was used at the Fraunhofer Institute for Solar Energy Systems ISE (Germany) to maintain the STC across all measurements of the PV devices. These results are presented in Chapter 7 also.

Test Conditions for the PV device in Dark Conditions

Chapter 8 includes test conditions which were applied to measure the I-V characteristic of the PV device with the LDC layers, under dark conditions. These measurements were taken after a LED light source was turned off to measure the I-V caused by the addition of the luminescent layers attached to the top or at the rear surface of the PV device under the photoluminescent "afterglow decay" as illustrated in Figure 3.15. This test condition used a LED light source containing 18 LED lights for maximum illumination, (using cold white colour, an illuminance of 3200 lux, a distance 0.05m view-angle 180°, and a Flux of 50.27 lm (lumen) at room temperature 25°C). The spectrum of a typical cold white LED used in this study, can be seen in Figure 3.23.

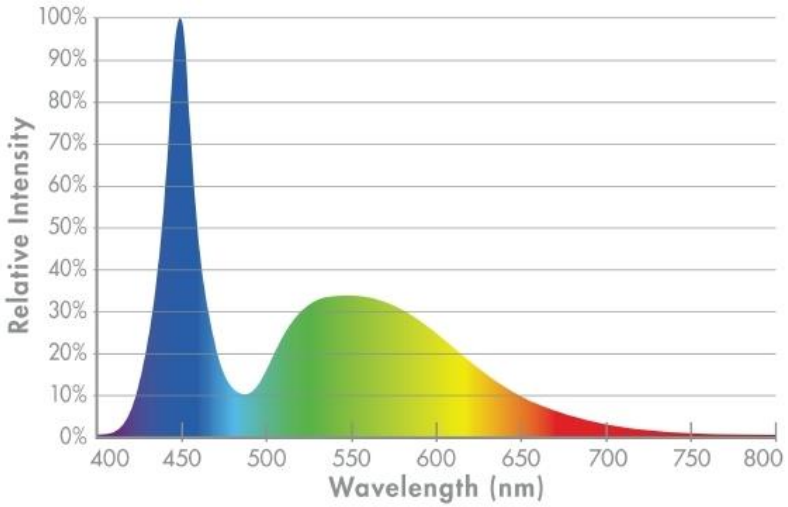

Figure 3.23. Light spectrum of a typical cold white LED, Source: Marineland.

Temperature control in the I-V curve measurement was monitored even if the illumination does not give many changes to the PV device temperature. Hence the devices remain at room temperature during measurement, in between 22-24°C, which still complies with the 25±5°C STC requirement.

Figure 3.24 shows the experiment set up used, the luminescent layers which are placed on the top of the PV device, before and after the cold LED light source is turned off. By applying this cold LED light source, it helps to maintain more stable conditions in terms of temperature and illumination.

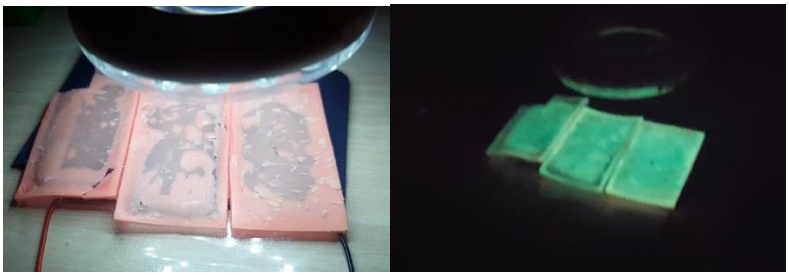

Figure 3.24. The luminescent layers which are placed on the top surface of the PV device, before and after the LED light source is turned off.

These measurements were carried out using an amperemeter, Fluke 289, and Voltmeter, Gold Precision PG10B, and high definition camera 30fps, to recode the measurements at room temperature. These results are presented in Chapter 8.

3.3.9 Quantum Efficiency Measurements of the PV Devices

The quantum efficiency, Q.E., is the ratio of the number of carriers collected by the PV device to the number of photons of a given energy incident on the PV device. The quantum efficiency may be given either as a function of wavelength or as an energy photon. This way, if all photons of a certain wavelength are absorbed and the resulting minority carriers are collected, then the quantum efficiency of that wavelength is unity. The quantum efficiency for photons with energy below the band gap is zero. The quantum efficiency can be described as External and Internal Quantum Efficiency, EQE/IQE.

The EQE is an important parameter because it includes the effect of optical losses such as transmission and reflection. On the other hand, IQE refers to the efficiency with which photons that are not reflected or transmitted out of the PV device can generate collectable carriers. By measuring the reflection and transmission of a device, the external quantum efficiency curve

can be corrected to obtain the internal quantum efficiency curve ("PVEducation," n.d.). Figure 3.25 shows a quantum efficiency measurement curve for an ideal PV device.

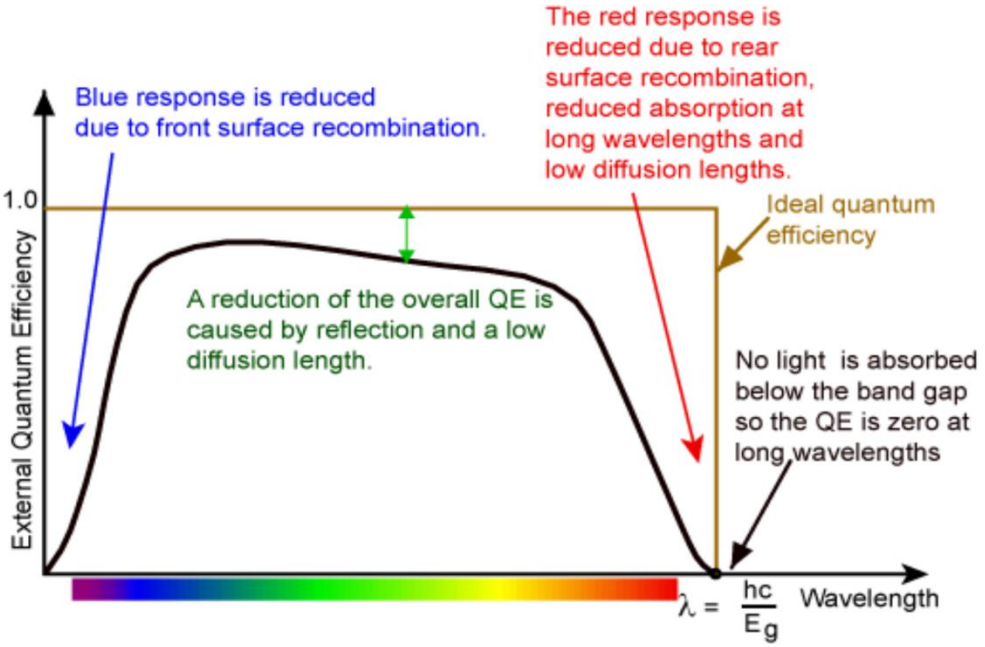

Figure 3.25. External quantum efficiency curve of a PV device showing the most important effect observed in this measurement ("PVEducation," n.d.).

In the present study, the system used to measure the QE of the PV device was a LOANA Solar cell analysis system, with PV-tools, at the Fraunhofer Institute for Solar Energy Systems ISE (Germany). It is an advanced instrument that includes all features of the IQE scan; and automatic spectral mismatch correction of subsequent I_{SC} measurements.

This instrument is composed of an advanced technology where part of the measurement procedures are conducted automatically, by itself, for instance, the IQE, EQE and reflectance are taken in one go. The calibration of the Light Beam Induced Current (LBIC) measurements is to global values. Correct sample thickness and grid shadowing as input for the automated IQE analysis is also conducted. Full area EQE and reflectance measurements were completed by moving the 4cm² illuminated area continuously. Monochromatic light can be positioned between 280-1600 nm from the monochromator (with two gratings, and slit width and order filter changed automatically). Typically, the bandwidth used is 8 nm FWHM and the wavelength accuracy is 1 nm. White bias light of up to 1.2 suns is restricted to the area of monochromatic illumination.

The reflectance is measured under an 8° tilted beam of 2 x 2 cm² area with a BaSO4-coated integrating sphere. Batch mode was employed for a series of measurements under different conditions. The PV device is held on a temperature-controlled vacuum chuck, 25°C, which can be moved by a motorized x-y-z stage, (see Figure 3.26). The temperature is measured directly at the back of the solar cell. A transimpedance amplifier (max. 200 mA) holds the PV device at short circuit with remote sense and a contact quality check. Automatic calibration of EQE and reflectance increases throughout and reduces the necessary time of operator interaction, making the operation safer against human errors (e.g. misalignment, bias light, etc). It avoids degradation of the reference solar cell by manual handling. Motorized contact-setting and change-over between EQE and reflectance measurements was also necessary. Data analysis was completed by comparison with the analytical, electrical and optical models. The duration is dependent on the size of the PV device, (1 sec. per wavelength of spot measurement, 2x2 cm²). (“PV-tools: LOANA system: methods: IQE measurement,” n.d.)

Figure 3.26. Loana PV Solar Cell Analysis system. The photo shows the outside and inside of the system, Fraunhofer Institute ISE (Germany).

The integrating sphere and capability of measuring the EQE and reflectance was one of the reasons which led to its use in this instrument, in order to measure the luminescent layer of a high concentration ratio on the PV device, (which may cause reflectance and scattering of light). This system was suited to measuring these effects with precision and in a single measurement.

However, one interesting measurement that it was not possible to conduct using these instruments, was determining the amount of light trapped inside the luminescent layer. Because in addition to the light bias of the instrument, there was also emitted light from the luminescent layers which was not possible to measure with this instrument.

The light trapping effect into the PV device has been investigated using mirror and photonic structures. According to (Goetzberger et al., 2008), the sunlight is coupled into a transparent medium and converted to diffuse radiation by randomization. *"It is well known that under these conditions light intensity is enhanced by a factor of $2n^2$ inside the medium"* (where n is refractive index). It has been stated also that *"efficiency depends on the ratio (solar cell area)/ (input area)"* and a more detailed analysis shows that *"under regular conditions part of the light is absorbed directly after entering the trap which results in higher efficiencies".* Thus, these concepts require practical applications to be proved and the conceptualization of the application of phosphorescent materials could require a new level of discussions because of its own light trapping mechanisms between the energy statistics of phosphorescence. In order to measure these effects, it requires a more advanced technology, along with a model which can take both fluorescence and phosphorescence effects to meet its needs. To this end, additional research is required, along with the necessary theory and equipment to carry out this measurement.

3.4 Conclusion

The detailed description of the materials and characterisation techniques used throughout this study was presented. The steady state spectrophotometry of solids and liquids and their principles of operation, to measure the light transmission, reflectance, scatter, absorptance were elaborated upon. Characterization techniques which were used to measure the emission, excitation, phosphorescent lifetime, and photoluminescence quantum efficiency were discussed. Confocal microscopy and its advantage in measuring the fabricated luminescent layer by mapping the internal and external areas of the solid was presented. PV device electrical characterization theory and the setups required during this study were discussed in

considerable detail. In the following chapter, the characterization of the synthesis of phosphorescent species and fabrication process of the luminescent layers will be discussed.

CHAPTER 4

PHOSPHORESCENT PHOSPHOR SYNTHESIS AND CHARACTERISATION

4.1 Introduction

As discussed in the Literature Review no standard method was found for synthesis or standard test conditions for characterization of the long persistent phosphor. The standard reference for this phosphor does not exist, which points to a need for meaningful understanding and deliberate investigation. The objective of this chapter was to synthesise a long persistent phosphor (LPP) for use in down conversion layers to enhance the efficiency of PV devices. The characterization of these LPP will be discussed using techniques available to investigate their physical and optical properties. Synthesis of a phosphorescent species, $SrAl_2O_4$: Eu^{+2}; Dy^{3+} (Strontium Aluminate, Dysprosium and Europium Doped) was undertaken and physical characterization analysis was used to confirm the successful synthesis, which involved thermo-gravimetric analysis (TGA) and differential scanning calorimetry (DSC). The final section of this chapter discusses the optical characterisation analysis applied in the attempt to measure the phosphorescent phosphor species.

4.2 Synthesis of the Phosphorescent Material $SrAl_2O_4$: Eu^{+2}; Dy^{3+}

In order to investigate the mechanisms of phosphorescence, the phosphor $SrAl_2O_4$: Eu^{+2}; Dy^{3+} (Strontium Aluminate, Dysprosium and Europium Doped) was reproduced by replicating the work conducted by Professor Matsuzawa in 1996 (Matsuzawa et al., 1996). The aim of this experiment was to synthesise the phosphorescent materials to verify its reproducibility, in order to check the possibility of its optimisation and adaptation to produce an enhanced luminescent species for PV device application.

This phosphorescent phosphor was selected because of its many properties which fulfil the prerequisites necessary for this project, such as a strong peak of emission at visible range, absorption in the ultraviolet range, high quantum yield, high chemical stability and also the

low cost of fabrication. These are some of the important optical characteristic necessary for PV device applications.

The phosphorescent sample was synthesised by a solid-state reaction, which is the widest approach due to its simplicity; raw solid powders where the desired phosphors are mixed then heated above their melting points and finally cooled down under different atmospheres until the ions incorporate into the host. These are the steps used for this reaction:

- The definition of chemical and physical elements, and facilities, where necessary, for the reproduction of $SrAl_2O_4$: Eu^{+2}; Dy^{3+} (Strontium Aluminate, Dysprosium and Europium Doped).
- The preparation of the raw powders and stoichiometry mixtures for calcination of the phosphors.
- The thermal calcination process of $SrAl_2O_4$: Eu^{+2}; Dy^{3+}, using thermo-gravimetric analysis (TGA), differential scanning calorimetry (DSC) (0-1500° C) and also the furnace (0-1300° C).

The phosphorescent $SrAl_2O_4$: Eu^{+2}; Dy^{3+} was prepared successfully through a process of the calcination of a mixture of these raw materials. The final stoichiometry mixture used in the calcination process, is shown in Table 4.1. Boron Oxide (B_2O_3) was added as a flux (5%wt).

Table 4.1. Final stoichiometry mixtures for the calcination of phosphor ($SrAl_2O_4$: Eu^{+2}; Dy^{3+}).

Stoichiometry Mixtures of the Raw Materials	
Eu and Dy Doped	0.01 and 0.02 mass(g)
Strontium Carbonate	1.697489(g)
Alumina	1.172363(g)
Europium Oxide	0.041717(g)
Dysprosium Oxide	0.088430(g)
Boron Trioxide (1wt%)	0.03(g)
Eu Doped	0.01 mass(g)
Strontium Carbonate	1.7495517(g)
Alumina	1.208320066(g)
Europium Oxide	0.042728256(g)

The powdered mixtures were then ground using a ball mill, and subsequently heated to different temperatures, ranging between 1000 to 1300 ° C for one hour, at a rate of 10° C ramp/min in Differential Scanning Calorimetry (DSC). This procedure was repeated several

times using the furnace and Thermal Gravimetric Analysis (DSC/TGA) in different atmospheres (air, oxygen, Argon).

Following the process of calcination in a furnace, the phosphors were ground and sifted through a 200-mesh screen to obtain a maximum range of particle sizes (approximately 30µm diameters). Subsequently, it was analysed through Thermal Gravimetric Analysis (TGA).

Figure 4.1 shows the final phosphorescent phosphor produced by the discussed method. This experiment has apparently successfully replicated the work done by Professor Matsuzawa in 1996, by confirming that this phosphor has a green emission colour with long persistence, which can absorb UV light and emit visible light after exposure to illumination. The long persistent phosphor showed a very good afterglow performance.

Figure 4.1. Final product phosphorescent phosphor ($SrAl_2O_4$: Eu^{2+}; Dy^{3}) powder after being exposed to UV light (254nm) for 5 minutes.

This result is also comparable to the work produced by Chang et al., (2006) in a similar process, with material resulting in a phosphorescent with “a high quantum efficiency, long persistence of phosphorescence, and good stability”. This work presents also the results of the thermal reaction analysis, DSC–TGA, which was used as a reference to compare with the analysis conducted in this research.

To investigate the reaction that took place in this calcination process of phosphor preparation, both analyses were used with the temperature range from 0 to 1300 ◦C, as shown in Figure 4.2.

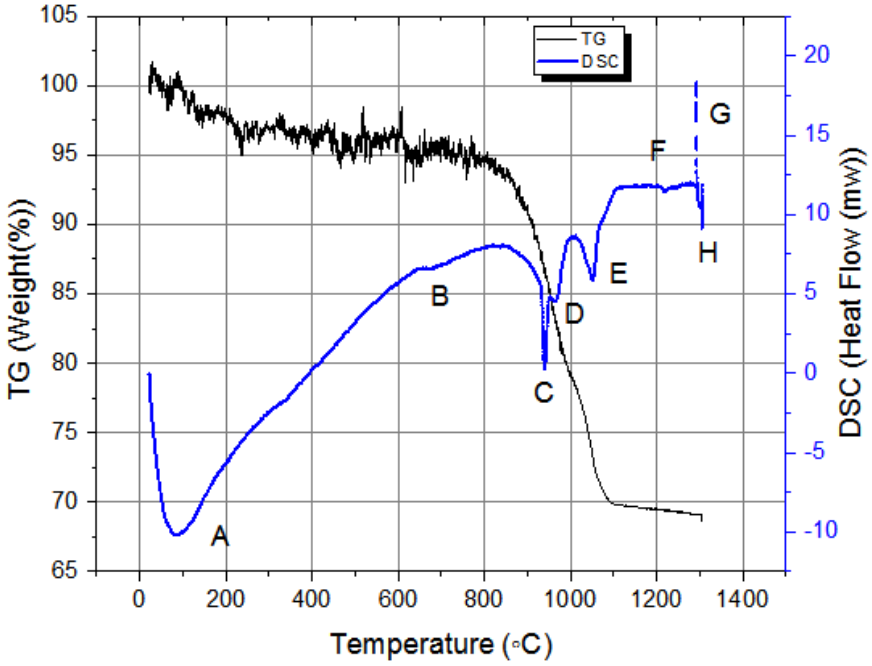

Figure 4.2. DSC and TG profile of the synthesis of phosphor, showing the reaction process during calcinations.

The endothermic peaks A and B in the differential scanning calorimetry (DSC) curve can be assigned to the dehydration of Al $(OH)_3$, and the other three endothermic peaks C, D and E can be assigned to the decomposition of $SrCO_3$, since the dehydration usually occurs at a relatively low-temperature. The thermogravimetric (TG) curve also concurs with the DSC result and is in agreement with Chang et al., (2006). It can be seen from the TG curve that the weight loss total is ~31%wt, during the dehydration and decomposition of the carbonate. Considering the phenomena that both the dehydration and decomposition processes reveal these endothermic peaks implies that these processes were well succeeded after the glass transition, crystallization and melting points.

According to this method and results, it's clear that changes can be applied to the characteristics of the phosphors (such as emission peak, photoluminescent, and also the main elements like dopants and chemical instability), if required and as deemed necessary, in future research.

Although many other studies could have been performed to characterize the physical properties of the phosphorescent species, (for example, X-ray diffraction using a Siemens D-

5000 diffractometer with Cu Kα, which may show the radiation structural characterization of tridymite, and Microstructural characterization, by means of electron diffraction (SAED) and High-resolution electron microscopy (HREM)), they were not utilised within this body of research.

These are structured properties analyses which take significant time and effort to investigate and they are not very deemed to be very relevant to this work. Therefore, more attention has been given to the optical characteristics of the phosphorescent species along with the application for PV devices.

A significant reason for this decision was due to the fact that it was not possible to find either standard reference, or standard methods for physical and optical characterization of the long persistent phosphor the LPP. In addition, very limited optical information, such as internal and external unity of photoluminescent quantum efficiency, was not found in the literature for the purposes of comparison with this prepared phosphor. For instance, Matsuzawa et al., (1996) merely mentions a “very bright and long-lasting phosphorescence” and an “extremely bright and long blue phosphorescence”, which cannot be directly compared to the current research findings.

For luminescent applications such as down-shifting and down-conversion mechanisms, the differences between them are mainly based on the unity of quantum efficiency of the luminescent species applied. Thus, unfortunately, some researchers (Lu et al., 2004). when arguing about a quantum efficiency for the phosphorescent species merely describe it as “high quantum efficiency”, Chang et al., 2006 described it as “a high quantum efficiency, long persistence of phosphorescence, and good stability” which also cannot be compared.
Additionally, when the researcher publishes the syntheses and unity of PLQY results, they cannot be compared either, as there is no standard method, or necessary reference available for phosphorescent species synthesis and characterization. On the contrary, for those prepared as fluorescent species, there is an abundance of research and readily available references which can be found in many different types of standards references.

4.3 Preliminary Tests for Optical Characterization of the LLP Phosphors

The aim of this experiment is to find a reliable method for the optical characterization of the phosphorescent phosphor species. The preliminary analysis was performed with a spectrometer, which has an integration sphere, as described in Section 3.3.1. The phosphorescent phosphor (approx. 200 mesh size (0.075mm) was compressed into tablet form before measuring the transmissions spectra, (see Figure 4.3 below).

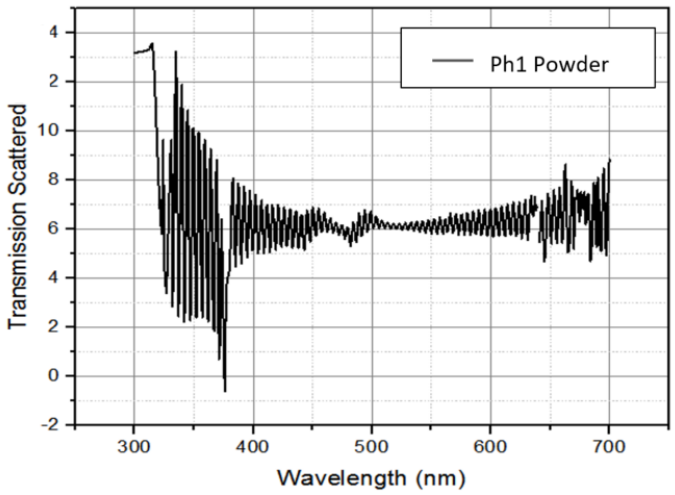

Figure 4.3. Preliminary measurement of the phosphorescent powder with UV/Vis LAMBDA 650 and a 150mm integrating sphere, resulting in significant photometric errors and showing a lot of light scattering.

It was observed that the micrometre sized particles and high emission of light from the phosphorescent phosphor was causing error in the instrument's detector, resulting in significant photometric inaccuracies and a lot of light scattering, as shown in Figure 4.3. Hence it cannot be measured using this instrument by applying the compressed solid. A new attempt was carried out for the purposes of this investigation by trying to dissolve the phosphor species using different types of solvents.

In the attempt to dissolve the phosphor materials, the following different types of solvents (both polar and nonpolar) were tested:

- Distilled water
- Methanol
- Ethanol
- Liquid acetic acid

- Acetone
- Toluene
- Benzene
- Chloroform
- Dimethylformamide (DMF)

It was established that the phosphor species are insoluble in the above solvents, because they are formed by rare-earth metals and exhibit a rigid structure of crystal. Hence, a different approach was needed to perform the optical characterizations of these materials.

After these unsuccessful attempts to obtain the optical characteristics of the phosphorescent species in powder form, a new approach was taken, which was to disperse the phosphor species in a polymer matrix material.

The application of the transparent host polymer material could be used, not just for the characterization of the phosphorous species, but also to develop the luminescent device in a solid layer, that could be subsequently applied to the PV device, as a passive approach to enhance the PV device efficiency, (as described in section 2.3). The next Chapter examines the preparation, production and application of the host polymer materials for the fabrication of the luminescent layers for these optical analyses.

4.4 Conclusion

More time has been allocated to investigating a reliable method which may be used to define a consistent method, to measure the internal and external unity of PLQY of the phosphorescent species. In addition, to define the energy converter mechanisms such as down-conversion or down-shifting, and better describes the application of these phosphors which will be used to enhance the PV device efficiency.

It was possible to identify similar phosphorescent species which had been synthesised and supplied by chemical companies such as Sigma-Aldrich which were used as samples, (see Table 3.2). However, unfortunately, these materials were still not fully characterized, and the unity

of PLQY were specified in the product specifications. Thus, it needed to be measured. For that reason, more attention will be given to the application of these phosphorescent species as luminescent materials to enhance the PV device efficiency. Accordingly, the following Chapter focuses on the examination of the ideal host material and method used to fabricate the host materials, as well as the luminescent layers for the optical characterization process.

CHAPTER 5

OPTIMISATION OF HOST MATERIALS AND FABRICATION OF THE LUMINESCENT LAYERS

5.1 Introduction

This Chapter investigates the ideal host materials and method of syntheses for the fabrication of the luminescent layers using the phosphorescent species. This chapter begins by testing different types of host materials and presenting their optical properties to identify a suitable host material for phosphorescent species. It was observed that an ultra-transparent host polymer matrix from the ultraviolet range (>200nm) is required to allow the Long Persistent Phosphors, LPP, to receive the required energy photons in order to activate its luminescent mechanism.

The synthesis process, degradation and storage methods of the fabricated polymer layer were explored to identify which are most suitable for this research application. All were investigated by testing different parameters in a sequence of analyses.

For the synthesis of the luminescent layers, two methods were tested for the concentration dependency studies. One of the methods, demonstrated by scientific evidence and presented to be more compatible with the scope of this project, was used to produce the luminescent layer for further analysis and applications.

5.2 Identifying A Desired Host Material for Phosphorescent Phosphors

In order to apply the phosphorescent phosphors to the PV device in a passive approach, that is outside of the PV device, the fabrication of a host material in the form of a transparent layer is required. This transparent layer will be used to disperse the LPP phosphor species by forming a luminescent layer that will be attached to the PV device. The main reason for the transparent layer material is that it will allow the maximum amount of energy photons from ultraviolet to the near-infrared (NIR) region. As the phosphorescent phosphors have demonstrated a high absorption in the UV range, it will allow for maximum transmittance in the host material layer without a reduction in the intensity of a light wave propagating through the layer.

Since UV, visible and infrared light are different frequency bands, both luminescent layers and PV devices are photosensitive devices and respond differently across these bands. By combining these properties, it will help them to work to a high-performance level and optimize the chances of any enhancement in efficiency of the PV device.

Another factor considered was the method of the syntheses required for the host material. Research has found that a simple method such as drop casting to produce the layer could help to avoid obstacles, and reduce time and cost, in the fabrication process.

Four different polymer products were tested with the purpose of obtaining a highly transparent layer to compare with those shown in Figure 2.21. The mean value of interest is high transparency in the UV range, and will be used to compare against those presented in the literature, to justify the selection of the best host material for the phosphorescent species and further analysis. As a result, different polymer products were examined including resins, silicone, and polyurethane which required different methods and combinations of mixtures, (see Table 5.1).

- Crystic 2446 Polyester Resin (GRS.LTD)
- Synolite 0328-A-1 Resin (GRS.LTD)
- Crystal Clear-202 (Smooth-on)
- Polysiloxane/Solaris Silicon (Smooth-on)

Some of these polymer materials were not listed in the literature review but were found through this research for suitable LDS host materials which were: inexpensive, easily processed, display UV transparency and UV resistance, and which also present with stability, low viscosity and a refractive index between 1 and 2.

Table 5.1. Different mixing and fabrication methods including; mixtures of parts or adding catalysts, for example:

Polymer Type	Mixing (A: B), ratio)	Adding Catalysts
Crystal Clear 202	100:90	No
Solaris Silicon	1:1	No
Crystic 2446 Polyester Resin	No	Yes
Synolite 0328-A-1 Resin.	No	Yes

The polymer samples were manually mixed for 10 minutes and then placed in a polypropylene mould to cure for 24 hrs and then fabricated into layers as shown in Figure 5.1, see below.

a) b)

Figure 5.1. (a) Host layer of Solaris material in the mould of Polypropylene, and (b) Solaris layer on a microscopy slide for various analyses.

UV-Vis spectroscopy was performed using a Perkin Elmer Lambda 650, (UV/Vis spectrophotometer, as described in Section 3.3.1). The absorbance was calculated from the percentage of transmittance (%T) data using Equation 3.3; Transmission and Absorbance Measurement of Host Materials.

Figure 5.2 shows the transmittance and absorbance of the different blank polymer layers. All the samples were fabricated almost the same size 40x40x1mm. Solaris silicon shows less than 10 absorbance in the UV region which is a great result and more than 90% of light has been transmitted when compared to the other polymers. This makes it a suitable host material candidate for the phosphor material and luminescent layers.

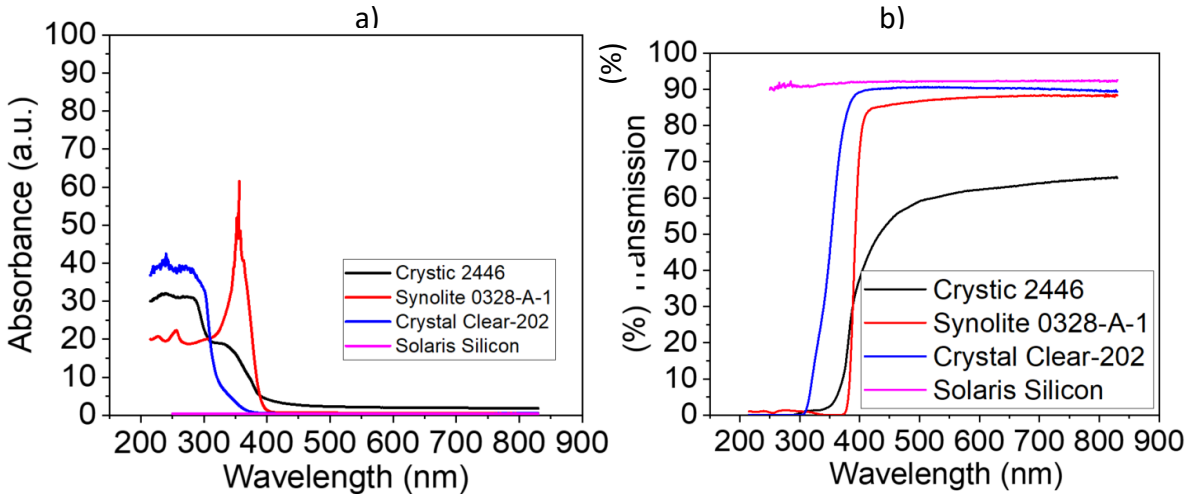

Figure 5.2. (a) Absorbance of the different polymer matrices used in this study and (b) Total transmissions of the different polymer matrices used in this study.

Figure 5.3 shows the transmission spectra for the Solaris layer. The transmission was observed to start at 215 nm and reached up to 95% transmission at 747nm, for a thinner layer of 1-3 mm. Therefore, Solaris Silicon was selected as the host material for the fabrication of the blank layers.

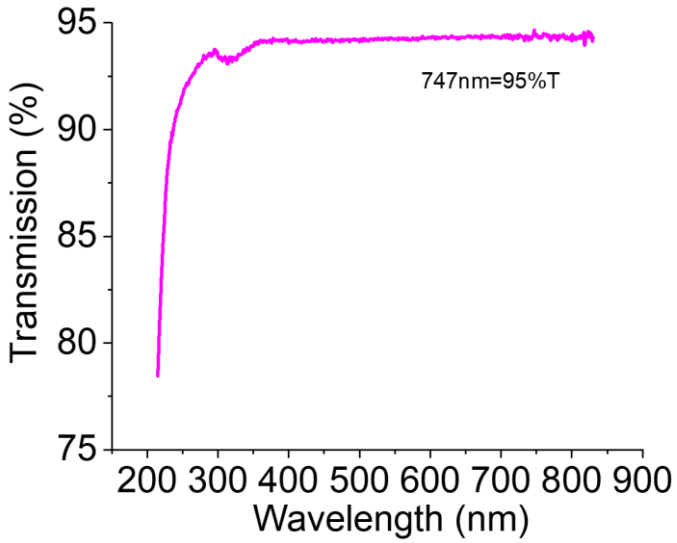

Figure 5.3. Shows the measured transmission spectra for a blank layer of Solaris Silicon, from 215 to 850 nm. A broad increase in transmission is clearly visible.

Apart from Solaris, all other tested polymer materials including those in Figure 5.1 showed transmission values below those present in Figure 2.21. Based on these results, it may be concluded that Solaris Silicon proved to be the best host material among all the tested and reported materials for this application.

Thus, it was possible to identify an ideal host material that can be used to disperse the phosphorescent species by forming a luminescent layer. Using this Polysiloxane material and method, the layer appears to be reproducible, reliable and allows direct mixing of the polymer and the phosphorescent species. In the same manner this host matrix and method can be used for further examinations and to help define a final fabrication technique and method for the production of the luminescent layers.

5.3 Weights and Dimensions Study of Host Polymer Layer

This study was to determine an ideal range of weights, thicknesses and dimensions to determine a reliable approach to producing a host layer of Solaris Silicon polymer. This investigation looked at two aspects, firstly the quality of the produced layers, and secondly exploring the method for the preparation of layers. Criteria such as thickness and reproducibility were used to evaluate the sample layers and their quality, to assure they are all reproducible and reliable under the same method.

In order to identify an ideal weight or thickness for the host material, (which can range from a thin-film to a thicker layer), it was important to consider that the desired thickness must be resistant to multiple tests and analyses (such as concentration dependency), without being damaged during the procedures.

Meanwhile, six different sample layers were produced with various amounts in weight of polymer, varying between 0.1g/mould for volume minimum (v_{min}) and 2.3g/mould for volume maximum (v_{max}), (which is the maximum amount of polymer that can be deposited on the mould). It was also necessary to observe and record the laboratory working conditions such as temperature, light exposure, curing time or any other factor which could affect the samples' reproducibility.

Table 5.2 show the internal dimensions of the 6 moulds used in the fabrication of the sample layers, and the average dimensions of length (46.44), width (25.64) and depth (1.89) mm. The measurement was taken using a Mitutoyo Absolute Digimatic Digital Calliper CD-6 CSX 6 (0-150mm/0.01mm). The mould is made of tough polypropylene and it is rugged and unusually

resistant to many chemical solvents, bases and acids, and so it appears to be an ideal material for this project.

Table 5.2. The mould internal dimensions measurements for 6 different moulds.

Mould	**Length (mm)**	**Width (mm)**	**Depth (mm)**
M1	46.44	25.60	1.90
M2	46.47	25.61	1.89
M3	46.41	25.69	1.88
M4	46.46	25.67	1.90
M5	46.46	25.68	1.90
M6	46.45	25.63	1.91
Average	46.44	25.64	1.89

Table 5.3 shows the dimensions of six fabricated sample layers. It was observed that the thinner the sample layer, the greater the possible error in measurement. For instance, the 0.1g layer has a length of 46.28mm. Comparing it with the 0.2g layer where the length was found to be 46.84mm, resulted in a change of 1.21% in length. This may be caused by the stretching effect created by the removal process or ease of expandability of the layer. However, this error was not found to be significant for a higher weight layer >0.3g.

Table 5.3. Dimension measurements of the fabricated sample layers at varying weights of Solaris Silicon polymer (varying between 0.1 to 2.3g).

Layer	Length (mm)	Width (mm)	Thickness (mm)
Blank E – 0.1g	46.28	25.43	0.41
Blank F – 0.2g	46.84	25.34	0.64
Blank G – 0.3g	46.40	25.55	0.99
Blank H– 0.4g	46.46	25.54	1.15
Blank I -0.5g	46.47	25.57	1.22
Blank J -2.3g	46.48	25.51	1.78
MITUTOYO SERIES 293-832 MDC Lite Micrometer 0-25mm/0.001mm			

Furthermore, the results show that the samples with volumes between 0.1g to 0.2g in weight total were too difficult to remove from the mould. For example, some sample layers of 0.1g were damaged during the removal process and appeared to be too thin, (approximately less than 1mm thick), which was verified using a micrometre, unlike the 0.3g sample layers which could be removed from their moulds. However, there was a high possibility of damage during

the removal or characterization process. Notably, the sample of Solaris Silicon above 1 mm appeared to be mechanically strong enough to be removed safely from its mould and easy to handle during the characterization processes.

As is demonstrated in Figure 5.4, total transmission spectra of the all sample layers at various thicknesses, were measured from between 215 to 850nm. It was observed that there is a small reduction in transmission as the thickness increases. The 0.1g sample layer was damaged during the removal process and it was only possible to measure it with the aid of a sample holder, which caused a significant reduction (by 18%) in the total transmission. The 2.3g sample layer resulted in the poorest total transmission in the range of interest, between 215-400nm. On the contrary, the 0.3g sample layer resulted in the highest transmission of 93% at the 350nm range, (as can be observed in the insert in same Figure). However, this sample layer does not appear to be thick enough and could be too fragile for further analyses. A critical evaluation of the layers containing 0.3g was carried conducted, and reproduced a total of 20 layers with the aim of testing reproducibility and fragility, and to be submitted to the same spectroscopy analysis. This test proved that not all the samples were successfully removed from the mould or instrument's port without being damaged. Indeed, more than 50% of the sample layers were damaged during this process of analysis.

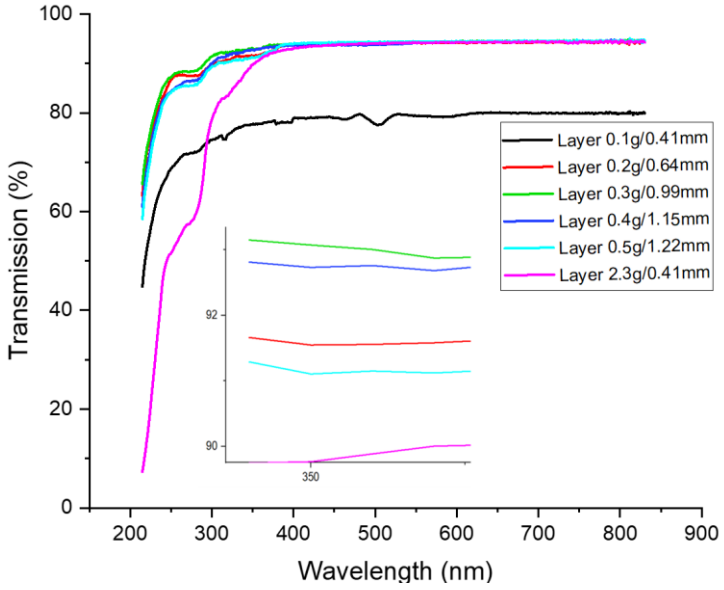

Figure 5.4. Total transmission spectra of the various sample layers at different weights (0.1 to 2.3g) of Solaris silicon. The insert shows zoomed spectra between 89 to 94% at 350nm.

As a result, the second-best sample layer according to the total transmission, (over 92% at 350nm) is the 1.15 mm thickness, which demonstrates as an ideal weight. Thus, the layers of 0.4 g or 1.15mm have shown the most desirable thickness and mechanical strength, which can be characterised without any damage. The weight of 0.4g was then adopted as a standard weight and applied in further layer analysis.

5.4 Optimization of the Host Material Fabrication Process

Subsequent to the identification of the ideal polymer matrix, and its thickness, an optimized method was developed to produce the layer which will be employed to fabricate the luminescent layer, in order to maintain quality and reproducibility. New investigations were carried out to establish the best approach for preparing multiple layers from a single batch of the host matrix, and to try to address the following identified issues:

- The poor manual mixing and pouring which caused trapped air in the host
- Mixing of the host and phosphorescent species may not be uniform
- The host polymer was mixed for 10 minutes in the same container, which is not an ideal process.
- Difficulty with the application of traditional Drop Casting or Lay-Up methods on the mould, (too much waste considering the small amount per layer)
- The polymer was not curing properly at room temperature
- It was difficult to weigh a precise amount of material

Due to the above issues, the new approach was investigated as a means of improving and addressing the issues wherever possible, as described in the following paragraphs:
After dispensing the required amounts of Solaris Silicon, Parts A and B into a container (1:1, by volume), it was mixed thoroughly using a magnetic stirrer at 30°C, at a speed of 250 rpm for 3 minutes. Then, the mixed parts were emptied into a second container, and mixed again for another 3 minutes. This process was repeated for a third time, into a third container and mixed for another 3 minutes. After the stirring, a total mass of 0.4 g of host material was poured into the mould for curing. The samples were placed on a level surface at room temperature to rest

for 30 minutes. After that the sample layers were placed in the incubator at 50 °C (Digital incubators, INCU-Line®, IL 10) to completely cure.

The curing process was completed using a microbiological incubator (see Figure 5.5, Digital incubators, INCU-Line®, IL 10). This instrument has Digital PID control with a PT100 sensor and LED display, temperature control which can be readjusted with a certified reference, excellent temperature stability, is easy to use, and is safe and reliable. It has a digital PID temperature control which can be freely adjusted in increments of 0.1°C up to a maximum of 70 °C and thermally insulated. The time of curing, and temperature of the incubator, were adjusted a number of times to achieve the best outcome.

Figure 5.5. Digital incubators, INCU-Line®, IL 10.

The new method was used to produce 5 batches of mixing; each batch consisted of five sample layers. All the layers were characterized following 24hr of the fabrication process and placed on a glass substrate (as shown in Figure 5.1). The characterization process was carried out using a Perkin Elmer Lambda 650 to measure the total transmission (UV/Vis spectrophotometer with integrating sphere 150 mm, as described in section 3.3.1).

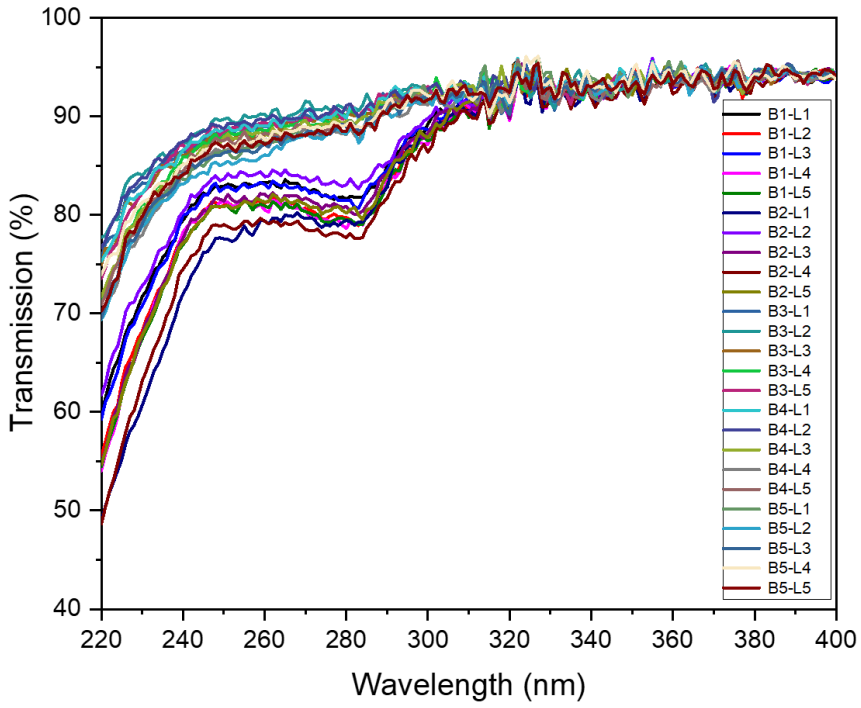

Figure 5.6. Total Transmission spectra measurement of five different batches of sample layers at 1.15mm thick, where B is Batch number and L is sample layer number

Figure 5.6 shows the measurements of the total transmission of the five batches, B1-5, and their respective sample layers, L1-5. It was observed that all sample layers have similar characteristics such as physically uniform composition and are reliable, but it resulted in an unexpected reduction of about 20% in the total transmission from 215 to 280nm for a total of 40% of all the sample layers measured. This reduction effect does not have an apparent reason because they were all prepared in the same way and measured in the same manner.

The production process where the samples are exposed to UV light, ambient temperature, mixing processes and many other effects, can result in poor uniformity of the samples and may cause instability and a polymerization effect in the total transmission of the samples.

The calculated absorbance spectra showing the layer had an undesirable discrepancy effect around 280nm that could be caused by the polymerization or degradation of the polymer, or the method used. As can be observed, the absorbance of 10 different layers was increased from 240 to 280nm. This discrepancy effect needs to be reviewed together with the establishing of the background correction for the host sample layer. This analysis is presented in the next section.

5.5 Establishing Background Correction

Attention was focused on determining the 'corrected' transmission and absorptance spectra of the host material by establishing a standard sample layer profile to avoid any undesirable inconsistencies during the analysis. The first step in this experiment was to verify if the discrepancy in the transmission spectra was caused by polymerization or degradation of the Solaris Layers, or whether it was the result of any other external factor.

With these considerations, a total of three new batches of sample layers were prepared by taking note of the following parameters after the mixing; the time of resting, exposure to the ambient light and ambient temperature, and aging for the characterisation.

The process of characterisation of the layer occurred 24 hours after the fabrication process and was carried out in the same manner as presented in section 5.4. Figure 5.7 shows the total transmission spectra of the 3 batches, B6-8, with three samples layers each, L1-3. The total transmission average spectrum was calculated and presented in Figure 5.7 below.

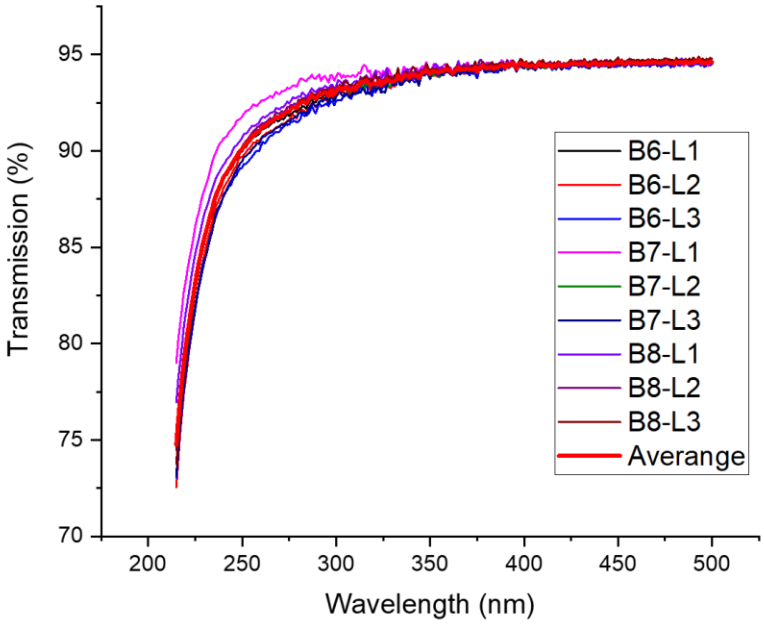

Figure 5.7. Total Transmission spectra of batches 6-8 with 3 sample layers each. The average spectra were calculated and displaying in the graph.

The spectroscopic analysis results indicated that with the new batches it was possible to reach good results, and that the shortages in the total transmission do not appear within 24 hours

of aging, or after the fabrication process. The transmission spectra demonstrated that all layers were measured with very consistently results across the entire spectral range. Despite the UV transmittance variation obtained for each layer, these results are consistent with the three different batches tested. Based on this evidence, it was possible to assume that the production process was causing the variation and not the polymer material as shown in the earlier batches (1-5), as discussed above.

Acknowledging the importance of establishing the optimum fabrication process parameters, it is recognised that they could help to control the inconsistent effects of instability or polymerization with ageing, beyond a 24hr period. Thus, two main parameters of fabrication were reviewed: resting time and exposure to ambient light. By testing these two parameters, we could avoid excess resting time during the polymer synthesis on the moulds and excess exposition of polymer material to the ambient light before and during the mixing process.
For the resting time parameter, tests were carried out to evaluate the total time needed for the fabricated layer to be put aside for resting, under light cover protection and before being transferred to the incubator.

Batch 9 was prepared to produce 6 layers of the host polymer without exposure to ambient light using a light protector cover during the curing time period. At five-minute intervals, a layer was removed from the resting time and transferred to the incubator, where they were kept for 24hrs for the curing process. The sample layers were measured for a period of 30 days after the first 24-hour measurement, Day 1.

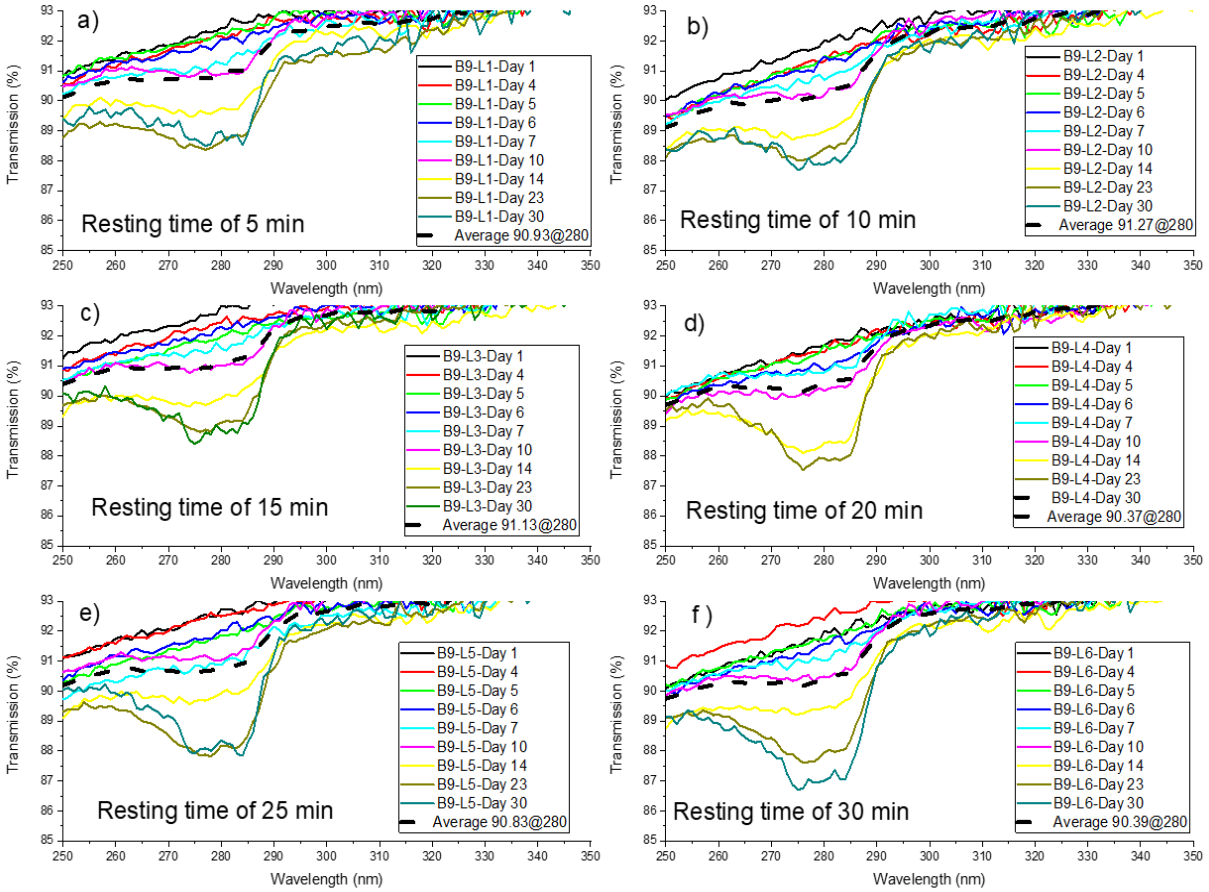

Figure 5.8. Time series analyses of the transmission measurement for Batch 9 and for all layers, with different resting times. The measurement analyses were taken from Day 1 to Day 30. Average spectra were calculated at the critical point of interest (280nm, and illustrated by a black dashed line, with calculated values for each).

Each of the layers on Figure 5.8 were plotted separately to compare their instability over the 30-day period. As can be observed, there is a common trend among all of them, the instability increased with age and showed a critical rating at 280nm. A significant variation in the transmittance were clearly observed after Day 7, where a 5% difference between Day 1 to Day 30 was established.

To analyse this data, the average values for each graph were calculated at the critical point (280nm) on each of the nine curves, and they are represented by a black dash line. It can be observed that Graph D shows less variation, with 90.37% at 280 wavelength range. In addition, on graph D, the curves appear to be more consistent and show that there is less variation at the critical point (280nm) than among all other graphs. With such a result, we have now

uncovered some evidence to merit the reproduction of more batches with 20 minutes of resting time, and can therefore test a new hypothesis, to determine if this can help to reduce the instability with aging.

In order to prove this hypothesis, another batch (batch 10) was produced with a resting time of 20 minutes, where all other parameters remained unchanged. This verification was necessary because it important to reach consistency in the obtained results with aging, which could represent a better profile for the host materials and subsequently the blank sample layer.

Figure 5.9. shows transmission spectra above 90% for all batches (batches 10-13) with a total of 3 layers in each batch and a curing time of 20 minutes, measured after 24 hours (Day 1) of production. Interestingly, initially all the batches appear to have the same transmission characteristics with 1.1% of difference between them, as can be observed in the insert.

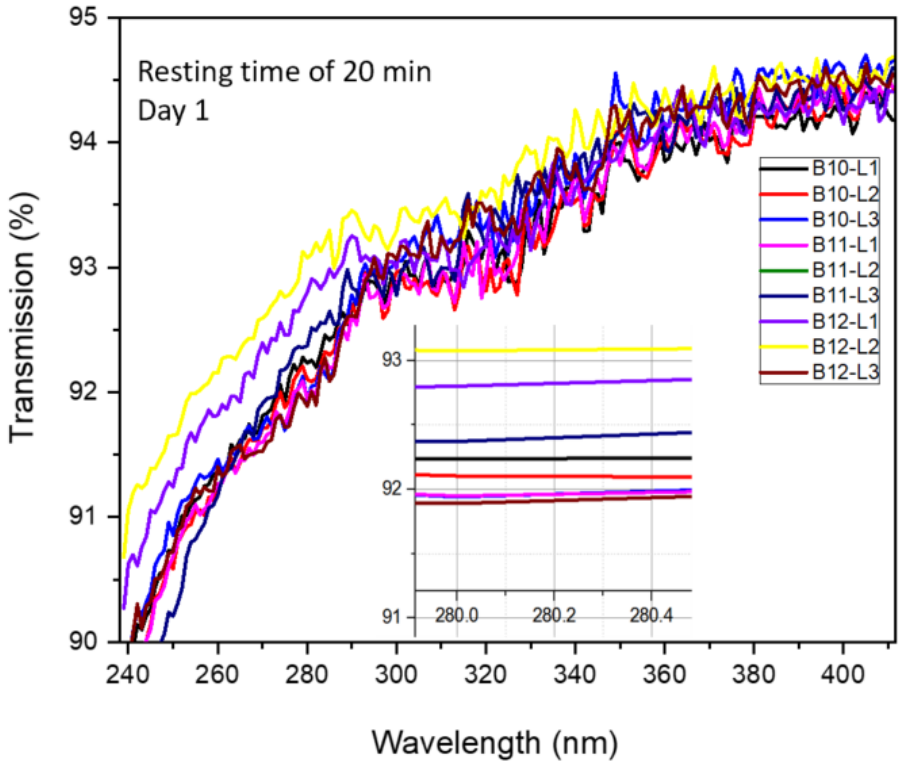

Figure 5.9. Total transmission of batches 10-12 with total of 3 layers in each batch, with a resting time of 20 minutes, measured on Day 1 after the fabrication. The insert shows the zoomed transmission at around 280nm.

As expected, it was found that the all three batches of the layer produced are fairly similar in their transmission, and for that reason only one of these three batches, B11, was selected for the time series analyses of the transmission measurement, during a maximum of thirty days. The measurements of the layers from this batch were plotted separately to compare their instability over the 30-day period, (see Figure 5.10).

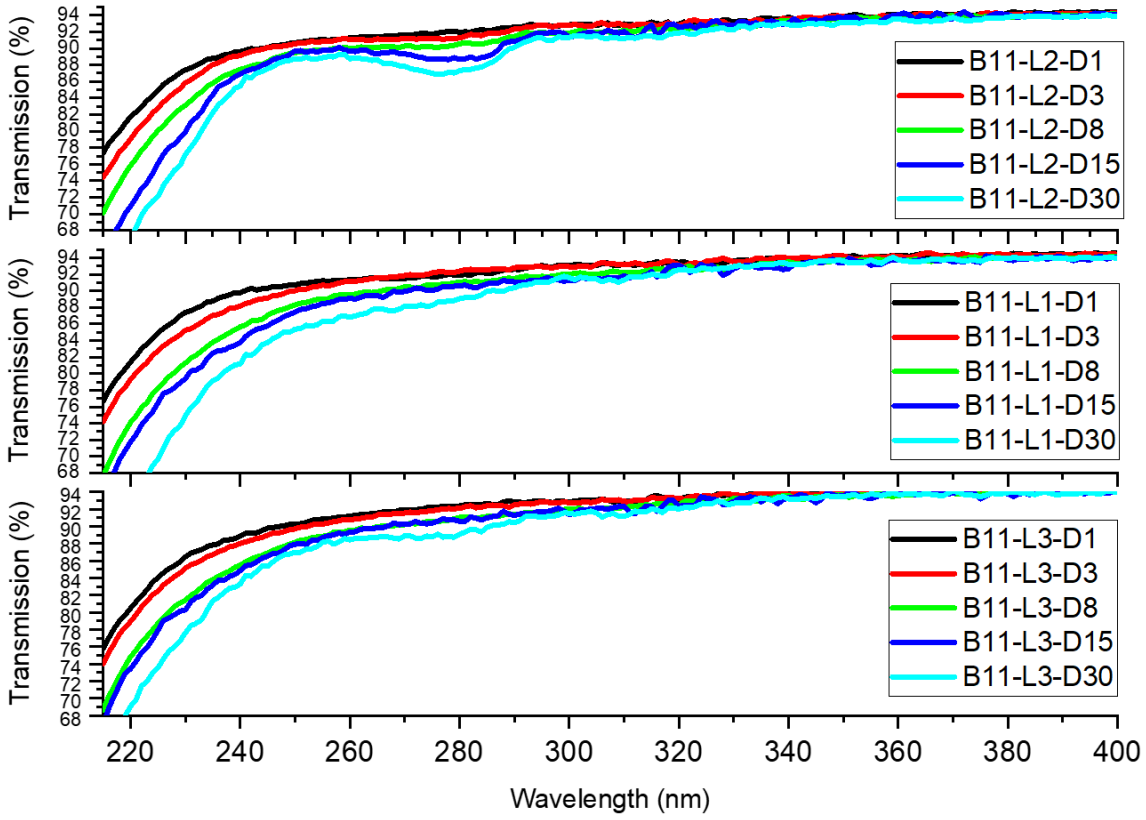

Figure 5.10. Change in UV–Vis light transmission spectra of batch 11 of all layers after production with 20 minutes of resting time, measured between Day 1 and Day 30.

As can be observed there are some similarities between Layers 2 and 3, and they appear to be more stable, showing a small variation at the critical point, 280nm, which was the main point of interest. On the other hand, Layer 1 appears to be less stable at 280nm, particularly between Day 8 and Day 30. With this hypothesis, it was possible to reach some improvement in the produced layers thus leading us to identify an improved production method. It also suggested that there might be no need to improve the layer optical result which was considered during a short-term analysis, between Day 1 and Day 8. This was because the critical effect at 280nm only appears on the first layer, leading the researcher to believe that the problem may be caused during the preparation process. Once these tests and hypotheses

were completed, it was possible to establish the background correction for the host material and blank samples layer without the appearance of the critical point at 280nm over a short-time period, (8 days).

This experiment shows that the host material layers have the same chemical instability over a longer-term period which resulted in a small variation (around 5%) in the transmission at 280nm, which may be characteristic of the material properties. The most uniform stability in transmission at the critical point was observed for sample Layer 3 which is about 3.85% for a period of 30 days. However, this reduction can be observed in the ultraviolet range from 220 to 340nm only. In order to define the stability of the host material it is important to investigate the instability of different ambient conditions for a longer period, by maintaining these same parameters.

5.6 Transmission Stability and Degradation of Blank Layers

This experiment aims to test the instability caused in total transmission of the host polymer layers, and to establish how the storage methods affect them. Degradation is considered to be a process that occurs in all types of polymers whether it is called a degradable or non-degradable polymer. The distinction between degradable and non-degradable polymers has not yet been fully established in the literature, as all polymers degrade (Göpferich, 1996). It was observed in the last experiment, that the host material in question has shown some unstable reactions which occur during the characterization process and which may be caused by the time that the Solaris layers are subjected to light, heat, oxygen, mechanical stress, or other types of degradation. The mechanisms of these reactions and stabilisation processes must be understood in order to develop the passive luminescent conversion layers such as DS, and DC. Also, they aim to produce a prolonged photostable layer designed to last during the extended periods of the PV device.

Degradation data was obtained by investigating the storage method of the fabricated layers. The layers were tested under different storage conditions. Three new batches, B13-15, were produced and kept indoors according to different storage conditions; inside of an incubator at

50^{o}C, at room temperature in the dark, and ambient light. The layers were characterized for a period between 4-15 days. The analyses were performed measuring transmission as a preliminary analysis, and then subsequently changing to infrared spectroscopy.

The degradation effect in the host layers has been carefully identified. During the production of layers, it was observed that this instability may start before the mixing process and continue after the layer has been produced. The degradation rate of polymers may be reduced in a controlled way using different storage methods and avoiding the ambient light during the premixing, so that polymer layers tend to degrade more slowly.

Figure 5.11 shows the total transmission of batches 13-15 produced with three layers each, L1-3, using the previously defined parameters. To optimise the analysis of the storage conditions, one layer of each batch was stored in a different place. Layer 1; an incubator at 50^{o}C, Layer 2 at room temperature in the dark and Layer 3, at room temperature under light conditions.

The Layers were plotted separately to compare the instability over time during a period of 15 days. As can be observed the curves are very similar and appear to be more stable across all spectra range and show only a slight reduction in the total transmission around the critical point, 280nm. The transmission for the three storage conditions is shown in the table above.

The summary of the calculations for the time series analyses of the transmission measurements, at the critical point of 280nm for batches 13-15, with each layer being stored under different conditions, is shown in Table 5.4.

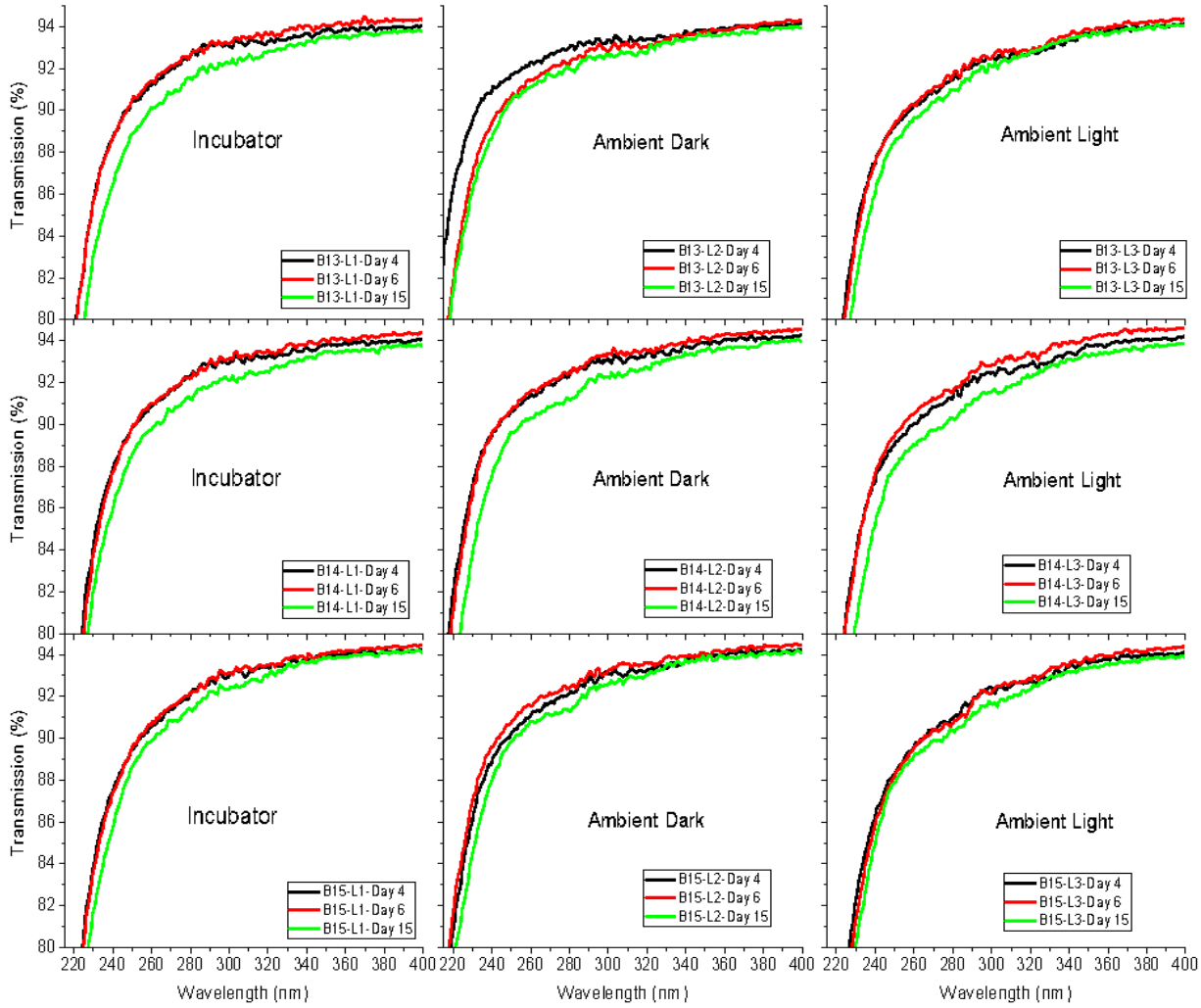

Figure 5.11. Change in UV–Vis light transmission spectra measurements for Batches 13-15 with each layer stored under different conditions, Layer 1s- incubator at 50°C, Layer 2s ambient dark and Layer 3s- ambient light at room temperature, samples measured between Days 4 and 15.

As can be observed, the highest percentage of transmission for the three different conditions is ambient temperature in the dark with 33.48, 33.46 and 33.49% for all batches. Thus, the results show that by storing the layers at the ambient temperature and in the dark helps to maintain the highest transmission at the critical point, 280nm. On the contrary, exposing the recently fabricated layers under light conditions decreases the transmission at the critical point, 280nm, and was also found to create the lowest percentages of 33.10, 33.12 and 33.04% among all three batches.

Table 5.4. Summary table of calculation of the changes in UV–Vis light transmission spectra measurements at the critical point of 280nm for batches 13-15, with each layer stored under different conditions.

Layer ID	Storage Condition	Day 4	Day 6	Day 15	Average	Min	Max	Percentage (%)
B13L1	Incubator 50 °C	92.50	92.55	91.51	92.19	91.51	92.55	33.41
B13L2	Ambient/Dark	92.98	92.18	91.97	92.38	91.97	92.98	33.48
B13L3	Ambient/Light	91.44	91.57	90.97	91.33	90.97	91.57	33.10
B14L1	Incubator 50 °C	92.21	92.12	91.22	91.85	91.22	92.21	33.42
B14L2	Ambient/Dark	92.25	92.46	91.14	91.95	91.14	92.46	33.46
B14L3	Ambient/Light	91.22	91.51	90.28	91.00	90.28	91.51	33.12
B15L1	Incubator 50 °C	92.01	92.12	91.40	91.84	91.40	92.12	33.47
B15L2	Ambient/Dark	92.09	92.38	91.27	91.91	91.27	92.38	33.49
B15L3	Ambient/Light	90.97	90.68	90.37	90.67	90.37	90.97	33.04

On the whole, the results show that the host materials react differently according to the ambient conditions, and independent of the fabrication process. Furthermore, monitoring the best storage methods over a longer period could help to define the percentage of the concentration ratio and profile in this host material.

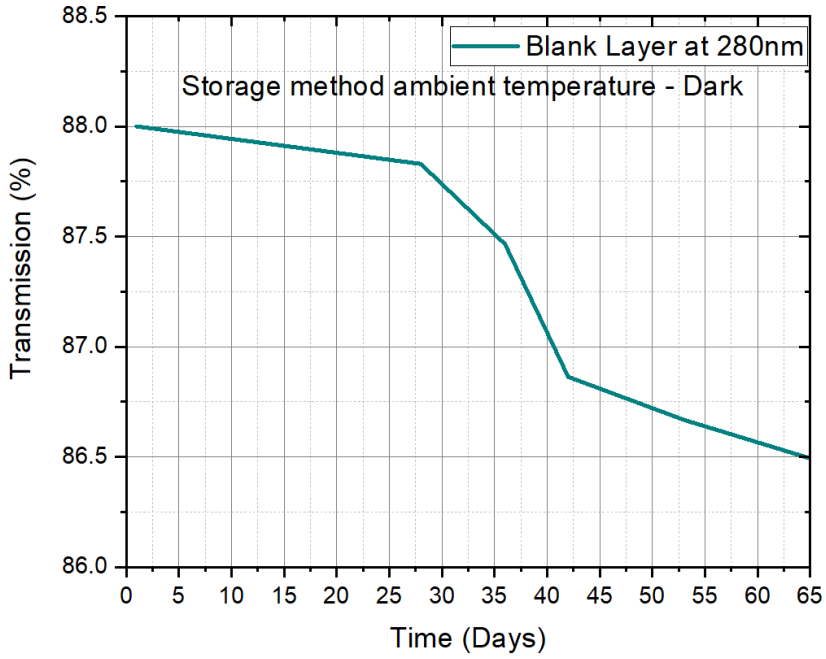

Figure 5.12. Shows the long-term effect in the transmission instability of the layer produced, at the critical point of 280nm, with storage in the dark at room temperature. The sample was measured between Day 1 and Day 65.

Figure 5.12 shows that there was some instability on this polymer causing variation of the transmission, although the size and shape of the layer remained apparently constant for a considerable period of time, (considering the reduction of less than 1.5% in the transmission for the critical wavelength, at 280nm, and the polymer layer was prepared for transmission over a total of a 65 days period). Thus, the final production process resulted in a more uniform photostability over the extended period of 65 days. In analysing this data, the yearly decrement rate for this indicator is 8.42% per 365 days at this critical point.

Infrared Spectroscopy – FTIR

The infrared spectroscopy was used to collect information to analyse instability, degradation and polymerization molecules through identification of basic structural components. A Fourier Transform Infrared (FTIR) spectrometer was used for the analysis of the host polymer layers. This FTIR technique allows the detection of traces and the deformation of polymers on the produced layers that could be verified between 4000–500 cm^{-1} (2500–20,000 nm) range.
This analysis was carried out with a new sample batch, B1F, with four different layers, L1-4, where the thickness range was less than 0.5mm. The sample layers were all produced using the optimised method described in the previous sections. The FTIR data are shown in Figure 5.13.

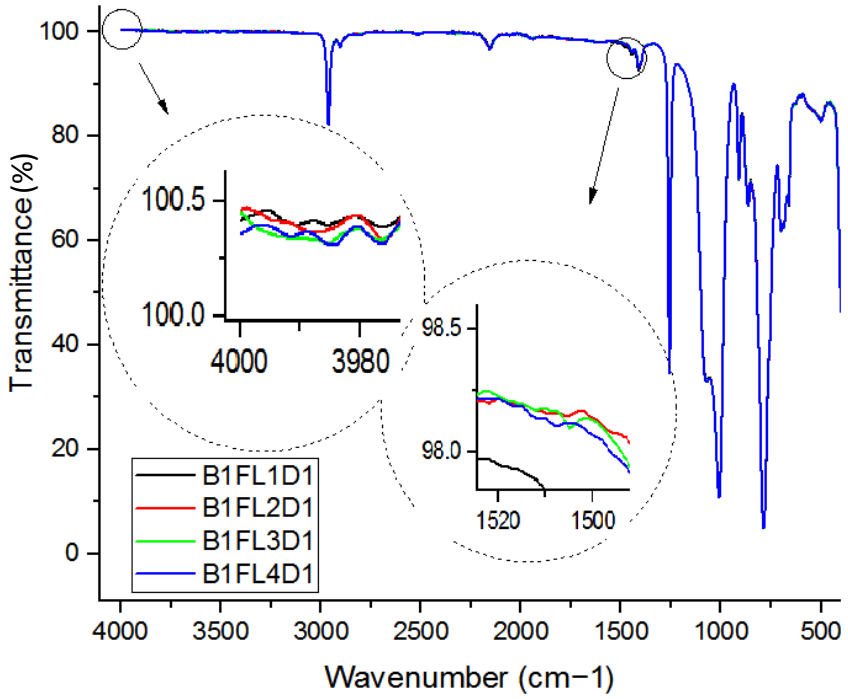

Figure 5.13. Fourier transform IR spectra of Batch B1F Layers 1-4, storage; dark at room temperature, measured on Day 1 of the fabrication.

It can be seen from Figure 5.13 that the FTIR spectra of the different layers do not show significant effect on the variation rate of light transmission between them. The amount of light transmittance variation at representative ranges are presented in the zoomed ranges, 400-3980 and 1520-1500cm^{-1}, which are about 0.125 to 0.25%. The experimental transmittance curves of light transmission show good agreement; the period in which layers were produced lasted 24h; the variation between them are insignificant and it did not appear necessary to repeat this analysis for all of them.

Layer 2 (B1FL2D1) was used as a reference of known composition and was examined by infrared spectroscopy to obtain a base data against unknowns, instability or degradation, and so could be compared, (see Figure 5.14).

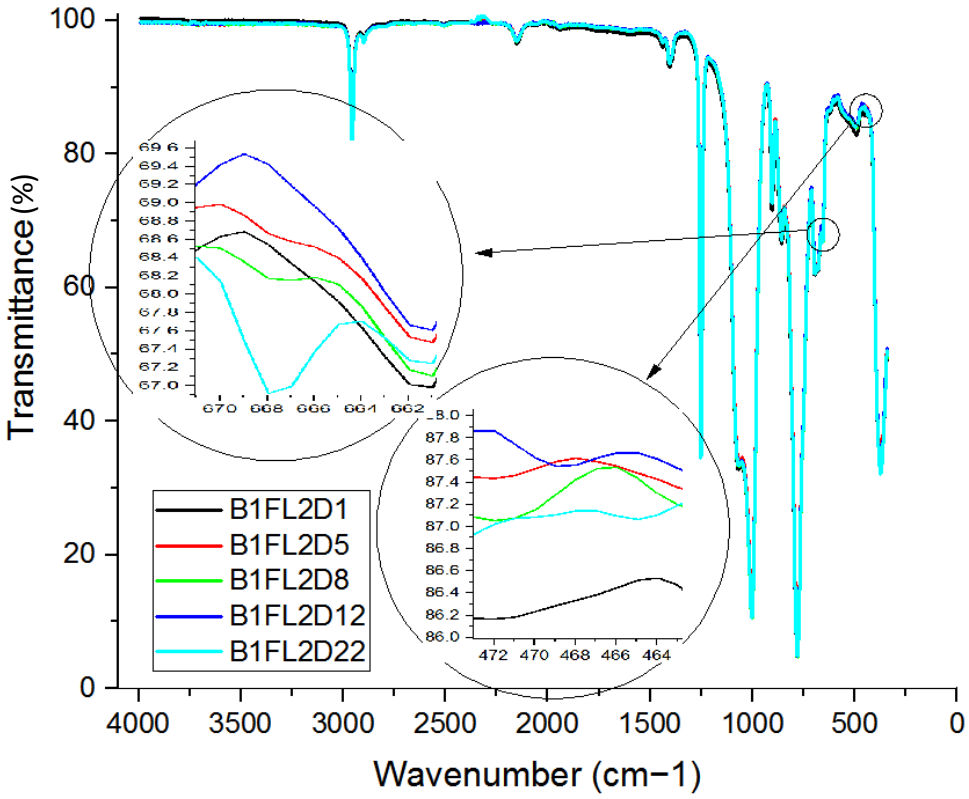

Figure 5.14. Fourier transform IR spectra recorded of the sample Layer 2, dark storage at ambient temperature, measured between Days 1-22.

The infrared spectra of these sample layers do not change substantially over the time period of 1-22 days. A slight loss of resolution is often observed, but the transmission and intensities remain almost constant. The multiple measurements of Layer 2 of the sample layer can be readily distinguished from 1-22 days, and the maximum difference in the peak is 2.5%, in the region of 674 to 669 cm^{-1}. To justify this instability, or to distinguish between the natural aging processes of host material can be difficult, especially if the sample has a small instability or is "contaminated" with other unknown substances such as impurities. Unfortunately, there is no available literature which compares the FTIR peaks. As shown in Figure 5.14, the spectrum of these two peaks at 668 and 472cm^{-1} are much more intense than the rest of the entire spectrum.

The displayed results cannot be discussed without a full review of the literature involved such as the Polymer Additives Spectra Database, (P/N 50002, 1.273 KBr& Liquid Film spectra of polymers, plastics and polymer additives). At the time of writing, this manner of database is

not yet available to the college. Therefore, we shall overview the behaviour of the host material with the luminescent application device. Aging does not appear to be a significant problem in the visible range of interest, where the phosphorescent materials emit their energy photons.

We conclude that UV-Visible spectroscopy can be used as a simple and reliable method for monitoring the stability of these polymer layers. As the instability occurs or destabilizes, the original peak will decrease with small changes in the optical properties due to the aging of the host material, Solaris Silicon.

These studies concluded that this last method of fabrication and storage of the sample layer, can be used as a standard method for the blank and luminescent sample layers. By using the UV/Visible spectroscopy as a characterization technique, this will provide information on whether the luminescent layer has destabilized over the time period and can be compared with these finds. However, this does not appear to be a problem in the luminescent application conception because these results demonstrated high transmission >90%, and low absorbance from the visible spectrum region >400nm, which is the most important requirement for this project application.

5.7 Index of Refraction of Host Material

The purpose of this experiment was to calculate optical constants of layer variation of the index of refraction versus wavelength or dispersion curve of the fabricated layer of the host material, Solaris Silicon. The Solaris product specification states that the selected host material has a Refractive Index of 1.41nm (ASTM-D1218) (see Appendix A for more details).

The host material is an ultra-transparent material between the UV and infrared spectrum and has high light transmittance characteristics, plus it is shown to be free from haze. Calculating the refractive index of the host material and its propagation within the layers helps to verify variation, and stimulate further analysis such as interactions of luminescent materials in the layers.

The computer program, PARAV, was used for calculating optical constants of layer, such as the dispersion of the refractive index, the optical absorption coefficient, optical thickness and optical bandgap from the measured UV-VIS sample data, and also transmission spectra (yaroslav, n.d.), (See Appendix C for more details about the calculated optical properties of the layer).

Figure 5.15 shows a Tauc plot of the host polymer Layer fabricated with Solaris Silicon. It was used to determine the practical optical properties of the host layer plus the linear region to evaluate the band-gap at the x-axis, (here about 3.9 eV).

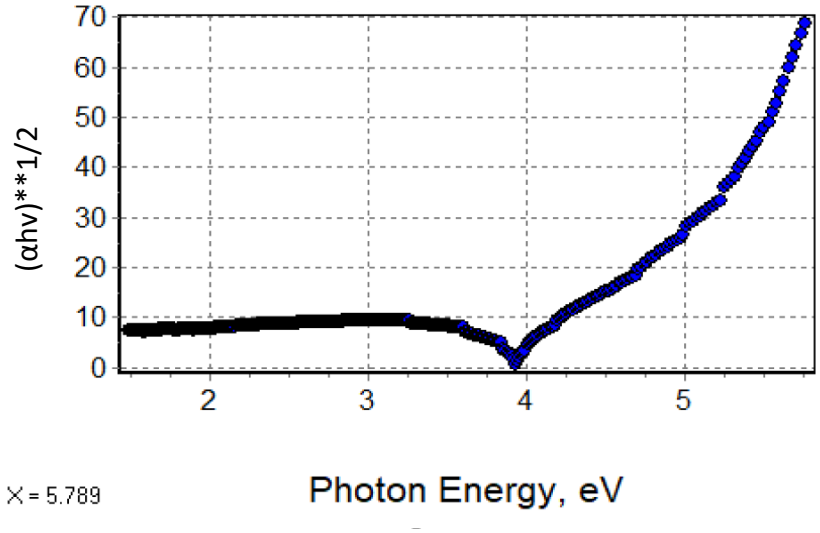

Figure 5.15. Tauc Plot from UV-VIS analysis of the host polymer layer fabricated with Solaris Silicon.

5.8 Defining Methods for Fabrication of the Luminescent Layers

A critical and comprehensive investigation of the various methods for the production and characterization of the luminescent layers doped with Long Persistent Phosphors (LPP), has been undertaken. Emphasis has been placed on the study of phosphor species concentration dependency in the layers. The LPP phosphors species are listed in Table 3.2.

The two methods used to prepare the luminescent layers containing the phosphorescent materials are weight and volume dependency. Method 1, utilises weight dependency studies which are used to measure each individual luminescence layer. Method 2 categorises the

amount of volume used to produce each individual luminescent layer for the device application.

The fabricated layers were characterized using the transmission and absorption measurement. Although the emphasis is on the qualitative methods of measuring the transmission, for completeness quantitative methods have also been used to help verify the saturation curve of the LPP. Both methods may not provide absolute saturation values of the luminescent layer, but they can be useful to investigate relative selections. In order to identify an ideal concentration of phosphor species a ratio of 1.25:1 per layer was applied, then 1.25 part of phosphors is mixed with one part of host material, or 0.5g phosphors is mixed with 0.4ml of polymer at 100wt%.

Method 1 - Weighing Method

This is a weighing method that was established for the fabrication of the luminescent layers in order to carry out the phosphor concentration dependence study. It considers the weighing of each produced layer containing the luminescent material of different concentrations. The required amount of LPP material was added to part A and B of the host polymer and then the standard fabrication process was applied. The initial LPP concentrations varied from 0.1-80% weight total (wt.).

Method 2 - Constant Volume

This is a constant volume method that was established for the fabrication of the luminescent layers using a volume total of 0.4 ml for each layer, thus carrying out the phosphor concentration dependence study. In addition, the advantage of this method is that the layer thickness remains constant, which is very important in terms of layer consistency.

The required amount of LPP materials was added to part A and B of the host polymer and then the standard fabrication process was applied. The concentrations varied from 1 - 70%wt.

Total transmission measurements of the luminescent layers were carried out after 24 hours, (Day 1), of fabrication, using a Perkin Elmer Lambda 650, UV/Vis spectrophotometer with integrating sphere 150 mm, in the range of 215-850nm and at room temperature, as described in section 3.3.1. The solid layers such as these luminescent layers, have various optical phenomena involved e.g. reflectance, scattering, diffusion, transmittance, and absorbance.

Overall transmittance, i.e. direct transmittance plus diffuse transmittance (including any deviation of the beam) can only be measured using the integrating sphere.

The emission measurements of the samples were performed after 48 hours of the production using a Horiba spectrofluorometer FluoroMax-4 & FluoroMax-4 p, (as described in section 3.3.2).

Method 1 Results

Figures 5.16 and 5.17 show the total transmission and absorptance spectra of the Phosphorescent Ph1 at various concentration ratios between 0.1-80%wt.

The total transmission shows that the luminescent layers increase to a concentration of 70%wt and then it remains fairly constant. 70%wt appears to be the point of maximum concentration, the saturation point for the phosphor Ph1, and the absorption range of the luminescent layers at this measure is between 200-450nm. As a result, the total transmission spectra measurement is above 70%wt concentration ratio which can be a problem because of the saturation level. However, for other measurements such as lifetime decay and quantum efficiency, these high concentration layers could be ideal and well suited for the current application.

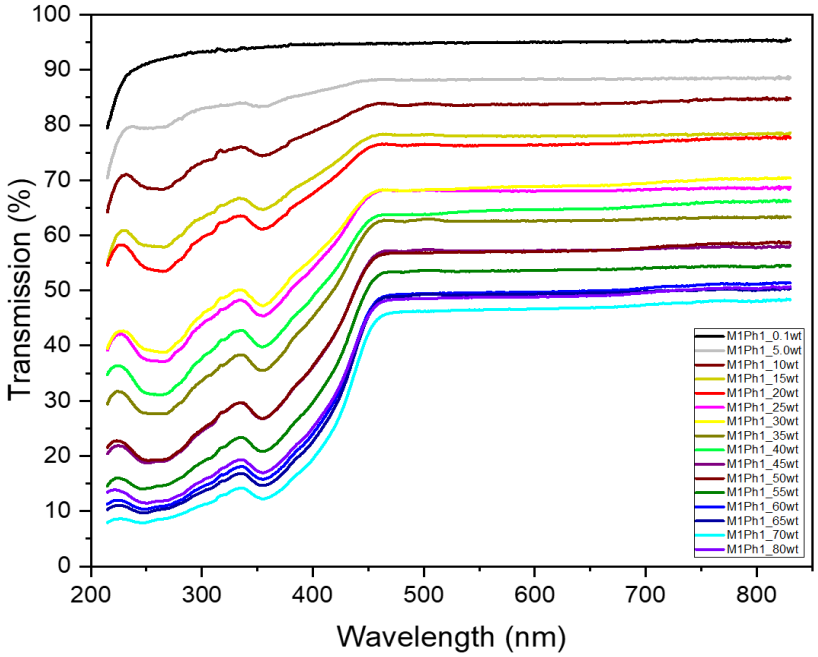

Figure 5.16. Total transmission spectra of the luminescent layers of phosphor (Ph1) fabricated with Method 1 (M1) at various concentration ratios; 0.1-80%wt.

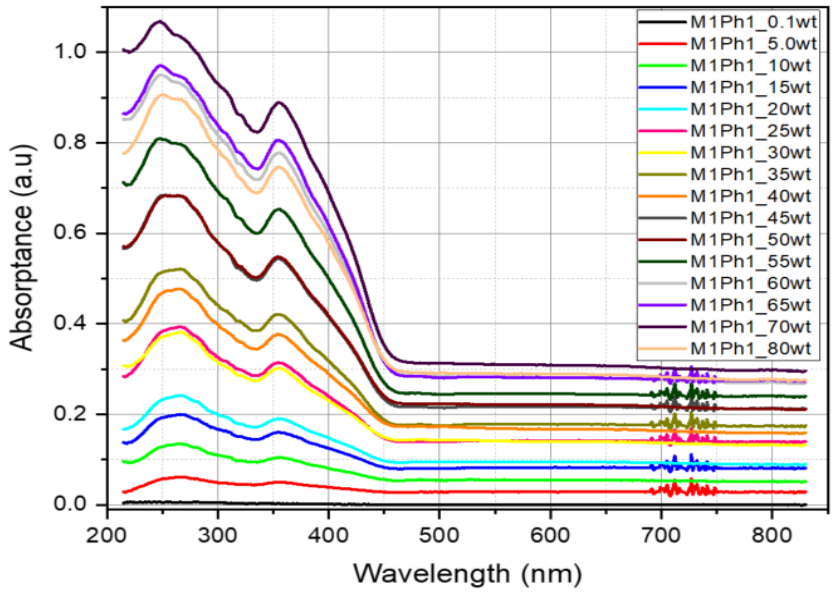

Figure 5.17. Absorptance spectra of the luminescent layers of phosphor Ph1 fabricated with Method 1 at various concentration ratios; 0.1-80%wt.

Figure 5.18, shows the emission spectra of the luminescent sample layers Ph1, produced by Method 1 of varying concentration ratio (0.1-80%wt). The maximum luminescence spectra were reached with a concentration of 60%wt at $1.2x10^9$ kcps, under excitation of 375nm. The emission peak positions are constant for all curves; however, the graph shows the changes of peak intensities. All the samples are excited with pulsed light at 375nm and the emitted phosphorescence is measured using an R928P photon-counting detector. The counting efficiency is determined by the quantum efficiency and any type losses that are present in the layers. The number of photons were measured per unit time or photon flux (count per second-CPS).

The measurements were taken under the same operating conditions for both Methods. Accordingly, Method 1 shows some significant intensity variations that could be caused by the saturation effect or thickness variation used in the experiment. Thus, comparing the intensities changes with the concentration ratio of Ph1, of 60%wt. appears to be ideal. The emission and absorption measurements show that this LPP appears to be a suitable candidate for the luminescent layer as the emission peak remains at a desired emission range, exhibiting a strong peak centred at 480nm. It is however important to note there is no need to subtract the background because 'background' is present in all of the measurements and this can be reviewed in further data analysis.

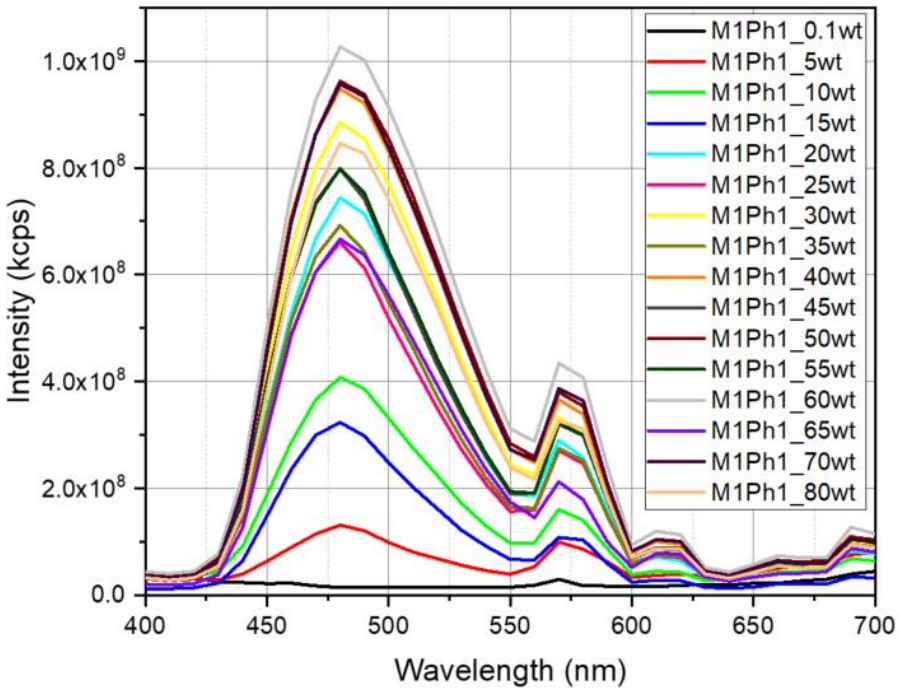

Figure 5.18. Emission spectra of luminescent layers phosphor Ph1 fabricated with Method 1 at various concentration ratios; 0.1-80%wt.

Method 1 results show that there are variations in thickness as it is inversely proportional to weight. A relationship between two variables in thickness and weight, in which the product or concentration is a constant, may lead to error. This is because when one variable increases the other decreases in proportion so that the product is unchanged, but the thickness does change and the layers get thinner within the higher concentration. Consequently, the optical properties measured such as transmission, absorptance and emission, will show a significant inconsistency because of the thickness changing.

Method 2 Results

The optimised method will be discussed here, with Figures 5.19 and 5.20 showing the total transmission and absorptance spectra of the luminescent phosphors Ph1, sample layers, at various concentration ratios between 0.1-70%wt.

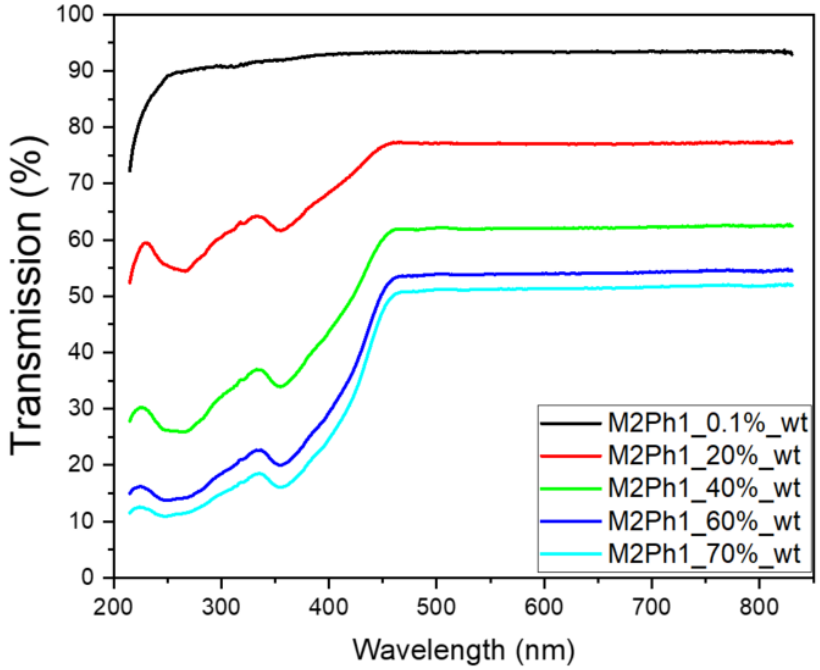

Figure 5.19. Total transmission spectra of luminescent layers phosphor Ph1 fabricated with Method 2 at various concentration ratios; 0.1-70%wt.

It was observed that the transmission increases up to 70%wt of LPP and above that concentration it remains fairly constant, in a similar manner to Method 1. This indicates the saturation concentration of LPP in the layers. To the best of our knowledge this is the first large-scale investigation of LPP concentration dependent analysis for phosphor Ph1. While our results do not exclude an additional effect of this 20%wt gap, independent of the accompanying change in lower concentration, we did not find such an effect within the concentration below 60%wt. This solely occurs when the concentration above 70%wt is plotted and the saturation curves are superimposed.

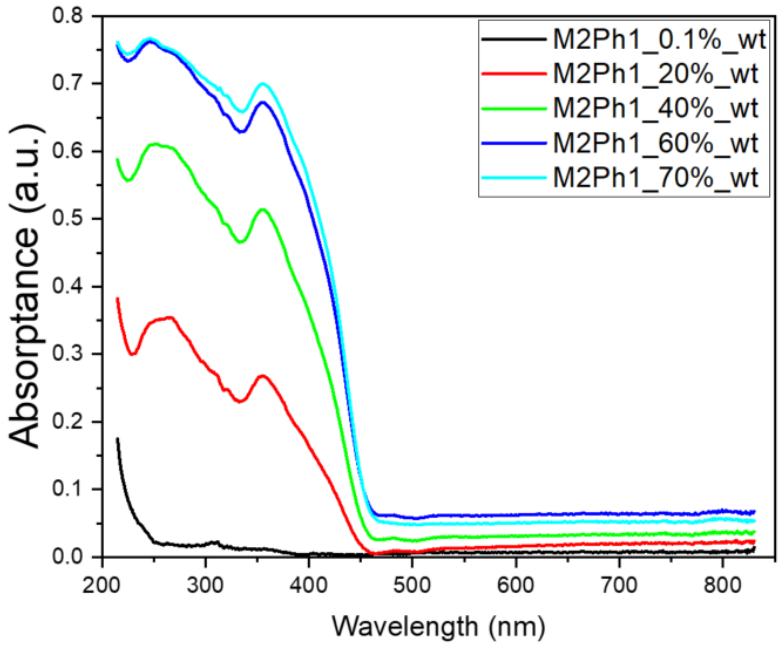

Figure 5.20. Absorptance spectra of luminescent layers of phosphor Ph1 fabricated with Method 2 at various concentration ratios; 0.1-70%wt.

Emission measurements were obtained and presented in Figure 5.21, where layers were excited at 375 nm. A maximum emission peak was observed at 480 nm and another small peak at 570 nm which is in accordance with Method 1. However, the intensity of luminescence curves for LPP Ph1 Method 2 differ from those observed for Method 1. In Method 2, the luminescence intensity increases in concentration and reaches a maximum point at 70%wt. It is not clear yet whether the differences between the luminescence intensities from Method 1 and Method 2 arise from the difference in layer concentrations or whether it is simply due to differences in sample thickness.

However, this experiment does not aim to determine whether or not the observed spectral differences between the intensities in Method 1 and Method 2 are due to the effect of different sample thicknesses.

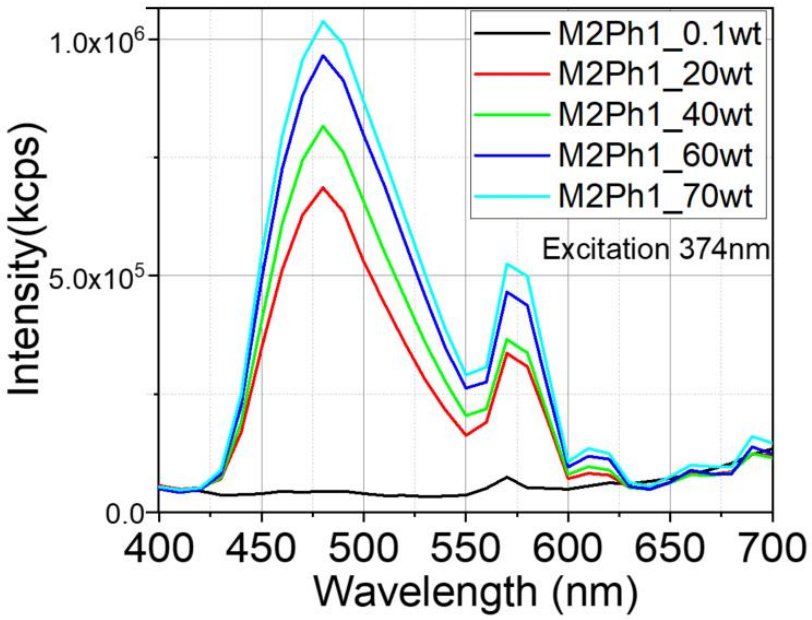

Figure 5.21. Emission spectra of luminescent layers of phosphor Ph1 fabricated with Method 2 at various concentration ratios; 0.1-70%wt.

Figure 5.22 shows some of the luminescent layers that were fabricated with the phosphorescent species, before and after exposure to ultraviolet radiation, as appears from left to right for Phosphors various different concentrations. Nevertheless, there are in total 6 different phosphorescent phosphors that will be used to fabricate the luminescent layers using Method 2. In addition to the new layers, the selection of the best phosphorescent species will be carried out by considering its optical properties, (such as quantum efficiency and lifetime decay), to develop the optimized layers formed by the mixing of these species. These optimized layers could result in an enhanced emission spectrum which could be a means to improving the PV device performance.

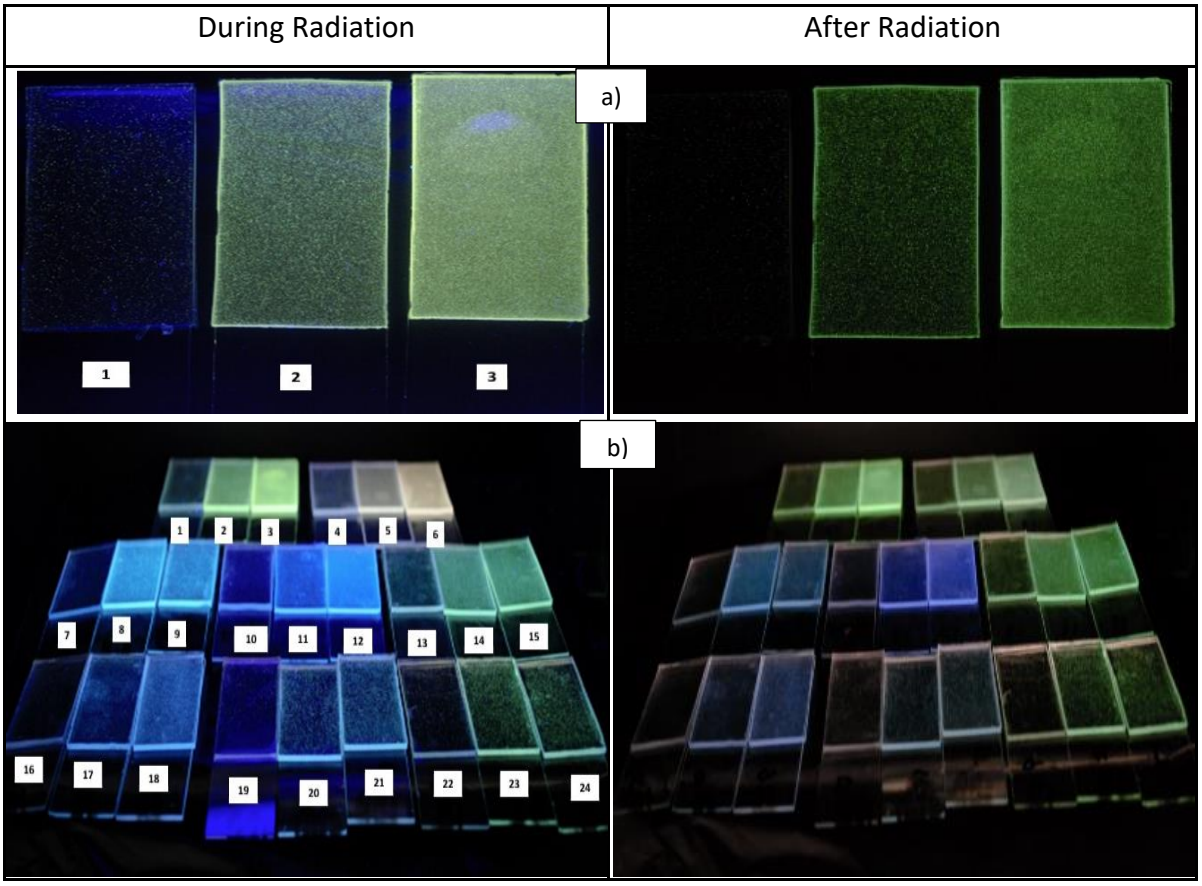

Figure 5.22. Luminescent layers **(a)** during and **(b)** after exposure to ultraviolet radiation (254 nm) for 3 minutes. **(a)** Ph3 at different concentrations (1) 0.1%, (2) 20% and (3) 60% wt; **(b)** Ph4 at different concentrations (1) 0.1%, (2) 20% and (3) 60% wt; Ph5 at different concentrations (4) 0.1%, (5) 20%, and (6) 60%wt; Ph1 at different concentrations 1% (7) 40% (8) 60% (9)wt; Ph2 at different concentrations (10) 1%, (11) 40% and (12) 60% wt; Ph3 at different concentrations (13) 1%, (14) 40% and (15) 60% wt; Ph1 at different concentrations (16) 0.1%, (17) 10% and (18) 20% wt.; Ph2 at different concentrations (19) 0.1% , (20) 10% and (21) 20% wt; Ph3 at different concentrations (22) 0.1% , (23) 10% and (24) 20% wt.

Ideally, one would like to measure the optical properties of the luminescent layers using the UV/Vis spectrometer, (i.e. transmission, absorptance and emission of the layers). But as pointed out earlier, the experiment measured in Method 1 could be inconsistent and may be too simplistic for this purpose, considering the solid sample, where thickness matters. Each method has their strengths and weaknesses, and accordingly, conclusions can be drawn from these experiments. Method 2 has a relationship between three variables; thickness, volume, and weight, where thickness and volume are constant and a multiple of the weight and its corresponding concentration, (as can be seen in Table 5.5). In that way it is possible to maintain the thickness of the layers by measuring the volume total for each layer. However, the weight will vary depending on the thickness of the layer.

Furthermore, the nature and extent of this thickness varies from method to method, with the result that the practical concentration values obtained by different methods may not be directly comparable, as their thicknesses are different. In addition, Method 2 is measured either in terms of the thickness, or weight and volume required to disrupt the unit area of the layer, and it appears to have less variation of the thickness, where the total area is known precisely. On the other hand, the values of Method 1 expressed in the weight of the layer differ considerably and cannot be directly related across sample thicknesses, as can be seen in Table 5.5.

Table 5.5. Comparing Methods.

	Method 1		**Method 2**	
Phosphor concentration ratio (%wt.)	**Weight (g)**	**Thickness (mm)**	**Volume (ml)**	**Thickness (mm)**
0.1	0.4	1.5	0.4	1.5
1	0.4	1.4	0.4	1.5
10	0.4	1.2	0.4	1.5
50	0.4	0.8	0.4	1.5
70	0.4	0.5	0.4	1.5

An ideal method test should be easily adaptable to assess the routine of fabrication of the layers: without risking damage to the sample, relatively simple to perform, applicable to all combinations of layer and phosphor species, valid over the range of the selected mould sizes, and independent of the manner of fabrication. However, this is not applicable here, as the samples get thinner. Furthermore, these points and other such idealization is not realized in practice as no method was tried which fulfilled all the above attributes.

However, both methods showed slightly comparable results for transmission, absorptance and emission. It is considered that Method 2 could provide an impetus for devising better methodologies in the progress of this ongoing work, by comparison to Method 1 where the production of the layers shows different thicknesses and has poor particle distribution on the mould (according to the mixing rates). An alternative explanation considers Method 1 with 100%wt concentration, although the total volume will not cover the entire mould area because there is not enough volume. Furthermore, the effects of the deposition rate may cause variation to the spectral and kinetic characteristics of the layer luminescence. It is interesting

to note that the maximum intensity curves for both methods are between 60-70%wt, which can be used as a maximum amount for the phosphor species.

A standard approach developed for the fabrication of the host matrix layers is described as follows:

- For the mixing process: it was achieved within 10 minutes using multiple containers on a Magnetic Stirrer at 30°C with a speed of 250rpm.
- After the stirring process, when a total mass of 0.4g was achieved, the Solaris silicon was deposited in the mould for the curing process.
- The samples were placed on a levelled surface at room temperature for a resting time of 20 minutes.
- After the resting time, the samples were placed in the incubator for 24 hours for curing. The incubator maintains optimal temperature, humidity and other conditions such as the carbon dioxide (CO2) and oxygen levels of the atmosphere inside.

5.9 Conclusion

A method was developed of preparing multiple samples and was based on the rapid mixing of the polymer resin mechanically. Thus, Solaris Silicon was revealed to be an ultra-transparent polymer, and hence had optical characteristics better than Crystic 2446 Polyester Resin, Synolite 0328-A-1 Resin, Crystal Clear-202 and many other polymers (such as Polyethylene, Poly(tetrafluoroethylene), PMMA and PVC, where they have poor or non-transmission in the UV range. It was considered that using a polymer which is invisible to the UV range could improve the workability of the luminescent device.

Therefore, Solaris was selected to be used as the host material for phosphors and the luminescent layer. However, this polymer has shown transmission variation in the range of 240-310nm, which could be caused by the polymerization or degradation of silicon, and does not seem to be a problem for the luminescent phosphor application because the phosphorescent species re-emit its absorbed energy photons > 400nm. A standard approach was developed for the fabrication of the host matrix layers and it was found to be easily

prepared, reliable, uniform in composition, with little or no trapped air and subject to a good curing process. Three different methods for storage were analysed and it was found that ambient temperature in dark conditions is the best method for maintaining the layer after fabrication. The Tauc plot of the host polymer layer which was fabricated using Solaris Silicon, and determined together with other optical properties of the host layer. Two different methods were presented for the fabrication of the luminescent layers, and it was found that Method 2 should be an impetus for devising better methodologies in the progress of this ongoing work.

CHAPTER 6

OPTICAL CHARACTERISATION OF LUMINESCENT LAYERS

6.1 Introduction

This chapter investigates the optical characteristics of the fabricated luminescent layers, produced by the development of Method 2, as discussed in the Chapter 5. The optical analysis was carried out to define the optical properties of the long persistent phosphor species that were acquired from chemical suppliers, (listed in Table 3.2). A series of various spectroscopy analyses including transmission, reflectance, absorptance, and scatter spectra of these layers were conducted. This chapter also presents the photoluminescence analysis: emission, excitation, fluorescent lifetime decay and the Photoluminescence Quantum Yield, PLQY, of these luminescent layers.

6.2 Spectrophotometric and Spectrofluorimetric Study of Luminescence Layers

The spectrophotometric and spectrofluorimetric studies of the luminescent layers produced at various concentration ratios of the selected phosphors are listed in the Table 3.2. The UV/Vis/NIR spectroscopy used to measure the transmittance, reflectance and scatter spectra of the luminescent layer the measurements were carried out using the Perkin Elmer Lambda 650 UV/Vis/NIR, in the range of 215-850nm at room temperature, as described in section 3.3.1. The spectrofluorimetric studies of the luminescent layers were carried out using a Horiba FluoroMax, as described in section 3.3.2.

The measured transmission, transmission scatter, reflectance and absorptance spectra of the luminescent layer of the various layers were produced using the Phosphorescent Phosphor Ph1, at various concentrations (1-70%wt) are shown in Figure 6.1. Table 6.1. summarises results for all phosphors samples, Ph1-6. The summarizing results, is given through the representation of specific wavelengths, showing that they are accountable to this project's applications. This already covers most of the spectral range where the AM1.5 spectrum has

significant contributions in these LDC layers. (See also the other graphs measured for Ph2-6, a full list is provided in Appendix D).

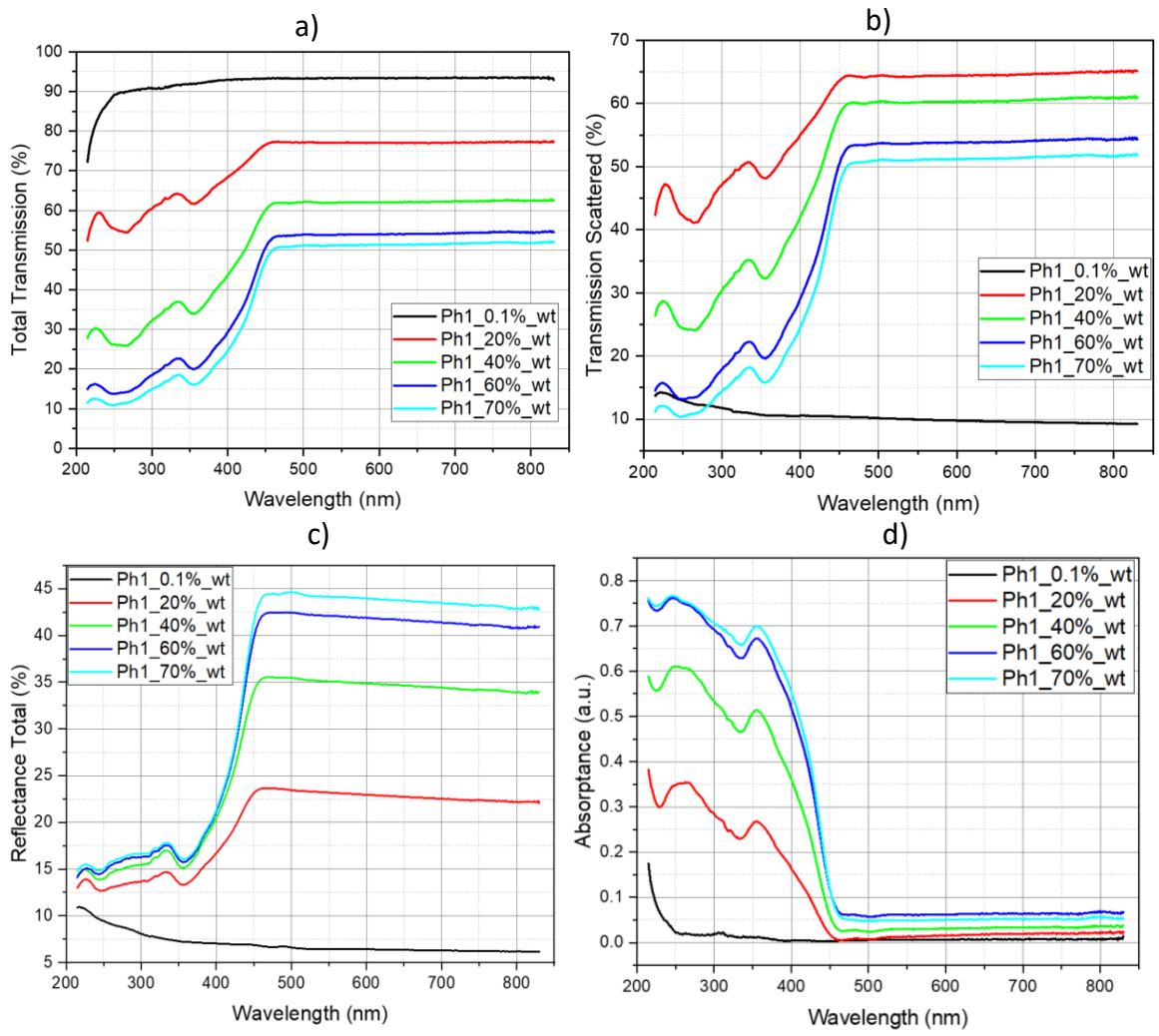

Figure 6.1. Optical (a) total transmission, (b) transmission scattered (c) reflectance total and (d) absorptance spectra of Ph1 luminescent layers at various concentration ratios; 0.1-70%wt.

As can be observed in Figure 6.1 (a) total transmission spectra, by increasing the concentration ratio from 0.1 to 60%wt, the layers reduced its visible light transmission significantly, and after that, 70%wt, it turns out that about 50% of the visible light are not transmitted through the layer. Thus, by applying a highly concentrated luminescent layer >20%wt on the top of the PV device could reduce the incident light into the PV device, reducing its efficiency under illumination. The transmission scatter spectra (b) shows the percentage of light scattering by phosphor species demonstrated that only high concentration ratio >20%wt were found to be contributed with the amount of light scattered by them. Thus, applying these higher

concentrated layers to the top surface of the PV device can result in the light passing several times through the PV device, increasing the effective path length. However, this benefit may be significant only if the layer received a reflecting coating on its side's surfaces, which is not the case here.

Regarding the reflectance spectra (c) by the luminescent layers, this can be observed as being directly proportional to the concentration of LPP- Ph1. This property could be exploited as a reflector with a luminescent layer for transparent PV devices, which may justify the application of such luminescent layers as reflectors at the rear or at the sides of the PV devices. These physical mechanisms may be able to improve the possibility of trapping light scattering from the luminescent layer to the rear surface of the PV device.

Figure 6.1 (d) shows that the phosphors of Ph1 have good absorption in the range of 200-450nm which indicate a good luminescent material for photovoltaic devices which happen to have poor absorptance in this same range. As can be observed, by increasing the concentration ratio above 20%wt more light is absorbed by layers.

The luminescent layers have similar physical properties such as particle size and distribution inside the host material (depending on concentration ratio, as was discussed in section 5.8). Thus, some of these optical properties such as transmission scatter will not be discussed any further, as similar findings are anticipated.

Figure 6.2 shows the photoluminescent emission and excitation spectra of the Ph1 at 60% wt. The emission spectra of Ph1_60%wt luminescent layer, the emission ranges between 400-650nm with an emission centred at 484nm, and at different excitation wavelengths, from 260-455nm are also displayed.

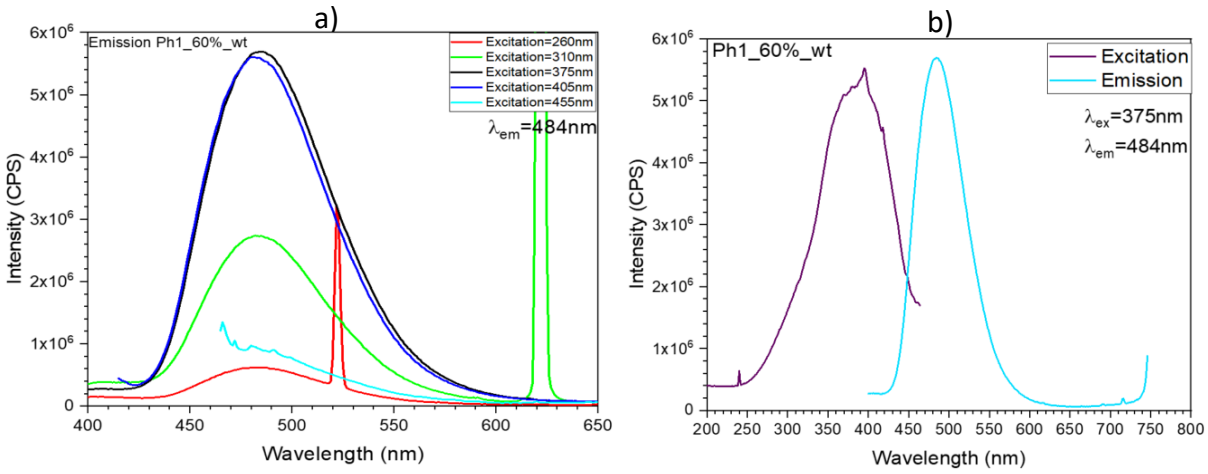

Figure 6.2. a) The emission spectra. b) The excitation, at 375nm, and emission spectra, at 484nm. Colour: rgb (0,222, 255).

Figure 6.2 (a) The graph shows the fluorescence emission spectra of the phosphorescent Ph1 layer with a concentration of 60%_wt. The excitation wavelength was at 375 nm, and the emission centred at 484 nm. The excitation and emission spectra results show that Ph1 down converts photons from the UV range, 200-450nm to the visible range, with an emission peak at 484nm. It is clear from these results that Ph1 has suitable spectral properties for transferring energy photons from the UV range to the visible range. As observed, this phosphorescent phosphors species demonstrated a higher spectra response at 375nm excitation, which resulted in a higher emission in the visible spectra range. Figure 6.2 (b) shows the emission and excitation spectra on its higher responses, and the gap between them is known as Stokes Shift (Daicho et al., 2018).

Table 6.1. Summary of the optical properties and fluorescence emission data relevant to the evaluation of all the luminescent layers, Ph1-6.

Phosphor ID	**Total Transmission**		**Reflectance Total**		**Absorption**	**Emission**
Sample Layer	**at 350 (nm)**	**at 500(nm)**	**at 350(nm)**	**at 500(nm)**	**(nm)**	**Peak λp(nm)** (λex=375nm)
Ph1_0.1%_wt	92%	94%	7.5%	4.0%	200-450	484
Ph1_60%_wt	20%	51%	16%	45%	200-450	484
Ph2_0.1%_wt	92.5%	93.5%	23%	26%	200-475	495
Ph2_60%_wt	37%	70%	24%	42%	200-475	495
Ph3_0.1%_wt	92.5%	95.8%	23%	24%	200-450	520
Ph3_60%_wt	36%	78%	19.5%	37.5%	200-450	520
Ph4_60%_wt	14%	43%	25.5%	50%	200-575	579
Ph5_60%_wt	14.7%	31%	23.5%	40%	200-625	602
Ph6_60%_wt	11%	52.5%	22%	55%	200-500	521

As observed in Sample Ph2 data, Table 6.1 shows that the total transmission spectra measurements of the two layers of Ph2 were very similar to the previously examined phosphors Ph1. Figure 6.1(a) however shows that at 60%wt only about 70% of visible light is transmitted through this layer. Reflectance total data of the layers shows that there is very low reflectance, 23-24%, in the UV range between 200-400nm and high reflectance 42% for high concentration samples above 60%wt > 400nm. Thus, the reduction in the UV range may be caused by the high absorption of the phosphor species. This LPP phosphor showed an absorptance between 200-475nm, resulting in an undesired absorption in part of the visible range, which can be useful under poor ultraviolet radiation conditions, (such as at the back of a PV device or in indoor applications).

Consider the emission data of the phosphorescent Ph2, with a concentration of 60%_wt into the luminescent layer. The excitation wavelength was 375 nm, and the emission peak centred at 495 nm, with an excitation peak at 395nm. The excitation and emission spectra results show that Ph2 down converts photons from the UV range, 200-450nm to 495nm, (emission peak). It is clear from these results that Ph2 has suitable spectral properties for transferring energy photons from the UV range to the visible range.

In the case of Ph3, transmission data were very similar to the two previously examined phosphors Ph1-2. The reflectance result (23% for low concentration, 0.1%wt), was not expected to be lower than the 60%wt sample layer and resulted in 19.5% only. However, the reason for this is probably the particle density, where a lesser amount of phosphor particles was need in this particular layer. Incidentally, there is low reflectance in the UV range between 200-400nm and high reflectance from visible range > 400nm. As discussed above, this may be caused by the high absorption of the phosphor species. The emission result shows that the Ph3 luminescent layer is also a good down convertor, it has absorptance in the UV range and below 500 and an emission peak at 520nm. It is clear from these results that Ph3 has suitable spectral properties for converting its energy photons (e.g. Ph1-2) and is also suited to enhancing the PV device application in the same manner.

Due to the lack of supplier and technical specifications such as chemical and physical properties for long persistent phosphorescent materials, Ph4, Ph5 and Ph6 at 60%wt were added to this study because of some important characteristics such as absorptance and emission range. However, as defined earlier, the ideal and optimum concentration is 60%wt, and it is for this reason that other concentrations will not be discussed here. It believed that they have more impurities than the phosphor Ph1-3. Thus, these luminescent devices already briefly summarised as being the most relevant for this investigation and applications.

Layers Ph4 and Ph5, show 43% and 31% of transmittance at the visible range, (500nm). These numbers are slightly lower than the value expected for them, and appear to be in contradiction with earlier findings, including Ph6. Accordingly, these findings need to be interpreted with caution due to the fact that they may have more impurities which contribute to these reductions.

Significant changes in the absorptance of Ph5 is observed, showing a slight increase in the absorptance range, in comparison with others samples. This slight increase in absorptance is linked to a shift in the reflectance of the layer. Significantly high absorptance value was found A=0.38 at 550nm, which resulted in an increase in the spectral absorptance range in the visible wavelength region. It can thus be suggested as the longest absorptance range, 200-624, amongst all samples. More interestingly, it was found that the reflectance of the sample Ph6 layer had a small peak at 500nm which resulted in the highest reflectance value, 55%, as can be observed in the Table.

As stated previously, these luminescent materials, Ph5, appear to absorb a wider range (200-625 nm), which in turn, absorbs a wider range of UV light compared to the other samples (Ph4 and Ph6). For that reason, this luminescent layer may not be a good candidate for the PV device as it has a similar spectra response or absorbs mostly within the same range. As a result of these various LPP phosphor species presented here, it is possible to use one or various types of phosphors species to fabricate a luminescent layer with a wider emission spectrum by combining multiple species of phosphorescent into the same layer.

Thus, it may be possible to improve the PV device efficiency and to generate current by PV technology in the dark, because of the long persistence phosphorescence given by these phosphors. To explore this possibility, two different layers were produced by mixing the LPP phosphors species. These new layers were named as PhX60%_wt and PhT60%wt. The PhX is composed of Ph1-3 with 20% concentration ratio of each phosphor. The PhT is composed of Ph1-6 with 10% concentration ratio of each phosphor. The decision for this specific concentration ratio was because most of the layers resulted in lesser transparency above 70%, thus 60%wt reduced the risk of this effect. These layers including PhX and PhT will be presented in PLQY analyses, in the following sections.

6.3 Spectrofluorimetric Study of Luminescent Layers - Standard Reference Samples

Apart from these optical studies of the phosphorescent samples, three additional standard reference phosphors were acquired from the Japan National Institute for Materials Science (NIMS) to aid the PLQY measurements using the "Mixed methods", as described in section 3.3.4. The characterisation of these standard reference phosphors is the subject of the following discussion and will be only used for quantum efficiency measurements of the LPP phosphors. These samples were only applied for photoluminescent studies and no spectroscopy measurements will be discussed here.

Figure 6.3 presents a comparative graph showing the photoluminescent emission and excitation spectra of the phosphors β-sialon: Eu^{2+}, α-sialon: Eu^{2+} and $CaAlSiN3:Eu^{2+}$ of the fabricated luminescent layers, PhNIMS-G, PhNIMS-O and PhNIMS-R, along with the photoluminescent emission and excitation spectra of the reference standard for phosphor species provided by the manufacturer ("Phosphors | Yuji International," n.d.).

Fluorescent Standard Reference Phosphors

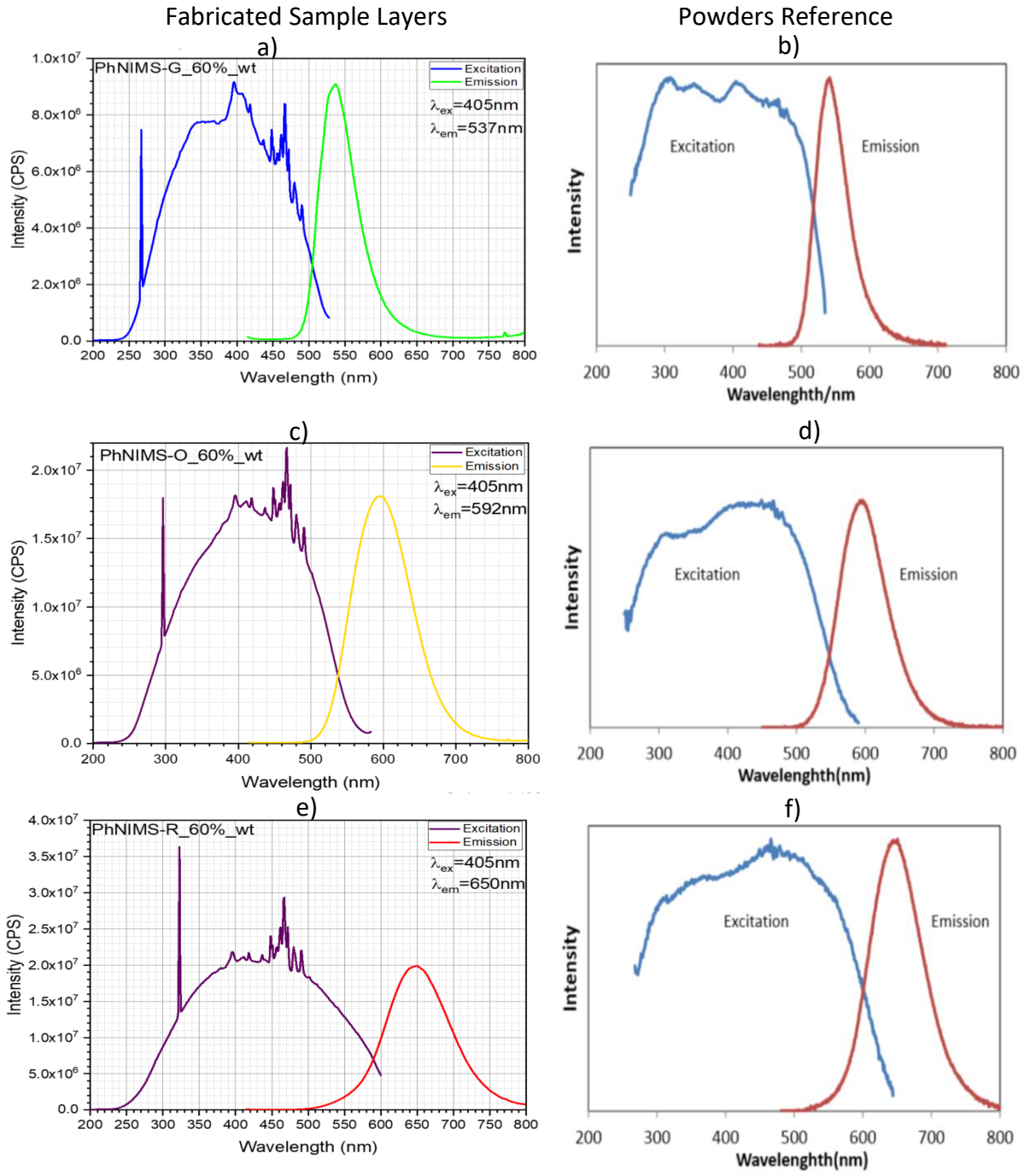

Figure 6.3. (a) Photoluminescence excitation and emission spectra of PhNIMS-G_60%_wt luminescent layer along with data reported by the manufacturer, Figure (b). (c) Photoluminescence excitation and emission spectra of PhNIMS-O_60%_wt luminescent layer, along with data reported by the manufacturer, Figure (d). (e) Photoluminescence excitation and emission spectra of PhNIMS-R_60%_wt luminescent layer, along with data reported by the manufacturer, Figure (f).

Figure 6.3 (a) shows the photoluminescent emission and excitation spectra of the PhNIMS-G luminescent layer with a concentration of 60%_wt. The excitation wavelength was at 405nm and the emission centred at 537nm. The results showed that the measurements of the standard phosphor species dispersed in the host material were identical with the NIMS standard references, Figure (b). Thus, this proved to be an ideal standard reference for the PLQY analysis of the luminescent layers.

Figure 6.3 (c) shows the photoluminescent emission and excitation spectra of the PhNIMS-O luminescent layer with a concentration of 60%_wt. The excitation wavelength was at 405nm and the emission centred at 592nm. Similarly, to the preview standard, the results showed that the measurements of the orange standard phosphor species dispersed in the host material were identical with the NIMS standard reference, (see Figure (d)).

Figure 6.3 (e) shows the photoluminescent emission and excitation spectra of the PhNIMS-R luminescent layer with a concentration of 60%_wt. The excitation wavelength was at 405nm and the emission centred at 650nm. This was the third reference sample and the results showed that the measurements of the standard phosphor powder were dispersed in the host material or luminescent layer and the predominant peaks are identical with the NIMS standard reference, (see Figure (f)). It has also proved to be an ideal standard reference for the PLQY analysis of the luminescent layers.

6.4 Quantum Efficiency Measurement of Luminescent Layers

6.4.1 External and Internal and Quantum Efficiency (EQE and IQE) of the Standard Reference

In order to measure the quantum yields of the different sample layers, we used a method described in section 3.3.4, based on the Mixed method, using an integrating sphere.
Figure 6.4 shows the photoluminescence spectra of the blank reference layer and the standard luminescent layers, PhNIMS-G, PhNIMS-O and PhNIMS-R, under the same excitation, 405 nm, wavelength characterized by the manufacture.

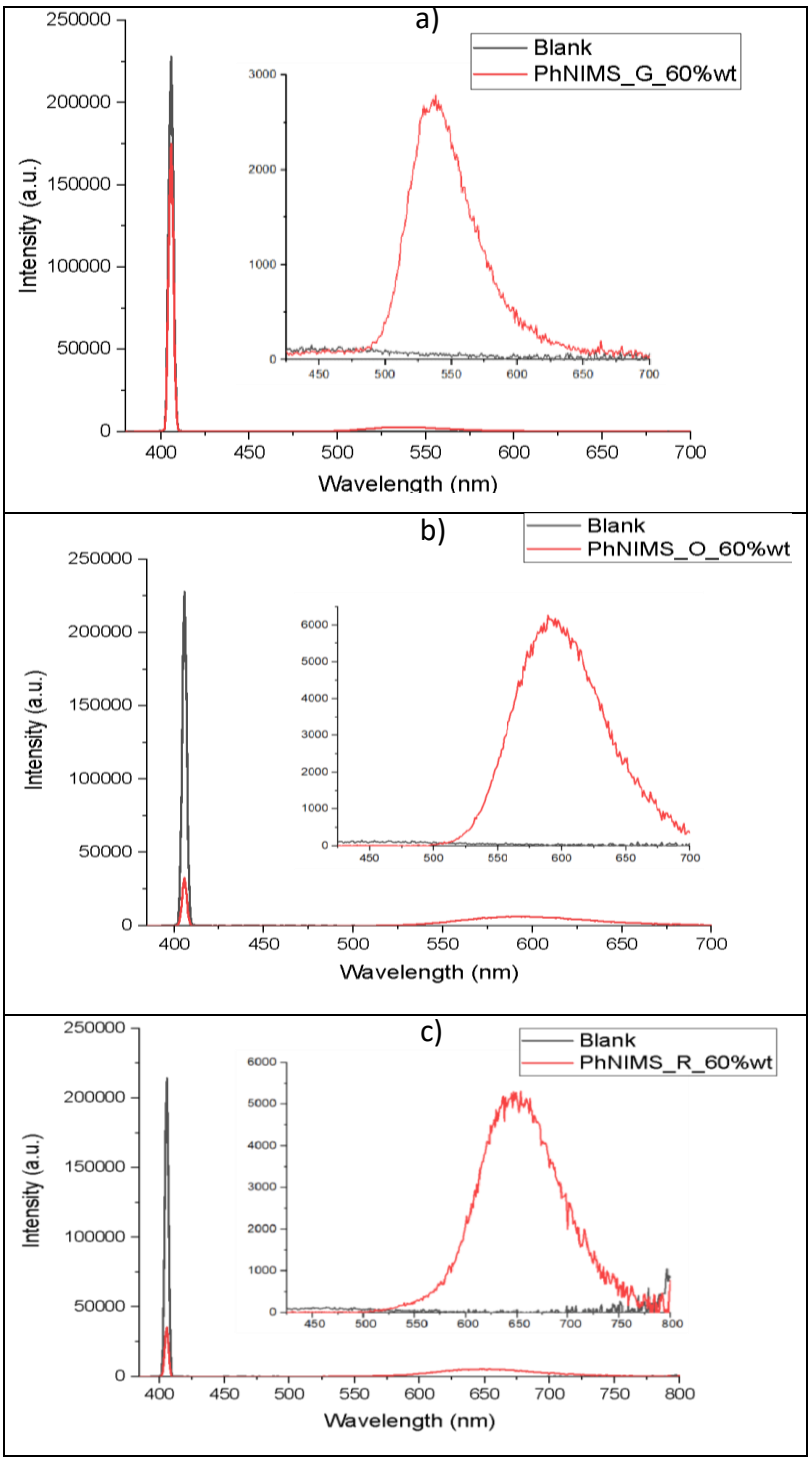

Figure 6.4. (a) Photoluminescence spectra of the standard phosphors β-sialon: Eu2+(PhNIMS-G) luminescent layers at 60%_wt, the emission ranges between 375-700nm at 405nm excitation wavelengths. Inset: zoomed in fluorescence spectrum around 500 nm peak. (b) Photoluminescence spectra of the standard phosphor α-sialon: Eu2+ (PhNIMS-O) luminescent layers at 60%_wt, the emission ranges between 375-700nm at 405nm excitation wavelengths. Inset: zoomed in fluorescence spectrum around 600 nm peak. (c) Photoluminescence spectra of the standard phosphor CaAlSiN3:Eu2+ (PhNIMS-R) luminescent layers at 60%_wt, the emission ranges between 375-700nm at 405nm excitation wavelengths. Inset: zoomed in fluorescence spectrum around 500 nm peak.

The EQE and IQE for β-sialon: Eu2+(PhNIMS-G) standard luminescent layer were calculated to be 0.21% and 0.94% respectively, at 60%_wt. The EQE and IQE for β-sialon: Eu2+ standard reference powder values reported in the manufacturer certificate of analysis were 0.62% and 0.82%, respectively, (see Table 3.3). These results indicate that β-sialon: Eu2+ standard phosphor powders and the fabricated luminescent layer (PhNIMS-G) are in agreement with data obtained from this report regarding this material, and showing the error associated with the PLQY measurement to be about 10%. The measurements were repeated three times per sample and the results are shown in Table 6.2, which summarises the calculation values.
These results indicate that β-sialon: Eu2+standard phosphor powder have similar optical characteristics to the luminescent layer (PhNIMS-G) and can be used as a comparative reference standard phosphor for the phosphorescent samples.

Figure 6.4 (b) shows the photoluminescent luminescence spectra of the blank reference layer and the standard luminescent layer Orange (α-sialon: Eu^{2+}), under excitation at 405 nm. The EQE and IQE for the α-sialon: Eu^{2+}(PhNIMS-O) standard luminescent layer were calculated to be 0.70% and 0.82% respectively, at 60%_wt. The EQE and IQE for α-sialon: Eu2+ standard reference values reported in the manufacturer certificate of analysis were 0.64% and 0.79%, (see Table 3.3). These results indicate that the α-sialon: Eu^{2+} standard phosphor powder value reported and the fabricated luminescent layer (PhNIMS-O) are in agreement with data obtained from this report, for this material, showing the error associated with the PLQY measurement about 10%. Table 6.2 summarises the calculations values. These results indicate that α-sialon: Eu2+ standard phosphor powder have also similar optical characteristics to the luminescent layer (PhNIMS-O) and can be used as a comparative reference standard phosphor.

Figure 6.4 (c) shows the photoluminescence spectra of the blank reference layer and standard luminescent layer Red (CaAlSiN3:Eu^{2+}), under excitation at 405 nm. The EQE and IQE for CaAlSiN3:Eu2+(PhNIMS-R) standard luminescent layer were calculated to be 0.74% and 0.88%, respectively at 60%_wt. The EQE and IQE for CaAlSiN3:Eu2+ standard reference powder values reported in the manufacture certificate of analysis were 0.64% and 0.79%, (see Table 3.3). These results indicate that CaAlSiN3:Eu^{2+} standard phosphor powder have similar

characteristics to the luminescent layer (PhNIMS-R) and can be used as a comparative reference standard phosphor.

These results suggest that the luminescent layers made of the standard reference phosphors from NIMS are suitable candidates for standard PLQY measurements, in particular, PhNIMS-G and PhNIMS-O because of their emission ranges, which are very similar to the LPP. These two standards present emission spectral properties which closely match those of the unknown samples and will be used to investigate the PLQY of long-persistent phosphor.
Also, it is important to observe that all three standard phosphors from NIMS have consistent and stable IQE and EQE data points, as well as spectral. The analysis confirmed that they can be used as absolute reference points for confirmation of the quantum efficiency method of the PLQY measurements for the phosphorescent samples, as presented in section 3.3.4.

6.4.2 External and Internal Quantum Efficiency (EQE and IQE) of the Luminescent Sample Layers Ph1-6, PhX and PhT.

The measurement of the quantum efficiency of luminescent layers Ph1-6, as referred to in Table 3.2, plus the two extra layers PhX and PhT, were produced by mixing phosphors. It was applied to the host polymer layer (blank) as a reference to calculate the spectrum of the excitation source. For a better representation of this study, highly concentrated samples (>60%wt) were applied because it was found that during measurement, the higher the amount of phosphors particles inside of the layer, the better the spectra data collection from the samples, due to the instrument photon detector.
After validating the method by applying the standard reference samples from NIMS, the samples Ph1-6, PhX and PhT were measured. Figure 6.5 shows the photoluminescence spectra of all the sample luminescent layers at 60 or 100%wt concentration ratio, under excitation at 375nm. This specific wavelength was selected based on the phosphorescent analyses described earlier in this Chapter. The total photoluminescence spectra were measured from 0-650 nm or 0-700nm, as discussed in section 3.3.4, but the graph summarizes and displays the emission ranges which were used in the PLQY calculations.

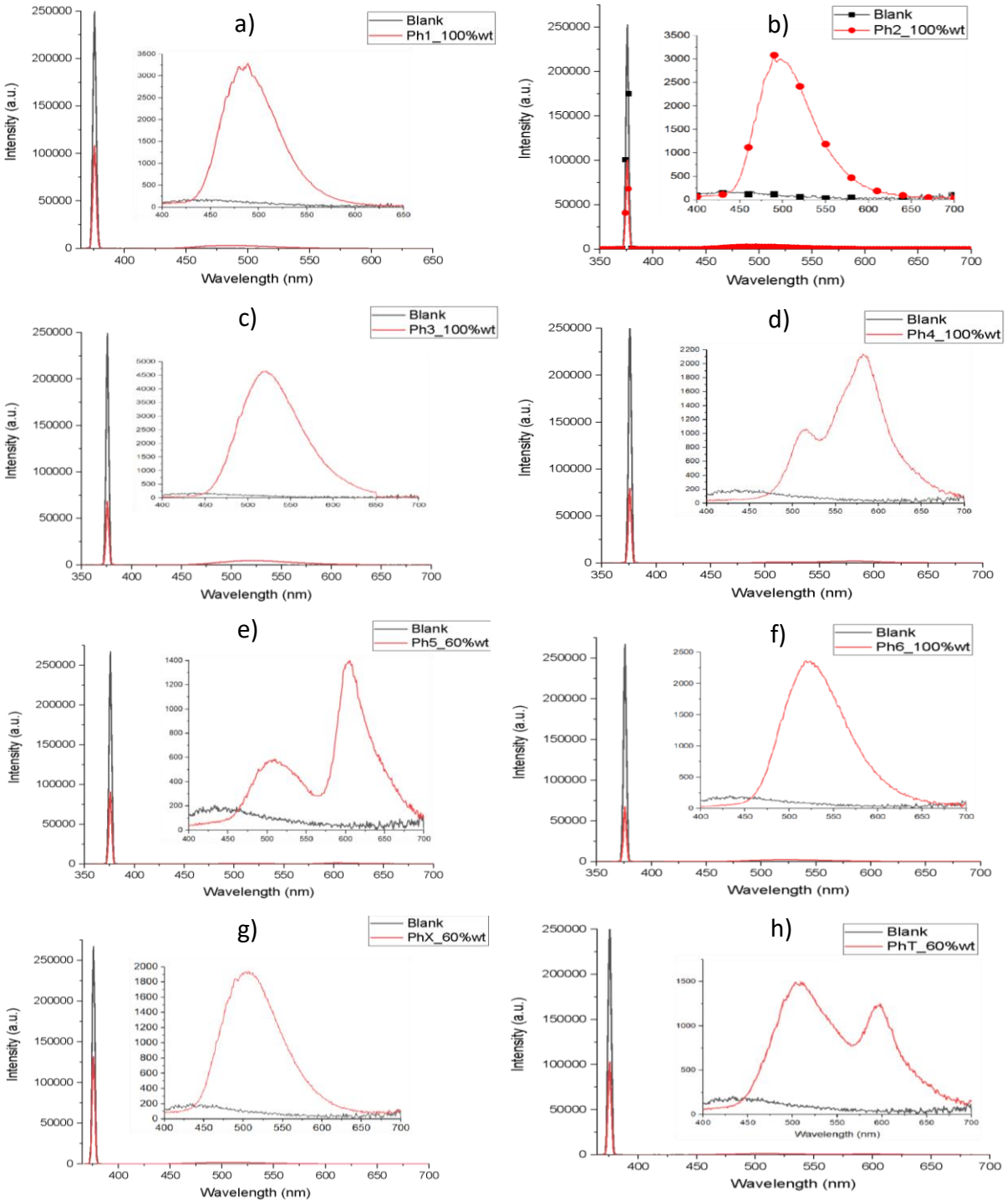

Figure 6.5. (a) Photoluminescence spectra of the sample Ph1 luminescent layer at 100%_wt. The emission ranges between 400-650nm. (b) Photoluminescence spectra of sample Ph2 luminescent layer at 100%_wt, the emission ranges between 400-700nm. (c) Photoluminescence spectra of sample Ph3 luminescent layer at 100%_wt, the emission ranges between 400-700nm. (d) Photoluminescence spectra of sample Ph4 luminescent layer at 100%_wt, the emission ranges between 400-700nm. (e) Photoluminescence spectra of sample Ph5 luminescent layer at 60%_wt, the emission ranges between 400-700nm. (f) Photoluminescence spectra of sample Ph6 luminescent layer at 100%_wt, the emission ranges between 400-700nm. (g) Photoluminescence spectra of sample PhX luminescent layer at 60%_wt, the emission ranges between 400-700nm. (h) Photoluminescence spectra of sample PhT

luminescent layer at 60%_wt, the emission ranges between 400-700nm. Inset: zoomed in fluorescence spectrum around its emission peaks.

To confirm reproducibility, three repeat measurements were made for each sample and this is shown in Table 6.2 (below), which summarises the calculation values. Internal quantum efficiency refers to the efficiency for photons which are absorbed by the ions. The external quantum efficiency is therefore much lower and depends strongly on the presence of defect states in the host lattice.

Figure 6.5 (a) shows the photoluminescence spectra of the bank reference and sample Ph1 luminescent layer at 100%_wt under excitation at 375nm. The EQE and IQE for the Ph1 luminescent layer were calculated to be 0.27% and 0.48% respectively, at 100%_wt. Figure (b) shows the photoluminescence spectra of the sample Ph2 luminescent layer at 100%. The EQE and IQE for the Ph2 luminescent layer were calculated to be 0.27% and 0.44% respectively, at 100%_wt. Figure (c) shows the luminescent layer Ph3, the EQE and IQE for Ph3 luminescent layer were calculated to be 0.43% and 0.62% respectively, at 100%_wt. Figure (d) sample Ph4 luminescent layer at 100%_wt, the EQE and IQE for the Ph4 luminescent layer were calculated to be 0.19% and 0.29% respectively, at 100%_wt. Figure (e) shows the sample Ph5 luminescent layer at 60%_wt, the EQE and IQE for Ph5 luminescent layer were calculated to be 0.11% and 0.17% respectively, at 60%_wt. Figure (f) shows sample Ph6 luminescent layer at 100%_wt. The EQE and IQE for the Ph6 luminescent layer were calculated to be 0.22% and 0.31% respectively, at 100%_wt. Figure (g) shows the photoluminescence spectra of Phx60%_wt, which is the mixing of phosphor Ph1, Ph2 and Ph3 containing weight of 20%_wt for each phosphor. This sample demonstrated emission peaks centred at 508nm. The EQE and IQE for the PhX luminescent layer were calculated to be 0.18% and 0.38% respectively, at 60%_wt. Figure (h) shows the photoluminescence spectra of the sample PhT60%_wt, which is the mixing of all phosphors, Ph1-Ph6, containing weight of 10%_wt for each phosphor. This sample demonstrated two emission peaks, 508 and 596nm. The EQE and IQE for Phx luminescent layer were calculated to be 0.19% and 0.32% respectively, at 60%_wt. To confirm the reproducibility three repeat measurements were made for each sample and this is shown in Table 6.2 below.

Table 6.2. Calculated results of photoluminescence quantum yields (PLQY) of the luminescent layers

Phosphor ID Sample	QY	1 PLQY	2 PLQY	3 PLQY	Average	Uncertainty	QY %
PhNIMS-G_60%_Wt	EQE	0.21	0.22	0.20	0.21	0.003	0.21
	IQE	0.95	0.93	0.95	0.94	0.003	0.94
PhNIMS-O_60%_Wt	EQE	0.69	0.70	0.70	0.70	0.002	0.70
	IQE	0.81	0.82	0.82	0.82	0.002	0.82
PhNIMS-R_60%_Wt	EQE	0.72	0.75	0.74	0.74	0.007	0.74
	IQE	0.86	0.90	0.89	0.88	0.008	0.88
Ph1_100%_Wt	EQE	0.22	0.34	0.26	0.27	0.033	0.27
	IQE	0.39	0.59	0.45	0.48	0.057	0.48
Ph2_100%_Wt	EQE	0.28	0.26	0.26	0.27	0.007	0.27
	IQE	0.47	0.43	0.43	0.44	0.013	0.44
Ph3_100%_Wt	EQE	0.48	0.38	0.42	0.43	0.027	0.43
	IQE	0.66	0.53	0.67	0.62	0.025	0.62
Ph4_100%_Wt	EQE	0.19	0.20	0.19	0.19	0.003	0.19
	IQE	0.27	0.28	0.32	0.29	0.015	0.29
Ph5_60%_Wt	EQE	0.11	0.11	0.11	0.11	0.000	0.11
	IQE	0.18	0.17	0.17	0.17	0.003	0.17
Ph6_100%_Wt	EQE	0.27	0.21	0.18	0.22	0.025	0.22
	IQE	0.37	0.29	0.28	0.31	0.028	0.31
PhX_60%_Wt	EQE	0.18	0.18	0.19	0.18	0.003	0.18
	IQE	0.38	0.38	0.38	0.38	0.000	0.38
PhT_60%_Wt	EQE	0.22	0.19	0.17	0.19	0.013	0.19
	IQE	0.37	0.32	0.27	0.32	0.025	0.32

As can be observed, the results show a very consistent and replicable measurement which is very important for this type of PLQY analysis. It is evident that all the standard luminescent sample layers from NIMS have a very high quantum efficiency value. For error associated for both reported values, see Table 3.3, and the PLQY measurement is approximately 10%.

The high PLQY values can be attributed to the fact that all standards reference are fluorescent phosphors and have an immediate emission and it is possible for one electron to absorb two photons; this absorption can lead to the emission of radiation by having a shorter wavelength than the absorbed radiation.

On the other hand, all other samples Ph1-Ph6 are phosphorescent materials and do not, necessarily, immediately re-emit the radiation they absorb. It is considered that excitation of electrons to a higher state is accompanied with the change of a spin of mechanically forbidden

energy state transitions. The transitions occur very slowly, and these absolved radiations may be re-emitted at a lower intensity for up to several hours after the original excitation, (as described in section 3.3.4).

The measurements illustrate the fact that the highest PLQY values of 0.43 and 0.62, EQE and IQE respectively, and of long persistent phosphor is to be found in Ph3, where it is slightly higher than the other samples. As expected, our measurements demonstrate that the Ph1-3 have the higher PLQY amongst all phosphorescent phosphor samples. The lowest PLQY values of 0.11% and 0.17% appear to be the phosphorescent phosphors Ph5. It was believed that these low measurement values can be attributed to many factors such as impurity or low quality phosphors, which can occur during the phosphor fabrication process, (for example, poor mixing process of raw materials, and poor synthesis process resulting in poor crystallization of the phosphorescent particles (Kitai, 2008; Shionoya and Yen, 1998; Yang et al., 2017).

Considering these low, <0.3, PLQY results, we could assume that half of these phosphors should be dismissed at this stage but, nevertheless, for the luminescent down converter application there are two possible mechanisms, (down-shifting and down conversion) and the difference between these two is the quantum efficiencies. In down conversion the converter emits two photons of low energy for each absorbed high energy photon, while DS layers emit a maximum of one low energy photon for each absorbed one. This means it is necessary to establish the emission lifetime of these phosphorescent phosphors to be able to check exactly if they are able to emit more than two photons and which of these materials is the best in terms of lifetime decay. The phosphorescent species demonstrate good properties such as absorption in the UV range, emission in the visible range, high reflectance, good chemical and physical stability, all of which are required to effectively enhance light-harvesting and lead to a higher photocurrent of the PV devices. However, it was found that PLQY values are lower than those reported in the Table 2.3.

The factors that may contribute to the low PLQY intensity or measurement is the intensity of the excitation source, light losses in the optical path, detector sensitivity or possible

photobleaching of the phosphorescent phosphor species. However, as discussed in section 2.4, there are no standard reference or measurement procedures for this type of long persistent phosphors. Nevertheless, these factors can be overcome with lifetime measurement, which is also a very important parameter to evaluate the impact of these emission lifetime decays on the performance to the luminescent layer and subsequently the PV device.

6.5 Phosphorescent Lifetime

Phosphoresce lifetime measurements were conducted through the analysis of the luminescence decay of the phosphorescent sample layers. In phosphorescent materials, optical excitation energy is stored in the lattice by the trapping of photo excited charge carriers. To investigate the lifetime of the luminescent layers of the long persistent phosphor and the standard phosphors from NIMS, six different sample layers of LPP (Ph1-Ph6) and all three standard layers selected at a concentration ratio of 60%wt were studied, to calculate and compare the behaviour during the charging and discharging time of the luminescent phosphor layers. In addition, weight-dependent phosphorescent decay lifetimes were measured for one of the LPP phosphors, Ph3 at various concentrations (0.1-80%_wt dispersed in the host polymer matrix under the single excitation wavelength). This investigation will confirm how the weight was dependent upon the lifetime emission of the phosphor samples. Photoluminescence decay curves were collected on a Horiba Jobin Yvon FluoroMax-4P spectrofluorometer using a pulsed Xenon lamp as the excitation source. After the sample is excited for 10 minutes with the pulsed lamp, the emitted phosphorescence is measured using an R928P photon-counting detector, as described in section 3.3.3.

Figure 6.6 shows the two different behaviours for these measurements; the first being measured during an excitation 10 minutes. After the light source was switched off the samples were measured for a further 10 minutes. During the excitation measurement the samples were excited for 10 minutes at 375 nm wavelength. Then the samples were measured according to the PL peak emissions for each sample, Ph1(λem 484nm), Ph2 (λem 495nm), Ph3 (λem 520nm), Ph4(λem 579nm), Ph5(λem 579nm), and Ph6 (λem 521nm). The decay curves after the light

was switched off, for all phosphorescent sample layers at 60%_wt, have been presented below, in order to compare the samples.

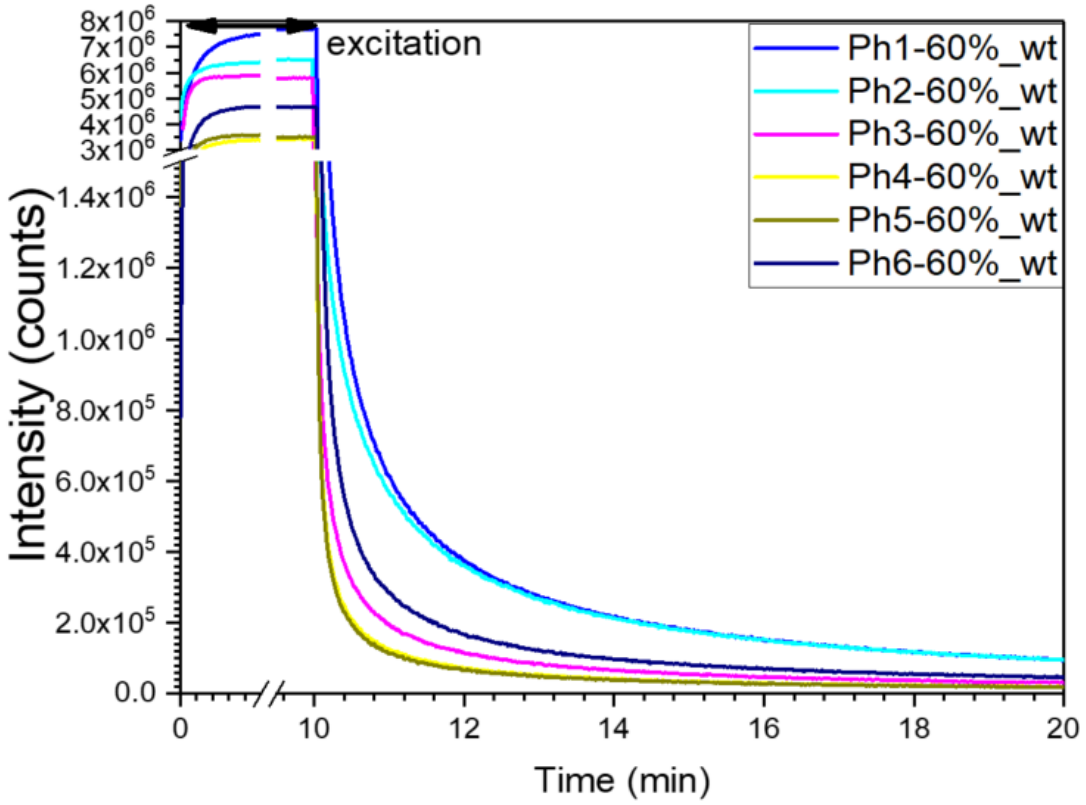

Figure 6.6. Excitation and lifetimes decay curves of all phosphorescent layers at 60%_wt. The plot of the intensity (counts) versus time (minutes) at 375nm excitation and various emission peaks is illustrated.

As can be seen from the above results, after 5 minutes under the light source the samples reach their excited state. The luminescent decay of the phosphorescence for all layers was fast initially, and gradually slowed down afterwards, where a stable emission was finally achieved. The phosphorescence for these layers can last for more than 10 minutes at high intensity, which can be observed for several minutes in the daylight, and several hours in the darkness with the naked eye, which explains the long persistent afterglow. The phosphorescent phosphors, Ph1 and Ph2, appear to have the longest lifetime during this timeframe, and probably also the highest purity and crystal structure quality, which triggers this behaviour. The luminescent effect observed here arises from the transition from a high-energy state to a lower-energy state, as discussed in section 2.4.

Many researchers debate these exponential equations when considering the calculation decay constants, so as to assess the phosphorescence characteristics of the phosphor (Berberan-Santos et al., 2005; Chang et al., 2010; Tsai et al., 2014). The afterglow attenuates exponentially, and its intensity time decay behaviour could follow the pattern of first-order, second-order, or general-order kinetic behaviour. However, single and triple order kinetic behaviour exponential equations have been verified, and both results appear to be a trend when comparing different phosphors. For that reason, the researcher applied the first order, which successfully fitted to the experimental long afterglow decay curves for all data collected. The photoluminescence decay time of all phosphors is presented in the Table 6.3.

Figure 6.7 shows the measurement of the standard luminescent layers of NIMS, Green, Orange and Red, that were used as standard reference samples. The samples were measured under the sample conditions and procedures as described previously, except for the PL emissions, which are; Green 537nm, Orange 594nm and Red 647nm respectively. The longer decay time observed in red PhNIMS-R can be ascribed to the spin and parity-forbidden of the electronic transitions. The decay time of the other two phosphors are much shorter and exhibit very typical behaviour for fluorescent phosphor materials.

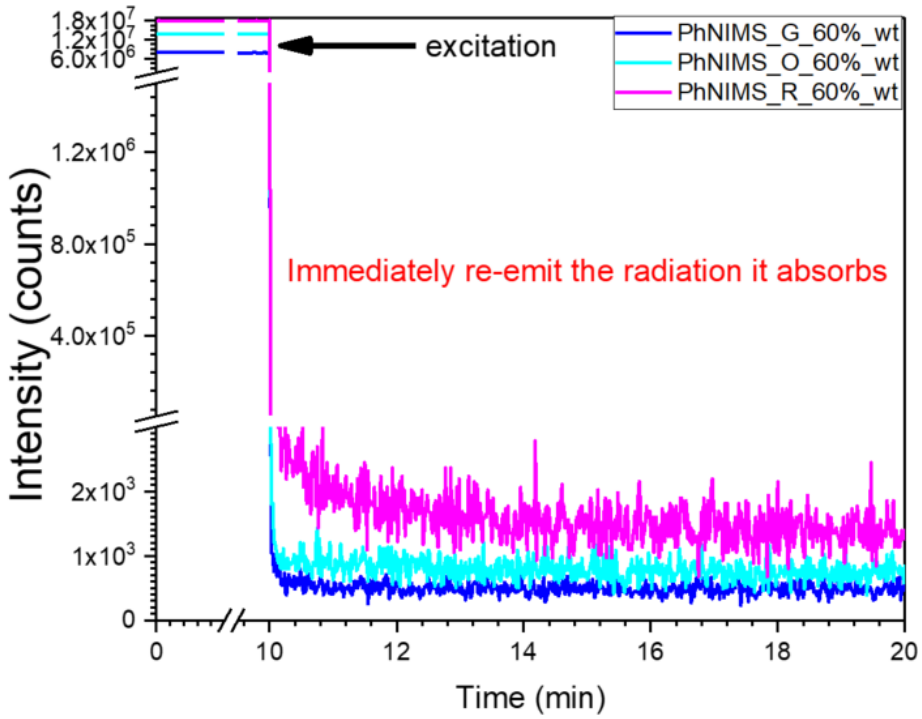

Figure 6.7. Excitation and lifetimes decay curves of the standard phosphor layers at 60%_wt. The plot of the intensity (counts) versus time (minutes) at 375nm excitation and with various emission peaks.

As we can observe, the standard phosphor layers have a very fast response, and show stable behaviour, under and after the excitation light source. The phosphor reaches its maximum value very quickly and remains constant. On the other hand, the decay curves are very typical of the fluorescent phosphors, which immediately emit the absorbed radiation. The photoluminescence decay curves of all three phosphors have a single exponential decay behaviour, and the decay time is presented in Table 6.3.

The results presented in Table 6.3 simulated those of the lifetime curves of all phosphor layers. The lifetime decay was calculated using OriginPro 2018 software by plotting the decay lifetime for each individual sample and subsequently calculating the tail for each measured sample data set. The tails of the decay curves were fitted to a single exponential decay function $I = I_o + \alpha_1 \, exp\left(-\frac{t}{\tau_1}\right)$, (see Equation 3.4).

Table 6.3. Lifetime Results for the afterglow curves of all luminescent phosphor samples layers.

Simulated Results	**I_0 (counts)**	**α_1 (counts)**	**$\tau_{1(s)}$**
Sample Phosphor ID	Value	Value	Value
PhNIMS-G_60%_Wt	501.859	7.88E+06	0.133
PhNIMS-O_60%_Wt	795.868	1.38E+07	0.002
PhNIMS-R_60%_Wt	2156.124	1.81E+07	0.123
Ph1_60%_Wt	123158.335	762046.899	90.057
Ph2_60%_Wt	122705.685	756727.501	91.424
Ph3_60%_Wt	55554.336	704185.695	32.752
Ph4_60%_Wt	40434.806	719619.034	19.079
Ph5_60%_Wt	27035.899	769095.937	4.578
Ph6_60%_Wt	74108.563	726360.846	44.230

As can be observed in Table 6.3, the NIMS phosphor materials have the shortest lifetimes (less than a second; PhNIMS-G at 0.13s, PhNIMS-O, 0.002s and PhNIMS-R, 0.123s) amongst all phosphors in the study. Ph2 has shown the longest lifetime and its value reached 91.424s. Again, a single exponential equation was used in the interpretation of the results of the largest deviations and the smallest values. Also, it indicates that the phosphorescent layers with the

largest luminescent decay profile does necessarily have the longest decay lifetime, as can be seen observed from the Ph1 and Ph2, (see Figure 6.6).

This result shows that the decay constants of the luminescent layer are a variant, and they are dependent on numerous factors such as the type of phosphor material, sample weight, thickness, and density of the sample layer. To gain a better understanding of the concentration or density dependent lifetime behaviour, one of the phosphorescent samples, Ph3, was subjected to concentration dependent lifetime analysis.

Figure 6.8 shows examples of the concentration-dependent phosphorescent decay lifetimes of one of the LPP phosphors, Ph3 at various concentrations (0.1-80%_wt) dispersed in the host polymer matrix, under the same excitation wavelength of 375nm and PL emission 520nm.

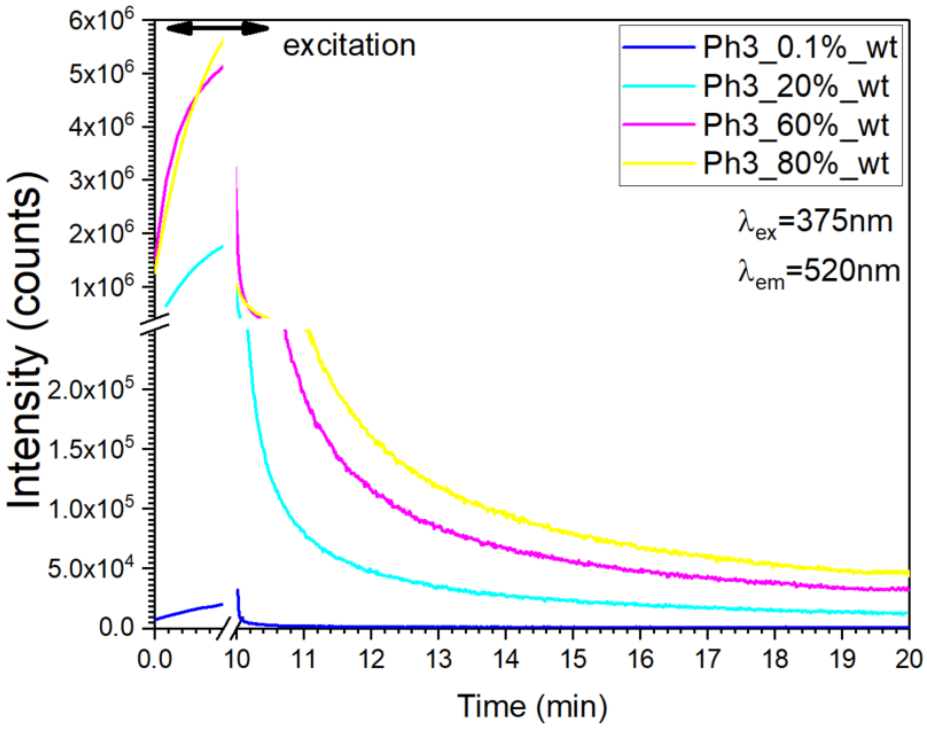

Figure 6.8. Excitation and lifetime thickness dependency decay curves of the Ph3 phosphor layers at various concentrations; 0.1 to 80%_wt. The plot of the intensity (counts) versus time (minutes) at 375nm excitation and PL emission at 520nm is presented.

As the concentration of layers increase from 0.1 to 80%wt, the lifetime decay tails also increased proportionally. This investigation confirms how the concentration was dependent upon the intensity of lifetime emission of the phosphor samples. Again, dispersion of a larger

amount of phosphorescent material corresponds to a longer afterglow behaviour. This may reveal that the afterglow mechanism is dependent upon the concentration or density of the sample layer. Similarly, having a higher number of energy photons at the higher concentration will result in increased energy storage being available in the luminescent layer, which can enhance the down converter layer by discharging more energy photons and subsequently be used to power the PV device in the dark.

The phosphorescent layers Ph1, Ph2 and Ph6, at higher concentrations resulted in very promising energy storage, but the DC converter was not useful as a down-shifting mechanism. Such long lifetime decay allowed absorbed ultraviolet energy to be stored for many hours generating more than two visible photons. These mechanisms were described in section 2.3.
These long lifetime decay properties allow absorbed ultraviolet energy and storage for many hours generating more than two visible photons (as we can see from these lifetime analysis), this process is defined as the down conversion mechanism (Hosseini et al., 2013; Spitzer et al., 2013; H. Sun et al., 2014b). The theoretical explanation for the use of these terms, (DS and DC), when describing the LPP impact on a PV device has not yet been agreed upon. It is standard practice to consider that DC can be achieved using host lattice states or ions to obtain quantum efficiencies larger than unity. For instance, schemes using single or double ions are possible. In the latter case, the excited ion can relax from the higher energy state into the lower energy state by transferring its energy to the second ion. After the energy transfer, both ions can emit a photon to reach the ground state (de la Mora et al., 2017).

It is believed that long persistence decay is generated by phosphors such as $SrAl_2O_4:Eu^{2+}$, and Dy^{3+}, which can be excited by high energy photons from the UV to the visible spectrum range. Its phosphorescence is derived from a transition from the 5d level to the 4f level of Eu^{2+}. In that case, the co-doped Dy^{3+} ions act as hole trap levels, as presented in section 2.4. This process explains the use of the term “down converter” in this research, because of the LPP phosphors caused by this forbidden process.
One of the biggest advantages of these luminescent materials, is that instead of only the singlet state, (from which the excited electron can easily return to its ground state, by emitting its excitation energy as fluorescent over a short lifetime (<0s)), the phosphorescent can also

transition from the triplet excited-state to a singlet state, (which results in these long excitation lifetimes), which can increase the luminescence by down converting this energy into photon efficiency. Accordingly, the luminescence originating in triplet states is of a longer duration which can improve the efficiency of the LDC. Apart from the two different types of phosphor materials, it is important to observe that the phosphor compounds investigated in this study were manufactured with different weights and particle sizes but were dispersed in the same volume into the host polymer matrix, to maintain a consistent thickness for each layer.

The NIMS phosphors were introduced in these investigations because unfortunately there are no standard references for long persistent phosphor materials available. Such optical characterization results for LPPs are not disclosed by the manufacturers, which makes results presented in the current research difficult to verify. Many researchers and manufacturers publish relative measurement data on their findings, yet this has its own shortcomings, since their reported measurements are relative to a specific situation or application, as defined by them.

In the same way, phosphorescent technologies are still subject to many debates and more knowledge is required to understand their chemical and physical properties. Moreover, this explains why so much important technical optical information is not provided by the manufacturers. A significant amount of work was focused on exploring such considerations, by investigating the long persistent phosphor technology for PV device applications and not just the bulk material itself. There parameters have been taken into consideration within the current body of work and will be used for the modelling, and final design and application of the luminescent devices.

6.6 Thickness Uniformity of Luminescent Layers

The study of the thickness and distribution of the phosphor particles in the luminescent layers was achieved using a confocal microscope to map the layer in 3D. A traditional method was used to measure the thickness of the layer using a micrometre (MITUTOYO SERIES 293-832

MDC Lite Micrometre 0-25mm/0.001mm) and Dektak tool, which purely measures basic considerations such as thickness and surface profiles.

The appropriate solution was to use a method that does not tarnish samples by touching it such as micrometre or profilometry, and furthermore allows the investigation of the luminescent layer composition from inside. That's why the Confocal Laser Scanning Microscopy (Leica TCS SP8) was used to record phosphorescent dispersion in the luminescent layers by painting the layer outside with fluorescent material, to map the internal and external area of the layer.

The three main parameters considered were: the position of the phosphor powders inside the host material, the space distribution of the phosphors, and particle size. Using a confocal instrument, it was possible to map the internal and external areas of the luminescent layer, which develops understanding of details such as formation inside and outside.
Using Method 2 to fabricate the luminescent layers, (as described in section 5.8), a 3D image for the outside and inside of the luminescent layer was produced (as shown in Figure 6.9). The external part of the layer was painted using a reference red fluorescent marker pen, whose known absorbance and emission wavelengths had a different range from those of the phosphor particles.

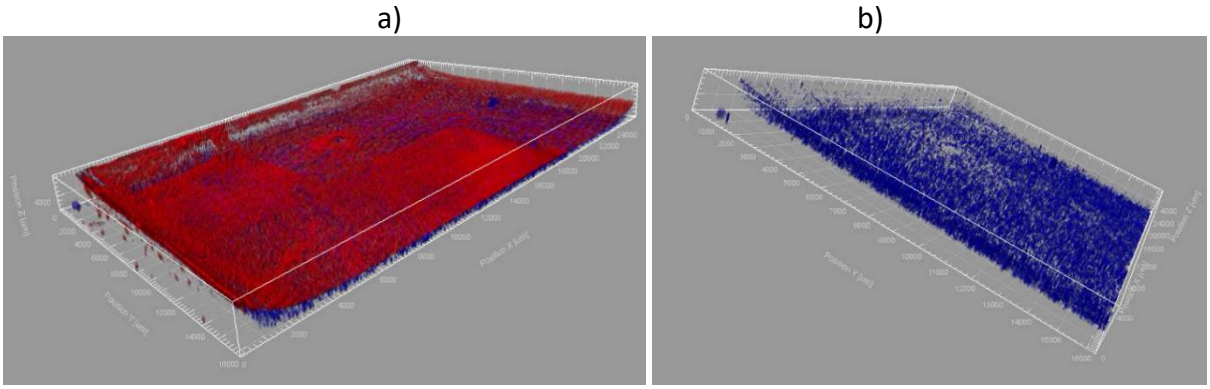

Figure 6.9. (a) 3D image of depth dispersion of the luminescent layer, showing the thickness across all surfaces (red) and the phosphorescent particle distribution inside the layer (blue). (b) 3D image of the luminescent layer (internal area), showing the particle size and dispersion.

The thickness distribution of the layer was obtained by laser scanning microscopy and does not depend upon particle position or concentration, but rather, on the shape of the layer; a condition which imposes a spatial distribution of phosphors on the polymer surfaces. The thickness of the layer is typically 2mm thick within a small edge of effect, approximately 1.5 mm from the bottom edge, and 4mm high.

It is considered that, when large phosphor particles are mixed with the host polymer matrix, both will result in different densities. The phosphorescent particles settle down at the bottom of the surface at an early stage and form a packed layer. The suspended polymer particles subsequently settle on the bottom and around the top surface edge, and fill the voids between the phosphor particles. These observed effects may be formed because of particles settling down on the surface due to gravitational forces, or when the polymer gets dried.

Both sides of the layer have been successfully mapped, and it has been shown that analytical Method 2 produced images of the layer, which verify the thickness dispersion of the different materials, fluorescent dye, phosphorescent particles and host polymer matrix. This confocal method may also be used to help analyse particle size, and particle distribution by scanning the luminescent layers in two-dimensional form, and at different depths, thus enabling the reconstruction of three-dimensional structures of the layer.

6.7 Conclusion

As can be observed from these studies, these results show that it is possible to fabricate a luminescent down-converting LDC layer using these phosphorescent phosphors. By applying Polysiloxanes (Solaris Silicon) as a host polymer material (which presents high transmittance, low scattering, low degrading, and good chemical and physical stability) critical project requirements will be fulfilled.

Careful selection of appropriate phosphorescent species, as the luminescent material demonstrated here, results in a very promising energy storage and LDC converter, since these luminescent LPP species can store the absorbed energy photons for many hours, even at low

intensities. One of the biggest advantages of these luminescent materials is that, instead of remaining in a singlet state, from which the excited electron can easily return to its ground state by emitting its excitation energy as fluorescent over a short lifetime, the phosphorescent can also transition from the triplet excited state to the singlet state, which results in a long excitation lifetime which can increase the luminescence down-converter efficiency. This means that the luminescence originating in triplet states has a longer lifetime which can improve the efficiency of the down convertor.

The fabricated luminescent layers with long persistent phosphors have also demonstrated a higher reflectivity, and higher excitation range extending from the UV-C to the visible bandwidth. This wide absorption is also present in the diffuse sunlight, and the down-converting mechanisms of those higher energy to lower energy photons into the middle visible spectrum band may also be absorbed by the PV device. These results demonstrate that it is possible to control the absorption and emission characteristics of the luminescent device, by applying single or various species of the LLP phosphor species to a better match of the PV technology, (as will be discussed in Chapter 7 and 8), in the electrical characterization of the PV devices.

Ultraviolet/Visible/Infrared spectroscopy was used to quantify the light that was transmitted, reflected, scattered and absorbed by the luminescent layers. These measurements are summarised together and compared at each concentration (0.1-80%wt) for transmission, reflectance, absorbance, and scattering.

The photoluminescent analyses revealed that all luminescent sample layers are suitable for the down-converting application, as they have emission on the visible spectrum range. However, some semiconductor materials of the PV devices such as a-Si, CdTe and mc-Si have been identified as having an external quantum efficiency (EQE) spectra that can absorb high energy photons in the same spectrum region of the LDC layer and therefore the LDC can weaken the power efficiency of these PV devices under illumination. In this case, the benefits of a very wide visible emission band of the luminescent layers, such as the LDC, can be to reduce the PV devices losses, such as transparency and lattice thermalisation. Contrary to

these dark conditions, the addition of the LDC layer on the top/rear of these PV could enhance its efficiency significantly due to the fact of this enhanced absorption on the visible range. This effect will be examined in Chapter 8.

Energy losses in the PV caused by spectral mismatch can be reduced by adapting the PV device spectrum, using a down convertor material such as LPP, where one higher energy UV photon generates two lower energy in the visible band to be absorbed by the PV device. These losses can be potentially reduced by applying the LDC on the top or at the rear of the PV device. However, as discussed earlier, high concentrate LDC applied on top of the PV device can potentially reduce the transmission of the layer, thus reducing the amount of incident light into the PV device.

Phosphorescent materials Ph1-3 represent the best samples for the LDC device, with the highest photoluminescent quantum efficiency amongst all others tested, (as described in Table 6.2). Their optimum optical properties are sensitive to size, shape, concentration, and dispersion/location in the host material. With the help of a UV/Vis spectroscopy tool, it was possible to identify, characterise, and study these luminescent materials.

Different phosphorescent materials which absorb photons in the UV portion and emit visible light to the spectrum, can be used as reflective layer. The application of these luminescent layers in the rear of the PV device may improve the efficiency due to the optical effects such as reflectance and scattering light, which does not rely on the lifetime effect.

The reflectance effect can randomize the direction of the reflected light inside the PV device. With high concentration layers, the device gains high reflection off the rear of the PV surface, which allows the light to reflect upwards and back into the PV, thus allowing for the possible absorption of sunlight. PV device functioning can be dramatically increased by this absorption effect, if both energy photons of light from the sunlight and phosphorescence are able to reach the PV device. It is expected that some of these photons will escape from the luminescent layer, and only those with an angle of incidence, smaller than the critical angle of incidence, will be internally reflected with a high probability of being transmitted towards the PV device.

The lack of description of the product specifications has influenced deductions as to alternative phosphor species, which created a variety of PL results. However, the following material characterizations (including trade-offs between product description accuracy, the ability to verify phosphor species, and covering the need for different material properties and materials of differing PL peaks and sizes etc.) are still under debate. However, this researcher believes it's a truly worthwhile venture, enabling the creation of new materials and furthering future research.

CHAPTER 7

LUMINESCENT LAYERS APPLICATIONS AND ELETRICAL CHARACTERISATION

7.1 Introduction

This Chapter assesses the electrical properties of the PV devices when combined with the luminescent layers on different applications, both as a light trap on top, and a reflector at the rear of the PV device. This chapter includes:

- Electrical characterisation of the PV device with and without the luminescence layers of various concentration ratios at the top and rear of the PV devices.
- Electrical characterisation of the PV device coupled with the luminescent layers at various concentration ratios at the top and rear of the PV devices.
- External quantum efficiency (EQE) of the PV devices coupled with the luminescent layers of various concentration ratios on the top surface of the PV devices.
- Reflectance of the PV devices coupled with the luminescent layers at various concentration ratios at the top (T).

7.2 Applications of the LDC Layers on Different Types of PV Devices

The principal focus of this section is to investigate the ideal applications for the luminescent layers (LDC) with different PV technologies. Despite the number of different types of PV technology, there are still issues with the establishment of an ideal PV technology as appropriate testing samples, because the degree of incompatibility between the PV device structure and the LDC layer applications. The two principal problems are the spectrum match with the LDC layers, and environmental condition, or degradation, of the PV devices. Accordingly, three different types of PV technologies were selected as candidate samples for the applications. (1) Dye-Sensitized Solar Cells (DSSCs), (2) a Monolithic Perovskite Solar Cell (MPC), and an amorphous silicon (a-Si) PV device.

The selected luminescent layers applied in these measurements, were the same luminescent layers, phosphorescent phosphors Ph1-6, PhX and PhT, fabricated and characterized for these

analyses, as described in Chapter 6. The layers can be easily attached and removed from the PV device surfaces, either on the top (T) or at the rear (R), as required during the measurements, and without causing damage, (which is considered a major advantage, by comparison to the same layers and applications on different PV technologies), as illustrated in Figure 3.15.

Current-voltage (I-V) measurements were carried out under standard test conditions, 1000 W/m² AM 1.5 global, 25°C, at Solaronix S.A., Switzerland (as described in section 3.3.8). EQE and reflectance measurements were carried out in a LOANA solar cell analysis system at the Fraunhofer Institute for Solar Energy Systems ISE, Germany (as described in section 3.3.9).

7.2.1 Dye-Sensitized Solar Cell (DSSC)

The Dye-sensitized solar cell was selected because it has well known absorption in both the ultraviolet and visible ranges, which establish it as a good candidate for the luminescent LDC layers. It has also demonstrated absorption on the ultraviolet range, and emission on the visible range. By doing this, the LDC layers can may be used to improve the light harvesting capabilities of the PV device.

The luminescent layers are electronically isolated from the PV device and prove to be a good ultraviolet absorber, with a suitable visible light scattering path length when applied on the top surface of the PV device. Another possible application is by applying the LDC layers at the rear surface as a reflector of the PV device, which may accordingly benefit light collection.

The Dye Solar cell was assembled with a Transparent Conductive Oxide (TCO) coating and an Ionic Liquid Electrolyte cell (TIC) containing a sensitizer (Ruthenizer 535-bis TBA). The total substrate size of the cell was 20x20mm and the active areas was 6x6mm. The dye sensitized solar cell was acquired from Solaronix S.A. (see Figure 7.1 below).

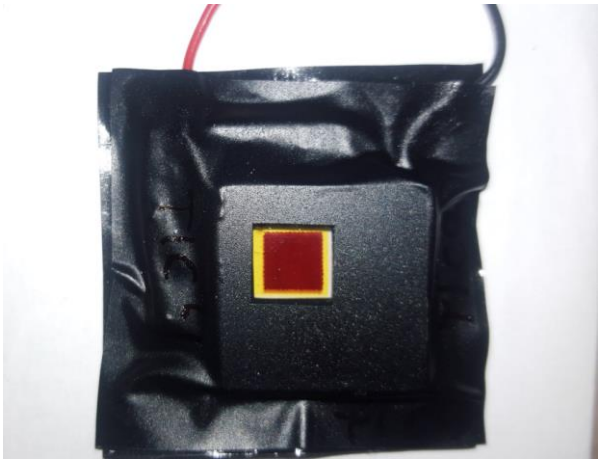

Figure 7.1. Photo of the DSSC PV device with the mask.

In order to conduct an accurate performance assessment of the PV device, it was tested with the cell mask measuring 40x40mm, with an aperture of 8x8mm. The mask is an opaque sticker with a tailored aperture that hides the non-active area of the cell while compensating for the optical losses inherent to masking.

The device was measured firstly without the layers, and subsequently by applying the layers. The first layer measured was the blank sample layer, which is the host matrix and does not contain luminescent particles. This was followed by different luminescent layers at various concentrations at the top (T) and at the rear (R) of the PV device.

7.2.1.1 DSSC with LDC Layers of Phosphor Ph1-3

Figure 7.2 shows the top two rows within the graphs presenting the J-V curves of the photovoltaic performance of the DSSC PV device, with the blank and various LDC sample layers, from the left to right Ph1 to Ph3, at various concentrations, (20-80%wt), applied to both the top (T) and the rear (R) of the PV device, respectively. The third row represents the EQE measurement, the bottom row represents the reflectance measurement. The summary of the measured IV characteristic is listed in separate Tables; Ph1 (Table 7.1 and Table 7.2); Ph2 (Table 7.3 and Table 7.4); Ph3 (Table 7.5 and Table 7.6).

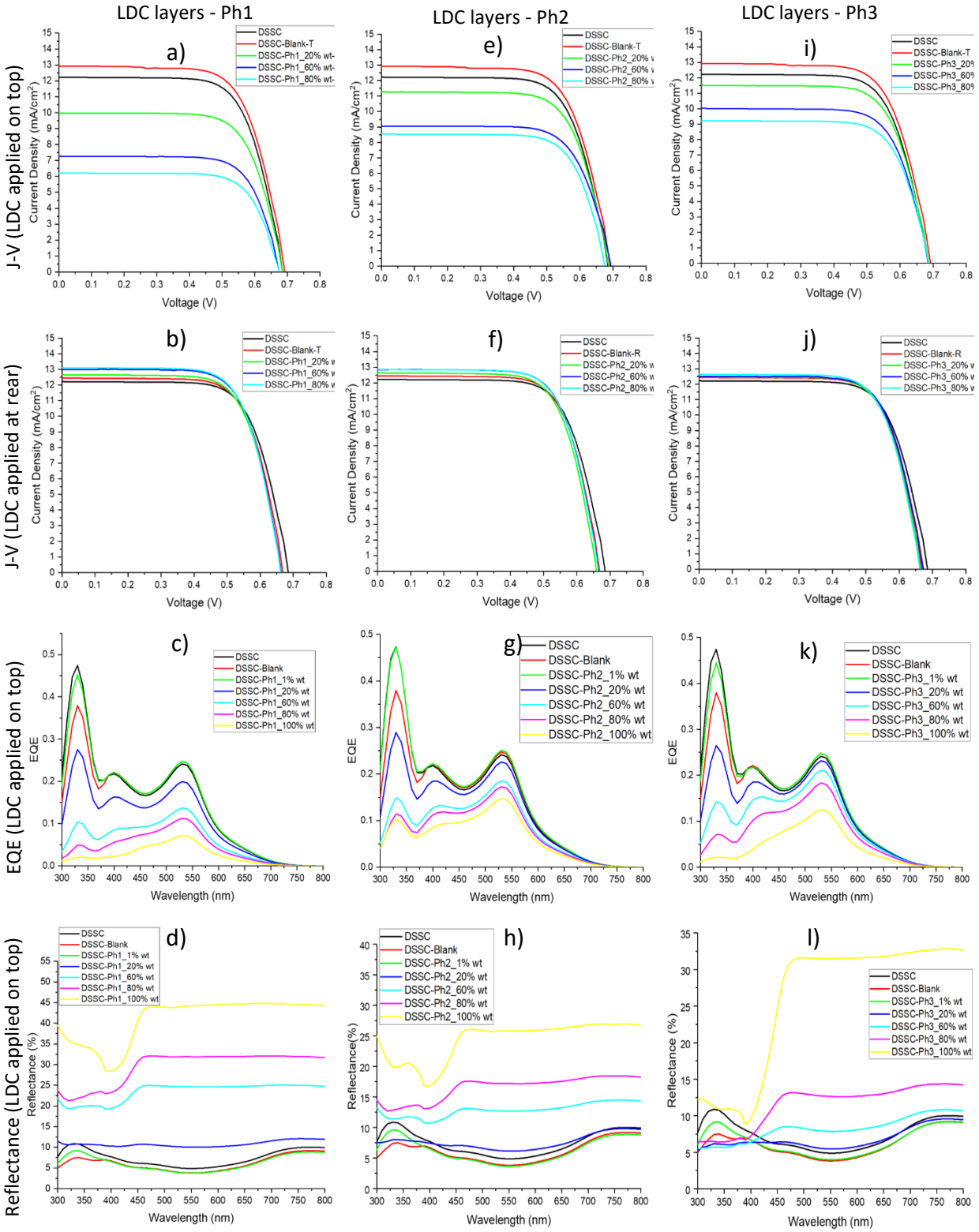

Figure 7.2. A matrix of the DSSC PV device illustrating the performance evaluation of the LDC sample layers, Ph1-3. A matrix of the DSSC PV device illustrating the performance evaluation of the LDC sample layers, Ph1-3, at difference concentrations. Ph1 (a) J-V measurements on the top of the PV device; (b) at rear of the PV device; (c) EQE measurements and (d) Reflectance spectra measurements. Ph2 (e) J-V measurements on the top of the PV device; (f) at rear of the PV device; (g) EQE measurements and (h)

Reflectance spectra measurements. Ph3 (i) J-V measurements on the top of the PV device; (j) at rear of the PV device; (k) EQE measurements and (l) Reflectance spectra measurements.

DSSC with LDC Layers of Phosphor Ph1 (a-d)

Referring to Figure 7.2 (a), it can be clearly observed from this graph, and Table 7.1, that when the blank layer was applied on the top of the DSSC PV device, the short-circuit current density (Jsc) increased from 12.23 to 12.93 mA/cm^2, and that the open circuit voltage, Voc, increased from 0.68 to 0.69V. However, these figures were found to decrease to 9.97, 7.26V and 6.21 mA/cm^2 subsequently, when increasing phosphorescent concentration content was added to the host matrix. The open-circuit voltage (Voc) reduced from 0.68 to 0.67V and remained at this level. Thus, they do not appear to appear do not respond in the same way as do the blank. This effect might be the result of transient effects due to an enhancement in carrier recombination zones resulting in a decrease of Voc (Scheer and Schock, 2011).

The observed efficiency of the PV device performance when LDC layers are applied on the top shows a decrease from 5.85 to 4.82, 3.54 and 3.03%, respectively. This may be because a greater number of phosphorescent particles were dispersed in the host matrix and corresponded to less effective light conversion into the PV device under the current light conditions. As the concentration ratio increases, the light gets trapped inside of the luminescent layer interfaces which are formed by the much higher ratio of doped ions of the phosphors. Furthermore, the amount of light trapped into the LDC layer results in increased or greater energy storage capability and a longer lifetime decay, simultaneous to the down-conversion, which may be considered as a desired effect during dark conditions.

In Figure 7.2 (b); when the luminescent layers were attached to the rear of the DSSC, the short-circuit current density (Jsc) showed an obvious increase as the concentration ratio increased. The photo current of the DSSC device increased to 13.11mA/cm^2 at 80%wt concentration ratio. This result was contrary to the blank layer which had the lowest Jsc, 12.45 mA/cm^2, among all the samples layers. Thus, the presence of more phosphor materials in the host matrix prevented the energy photons from being transmitted though the luminescent layer, by

reflecting and emitting them into the PV device. In addition, the down-conversion process happens simultaneously.

Additionally, the decrease in Voc from 0.68 to 0.66V can also be caused by transient effects which are due to an enhancement in carrier recombination, particularly in the case of a highly reflective layer at the rear of the device, where the local generation rate may be decreased, thus reducing the Voc. A significant improvement is observed in the efficiency of the PV device performance, with a 3.58% increase, from 5.85 to 6.06% at 80%wt. This can be explained by the enhancement due to the presence of the luminescent layers at the rear surface.

Table 7.1. Summary of DSSC photovoltaic performance with luminescent layers of phosphor Ph1 at various concentrations on the top (T) and at the rear (R) along with the reference blank layer.

LDC Layer Application	Jsc (mA/cm^2)	Voc (v)	FF (%)	η (%)
DSSC	12.23	0.68	0.69	5.85
DSSC-Blank-T	12.93	0.69	0.68	6.16
DSSC-Ph1_20%wt-T	9.97	0.68	0.70	4.82
DSSC-Ph1_60%wt-T	7.26	0.67	0.72	3.54
DSSC-Ph1_80%wt-T	6.21	0.67	0.72	3.03
DSSC-Blank-R	12.45	0.66	0.70	5.88
DSSC-Ph1_20%wt-R	12.66	0.66	0.69	5.88
DSSC-Ph1_60%wt-R	13.00	0.66	0.69	6.03
DSSC-Ph1_80%wt-R	13.11	0.66	0.69	6.06

The prepared luminescent layers, with Phosphor Ph1 at various concentration ratios, from a 1 to 100%wt, were evaluated as LDC layers on top of a DSSC PV device, by recording the external quantum efficiency (EQE) of the PV device as a function of wavelength, (see Figure 7.2 (d)). The layers were measured for comparison with the blank layer without the phosphors. The comparison was conducted in this manner to check for additional reflections caused by the introduction of an extra layer on top of the PV device. The reflectance spectra were measured as a function of the incidental light wavelength, (as shown in Figure 7.2 (e)). In addition, a summary of the short-circuit current, Jsc, of the DSSC PV device from the I-V measurement and the Jsc, was calculated from the EQE, as shown in Table 7.2.

With an increased luminescent concentration ratio in the host material, the DSSC EQE increased the absorption in the ultraviolet region, while the light harvesting capability of the PV device is also enhanced in the visible spectra region between 400-550nm, but only for a very low concentration ratio. This enhancement can be observed in Table 7.2, which shows the calculated Jsc increasing, from 2.86 to 2.98 mA/cm2, resulting in a 4.1958% increase at 1%wt concentration ratio.

The high-energy photons are absorbed by the phosphors and emitted at lower energy, reaching the PV device either directly, by reabsorption and re-emission, or via total internal reflection at the low concentration ratio LDC layer. This optimized EQE was obtained for the lowest concentration only, as can be observed in the green line, DSSC-Ph1_1%wt. Lower energy photons are transmitted through the LDC layer and reach the PV device directly, which is not significantly different from the result observed from the blank layer. This confirms that the presence of a critical amount of phosphor Ph1 in the host matrix layer plays a key role in increasing the light harvesting efficiency in the DSSC device. The comparison between the blank and lower concentration luminescent layer was conducted in this manner to check for additional reflections caused by the introduction of higher concentration layers on top of the PV device. The introduction of the higher concentration LDC layer resulted in a reduction of the cell's EQE in the region where the DSSC absorbed light.

This EQE efficiency reduction can be attributed also to the reflection effects, where the energy photons may escape through the front escape cone and sides, or may be due to the low PLQY of the phosphorescent phosphor Ph1. In this way, if the amount of luminescent particles in the host matrix is above 1%wt, the overall PV's quantum efficiency is reduced. This may be caused by the amount of light reflected or scattered before it reaches the PV device. However, this phosphor could absorb near ultraviolet photons, giving rise to characteristic visible energy photons which is a unique property that this LDC layers imposes. The significant blue light (around 480nm) emitted from the excited phosphorescent could be useful in the generation of electricity under a no light condition, during afterglow or lifetime decay. This result concurs with the results obtained by PL spectroscopy. Thus, by having a lower concentration LDC layer <1, the solar energy was converted to electric energy more effectively than by the DSSC

without phosphors, resulting in an increase in quantum efficiency. However, the application of phosphorescent phosphors does not focus on the beneficial effect of the down-conversion of the solar spectrum to a higher EQE alone, but also on the generation of the electrical power from the emitted photons at 400-600nm, which were observed as being significantly higher with the higher concentration ratio.

The luminescent layers of Ph1 have demonstrated a low reflectivity in the ultraviolet range with an increase in the concentration ratio, resulting in a higher reflectivity, from the visible region. The optimised reflectance was obtained for concentrations above 20%_wt. Therefore, in view of this reflectance effect, we can assume that the broadband enhancement in EQE above 400nm corresponds to the increased carrier collection efficiency, and of light harvesting efficiency, in this type of transparent DSSC device. It can drastically increase the reflectance values in that region by applying the LDC at the rear, instead of on the top. Therefore, it is feasible that the luminescent layers with higher concentration, i.e. greater 20%wt, could serve as a reflector coating to further increase the reflectance from this region.

As listed in the device efficiency, (see Table 7.1), it can be seen that η (%) is significantly higher as the concentration ratio increased from 5.85 to 5.88, 6.03 and 6.06%, respectively, when the layers are placed at the rear of the PV device. This implies that the PV device property is improved without creating additional defects inside the PV device, leading to a boost of the device's efficiency under sunlight.

Calculated Jsc from EQE

It was possible to calculate the Jsc short-circuit current from EQE measurements data of the DSSC PV device with the LDC layers of Ph1 on top, at various concentration ratios, between 1-100%wt, by applying equation 7.1 below. The calculated Jsc from EQE measurements are shown in Table 7.2, ("PVEducation," n.d.).

$$Jsc = q \int \varphi(\lambda) \cdot EQE(\lambda)\, d\lambda \quad \textit{Equation 7.1}$$

where q is the charge of the electron, and φ is the photon flux.

The EQE measurement was performed considering the entire active area of the DSSC PV device. However, a standard procedure was applied during the EQE measurement which was performed at 0.3 sun (AM1.5G solar spectrum) using the LOANA system, (as described in section 3.3.9). It is important to point out that DSSC and PSC PV devices have a long-time constant regarding both the chopped monochromatic light (375Hz) and I-V measurement, under light conditions. This can raise issues in relation to charge carrier dynamics and LDC behaviour under such light conditions. Unfortunately, these results were not cross examined for an underlying bias at 1 sun or higher, to check for differences in carrier lifetime or collection efficiency due to the illumination level, which can be a problem considering this type of non-silicon device. One of the main concerns of EQE measurement of DSSC is that it's arbitrary, (according to a similar studies prepared by Ananda, (2017)). Although Ananda systematically drew the comparison between current density value from I-V and Spectral Response, SR, of DSSC and found that current density 1.21mA/cm^2 measured for I-V measurements was 0.28 mA/cm^2 from EQE. Ananda also stressed that DSSCs often exhibit nonlinearity of SR versus light intensity because of mass transport limitations in the electrolyte, or the dependency of electron concentration with its diffusion length. Another factor associated with this difference could be the slow photocurrent response time due to electron trapping (Halme et al., 2010). Thus, the results discussed below were not directly comparable to each other due to the use of two different type of measurements. This was appropriate since such hysteresis effects were anticipated for these types of PV devices, (DSSC and Perovskite), and experts do achieve similar results for these measurements.

Table 7.2. The short circuit current (Jsc) of the DSSC PV device from J-V curves and calculated Jsc from the integration of the EQE curves, with LDC layers of phosphor Ph1 at various concentrations ratio, (1 to 100%wt), on the top (T) surface of the device.

LDC Layer Application	I - V Jsc (mA/cm^2)	EQE (280-800nm) Jsc (mA/cm^2)
DSSC	12.23	2.86
DSSC -Blank-T	12.93	2.89
DSSC-Ph1_1%wt	Not Available	2.93
DSSC-Ph1_20%wt-T	9.97	2.29
DSSC-Ph1_60%wt-T	12.66	1.47
DSSC-Ph1_80%wt-T	6.21	1.16
DSSC-Ph1_100%wt-T	Not Available	0.69

As observed from the Table above, the calculated Jsc from EQE provided results much lower than those established from the I-V measurement. As listed, the DSSC reduced from 12.23 to 2.86mA/cm^2, which is a direct result of the measurement method. The calculated results show that increasing the concentration ratio from 1 to 100%wt, results in a decrease of Jsc proportionally reaching 0.69 mA/cm^2, at a 100%wt concentration ratio. Thus, these comparison results demonstrate the effects of non-identical incident radiation in both cases. The external quantum efficiency and the J-V curve measurements can vary, as noticed in Table 7.2. However, the values of the Jsc followed the same pattern, showing a downward trend. Although the comparison between J-V to EQE is significant for this reason and complies with all discussed results for these LDC Ph1.

It was found that there are several factors that could lead to a lower J_{sc} value or incorrect results from the EQE measurement, and some experts (Scheer and Schock, 2011) describe that these effects can occur in many types of PV device, with the reasons attributed to EQE being lower than Jsc as, for example; a) a barrier to the photo current which is large under low light intensity or monochromatic illumination, but becomes lowered by photodoping of the buffer at AM1.5 illumination, and b) a large number of micro shunts. If the PV device is irradiated only on a limited area (as in the QE measurement), the non-illuminated part acts as a shunting load. Seen from the active PV device, this load is in parallel with the input resistance of the QE current amplifier. Although the total shunt resistance of the device (measured as a macroscopic quantity by J-V analysis) is high, the local shunt resistance seen from the active PV device part may be small. Thus, the current is drained through the shunting load. Reducing the PV area to the area of illumination may increase the QE. These effects therefore show that with regards to the non-identical incidental radiation in both cases, the external quantum efficiency and the J-V curve measurements can vary, as seen in the tabulated results. The values of the Jsc followed the same trend, showing a downward profile. Although the comparison between J-V and EQE is significant for this very reason, it may not represent the PV device total power output under STC.

DSSC with LDC Layers of Phosphor Ph2 (e-h)

Figure 7.2 (e) and the Table 7.3 summary show that, for the LDC layers, Ph2 was applied on the top surface of the PV device, and similar behaviours to the Ph1 previously presented were clearly observed. As listed in Table 7.3, it was found that apart from the blank layer, the short-circuit current density (Jsc) subsequently decreased from 12.23 to 11.27, 9.04 and 8.54 mA/cm^2, with increasing phosphorescent content added to the host matrix. The open-circuit voltage reduced from 0.68 to 0.67V.

Table 7.3. Summary of DSSC photovoltaic performance attached to the host matrix, blank, and the luminescent layers of phosphor Ph2 at various concentration ratios on the top (T) and at the rear (R).

LDC Layer Application	Jsc (mA/cm^2)	Voc (v)	FF (%)	η (%)
DSSC	12.23	0.68	0.69	5.85
DSSC-Blank-T	12.93	0.69	0.68	6.16
DSSC-Ph2_20%wt-T	11.27	0.68	0.70	5.42
DSSC-Ph2_60%wt-T	9.04	0.69	0.70	4.40
DSSC-Ph2_80%wt-T	8.54	0.67	0.71	4.13
DSSC-Blank-R	12.45	0.66	0.70	5.85
DSSC -Ph2_20%wt-R	12.64	0.65	0.70	5.83
DSSC -Ph2_60%wt-R	12.85	0.66	0.69	5.98
DSSC-Ph2_80%wt-R	12.87	0.66	0.70	5.99

With regards to efficiency, the PV device performance when LDC layers were applied on the top, showed a decrease from 5.85 to 5.42, 4.40 and 4.13%, respectively. This may be caused by a greater number of phosphorescent particles dispersed in the host matrix, which corresponded to less effective light conversion into the PV device, under the light condition. As the concentration was increased from 20 to 80%wt, the light gets trapped inside of the luminescent layer interfaces, which have been formed by the much higher ratio of the doped ions of the phosphors.

Figure 7.2 (f), indicates LDC layers applied at the rear of the DSSC, where the short-circuit current density (Jsc) showed a clear increase, in accordance with an increase of concentration ratio. The photocurrent of the DSSC device increased to 12.87mA/cm^2 at 80%wt concentration ratio. The decrease in Voc from 0.68 to 0.66V can be caused by transient effects, which were

an undesirable side-effect. A significant improvement was observed in the efficiency of the PV device performance from 5.85% to 5.99%, which represent a 2.39% increase. This can be explained by enhancement due to the presence of a higher concentration of luminescent materials at the rear surface of the PV device, (acting as reflective layer as well as down converting).

EQE Measurement and Reflectance

Figure 7.2(g), as observed with Ph1, represents an increase of the luminescent concentration ratio in the host matrix. The DSSC EQE increased the absorption in the ultraviolet region, while the light harvesting capability of the PV device was enhanced in the visible spectra region between 450-600nm, (in the case of Ph2). This enhancement can be seen in Table 7.4, which shows the calculated Jsc increasing from 2.86 to 2.97 mA/cm2, which is a 3.84% increase at 1%wt concentration ratio. The high-energy photons are absorbed by the phosphors and emitted at lower energies, reaching the PV device either directly, or via reabsorption and re-emission, or via total internal reflection at the low concentration ratio LDC layer. This optimized EQE was obtained at 1wt% as can be observed in the green line, DSSC-Ph2_1%wt, in the graph above. Lower energy light is transmitted through the LDC layer and reaches the PV device directly; not significantly different from the result observed from the blank layer. This confirms that the presence of a small amount of phosphor Ph2 in the host matrix layer plays a key role in increasing the light harvesting efficiency in the DSSC device. The introduction of the higher concentration LDC layer resulted in a reduction of the cell's EQE in the region where the DSSC absorbed light.

The EQE efficiency reduction can be attributed to the reflection, which may escape through the front escape cone and sides, due to the low PLQY of the phosphorescent phosphor, Ph2. In this way, if the amount of the luminescent particles in the host matrix is too large, the overall quantum efficiency of the PV is reduced. This may be caused by the amount of light reflected or scattered before it reaches the PV device.

A significant luminous vivid green cyan light, around 495nm, was emitted from the excited phosphorescent which may be useful to generate electricity under a no light conditions, during afterglow or lifetime decay. This compliments results obtained by the PL spectroscopy. By having a lower concentration LDC layer <1%wt, the solar energy was converted to electric energy more effectively than by the DSSC without phosphors, resulting in an increase of quantum efficiency. On the contrary, the higher the concentration, the longer the lifetime decay or long persistence effect which is the main focal point of this project application on the PV device. Thus, the application of phosphorescent phosphors does not focus solely on the beneficial effect of the down-conversion of the solar spectrum to a higher EQE alone, but also on the generation of the electrical power from the emitted photons, from 450-600nm, in the dark, which were also observed to be significantly higher with the higher concentration ratio.

Interestingly, the LDC layers of phosphor Ph2 similarly resulted in low reflectively, below 15%, in the ultraviolet and visible range, for concentrations below 60wt%. The 20%wt shows almost no difference between 0.07-0.1%, across all spectra in the range. Thus, the optimised reflectance was obtained for a concentration above the 60%_wt.

Thus, from this reflectance effect, we can assume that the broadband enhancement in EQE, above 400nm, corresponds to the increased carrier collection efficiency. In addition, light harvesting efficiency in this type of transparent DSSC device can drastically increase the reflectance values in that region, by staking the LDC at the rear, instead of at the top.

Thus, it is feasible to consider that the luminescent layers with higher concentrations, greater than 60%wt, could serve as reflective layers, to further increase the reflectance from this region. According to the PV device efficiency presented in Table 7.3, as observed, the η (%) is significantly higher as the concentration ratio increased from 5.85 to 5.83, 5.98 and 5.99% at 80%wt, implying the PV device property is improved without creating additional defects inside the PV device, leading to a boost of the device's efficiency.

Calculated Jsc from EQE

Table 7.4. The short circuit current (Jsc) of the DSSC PV device from J-V curves and calculated Jsc from the integration of the EQE curves of AM1.5G, with LDC layers of phosphor Ph2 at various concentration ratios (1-100%wt), on the top (T) surface of the device.

LDC Layer Application	I - V Jsc (mA/cm^2)	EQE (280-800nm) Jsc (mA/cm^2)
DSSC	12.23	2.86
DSSC-Blank	12.93	2.89
DSSC-Ph2_1%wt	Not Available	2.97
DSSC-Ph2_20%wt	11.27	2.59
DSSC-Ph2_60%wt	9.04	2.03
DSSC-Ph2_80%wt	8.54	1.87
DSSC-Ph2_100%wt	NA	1.57

As observed in Table 7.4, the calculated Jsc from EQE was much lower than that of the I-V measurement. As listed, the DSSC reduced from 12.23 to 2.86mA/cm^2. The calculated results show that increasing the concentration ratio from 1 to 100%wt, results in a decrease of Jsc proportionally reaching 1.57mA/cm^2 at a 100%wt concentration ratio. The reasons were found to be the same as for Ph1.

DSSC with LDC Layers of Phosphor Ph3 (i-k)

Figure 7.2(i) shows the LDC layers Ph3 applied on the top surface of the PV device, following a similar pattern to Ph1-2 presented in the earlier sections, (see Table 7.5). It was established that apart from the blank layer, the short-circuit current density (Jsc) subsequently decreased from 12.23 to 9.21 mA/cm^2 as increasing phosphorescent content was added to the host matrix. Interestingly, the open-circuit voltage remained the same at 0.68V and did not reduce. In terms of the efficiency of the PV device performance, when LDC layers are applied on the top, it shows a decrease from 5.85 to 5.53, 4.85 and 4.49%, respectively. However, this reduction of Jsc and efficiency was caused by a greater amount of phosphorescent particles dispersed in the host matrix, and corresponded to less effective light conversion into the PV device under these light conditions. As the concentration ratio increases the light gets trapped inside of the luminescent layer interfaces which are formed by the much higher ratio of doped ions of the phosphors. Furthermore, the amount the light trapped into the LDC layer resulted in greater energy storage, and a longer decay, as a result of down-conversion.

Table 7.5. Summary of the DSSC photovoltaic performance attached to the host matrix and the luminescent layers phosphor of Ph3 at various concentration ratios, (20-80%wt) on the top (T) and at the rear (R) of the PV device.

LDC Layer Application	Jsc(mA/cm^2)	Voc(v)	FF (%)	η (%)
DSSC	12.23	0.68	0.69	5.85
DSSC-Blank-T	12.93	0.69	0.68	6.16
DSSC-Ph3_20%wt-T	11.51	0.68	0.70	5.53
DSSC-Ph3_60%wt-T	10.01	0.68	0.70	4.85
DSSC-Ph3_80%wt-T	9.21	0.68	0.71	4.49
DSSC-Blank-R	12.45	0.66	0.70	5.85
DSSC-Ph3_20%wt-R	12.51	0.66	0.70	5.84
DSSC-Ph3_60%wt-R	12.52	0.67	0.70	5.90
DSSC-Ph3_80%wt-R	12.66	0.66	0.70	5.88

Regarding Figure 7.2(j), and the LDC layers Ph3 placed at the rear of the DSSC, the short-circuit current density, Jsc, showed a slight increase as the concentration ratio increased. The photocurrent of the DSSC device increased from 12.23 to 12.66mA/cm^2 at 80%wt concentration ratio. This Jsc increase was caused by the presence of more phosphor materials in the host matrix, which prevented the energy photons from being transmitted through the luminescent layer by reflecting and emitting energy photons into the PV device.

The decrease in Voc from 0.68 to 0.67 and 0.66V can be caused by transient effects due to an enhancement in carrier recombination, specifically in the case of a highly reflecting layer at the rear. The local generation rate may be decreased, thus reducing the Voc.

The improvement observed in the efficiency of the PV device performance increased from 5.85% to 5.88%, much higher than that of the blank layer at 5.85%, which represents a 0.51% increase. This increase can be explained by the enhancement due to the presence of the luminescent.

Figure 7.2 (k), presents an increase of the luminescent concentration ratio in the host material, where the DSSC measurements show that EQE increased the absorption in the ultraviolet region, while the light harvesting capability of the PV device was enhanced in the visible spectra region between 450-600nm. Interestingly, both the DSSC and luminescent Ph3 have peaks centred around 520nm. The optimized EQE was obtained for 1wt% as can be observed in the green line, DSSC-Ph3_1%wt, and this enhancement can be noted in the Table 7.6, which

shows the calculated Jsc increasing from 2.86 to 2.92 mA/cm2, (a 2.09% increase). The high-energy photons are absorbed by the phosphors and emitted at lower energies reaching the PV device either directly, or via reabsorption and re-emission, or via total internal reflection at the lower concertation ratio.

However, lower energy light is transmitted through the LDC layer and reaches the PV device directly, a result not entirely different from that observed in the blank layer. This confirms that the presence of a critical amount of phosphor Ph3 in the host matrix layer plays a key role in increasing the light harvesting efficiency in the DSSC device. The EQE efficiency reduction can be attributed to the reflection effects, in a similar manner to Ph1-2.

The green light around 524nm was emitted from the excited phosphorescent phosphor species which could be useful in the generation of electricity under a no light condition, during afterglow or lifetime decay. This agrees well with the results obtained by the PL spectroscopy. Thus, within a lower concentration luminescent layer <1%wt, the solar energy was converted to electric energy more effectively than by the DSSC without phosphors, resulting in an increase in quantum efficiency. On the contrary, the higher the concentration ratio the longer the lifetime decay or long persistence effect and its impact on the PV device, which is of specific interest to this research.

In Figure 7.2 (I) the LDC layers of phosphor Ph3 have resulted in a low reflectivity in the ultraviolet range for all concentrations, (maximum of 0.125%), and with the lowest compared to Ph1 and Ph2. However, the increase in the concentration ratio resulted in high reflectivity, particularly in the visible wavelength region. The optimised reflectance was obtained for concentrations above 60%_wt. Therefore, from this reflectance effect, we can assume that the broadband enhancement in EQE above 400nm corresponds to an increased carrier collection efficiency and of light harvesting efficiency in this type of transparent DSSC device, and it can drastically increase the reflectance values in that region by staking the LDC at the rear, instead of at the top. Therefore, it can be stated that the luminescent layers with higher concentrations, greater than 60%wt, could serve as a reflector coating to further increase the reflectance from this region, in addition to down conversion.

According to the device efficiency in Table 7.5 the η (%) is suppressed at significantly higher levels as the concentration ratio increased, from when the concentration ratio is above 20%wt, reaching 5.90 at 60%wt and 5.88% at 80%wt, thus implying that the PV device property is improved without creating an additional defect inside the PV device, leading to a boosted device efficiency.

Calculated Jsc from EQE

Table 7.6. The short circuit current (Jsc) of DSSC PV device from J-V curves and calculated Jsc from the integration of the EQE curves of AM1.5G, with LDC layers of phosphor Ph3 at various concentration ratios (1-100%wt), on the top (T) surface of the device.

LDC Layer Application	I - V Jsc (mA/cm^2)	EQE (280-800nm) Jsc (mA/cm^2)
DSSC	12.23	2.86
DSSC-Blank	12.93	2.89
DSSC-Ph3_1%wt	Not Available	2.92
DSSC-Ph3_20%wt	11.51	2.63
DSSC-Ph3_60%wt	10.01	2.31
DSSC-Ph3_80%wt	9.21	1.92
DSSC-Ph3_100%wt	Not Available	1.22

As observed from the Table above, the calculated Jsc from the EQE resulted in a much lower statistic than that achieved by the I-V measurement as listed with the DSSC, when concentrations were reduced from 12.23 to 2.86mA/cm^2. The calculated results show that by increasing the concentration ratio from 1 to 100%wt, the Jsc decreased proportionally, reaching 1.22mA/cm^2 at a 100%wt concentration ratio. Thus, these comparison results demonstrate the effects a non-identical incident radiation had in both cases. The external quantum efficiency and the J-V curve measurements can vary, as noticed in the tabulated results. However, the values of the Jsc followed the same trend, showing a downward profile. Yet, the comparison between J-V to EQE is significant due to this reason and complies with all discussed results for the LDC layers Ph3, as described above.

7.2.1.2 DSSC with LDC Layers of Phosphor Ph4-6

Figures 7.3 and 7.7 present the photovoltaic performance of the DSSC device, (blank) and Ph4-6 luminescent layers at 60%wt concentration applied on the top (T) and at the rear (R) of the PV device, respectively. The summary of the measured IV characteristics is listed in Table 7.7.

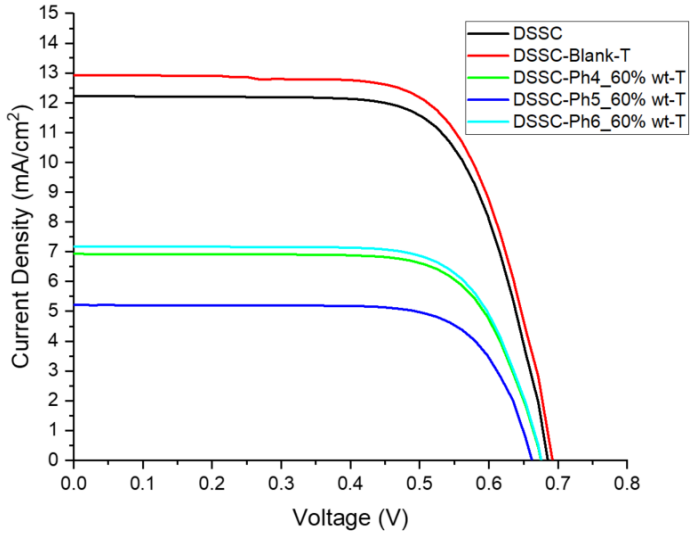

Figure 7.3. J-V curves of the DSSC device attached to the host (blank) matrix and the LDC layers of phosphors (Ph4-6 at 60%_wt), on the top (T) of the PV device.

The luminescent layers prepared with the Phosphorescent materials Ph4, Ph5 and Ph6, have demonstrated a similar behaviour as the Ph1-3 layers presented in earlier sections. It was established that the layers, when applied at the top surface of the PV device, at 60%wt concentration, decreased the photocurrent density from 12.23 to 6.93, 5.21 and 7.18 mA/cm^2, respectively. Considering the different luminescent materials, Ph6 demonstrated the lowest current density among all three LDC layers. The open-circuit voltage reduced from 0.68 to 0.67, 0.66 and 0.67 V respectively, and the Ph5 resulted in the lowest Voc value which can lead to a higher transient effect.

With regards to the efficiency results, the PV device performance when LDC layers are applied on the top it, shows an expected decrease from 5.85 to 3.37, 2.52 and 3.49%, respectively. Having these highly concentrated LDC layers with a greater amount of phosphorescent particles dispersed in the host matrix corresponded to less effective light conversion into the

PV device under illumination. As observed in previous sections, by increasing the concentration ratio, the light gets trapped inside of the luminescent layer interfaces which are formed by the much higher ratio of doped ions of the phosphors.

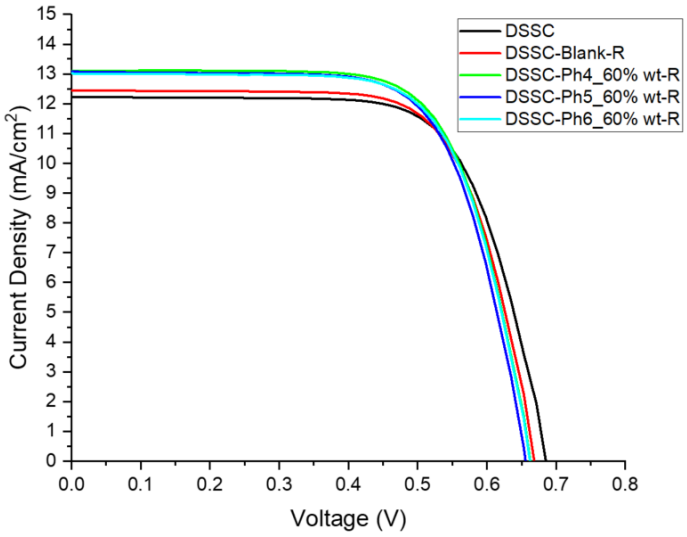

Figure 7.4. J-V curves of the DSSC device attached to the host (blank) matrix and the LDC layers of phosphors Ph4-6 at 60%_wt, at the rear (R) of the PV device.

The three LDC layers were attached at the rear of the DSSC following the same procedures and the results as previous measurements (Ph1-3) and shows that short-circuit current density (Jsc) resulted in an increase from 12.23 to 13.11, 13.07 and 13.01mA/cm^2 respectively at this 60%wt concentration ratio. The most significant gain was observed in Ph4 among all 6 phosphors examined. This Jsc increase was caused by the presence of these phosphor materials in the host matrix, which prevented the energy photons from being transmitted though the luminescent layer, by reflecting and emitting into the PV device. Additionally, the down-conversion process occurred simultaneously.

The open circuit voltage resulted in a decrease from 0.68 to 0.66, 0.65 and 0.66V, respectively. This can be caused by transient effects which are due to an enhancement in carrier recombination, specifically in the case of a highly reflecting layer at the rear, where the local generation rate may be decreased, thus reducing the Voc.

The differences observed in the efficiency of the PV device performance from 5.85% to 6.07, 5.96 and 6.00%, respectively, were subsequently higher than the blank layer, 5.85%. This

increase can be explained by enhancement due to the presence of the luminescent layers at the rear surface of the PV device.

Table 7.7. Summary of DSSC photovoltaic performance attached to the host matrix, (blank), and the luminescent layers of phosphor Ph4-6 at 60%wt concentration ratio on the top (T) and at the rear (R).

LDC Layer Application	Jsc (mA/cm^2)	Voc (v)	FF (%)	η (%)
DSSC	12.23	0.68	0.69	5.85
DSSC-Blank-T	12.93	0.69	0.68	6.16
DSSC-Ph4_60%wt-T	6.93	0.67	0.72	3.37
DSSC-Ph5_60%wt-T	5.21	0.66	0.73	2.52
DSSC-Ph6_60%wt-T	7.18	0.67	0.71	3.49
DSSC-Blank-R	12.45	0.66	0.70	5.85
DSSC-Ph4_60%wt-R	13.11	0.66	0.69	6.07
DSSC-Ph5_60%wt-R	13.07	0.65	0.69	5.96
DSSC-Ph6_60%wt-R	13.01	0.66	0.69	6.00

EQE measurements and Reflectance

The prepared luminescent layers, Phosphor Ph4 and Ph5, at 60%wt concentration ratio, were evaluated as LDC layers on top of a DSSC PV device by recording the external quantum efficiency (EQE) of the PV device as a function of wavelength, (see Figure 7.5). The reflectance spectra were measured as functions of the incidental light wavelength as shown in Figure 7.6. In addition, the summary of the short-circuit current Jsc of the DSSC PV device from the I-V measurement, and the Jsc calculated from using the EQE, is shown in Table 7.8. Unfortunately, the EQE and reflectance of the luminescent layer Ph6 was not included in this analysis because the file was corrupted during the analysis process.

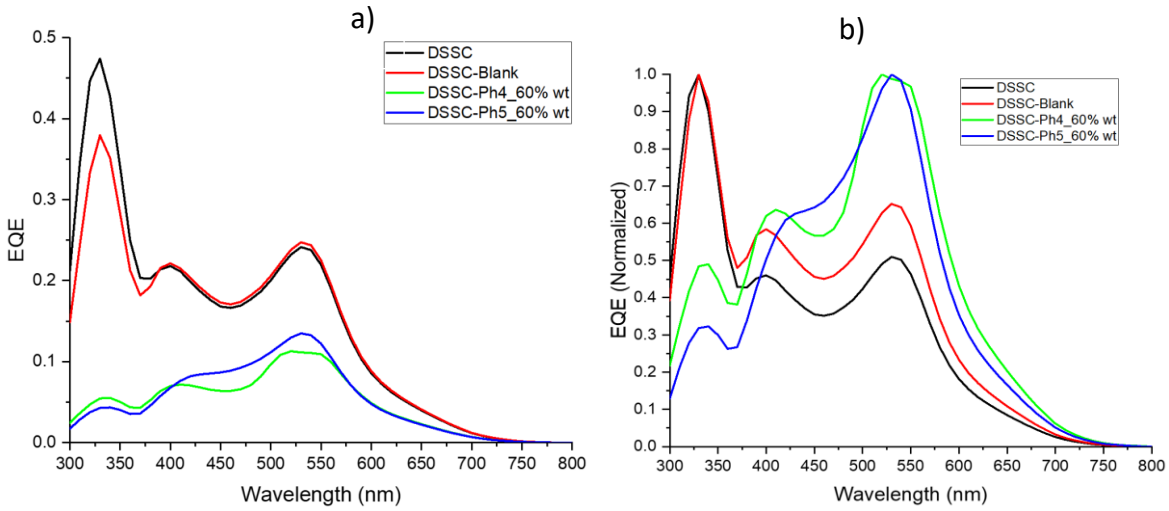

Figure 7.5. a) EQE measurements of the DSSC PV device attached to the host (blank) matrix and the LDC layers of phosphors Ph4-5 at 60%_wt, at the Top (T) surface of the PV device. b) Normalized EQE measurement data.

Figure 7.5 (a) shows that by applying the luminescent layers at a 60%wt concentration ratio in the host material, the DSSC EQE is reduced. This reduction can be verified in Table 7.8, which shows the calculated Jsc increasing from 2.86 to 1.24 and 1.39 mA/cm2, with Ph4 and Ph5 at 60%wt concentration ratio. However, an increased absorption in the ultraviolet region was observed, while the light harvesting capability of the PV device is enhanced in the visible spectra region between 400-700nm, (as seen in the normalized graph spectra Figure 7.5 (b)). Thus, the luminescent layer, Ph4, has emission peaks centred at 579nm and Ph5 at 602nm, which were examined in the PL spectroscopy analysis. The high-energy photons were absorbed by the phosphors and emitted at lower energies reaching the PV device.

The comparison between the blank and 60%wt concentrations layers, for these two different luminescent species, demonstrated that the introduction of the higher concentration LDS layers resulted in a reduction of the cell's EQE in the region where the DSSC absorbed light. The external quantum efficiency of the luminescent layer Ph4 resulted in a higher EQE in the ultraviolet range, (300-400nm) and a lower EQE in the visible range, (400-550nm). On the contrary, with Ph5, it has proved markedly to be in the visible range, between 400-550nm. The EQE reduction can be attributed to the low PLQY of the phosphorescent phosphors Ph4 and Ph5. As discussed earlier, if the amount of the luminescent particles in the host matrix is too

large, the overall PV's quantum efficiency is reduced. This may be caused by the amount of light absorbed, reflected or scattered before it reaches the PV device. However, these phosphors could absorb near ultraviolet photons, giving rise to the characteristic emission of visible photons which is a feature unique to this LDC. These emission ranges from the excited phosphorescent layers could be useful in the generation of electricity under a no light condition, during afterglow or lifetime decay of the phosphorescent. This corresponds with the results obtained by PL spectroscopy, as discussed in Chapter 6.

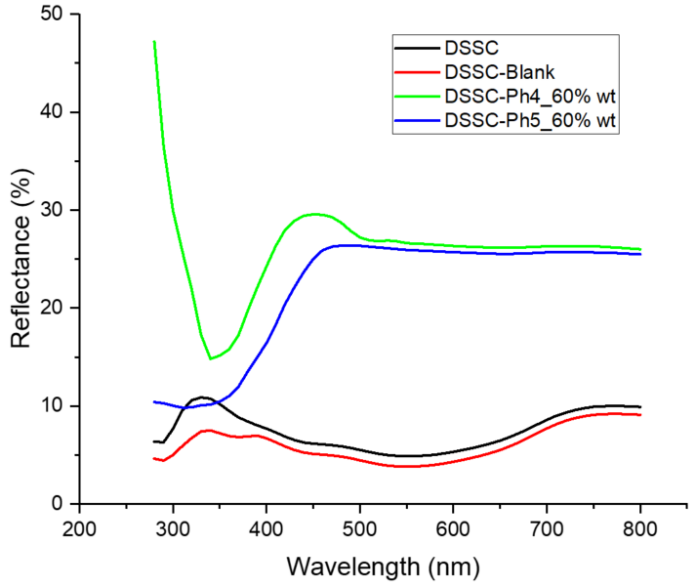

Figure 7.6. Reflectance spectra of the DSSC PV device attached to the host (blank) matrix and the LDC layers of phosphors Ph4-5 at 60%_wt, at the Top (T) of the PV device.

Figure 7.6 shows the LDC layers of Ph4 and Ph5 have demonstrated a low reflectivity in the ultraviolet range and interestingly Ph5 was the lowest among all LDC layers, (Ph1-6). Accordingly, from this reflectance effect, we can assume that the broadband enhancement in EQE above 400nm corresponds to the increased carrier collection efficiency and light harvesting efficiency in this type of transparent DSSC device. Furthermore, it can significantly increase the reflectance values from that spectrum region, by installing the LDC at the rear, instead of at the top.

It can also be asserted that the luminescent layers with 60% or higher concentration ratio could serve as reflector coating to further increase the reflectance from this region on this type of

transparent PV device. According to the device efficiency, as presented in Table 7.7, it can be seen that η (%) is significantly higher for these three different LDC layers, (Ph4-6, from 5.85 to 6.07, 5.96 and 6.00% at 60%wt), implying the PV device property is improved without creating an additional defect inside the PV device, leading to boosted device efficiency.

Calculated Jsc from EQE

Table 7.8. The short circuit current (Jsc) of the DSSC PV device from J-V curves and calculated Jsc from the integration of the EQE curves of AM1.5G, with LDC layers of phosphor Ph4-5 at 60%wt concentrations ratio, on the top (T) surface of the device.

LDC Layer Application	I - V Jsc (mA/cm^2)	EQE (280-800nm) Jsc (mA/cm^2)
DSSC	12.23	2.86
DSSC-Blank	12.93	2.89
DSSC-Ph4_60%wt-T	6.93	1.24
DSSC-Ph5_60%wt-T	5.21	1.39

As observed in Table 7.8, the calculated Jsc results from EQE were much lower than those of the I-V measurement, and as listed, the DSSC reduced from 12.23 to 2.86mA/cm^2. These comparison results demonstrate the effects a non-identical incidental radiation had in both cases. The external quantum efficiency and the J-V curve measurements can vary, as noticed in these tabulated results, (these were explained in the earlier sections). The values of the Jsc followed the same pattern showing a downward trend, although the comparison between J-V to EQE is significant for this reason and complies with all discussed results presented previously. The calculated results show that for a concentration of 60%wt, the result was a decrease of Jsc for both layers, Ph4-5, reaching 1.24 and 1.39mA/cm^2.

7.2.1.3 DSSC with Optimized Luminescent Layers – PhX and PhT

Current- Voltage Measurements

Figure 7.7 presents the photovoltaic performance of the blank DSSC device, and the optimized PhX and PhT luminescent layers at 60%wt concentration ratio applied on the top (T) of the PV device. The optimized luminescent layers PhX and PhT were fabricated with the mixing of various phosphors species, (as explained in Chapter 6). The PhX layer, produced with the

mixing of Ph1-3 with 20%wt for each phosphor, presented with the highest (>30% PLQY) quantum efficiency. PhT, was a combination of all phosphors, Ph1-6, 10%wt for each phosphor. The layers were measured to compare with the blank layer (which is the host matrix without the phosphors). The summary of the measured IV characteristics are listed in Table 7.9.

These measurements were carried out a few months later than the date of the initial characterizations, but all the measurements were performed under standard test conditions (STCs), (as described in section 3.3.8, at the Fraunhofer Institute for Solar Energy Systems ISE, Germany). Between measurements, the PV device had shown some signs of degradation, which resulted in a reduction of its performance characteristics. For example, the efficiency of PV device was measured initially at 5.85%, (which was displayed earlier), and during this measurement it was found to be 4.71%, resulting in a decrease of 19.48%.

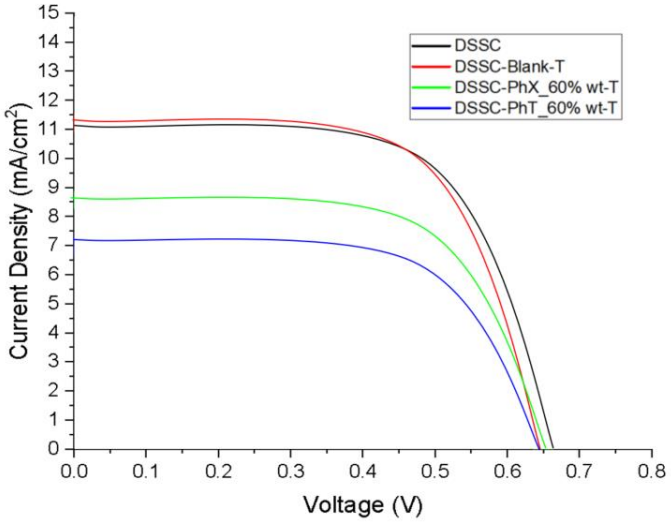

Figure 7.7. J-V curves of the DSSC device attached to the host (blank) matrix and the LDC layers of phosphor PhX and PhT- at 60%_wt concentration, on the top (T) of the PV device.

When the blank layer was applied on the top of the DSSC device, it was observed that the short-circuit current density (Jsc) increased in Jsc from 10.97 to 11.22 mA/cm^2 and that the open circuit voltage, Voc, decreased from 0.66 to 0.64V. For the luminescent layers PhX and PhT, the short-circuit current density (Jsc) decreased to 8.48 and 7.13 mA/cm^2 respectively, with phosphorescent content added to the host matrix. This may be caused by a greater number of phosphorescent particles dispersed in the host matrix which corresponded to less effective light conversion into the PV device under illumination. It is considered a high concentration ratio, at 60%wt, and the light gets trapped inside of the luminescent layer

interfaces which are formed by the much higher ratio of doped ions of the phosphors. The open-circuit voltage of both layers, PhX and PhT, reduced from 0.66 to 0.65, 0.64V. This effect can be due to transient effects, as described in earlier sections. Interestingly, the device resulted in a higher Fill factor, with both optimized layers increasing from 0.65 to 0.67 and 0.68%, respectively. This may be due to the energy conversion efficiency increases as a result of reducing the reflection of incidental light. With regards to efficiency, the PV device performance shows a decrease from 4.71 to 3.73 and 3.17%, respectively. Thus, the amount of light trapped into the LDC layer resulted in further energy storage and a longer decay, occurring simultaneously with down-conversion.

Table 7.9. Summary of the DSSC photovoltaic performance attached to the host matrix, (blank), and the luminescent layers of phosphor PhX and PhT, at 60%wt concentration ratio on the top (T) of the PV device.

LDC Layer Application	Jsc (mA/cm^2)	Voc (v)	FF (%)	η (%)
DSSC	10.97	0.66	0.65	4.71
DSSC-Blank-T	11.22	0.64	0.65	4.72
DSSC-PhX_60%wt-T	8.48	0.65	0.67	3.73
DSSC-PhT_60%wt-T	7.13	0.64	0.68	3.17

EQE measurements and Analysis of the Area Under EQE

The prepared optimized luminescent layers, PhX and PhT, were evaluated as LDC layers on top of a DSSC PV device by recording the external quantum efficiency (EQE) of the PV device as a function of wavelength, (Figure 7.8). The areas under those curves were evaluated, and displayed in percentages, for all LDC layers, (Ph1-5, Ph6 was not measured, PhX and PhT). Results are shown in Figure 7.9.

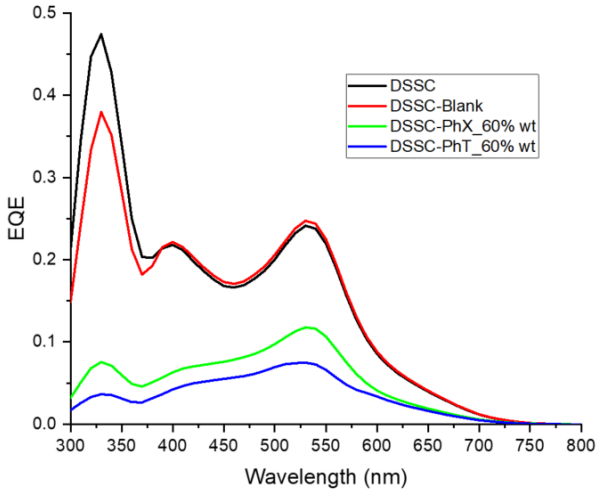

Figure 7.8. EQE measurements of the DSSC PV device attached to the host (blank) matrix and the LDC layers, of phosphors PhX and PhT, at 60%wt concentration ratio, on the top (T) of the PV device.

As observed with the high concentration LDC layers, PhX and the PhT, on the top surface of the DSSC, there was a reduction of EQE. However, the absorption in the ultraviolet region, (while the light harvesting capability of the PV device is enhanced in the visible spectra region between 400-750nm), was enhanced in both cases. This enhancement can be verified (see Figure 7.9 which shows the normalized EQE measurements of the PV device as a function of the wavelength for both these layers and also includes other LDC layers, (Ph1-5)). The EQE were normalized to more clearly demonstrate the effects of each LDC layer. In order to compare the EQE effects caused by the introduction of the different LDC layers on the top surface of the PV device, the areas under those curves were evaluated, and displayed in percentages. After evaluation of the normalized curves, it was revealed that the maximum area does not lie either under the curves of the PhX or the PhT layers, and hence does not represent the maximum EQE, resulting in only 11.44 and 11.95% respectively. The maximum area under the curves was found to be LDC Ph2 with 12.38%, followed by Ph3 at 12.03%. thus, lies on single phosphors species used in the production of the layer, it is perhaps because the total quantum efficiency of the LDC layer has decreased using the mixing species with lower quantum efficiency.

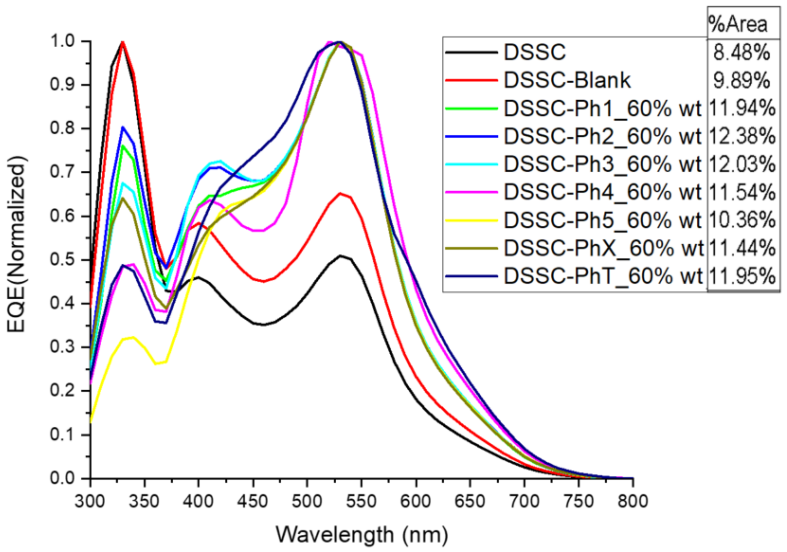

Figure 7.9. Normalized EQE measurements of the DSSC PV device attached to the host (blank) matrix and the all LDC layers, with phosphors Ph1-5, PhX and PhT, at 60%wt concentration ratio, on the top (T) of the PV device. The EQEs were normalized to more clearly demonstrate the effect of each LDC layer. Inserted values of each individual area, beneath the curve, were calculated and a percentage displayed for each LDC layer.

From the normalization procedure, the calculate percentage of peak area in relation to total area of peaks under interest,(which is inserted in the graph, %Area), show that the PhT layer is one of the most remarkable light harvesting devices, and was found to have a wider enhanced energy in the visible spectrum range. This effect becomes significant between 425-700nm and may be caused by the mixing of different phosphorescent species, (Ph1-6), which results in a wider emission spectra. Interestingly, both graphs, PhT and Ph1, show almost the same area in the percentage, 11.95 and 11.94%. However, this area has not arisen because of the high amount of UV light absorbed by PhT, which is subsequently trapped into the layer. Similarly, with respect to Ph2 and Ph3; they were found to have the largest areas in the percentage. Yet the emission in the visible range was lower than PhT. The EQE increase around 430nm and benefits were found to enhance DSSC absorption.

However, kept in perspective, this enhancement is seen to be moderate, with reference to the LDC layer concentration ratio achieved in the top surface of the PV device. Furthermore, by representing the integrated areas beneath a curve as a function of the wavelength, all the data, regardless of the type of luminescent species, seem to follow a common trend which is linked to the quantum efficiency of the phosphors, where Ph1-3 demonstrate high PLQY values.

The high-energy photons are absorbed by the phosphors and emitted at lower energies, reaching the PV device either directly, via reabsorption and re-emission, or via total internal reflection at the low concertation ratio LDC layer. Thus, the EQE efficiency reduction can be attributed to reflection where light escapes through the front escape cone and sides due to low PLQY achieved by the mixing of the phosphorescent phosphors. Accordingly, if the amount of the luminescent particles in the host matrix is too large, the overall quantum efficiency of the PV is reduced. This may be caused by the amount of light reflected, scattered or absorbed before it reaches the PV device.

Due to the wide spectrum range demonstrated by these two LDC layers, the application of phosphorescent phosphors can have a positive impact on the down-conversion of the solar spectrum in the generation of the electrical power from the emitted photons, (between 400-750nm in the dark, and which were observed as being significantly higher with higher concentration).

7.2.2 Monolithic Perovskite Solar Cell (MPC)

The Monolithic Perovskite Solar Cell (MPC) is a non-transparent PV device with an electrode of Titania, mesoporous TiO_2, mesoporous ZrO_2 and carbon layers, thus creating a particularly stable device (Hashmi et al., 2017; Hu et al., 2014). This particular type of Perovskite Solar Cell (PSC) was selected because it has high power conversion efficiency, and highly stable PV with low hysteresis effect. The MPC was acquired from Solaronix S.A. The total substrate size of the cell is 20x25mm and the active area was $1cm^2$. For the accurate performance assessment of the PV device the test cell mask was 50x50mm, with an aperture of $1cm^2$. The mask is an opaque sticker with a tailored aperture that hides the non-active area of the cell while compensating for the optical losses inherent to masking. Figure 7.10 shows the MPC PV device used in this assessment with the device architecture illustrated in Figure 2.6.

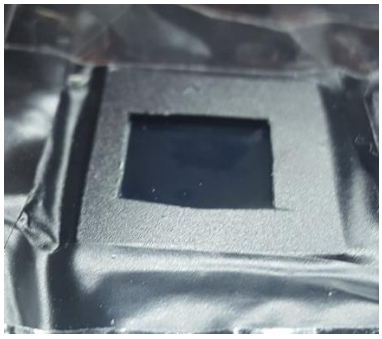

Figure 7.10. (a) Photo of the MPC PV device with the mask.

The luminescent layers applied in these measurements were the same luminescent layers, (Ph1-6), fabricated and characterized as described in Chapters 5 and 6. The layers can be easily attached to and removed from the PV device surfaces, both on the top (T) or at the rear (R), as required, without damaging the layers. The device was measured first without the layers and subsequently by applying the layers. The first layer measured was the blank sample layer, which is the host matrix and does not contain luminescent particles. This was followed by different Luminescent layers at various concentrations, both on top (T) and at the rear (R) of the PV device, as illustrated in Figure 3.15.

Current- Voltage curves Measurements

Figure 7.11 presents the photovoltaic performance of the MPC cell, (blank) and Ph1-3 luminescent layers at various concentrations, 20-80%wt, applied on the top (T) and at the rear (R) of the PV device, respectively. The summary of the measured IV characteristics is listed in separated Tables; Ph1 (Table 7.10); Ph2 (Table 7.11); Ph3 (Table 7.12).

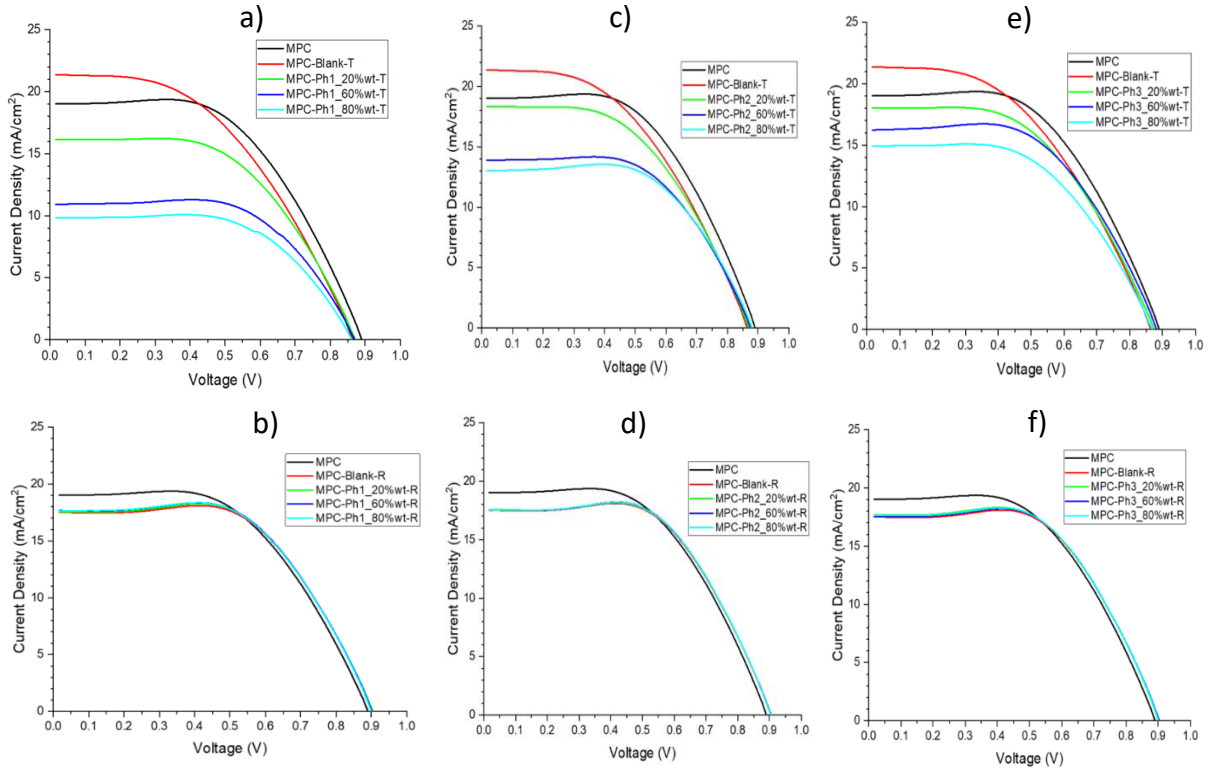

Figure 7.11. J-V curves of the MPC device attached to the host (blank) matrix and the LDC layers of phosphor Ph1-3 at various concentration 20 to 80%_wt, on the top (T) and at rear (R) of the PV device.

Figure 7.11 (a) and Table 7.10 show that with the application of the blank layer on the top of the MPC device, it was clearly observed that the short-circuit current density (Jsc) increased in Jsc from 19.02 to 21.39 mA/cm^2. This may be caused by incidental light, which is absorbed by the layer and then increases the light harvesting ability and probability of light trapping inside of the layer. However, the open circuit voltage, Voc, decreased from 0.90 to 0.87V, the fill factor (FF) and efficiency reduced also, from 0.55 to 0.47%. The efficiency decreased by a total of 6.7%.

When the luminescent layers, Ph1, were applied on the top of the MPC-PV device, the short-circuit current density (Jsc) resulted in a decrease from 19.02 to 16.13, 10.92 and 9.83mA/cm^2 respectively, increasing phosphorescent content added to the host matrix. With the presence of the higher concentration of LDC phosphors inserted into the top of MPC, the open-circuit voltage (Voc) reduced from 0.89 to 0.87 reaching 0.86V at 80%wt. This effect could be the

result of transient effects that occur also with a perovskite PV device, due to an enhancement in the carrier recombination zone causing a decrease of Voc (Scheer and Schock, 2011).

The efficiency characteristic of the PV device performance when the layers were applied on the top surface, resulted in a decrease from 9.24 to 7.68, 5.84 and 5.17%, respectively. This was because a greater amount of phosphorescent particles dispersed in the host matrix, and corresponded to less effective light conversion into the PV device under illumination. As the concentration ratio were increased, the light was trapped inside the luminescent layer interfaces (these were formed by the much higher ratio of doped ions in the phosphor). As discussed for DSSC, the bigger the amount of light trapped into the LDC layer, the greater the energy storage and the longer the decay, similar to the down-conversion process.

As shown in Figure 7.11 (b) when the luminescent layers were placed at the rear of the MPC, the short-circuit current density (Jsc) showed an unexpected reduction, independent of the concentration ratio which also included the blank layer, (host matrix). The photocurrent of the MPC device decreased from 19.02 to 17.52, 17.58, 17.68, 17.67mA/cm^2 respectively. With the presence of any phosphors species layer inserted at the rear surface of the MPC device, the result was a constant open-circuit voltage (Voc) of 0.90V. Interestingly the Fill factor has significantly increased from 0.55 to 0.59 for any layer added to the rear surface, independent of the concentration ratio.

Observing the efficiency of the PV device, a small increase in performance has been noted. By adding any of these phosphors layers at the rear it was found that the blank layer resulted in a 1% improvement from 9.24 to 9.34%. Furthermore, by increasing the concentration ratio this increased to 9.40, 9.41, and 9.38%. Surprisingly, there was a small unexpected reduction, 9.38% at 80%wt. These results demonstrate overall, a very small enhancement, around approximately 1.8% on the PV performance by comparison to the DSSC device, 8.9%, and almost the same efficiency as the blank layer, 1%. This minor enhancement, (regardless of the stability of measurement procedures, including light and temperature, and assuring homogeneity of replication), could readily be obscured by a nondifferential measurement error. It was confirmed that this PV device is not transparent, which means it may be blocking

or absorbing the light before it is being transmitted to the LDC layers at the rear. Therefore, this small improvement shows that the application of these layers at the rear as a reflector does not improve the light enhancement into the PV device under light conditions.

Table 7.10. Summary of MPC photovoltaic performance attached to the host matrix, (blank), and the luminescent layers phosphor Ph1 at various concentrations ratio on the top (T) and at the rear (R) of the PV device surface.

LDC Layer Application	Jsc (mA/cm^2)	Voc (v)	FF (%)	η (%)
MPC	19.02	0.89	0.55	9.24
MPC-Blank-T	21.39	0.87	0.47	8.63
MPC-Ph1_20%wt-T	16.13	0.87	0.55	7.68
MPC-Ph1_60%wt-T	10.92	0.87	0.61	5.84
MPC-Ph1_80%wt-T	9.83	0.86	0.61	5.17
MPC-Blank-R	17.52	0.90	0.59	9.34
MPC-Ph1_20%wt-R	17.58	0.90	0.59	9.40
MPC-Ph1_60%wt-R	17.68	0.90	0.59	9.41
MPC-Ph1_80%wt-R	17.67	0.90	0.59	9.38

The J-V analysis shows that MPC PV and LDC layers of Ph1 applied on the surface of this PV device resulted in a very small enhancement for this research application. For that reason, the external quantum efficiency (EQE) and reflectance analysis will not be presented or discussed here.

MPC with LDC Layers of Phosphor Ph2

As shown in Figure 7.11(c) and Table 7.11, when the luminescent layers, Ph2, were applied on the top of the MPC device (and apart from blank layer), the short-circuit current density (Jsc) resulted in a decrease from 19.02 to 18.36, 13.89 and 13.01mA/cm^2. This resulted in a change, with increasing phosphorescent content being added to the host matrix. With the presence of the higher concentration of LDC phosphors inserted into the top of MPC, the open-circuit voltage (Voc) decreased from 0.89 to 0.87, 0.88 and 0.88V, respectively, and maintained the amount of voltage constant at 0.88V, for the three different concentrations of phosphor analysed. It was observed that the fill factor increased from 0.55 to 0.51, 0.58 and 0.60%. However, the efficiency responded differently, with a decrease in performance when the layers were applied to the top surface, resulting in a decrease from 9.24 to 8.13, 7.04, and

6.91%. This means that the amount of phosphorescent particles dispersed in the host matrix resulted in a less effective light conversion into the PV device under light conditions. As observed for the LDC of Ph1, the Ph2 sample also demonstrated that with an increase of concentration ratio the light became trapped inside the luminescent layer interfaces. These were formed by the much higher ratio of doped ions of the phosphors. Furthermore, the greater the amount of light trapped into the LDC layer, the greater the energy storage. There was also a longer decay, as with the down-conversion process.

As shown in Figure 7.11 (d), when the luminescent layers were placed at the rear of the MPC the short-circuit current density (Jsc) showed an unexpected reduction which appeared to be independent of the concentration ratio, (between 20-80%wt). The photocurrent of the MPC device decreased from 23.01 to 17.58 and maintained 17.55 mA/cm^2 between 60 and 80%wt. With the presence of the higher concentration of LDC phosphors inserted at the rear surface of the MPC device, the results were a reduced, and almost constant open-circuit voltage (Voc) of 0.90, 0.91 and 0.90V. The fill factor has increased from 0.55 to 0.59 for any layer added to the rear surface, independent of the concentration ratio.

The improvement observed in the efficiency of the PV device performance from 9.24 to 9.38, 9.40 and 9.39%, respectively, was nonetheless considered small and just above the efficiency measured for the blank layer, 9.34%. Therefore, this 1.8% improvement shows that the application of these layers at the rear as a reflector does improve the light enhancement into the PV device under illumination, similar to the LDC of Ph1.

Table 7.11. Summary of MPC photovoltaic performance attached to the host matrix, (blank), and the luminescent layers of phosphor Ph2 at various concentration ratios on the top (T) a and at the rear (R) of the PV device surface.

LDC Layer Application	Jsc (mA/cm^2)	Voc (V)	FF (%)	η (%)
MPC	19.02	0.89	0.55	9.24
MPC-Blank-T	21.39	0.87	0.47	8.63
MPC-Ph2_20%wt-T	18.36	0.87	0.51	8.13
MPC-Ph2_60%wt-T	13.89	0.88	0.58	7.04
MPC-Ph2_80%wt-T	13.01	0.88	0.60	6.91
MPC-Blank-R	17.52	0.90	0.59	9.34
MPC-Ph2_20%wt-R	17.58	0.90	0.59	9.38
MPC-Ph2_60%wt-R	17.55	0.91	0.59	9.40
MPC-Ph2_80%wt-R	17.55	0.90	0.59	9.39

MPC with LDC Layers of Phosphor Ph3

As shown in Table 7.12, below, when the luminescent layers, Ph3, were applied to the top of the MPC device which was separate to the blank layer, the short-circuit current density (Jsc) resulted in a decrease from 19.02 to 18.04, 16.24 and 14.94mA/cm^2, respectively, with increasing phosphorescent content added to the host matrix, (see Figure 7.11 (e)). The open-circuit voltage (Voc) decreased from 0.89 to 0.87, 0.88 and 0.87V, respectively, and maintained a constant voltage, 0.87V, for the three different concentrations analysed.

A fluctuation of the fill factor was observed, which decreased from 0.55 to 0.52, 0.57% and back to 0.55% and did not show a clear sign of transient effects. However, the efficiency results showed a clear decrease in performance when the layers were applied to the top surface, resulting in a decrease from 9.24 to 8.21, 8.12 and 7.07%. A greater amount of phosphorescent particles dispersed in the host matrix corresponded to a less effective light conversion into the PV device under this specific light condition. As the concentration ratio were increased, the light became trapped inside the luminescent layer interfaces.

As shown in Figure 7.11 (f), when the luminescent layers were placed at the rear of the MPC, the short-circuit current density (Jsc) showed an unexpected reduction which appeared to be independent of the concentration ratio, 20-80%wt, and the photocurrent decreased from 19.02 to 17.69, 17.59 and 17.66mA/cm^2, respectively.

The presence of the higher concentration of LDC phosphors inserted at the rear surface of the MPC device, resulted in a reduced and constant open-circuit voltage (Voc) of 0.90V. The fill factor has significantly increased from 0.55 to 0.59 for any layer added to the rear surface, independent of the concentration ratio. Similar results were observed in the Ph2 layers. The improvement observed in the efficiency of the PV device performance from 9.24 to 9.38 and 9.39% for layers at both 60% and 80% respectively, were still considered negligible and just above the measured efficiency for the blank layer, 9.34%. This small improvement shows that the by applying these layers at the rear as a reflector does improve (by up 1.5%) the light

enhancement into the PV device under illumination, but it appears to be even lower than the earlier layers, Ph2 and Ph3.

Table 7.12. Summary of the MPC photovoltaic performance attached to the blank host matrix, and the luminescent layers of phosphor Ph3 at various concentration ratios on the top (T) and at the rear (R) of the PV device surface.

LDC Layer Application	Jsc (mA/cm^2)	Voc (V)	FF (%)	η (%)
MPC	19.02	0.89	0.55	9.24
MPC-Blank-T	21.39	0.87	0.47	8.63
MPC-Ph3_20%wt-T	18.04	0.87	0.52	8.21
MPC-Ph3_60%wt-T	16.24	0.88	0.57	8.12
MPC-Ph3_80%wt-T	14.94	0.87	0.55	7.07
MPC-Blank-R	17.52	0.90	0.59	9.34
MPC-Ph3_20%wt-R	17.69	0.90	0.59	9.38
MPC-Ph3_60%wt-R	17.59	0.90	0.59	9.39
MPC-Ph3_80%wt-R	17.66	0.90	0.59	9.39

MPC with LDC Layers of Phosphor Ph5

The discussion below provides a summary of the measurement of the MPC with the luminescent phosphor Ph5 layer at 60%wt, to show how this lower quantum efficiency, <30%, sample phosphor will behave with these top and rear applications. As was established, this PV device did not show much enhancement with LDC layers under light conditions. For that reason, the Ph4 and Ph6 applications will not be discussed.

Current- Voltage curves Measurements

Figure 7.12 presents the photovoltaic performance of the MPC cell with the blank layer and the Ph5 luminescent layers at 60%wt concentration, applied to the top (T) and the rear (R) of the MPC PV device. The summary of the measured IV characteristic is listed in Table 7.13.

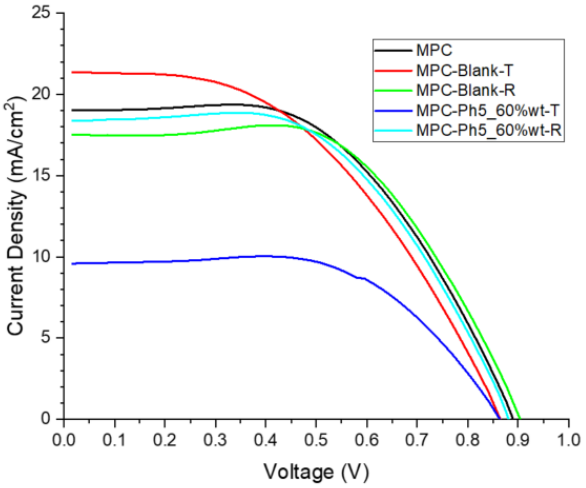

Figure 7.12. J-V curves of MPC device attached to the host (blank) matrix and the LDC layers of phosphor Ph5 at 60%_wt concentration, on the top (T) and at the rear (R) of the PV device.

In Figure 7.12, when the luminescent layer, Ph5, was applied on the top of the MPC device, (apart from the blank layer), the short-circuit current density (Jsc) resulted in a decrease from 19.02 to 9.60 mA/cm^2. The open-circuit voltage (Voc) reduced from 0.89 to 0.87V which contributed to the increase in the fill factor from 0.55 to 0.62%. A decrease in the performance of the PV device was observed when the LDC layers applied on the top, fell from 9.24 to 5.16%, which was subsequently lower than the blank layer, 8.63%. This decrease can be explained by the deposition of the blank and luminescent layers on the top; they do not improve the PV device performance at this concentration.

On the other hand, when the luminescent layers were placed at the rear of the MPC, the short-circuit current density (Jsc) of the MPC device decreased from 19.02 to 18.37 mA/cm^2. The efficiency of the PV device showed a reduction in performance from 9.24 to 8.99%, which is below the efficiency of the blank layer, 9.34%. This decrease shows that the application of the luminescent layer at the rear will not result in a good reflector or light scattered device, and subsequently will not improve the device performance under illumination. Within these results is a minor enhancement due to the presence of the luminescent layer.

The J-V analysis shows that the MPC, PV and LCD layers with Ph5 at 60%wt applied on both surfaces, i.e. to the top and rear of this PV device, resulted in a reduction of the photovoltaic effect of the PV device. Therefore, this device does not show any enhancement to the PV

device performance with this layer. However, this device could show a different result under the afterglow or lifetime decay applications and some measurements were taken to examine that.

Table 7.13. Summary of the MPC photovoltaic performance attached to the host matrix, (blank), and the luminescent layers of phosphor Ph5 at 60%wt concentration ratio to the top (T) and at the rear (R) of the PV device surface.

LDC Layer Application	Jsc (mA/cm^2)	Voc (V)	FF (%)	η (%)
MPC	19.02	0.89	0.55	9.24
MPC-Blank-T	21.39	0.87	0.47	8.63
MPC-Ph5_60%wt-T	9.60	0.87	0.62	5.16
MPC-Blank-R	17.52	0.90	0.59	9.34
MPC-Ph5_60%wt-R	18.37	0.88	0.56	8.99

MPC PV Device and LDC layers Photoluminescence lifetime

Figure 7.13 shows the photovoltaic performance of the MPC cell which was tested with one of the better layers with a higher PLQY quantum yield, Ph1, at 60%wt concentration, and also a blank layer. Both layers were applied on the top (T) of the PV device to measure the short circuit current over a period of time; before and during the photoluminescence lifetime decay or afterglow.

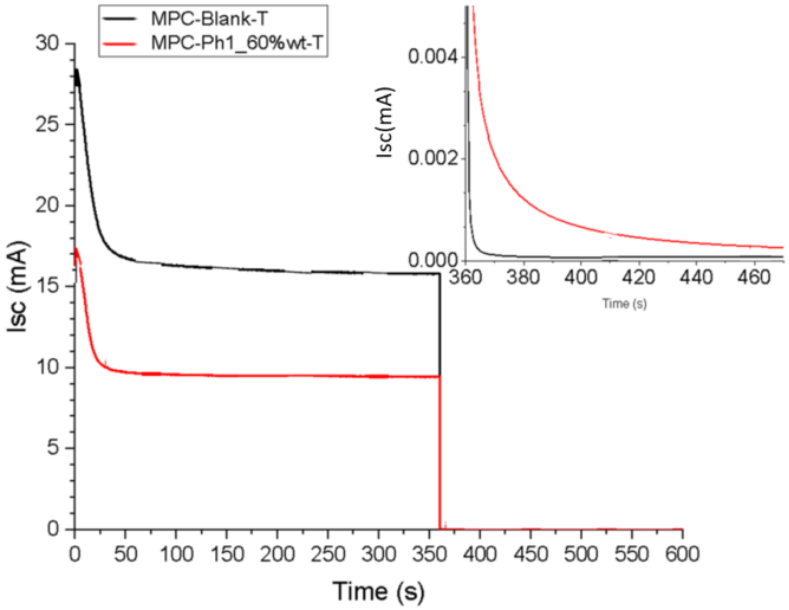

Figure 7.13. Fixed Isc x time curves of the MPC device attached to the LDC layer of phosphor Ph1 at 60%_wt concentration on the top (T) of the PV device. The insert shows the zoomed afterglow effect of the Blank and Ph1 layers.

The short-circuit current (Isc) versus time seconds (s) curves were obtained from the devices, with the layers placed on the top of the surface of the PV device, under both biased test conditions, and also the dark condition. This was achieved by monitoring the short-circuit current until it reached a constant value, which was around 360s at 15.96mA. Then the samples were covered with a metal cover to avoid any external light infiltrating the PV device, and measured for another 340s.

As can be observed in the PV device itself, by merely adding the blank layer without phosphorescent particles, a very fast response by the device, with the Isc as a function of time decay, (black curve during the measurement) was detected. On the contrary, the PV device with the Ph1 resulted, as expected, with a very long Isc decay when it was compared to the blank layer, which is similar to the phosphorescent lifetime decay curves discussed in section 6.5. Thus, this measurement shows that the luminescent decay of phosphors irradiated by sunlight was found to occur for several seconds. This suggests that the afterglow of phosphors Ph1 did significantly affect the photovoltaic performance of the MPC device.

Figure 7.14 shows the performance of the MPC device with various luminescent layers, Ph1-3, and LDC layers at 80%wt, at the top and rear surface of the PV device, as illustrated in Figure 3.15. The measured current density as a function of voltage (V) examinations were conducted under the same test conditions as described above.

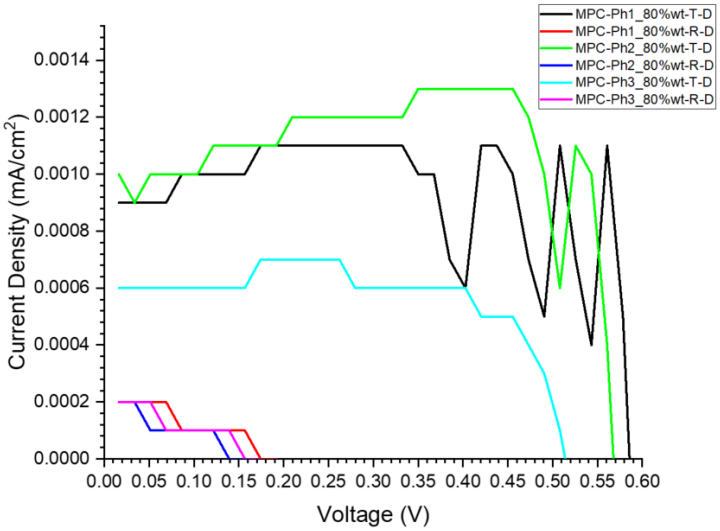

Figure 7.14. J-V curves of the MPC device attached to the LDC layers of phosphor Ph1-3 at 80%wt concentration, on the top (T) and at the rear (R) measuring dark conditions.

After removing all the illumination from the devices, weak power produced by the LDC layers, attached on the top or rear the of the MPC PV device was observed. The afterglow properties of the Ph1-3 phosphor layer provided a light source under dark conditions enabling the MPC device to produce electrons. The LDC layers on the top surface of the PV device demonstrated a much higher power than at the rear surface. Among all three LDC layers, Ph2 demonstrated the highest current density; $1.28x10^{-3}$ mA/cm^2, followed by Ph1, at $1.12x10^{-3}$ and Ph3 at $7.2x10^{-4}$ mA/cm^2.

Nevertheless, the application of the luminescent layers on the surfaces of the MPC device under dark conditions resulted in a low power conversion efficiency, as demonstrated earlier (see Figure 7.14). It was an interesting result to have this phosphorescent behaviour caused by a highly concentrated phosphorescent layer. Thus, these results show that the LDC layers can transfer the absorbed or stored energy photons and could contribute to the electrical energy power conversion in the dark and under a low light intensity application because the photons down converted from the LDC layers, and transferred to the MPC PV device, thus generating electricity.

7.2.3 Amorphous Silicon (a-Si) PV Device

The Amorphous Silicon (a-Si) was the only multijunction PV device selected for this application. It is a non-crystalline form of silicon with a double sequence of p-i-n structure. This type of PV device is manufactured on a layer of TCO (transparent conductive oxide) on glass, which is similar to the DSSC, examined earlier. However, this is an industrial PV device which was deposited on the glass followed by a P2 and P3 laser scribing structure, (reflective metal placed at the rear, and has a lifespan of 50,000 hours, see Figure 2.2). It is understood that this PV device has a superior performance under weak light conditions and that TCO conductive film increased the ultraviolet and visible light transmissibility of bands. The a-Si was acquired from Xiamen Mars Rock Science Technology Co., Ltd. The total active area of the device was 22.11cm^2(6.7x3.3cm). It is a module because it was formed by a series of PV devices. For that reason, it was not necessary to apply the mask during the measurement, and two similar LDC

layers were applied to cover the entire active area of the PV device, (see Figure 3.24). Figure 7.15 shows the a-Si PV device.

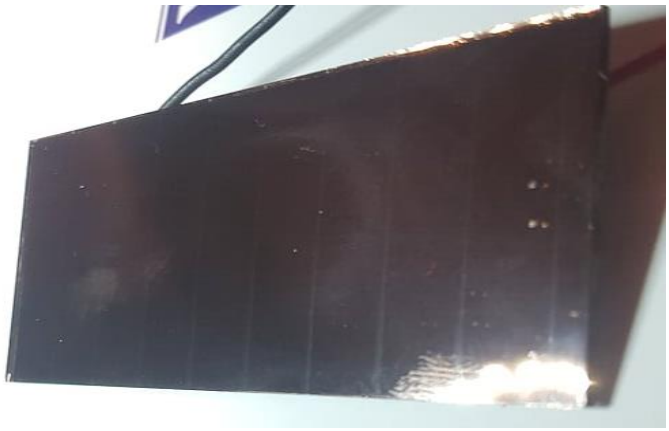

Figure 7.15. Amorphous silicon, a-Si, mini-module PV device, module consisting of 10 series connected PV devices.

The luminescent layers selected for this measurement were of a higher PLQY quantum efficiency >30, (Ph1-3), and the layers were the same luminescent layers fabricated and characterized as described in Chapters 5 and 6. The layers were easily attached and removed from the PV device surfaces, on the top (T) or at the rear (R), as required, without damaging them, as illustrated in Figure 3.15. The device was measured first without the layers and subsequently by applying the layers. The LDC layers at various concentrations were measured on the top (T) and at the rear (R) of the PV device.

The current-voltage measurements were carried out under standard test conditions, 1000W/m² AM 1.5 global, 25°C, at Solaronix S.A, Switzerland; details of the measurements are described in section 3.3.8.

A-Si with LDC Layers of Phosphor Ph1-3

Current- Voltage Measurements

Figures 7.16 and 7.17 present the photovoltaic performance of the a-Si device and Ph1-3 luminescent layers at an 80%wt concentration ratio, applied on the top (T) and the rear (R) of

the PV device, respectively. The summary of the measured IV characteristic is listed in Table 7.14.

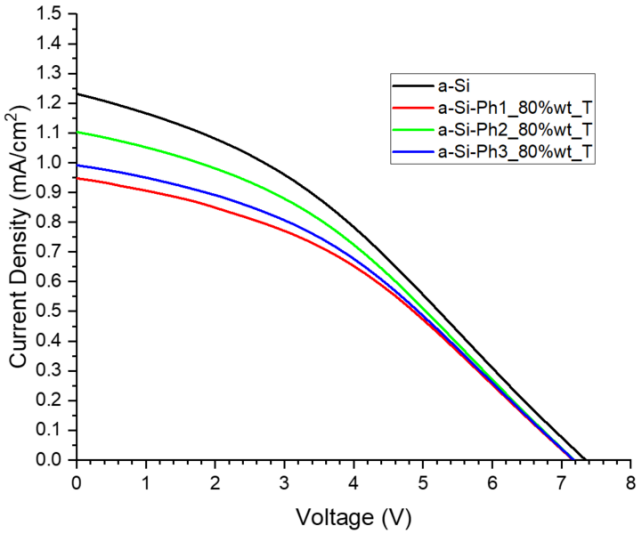

Figure 7.16. J-V curves of the a-Si device attached to the LDC layers of phosphor Ph1-3, at 80%wt concentration ratio, on the top (T) of the PV device.

When the luminescent layers, Ph1-3, were applied to the top of the PV device, the short-circuit current density (Jsc) resulted in a decrease from 1.23 to 0.95, 1.10 and 0.99mA/cm^2 respectively. On the contrary, the open-circuit voltage (Voc) reduced from 7.29 to 7.08V, independent of the type of LDC layer or phosphors species. This Voc reduction could be as a result of transient effects due to an enhancement in carrier recombination zones, resulting in a decrease of Voc, as mentioned in the earlier sections. An increase in the fill factor results, from 0.34 to 0.38, for LDC Ph1 and Ph3, and 0.37% for LDC Ph2 was observed. Thus, the reduction is clearly observed on the PV device efficiency performance; when LDC layers were applied to the top it showed a decrease from 3.14 to 2.61, 2.90 and 2.71%, respectively.

This effect was due to a greater amount of phosphorescent particles dispersed in the host matrix, which in turn corresponded to a less effective light conversion into the PV device under this illumination condition. Having a higher concentration LDC layer reduced the amount of light that got trapped inside of the luminescent layer interfaces (which were formed by a higher ration of doped ions in the phosphors). As discussed previously, the greater the amount of light trapped in the LDC layer resulted in increased energy storage and a longer decay in a simultaneous down-conversion process.

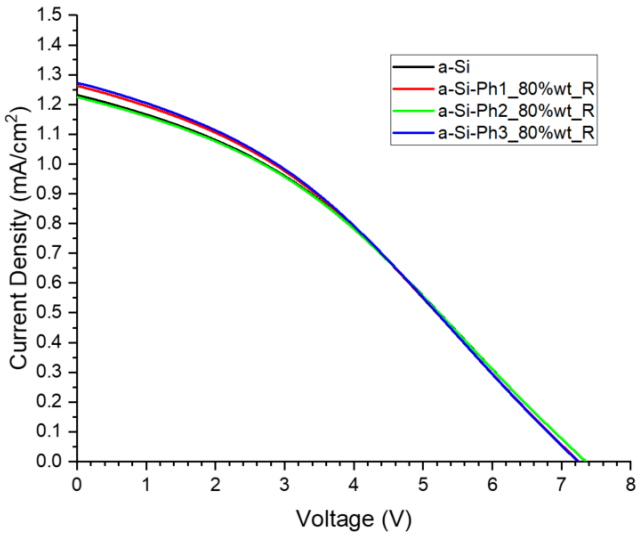

Figure 7.17. J-V curves of a-Si device attached to the LDC layers of phosphor Ph1-3 at 80%wt concentration ratio, at the rear (R) of the PV device.

Figure 7.17 shows the J -V effect when the luminescent layers were placed at the rear of the a-Si device, where the short-circuit current density (Jsc) showed a small increase from 1.23 to 1.26 and 1.27mA/cm^2 for both LDC layers. A small increase was only observed on the open-circuit voltage (Voc) of LDC Ph2, which appeared to be 7.31V. The results showed that the LDC layers did not cause any change in the fill factor of the PV device, remaining the same at 0.34%. Thus, the efficiency of the PV device performance was increased from 3.14 to 3.16, 3.15 and 3.17%, respectively, which is quite a negligible result and expected for this PV device. This proved that the back-contact metal or reflective layer retains the energy photons that cross from one side to the other.

These are very small improvements, on consideration that this silicon device, (which uses a transparent glass material), shows good performance in both the ultraviolet and visible spectra ranges. However, the improvement of this device may be limited because of the multijunction structure, which resulted in a very wide absorption, with a high from the upper surface, to lower energy photons at the lower surface of the PV device. Therefore, this technology may have filtered or absorbed a significant amount of light which prevented the energy photons from reaching the luminescent layer at the rear surface by reflecting them or scattering them back into the PV device under these light conditions. In addition to that, it absorbs both UV and visible light very efficiently compared with the DSSC and perovskite PV devices.

Table 7.14. Summary of a-Si photovoltaic performance attached to the luminescent layers of phosphor Ph1-3 at 80%wt concentration ratio on the top (T) and at the rear (R) of the PV device surface.

LDC Layer Application	Jsc (mA/cm^2)	Voc (v)	FF (%)	η (%)
a-Si	1.23	7.29	0.34	3.14
a-Si-Ph1_80%wt-T	0.95	7.08	0.38	2.61
a-Si-Ph2_80%wt-T	1.10	7.08	0.37	2.90
a-Si-Ph3_80%wt-T	0.99	7.08	0.38	2.71
a-Si-Ph1_80%wt-R	1.26	7.29	0.34	3.16
a-Si-Ph2_80%wt-R	1.27	7.30	0.34	3.15
a-Si-Ph3_80%wt-R	1.27	7.29	0.34	3.17

The J V analysis shows that the a-Si PV device and LDC layers with Ph1-3 applied on the surface is a negligible result, and accordingly the external quantum efficiency (EQE) and reflectance analysis will not be presented or discussed here.

a-Si PV Device and LDC Layers in Dark Conditions

Figure 7.18 shows the photovoltaic performance of the a-Si device measured with the three selected best layers with a higher PLQY quantum yield, and Ph1-3 layers at 80%wt concentration levels. These were applied on the top (T) of the PV device to measure the short-circuit current density (J_{SC}) in dark (D) conditions, during the afterglow. Prior to the measurements, the samples were kept under bias test conditions for 5 minutes. Then the samples were covered with a metal cover to avoid any external light accessing the devices, and measured immediately.

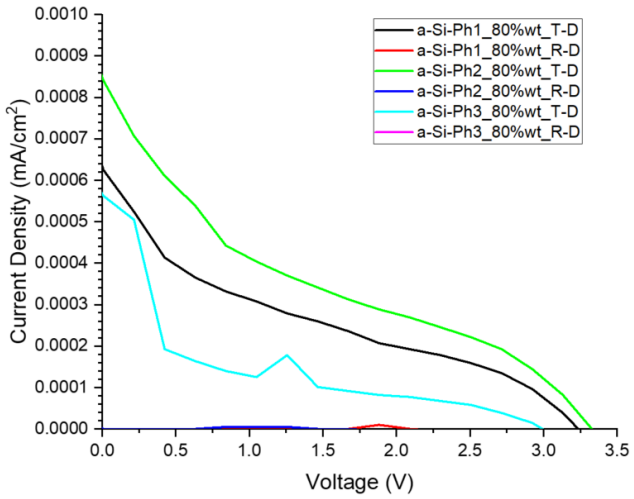

Figure 7.18. J-V curves of a-Si device attached to the LDC layers of phosphor Ph1-3 at 80%wt concentration ratio, on the top (T) and at the rear (R) of the PV device, measure in dark (D) condition.

This measurement shows that the luminescent decay of phosphors irradiated by sunlight was found to occur within several seconds as expected. It was observed that the weak power was obtained by the addition of the LDC layers attached to the top of the a-Si PV device. The afterglow properties of the Ph1-3 phosphor layers provided a light source under dark conditions for the a-Si to generate electrical current. The LDC layers on the top surface of the PV device demonstrated a much higher power compared to the rear surface. Among all three LDC layers, the Ph2 demonstrates the highest current density 0.0175 mA/cm^2, followed by Ph1, 0.013 and Ph3, 0.0115 mA/cm^2. This suggests that the afterglow of phosphors, Ph1-3, did strongly affect the photovoltaic performance of a-Si, but only when the LDC layers are placed at the top surface of the PV device.

7.3 Conclusion

This chapter presented the electrical characterization and optical reflectance of three different PV devices, DSSC, MPC and a-Si; which were used to examine the performance of various luminescent layers attached on the top or at rear of the PV device. It was found that luminescent layers with a low concentration ratio (1%) applied on top of the PV device, may improve the PV devices performance due to light scattering and down conversion mechanisms. It has been observed that a concentration >20%wt on top of the PV devices under illumination contributed to a reduction in the efficiency of the PV devices due to the reduction of light

reaching the PV device. However, highly concentrated luminescent layers appeared to be good reflectors at the rear of the DSSC PV device and have contributed to considerably improving the performance of the PV device. The next Chapter presents the electrical characterisation of these PV devices under dark conditions and practical applications.

CHAPTER 8

DETERMINATION OF ENERGY OUTPUT OF LDC LAYERS ATTACHED TO THE PV DEVICES IN THE PHOTOLUMINESCENCE DECAY

8.1 Introduction

In the previous section, the LDC layers were examined under Standard Test Conditions (STCs), to determine the effect of the application of the LDC on the top and at the rear surface of the PV devices. The selection of the long persistent phosphors for LDC was motivated because, in addition to down conversion, these luminescent materials demonstrate long photoluminescence decay or lifetime decay, which can enhance the LDC device and subsequently the PV device performance. This LDC device with a long lifetime decay can be described as an energy storage device, because it has a function of absorbing high energy photons when exposed to radiation, and in the dark its absorbed energy has a slower time scale of re-emission. This re-emission occurs at a visible band in two different mechanisms; a short and long lifetime which can be converted to the PV device, and subsequently a PV power output. This chapter presents the different LDC layers under tests that were taken in dark conditions, to determine the effect of the application of the LDC on the top and at the rear surface of the PV devices in the photoluminescence decay “afterglow”.

This section describes the analyses procedures, which were used for this assessment of LDC layers and with the same set of PV devices, (DSSC, MPC and silicon-based a-Si, which were examined in Chapter 7). These procedures include a) determining which LDC layers demonstrate more energy storage capacity, and b) describing performance in the context of real application settings and function by powering a LED light in the dark, (which describes the application in terms of real-world usage). Thus, there are compelling reasons to examine the evidence to confirm if it is possible to power a LED light during the afterglow, under dark conditions. This test setup used was discussed in section 3.3.8.

8.2 LDC layers and Energy Storage Performance

Prior to the real application testing, it was important to establish two important parameters in order to identify the ideal PV device and also which is the best LDC layer. For the PV device a-Si was selected because it is a mini module of a multijunction PV device, with a quick spectrum response, a wide absorption spectrum range and photostability, compared to DSSC and MPC PV devices. All the LDC layers were considered, Ph1-6, PhX and PhT at the 60%wt concentration ratio for both Layers, (see Figure 8.1).

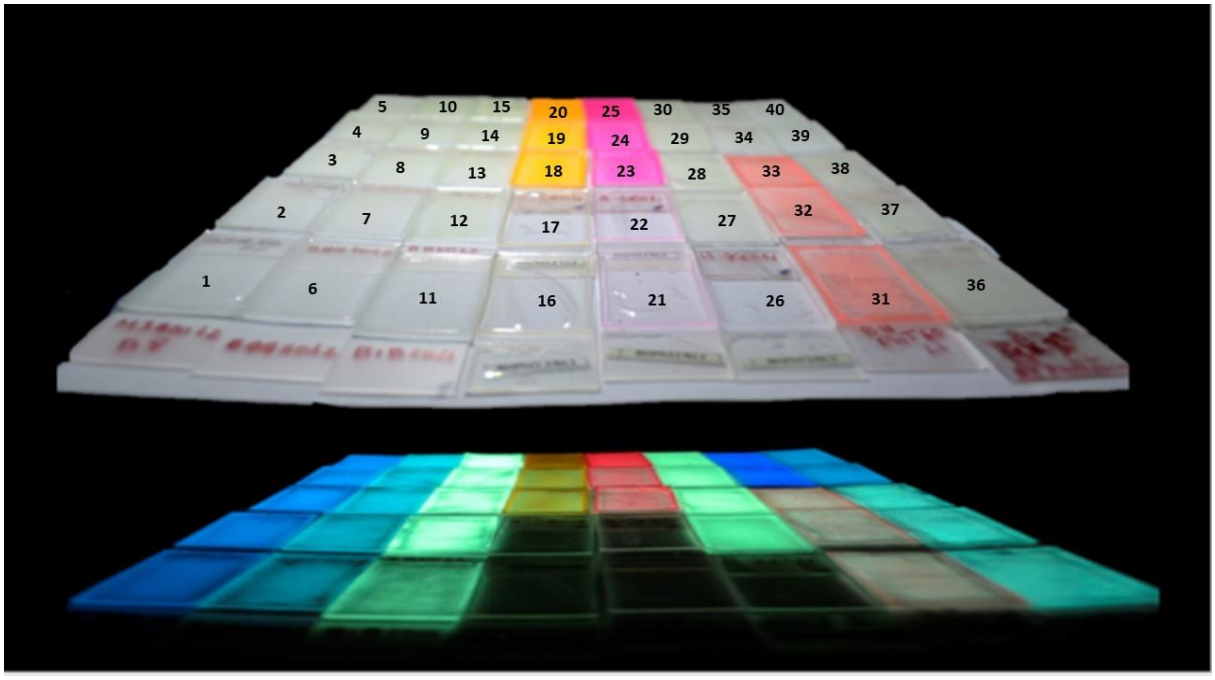

Figure 8.1. All Luminescent layers during and after exposure to ultraviolet radiation (254 nm) for 5 minutes. (Ph1) at different concentrations (1) 1%, (2) 20%, (3) 40%, (4) 60%, and (5) 80% wt.; (Ph2) at different concentrations (6) 1%, (7) 20%, (8) 40%, (9) 60%, and (10) 80% wt.; (Ph3) at different concentrations (11) 1%, (12) 20%, (13) 40%, (14) 60%, and (15) 80% wt.; (Ph4) at different concentrations (16) 1%, (17) 20%, (18) 60%, (19) 80%, and (20) 100% wt.; (Ph5) at different concentrations (21) 1%, (22) 20%, (23) 60%, (24) 80%, and (25) 100% wt.; (Ph6) at different concentrations (26) 1%, (27) 20%, (28) 60%, (29) 80%, and (30) 100% wt. ; (PhT) at 60%wt concentration (31-33); (Ph1) at 100%wt concentration (34-35); (PhX) at 60%wt concentration (36-38); (Ph2) at 100%wt concentration (39-40).

As discussed in section 6.3, it was observed that PhX and PhT are the best layers of all because of the broadened spectrum achieved by the mixing of LDC layers; establishing it as a good candidate for this analysis. However, these LDC layers were only prepared at a 60%wt concentration ratio.

Furthermore, for the type of LDC layer needed, the ideal number of LDC layers were compared with a single layer or multiple layers of LDC placed on top of each other, to be tested with the PV device, with multiple layers of LDC to enable the increase of the quantity of luminescent phosphorescence in level of thickness. Figure 8.2 shows a double level of three LDC layers placed in parallel on top of the a-Si PV device.

a) Under light conditions b) Under dark conditions

Figure 8.2. a) Double level PhX60%_wt and PhT60%_wt LDC attached to top of the a-Si PV device under light conditions, b) Double level LDC Layers during the afterglow decay, under dark conditions.

The PV device performance was measured first without the layer, then with a single and double level of LDC layers placed in parallel to cover the entire active area of the PV device. Results are shown in Table 8.1.

Table 8.1. a-Si photovoltaic performance under light and dark conditions, with a single and double LDC layers PhX and PhT at a 60% concentration ratio on the top (T) of the PV device.

Power/Time	Time (s)	Current (µA)	Voltage (V)	Current (µA)	Voltage (V)	Power (µW)	Power (µW)	% of total Power	% of total Power
a-Si PV under light		246.93	1.59	246.93	1.59	392.62	392.62		
a-Si PV - Dark	0	0	0.05	0	0.05	0.00	0.00		
LDC Layer Application		**Single LDC layer**		**Double LDC layers**		**Single LDC**	**Double LDC**	**Single LDC**	**Double LDC**
a-Si + LDC under light	0	150.12	1.55	23.5	1.45	232.69	34.08		
a-Si + LDC - dark	1	0.70	1.46	0.66	1.28	1.02	0.84	20.26%	17.21%
a-Si + LDC - dark	2	0.60	1.26	0.56	1.26	0.76	0.71	14.99%	14.38%
a-Si + LDC - dark	3	0.54	1.26	0.50	1.25	0.68	0.63	13.49%	12.74%
a-Si + LDC - dark	4	0.45	1.48	0.48	1.24	0.67	0.60	13.20%	12.13%
a-Si + LDC - dark	5	0.41	1.24	0.46	1.24	0.51	0.57	10.08%	11.62%
a-Si + LDC - dark	6	0.40	1.23	0.44	1.24	0.49	0.55	9.75%	11.12%
a-Si + LDC - dark	7	0.39	1.23	0.42	1.23	0.48	0.52	9.51%	10.53%
a-Si + LDC - dark	8	0.36	1.22	0.41	1.23	0.44	0.50	8.71%	10.28%
Total Energy Converted						**5.04**	**4.91**	**Fast Decay**	**Slow Decay**

The a-Si PV device performance without the LDC Layers under illumination was 392.62 µW. In dark conditions, after a second, the power measured 0.05V and there was no current. This PV device had a consistent and very fast response to light conditions, as expected.

When a single level of layer was placed on the top of the PV device it caused a power reduction from 392.62 to 232.69µW. When a double level of layers was placed on the top of the PV device, the power reduced from 392.62 to 34.08µW, which was caused by a significant reduction in the current, which fell from 246.93 to 23.5 µA.

As discussed earlier, when the LDC layer was exposed to light illumination, the light gets absorbed as well as trapped or reflected into the LDC layer before it reaches the PV device, thus reducing the PV device performance. During this period of approximately 5 minutes, LDC

layers are charging or absorbing radiation light, which is a storage device that will provide a source of energy to the PV in dark conditions.

After this charging period, the illumination is removed, and the PV device can generate electricity from the photon's energy storage in the LDC layer. The total energy converted from the single and double level LDC layers was found to be 5.04 and 4.91 μW. These electric powers were converted or generated through the charged LDC layers, which were released in dark conditions during the first 8 seconds.

The PV device with a single level layer demonstrated a higher electric power conversion, however, it also displayed a shorter lifetime decay than with double level layers, reduced from 232.69 to 0.44 μW and the double layers from 34.08 to 0.50 μW, which was expected. As can be observed, after 8s in the dark, a single layer loss of 149.76μA occurs in the same time that the double level layer losses only 23.09μA. This is because more light was absorbed or stored inside the LCD layers, thus increasing the lifetime decay of the LDC layers. The double level LDC layers resulted in more electric power generated over a long period of time, 10.28% comparing with the 8.71% within the same period.

By observing this data, it was possible to establish that a double layer should result in a large enough amount of phosphorescent emission to generate power by the PV device and power an LED, as double layers stacked on the top of the PV device results in a longer lifetime decay. As a result, more electrical power will be generated to the LED test, creating a much longer LED lighting time. The usage of double layers LDC PhT and PhX at 60%wt represent the best arrangement and they were applied on the top surface of the PV device for the following test. After exposing the LDC layer to the light source for 5 minutes, an interesting fact was observed. Details are presented in Figure 8.3 where; a) after the light source is removed, it was observed that the underneath layers receive less light than the top layer thus creating a shadow effect, and b) the bottom layer obstructs the light path to the layers beneath. A reduction in the light intensity thus causes a reduction of the photovoltaic effect in the PV device. The remaining reduction can also be explained by the high amount of UV light absorbed in the top layer, resulting in UV protection for the PV devices, which degrade following exposure to UV light.

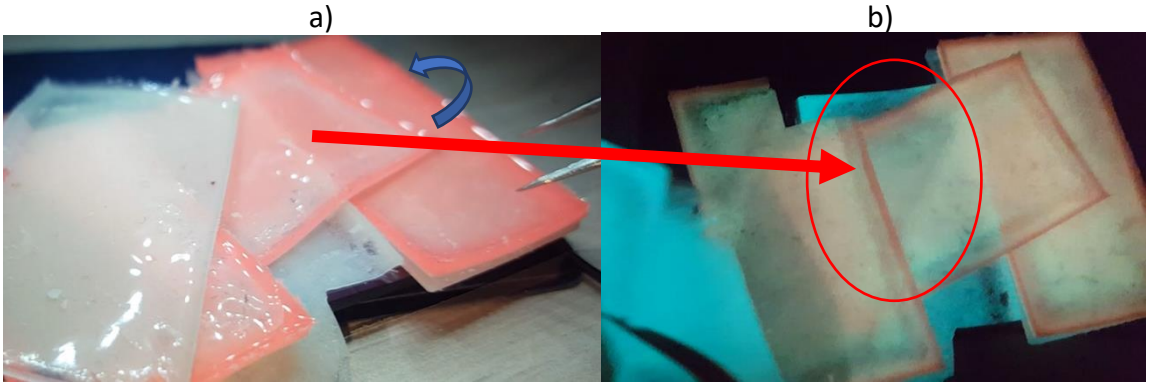

Figure 8.3. a) Different LDC stacked on top of each other under light conditions, b) different LDC stacked on top of each other under dark conditions, the red circle showing the shadow effect caused by the removed LDC layer.

Light is absorbed, scattered or reflected by these layers and that is why there is a reduction in the light reaching the PV, therefore reducing the power output.

8.3 Real Application Setup

8.3.1 LDC Layers and Energy Storage Performance on a-Si PV Device

These were the two relevant experimental methods that were developed to verify the performance of the proposed devices in a real application setting. Both methods are presented with diagrams. Figure 8.4 helps to explain the internal energy flow of the LDC layer to the PV device and subsequently to the LED light, after being exposed to the light.

The PV device cannot generate electricity in the dark condition but the LDC layers have the capability of transferring its energy in the dark, as discussed in the previous section. So, by combining them, they may be able to work together to power the LED in the dark. Figure 8.4 (a) and (b), shows these equivalent circuit diagrams.

The intensity and speed of the photon's conversions to electricity depends on the phosphorescent lifetime decay of the LDC layer and the PV device electrical structure. Thus, this phosphorescent lifetime decay (I), P_{dec} versus Time can last for some time, (as long as 20 hours), before discharging its energy to the PV device (II). However, the usage of this electrical energy generated by the PV device (which is the power output), depends upon a load

connected to it (L dis), (V). It means that the size and efficiency of the LDC layer and the PV device result in the electrical power output generated by them. So, if the required amount of the power load is lower than the power source generated, it can be used to power a load for a very long time.

For this reason, the current research provides two different methods by which to verify this conversion, and the two proposed diagrams are shown in Figure 8.4; a) firstly, the circuit diagram shows the power source which is an LDC layer and PV device, a load that is a LED (LD1), and instrumentation, amperemeter (M1) and voltmeter (M2). b) secondly, the optimized circuit diagram has in addition a capacitor (C1) and a push button (Push to Test), and the LED is operated by pressing the button. This is an Avago LED HLMP-D150, (minimum luminous intensity specified at 1mA, forward voltage 1.6V, and luminous Intensity 3 mcd, the capacitor can store up to 47µF, 16V, see Table 3.1).

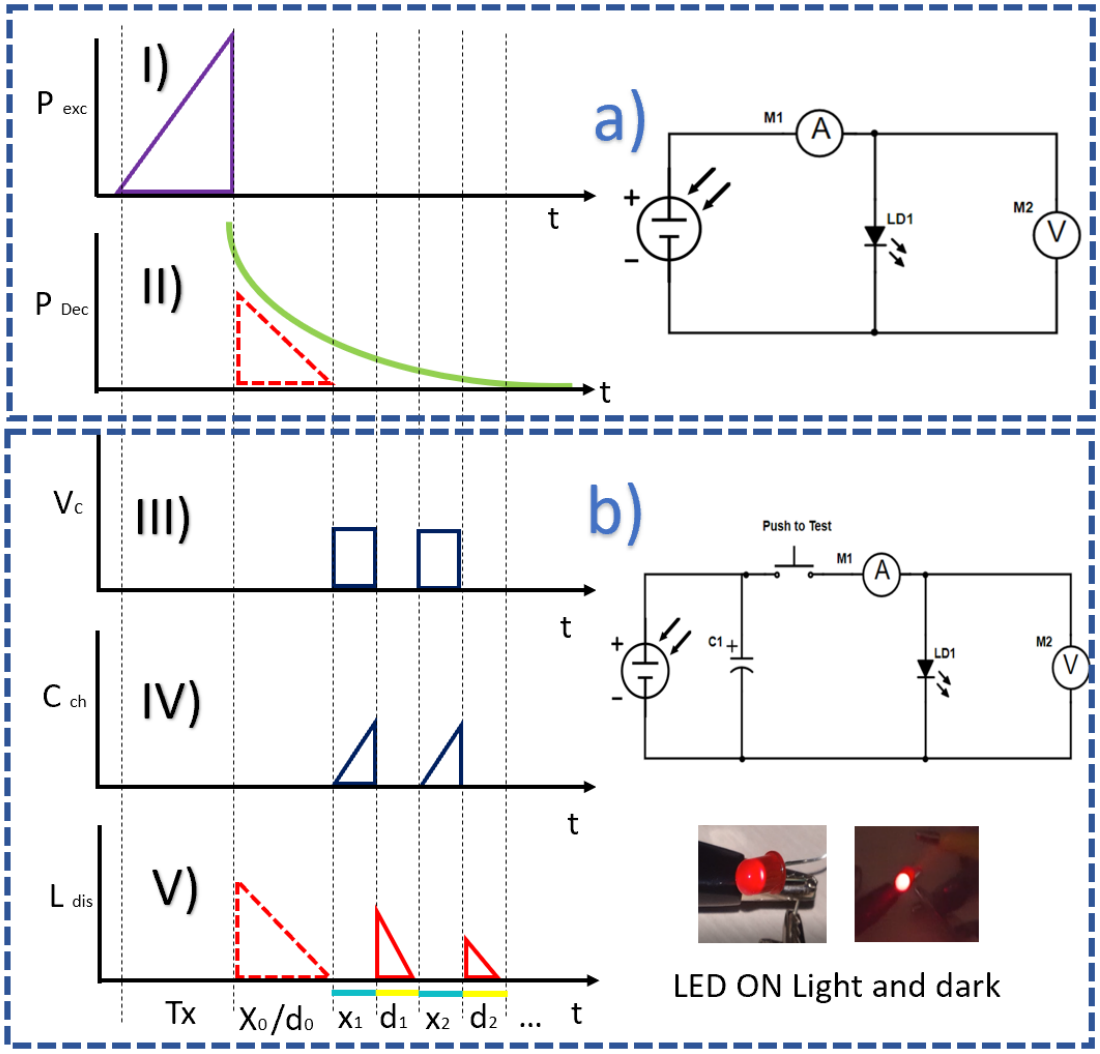

Figure 8.4. a) Measuring afterglow theoretical decay and equivalent circuit diagram of measuring method 1. b) Measuring afterglow theoretical decay and equivalent circuit diagram of measuring method 2. Photos of the LED under light and dark conditions.

The primary diagram and method operates as follows; with the double LDC layer attached on the top surface of the PV device, and exposed to the LED for 5 minutes, T_x, (I). Then, after 5 minutes the light source is turned off before starting the measurements. Both measurements (voltage and ampere) were recorded until the LED light output could be seen by the naked eye, d_0. The summary of the measured IV characteristic is listed in Table 8.2. It was observed that under the light condition, the PV device current measured was 406.66µA and voltage 1.59V, this is the initial value d_o. After 6s the current reduced to 1.37µA and voltage to 1.37V, as a result of switching off the LED light. Under this Method 1, the electrical power generated from the LDC layer was enough only to power the LED for the first 6 seconds. It decreased from

646.58 to 6.19 µW, which is the minimum amount of power required from the load; the LED light, (this is in accordance with the LED specification). However, the LDC layers were still emitting absorbed energy.

Despite the LED being off it can be turned back on again by applying Method 2 (see the second diagram). In Figure 8.4 b) the second circuit has a capacitor to store the power for a load, and the LED is operated by a push button. These features and advantages are beneficial, for instance, when the power goes below the minimum amount of power required for a load, or when the LED is turned off which allows the power to be stored in the capacitor and after a few seconds the LED can be turned on again, (when the electrical power re-establishes above the power level required for a load turning the LED on).

This is because the PV device is generating an electrical charge and it is flowing in the circuit, although it is not enough to power the LED. However, this charge can be stored in the capacitor ($C_{ch,}$ versus X_1, X_2…); since the capacitor is directly connected to the PV device it keeps charging the capacitor to the store power source for a load. The voltage on the storage capacitor does not vary with the load power, LED. Moreover, the variation of the level of storage energy is determined by time and electric output of the PV device. The stored power source for a load (Vc versus $X_{0,}$ X_1…) may not be released whilst the button is not pressed. When the button is pressed down, closing the LED circuit, the capacitor and the PV device will transfer its electric power to the LED, lighting it. Table 8.2 listed the voltage and current measured during the time that the LED is turned on. It was observed that the voltage decreased over time from 1.13 to 1V at 300s and the current varied depending on the amount of charge storage in the capacitor.

The capacitor stores energy, but also acts as the power source, giving current to the LED so that the LED remains on (L_{dis} versus $d_{1,}$ d_2…), despite not being powered anymore, (only by the PV device). When the capacitor acts as to store power, it discharges its voltage very quickly and the LED is on only for a short period of time, (the observed voltage was approximately 1vV and current about 40µA at 300s). Nonetheless, it can still provide power for the LED so that it can remain on for a lot longer than without the capacitor.

Table 8.2. Summary of a-Si photovoltaic performance of the double LDC layers on the top (T) of the PV device measured under light and dark conditions for 5 minutes.

	Time (s)	Capacitor Charging(x)	LED on (d)	Current (μA)	Voltage (V)	Power (μW)	% of total Power
PV-LDC under light	0			406.66	1.59	646.58	
a-Si-PhT60-PhX60	1	X_0	d_0	319	1.57	500.83	72.26%
a-Si-PhT60-PhX60	2			21.82	1.49	32.51	4.69%
a-Si-PhT60-PhX60	3			8.87	1.41	12.50	1.80%
a-Si-PhT60-PhX60	4			6.28	1.4	8.79	1.27%
a-Si-PhT60-PhX60	5			5.07	1.38	6.99	1.01%
a-Si-PhT60-PhX60	6			1.37	4.52	6.19	0.89%
a-Si-PhT60-PhX60		X_1					
a-Si-PhT60-PhX60	25		d_1	16.69	1.13	18.85	2.72%
a-Si-PhT60-PhX60	26-29	X_2					
a-Si-PhT60-PhX60	30		d_2	13.14	1.12	14.71	2.12%
a-Si-PhT60-PhX60	31-39	X_3					
a-Si-PhT60-PhX60	40		d_3	5.7	1.37	7.80	1.13%
a-Si-PhT60-PhX60	41-64	X_4					
a-Si-PhT60-PhX60	65		d_4	5.25	1.28	6.72	0.97%
a-Si-PhT60-PhX60	66-79	X_5					
a-Si-PhT60-PhX60	80		d_5	16.32	1.21	19.74	2.85%
a-Si-PhT60-PhX60	81-99	X_6					
a-Si-PhT60-PhX60	100		d_6	55.73	1.03	57.40	8.28%
a-Si-PhT60-PhX60	300	x continues	d continues	~40.00	~1.0		
Total Energy Converted						**693.08**	

It was observed that both methods make use of the storage energy of LDC layers to power the LED light and to measure the electrical power output. However, only the second method can produce a flashing light afterwards using the lower intensity energy photons. The total amount of energy converted, or power generated was 693.08 μW during these 300 seconds. In the last measurement registered, d6, the total percentage of energy converted, and consumption used for the LED lighting was 8.28%. With these high energy photons and LDC layers combined with this PV device under dark conditions, more than the same amount of electric power is supplied to the load, LED, under illumination. As much as 1.07% of the electrical power is being generated, since the energy of the LDC layers are transferred to the PV device. This means the energy storage in the down converter's layers is generating electrical charges into the PV device under dark conditions for my than 5 minutes.

8.3.2 LDC Layers and Energy Storage Performance on the DSSC PV Device

The second method was used to experimentally verify the performance of the LDC layers attached to the DSSC PV device, (see schematic shown in Figure 8.4 b). The same circuit and apparatus were used for these measurements. The PV device and some of the LDC layers are shown in Figure 8.5, and the measured values are shown in Table 8.3.

This type of PV device has good efficiency even under low light conditions. However, a major drawback of this application is the small size of the active area, and the slow response sensitivity of the liquid electrolyte which is caused by parasitic effect. This parasitic effect caused by internal resistances, (series and shunt resistance), leads to a slow response by the LDC layer, and subsequently to power loss in a PV device.

One way to increase the size of the active area's power output is to connect various PV devices in series. However, this would also increase the amount of series and short resistances in the circuit. In addition, having PV devices connected in series with different power efficiencies can result in even more resistance. Thus, in order to avoid these extra losses, only one PV device is used for this method.

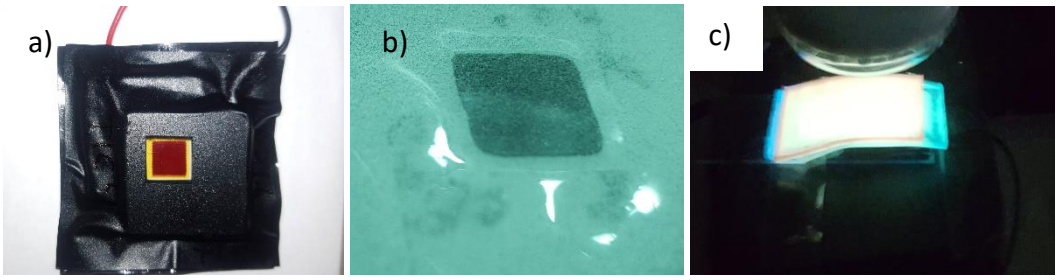

Figure 8.5. a) The same DSSC PV device used in Chapter 6, b) LDC layer on top of DSSC PV device, after removing the air bubble between the layer and the PV device, c) multilayers of LDC applied on top and at the rear surface of the PV device, after being exposed to light.

The first measurement was taken after 5 minutes to allow the PV and LDC layers to stabilise, then the voltage and current were taken to calculate the power output of the PV device under light conditions and time (0s). Under this light condition the measured power of the PV device without a layer was 0.036 μW. After that, three subsequent I-V measurements were obtained in dark conditions, measured at 1, 5 and 300 seconds after being removed from the light. The power calculated for these measurements were 0.027, 0.016 and 0.001 μW respectively. As

observed, these are the internal capacitances measured in the DSSC PV device over time, which is described as chemical capacitance. Essentially, this describes the fundamental mechanism whereby photogenerated carriers store free energy and produce a voltage and current in the external circuit over time; this power was calculated to be **0.0433**μW. After these PV characteristic parameters were identified, the tests were carried out with the LDC layers attached, to compare these results.

Table 8.3. Summary of DSSC photovoltaic performance of the single and multilayers of LDC attached on the top (T) and at the rear (R) of the PV device measured under light and dark conditions for 5 min.

Light/Dark Conditions	**Light (0s)**	**Dark (1s)**	**Dark (5s)**	**Dark (300s)**	**Dark (1s)**	**Dark (5s)**	**Dark (300s)**	**Total**	**Total (%)**
Power/Time	(μW)	(μW)	(μW)	(μW)	%(μW)	%(μW)	%(μW)	Energy in Dark	Energy Converted
DSSC	0.036	0.027	0.016	0.001	62%	36%	2%	0.0433	
DSSC-Ph1_20%wt-T	0.032	0.026	0.016	0.001	60%	37%	3%	0.0430	-1%
DSSC-Ph1_60%wt-T	0.029	0.018	0.016	0.002	51%	53%	7%	0.0355	-18%
DSSC-Ph1_80%wt-T	0.030	0.025	0.017	0.002	57%	38%	5%	0.0430	-1%
DSSC-Ph1_100%wt-T	0.029	0.023	0.015	0.003	55%	36%	8%	0.0411	-5%
DSSC-*R + Ph1_100%wt-T	0.029	0.021	0.0112	0.0022	61%	33%	6%	0.0344	-21%
DSSC-*R + Ph2_100%wt-T	0.029	0.027	0.0165	0.0036	57%	35%	8%	0.0471	9%
DSSC-*R + Ph3_100%wt-T	0.029	0.0258	0.0175	0.003	56%	38%	6%	0.0463	7%
DSSC-*R + Ph4_100%wt-T	0.006	0.0051	0.0024	0.0003	65%	31%	4%	0.0078	-82%
DSSC-*R + Ph5_100%wt-T	0.023	0.0216	0.015	0.0014	57%	39%	4%	0.0380	-12%
DSSC-*R + Ph6_100%wt-T	0.028	0.0185	0.0124	0.002	56%	38%	6%	0.0329	-24%
DSSC-*R + 2x(Ph3_100%wt)-T	0.029	0.024	0.018	0.006	50%	38%	12%	0.0477	10%
DSSC-*R + 3x(Ph3_100%wt)-T	0.029	0.024	0.019	0.008	47%	36%	17%	0.0509	18%
***R=Ph1_70%wt at Rear surface of the PV device**									

For that reason, the following experimental parameters were examined: the increasing of the concentration ratio with the LDC layer, the difference between each type of LDC layer at the highest concentration ratio and the addition of the multiple LDC layers on top of the PV device.

For the first experimental parameter, the concentration ratio with the LDC layers were increased, for the purpose of calculation. The electrical power of the PV device with different LDC layers at different concentration ratios was: 1-100%wt on the top surface of the PV device. For this analysis the LDC of phosphor Ph1 was selected. As discussed in section 6.4, the Ph1-3 were found to have a very high PLQY, which is important for this test. Then, each LDC layer Ph1 was placed on top of the PV device and the I-V measurements were taken subsequently, under light and dark conditions, as described above.

Under light conditions, the power calculated for these measurements were 0.032, 0.029, 0.030 and 0.029 μW, values which are very similar to the PV device without the LDC layer on top. Under dark conditions, the results show that the only significant differences were found after 300s, for the highest concentration ratio >60%wt, which demonstrated an increase of 7, 5, and 8% of power. Thus, the decrease in total energy in the dark was lost due to the internal capacitance, which became difficult to extract from the DSSC PV device.

The second experimental parameter examined the difference between each type of LDC layer, Ph1-6, at highest concentration ratio, 100%wt, placed on the top surface of the PV device. In addition to each LDC layer placed on the top surface, an extra layer, Ph1_70%wt- was added at the rear surface of the PV device to act as a Reflector (*R) as well as a down-convertor under dark conditions, which is an advantage in this type of PV device, as it does not have an anti-reflecting coating at the rear surface.

The power measurements under light conditions were calculated as 0.029, 0.029, 0.029, 0.006, 0.023 and 0.028μW. These results are slightly lower than the PV device without the LDC layer on top. As expected, the low power ratings were found to exist in the LDC layers with low PLQY values, Ph4 and Ph5, (as discussed in section 6.4). However, an unexpected result was found with the LDC layer at the rear surface, in so far as it does not improve the efficiency of the PV device.

The experimental results obtained for the LDC layer under dark conditions, were only slightly encouraging; 9% for Ph2 and 7% for Ph3, which were found to increase due to the application

of the LDC layers to this PV device. Interestingly, significant amounts of energy in the dark were obtained for the LDC layers which were found to have high PLQY, Ph1 and Ph3, (as discussed in section 6.4). In contrast, a significant decrease was found for Ph1 with -21%, which may be caused by adding the same type of phosphorescent at the rear surface of the PV device.

The final experimental parameter saw the addition of the multiple LDC layers on top of the PV device. For this analysis, the addition of double and triple layers of Ph3 at 100%wt were measured on top of the PV device. These final arrangements appeared to be the most significant in terms of energy in the dark. After 5 seconds, the power calculated for the double and triple layers was found to be 0.018 and 0.019 μW. Clearly, these figures indicate a major energy conversion with 10 and 18%, respectively. However, these low powers were not enough to power the LED light under light or dark conditions because of the small active area of the PV device. It resulted in power much lower than the minimum amount required for the load.

8.3.3 LDC Layers and Energy Storage Performance on MPC PV Device

Similar steps were taken to verify the performance of the LDC layers attached to the MPC PV device, (see the schematic shown in Figure 8.4 b). The same circuit and apparatus were used for these measurements. The measured values are shown in Table 8.4. This type of PV device does not have a reflective coating at the rear similar to a DSSC. Despite having a larger active area than the DSSC, this is still smaller than a-Si PV, which results in a lower power output.

Among the three different experimental parameters applied to the DSSC PV device, the following were most appropriate to evaluate the MPC device with the LDC layers: verify the difference between each type of LDC layer at its highest concentration ratio and test the optimised layer, PhX and PhT, with lower concentration ratios as single and multiple LDC layers on top of the PV device.

For the first experimental parameter, (verify the difference between each type of LDC layers), the following factors were observed; Ph1-6, at highest concentration ratio, 100%wt, maintaining an extra layer LDC layer, Ph1_70%wt, at the rear of the PV device. As stated,

before the measurement of the LDC layers, the I-V characteristic of the PV device was taken to calculate the power without any LDC layer attached to it.

Under light conditions, the calculated power for the MPC PV device was 0.070 μW. When the LDC layers, Ph1-Ph6, are attached to the PV device these measurements were also taken for each layer: 0.068, 0.069, 0.070, 0.069, 0.068 and 0.068 μW, respectively. These are the same or slightly lower than the PV device without the LDC layer.

With regards to the experimental result obtained for the PV device with the LDC layers under dark conditions, the calculated powers were equal to, or higher than, the PV device without any LDC layer, (these can be observed at 1 and 5 seconds). At 300 second, Ph5 was the only one which resulted in the lowest power 0.003 μW of all. This was expected because this LDC layer, Ph5, had the lowest PLQY, as discussed in section 6.4. However, the increase in percentage of the total amount of energy converted for each different type of LDC layer was 27, 5, 75, 8, 28, and 57%, which were higher than the PV without the LDC layer. This increase was observed in the total energy in the dark, which was demonstrated as being higher than the internal capacitance, and possible to be extracted from the MPC PV device.

Table 8.4. Summary of MPC photovoltaic performance of the single and multilayers of LDC attached on the top (T) and rear (R) of the PV device measured under light and dark conditions for 5 min.

Light/Dark Conditions	Light (0s)	Dark (1s)	Dark (5s)	Dark (300s)	Dark (1s)	Dark (5s)	Dark (300s)	Total	Total (%)
Power/Time	(μW)	(μW)	(μW)	(μW)	%(μW)	%(μW)	%(μW)	Energy Converted	Energy Converted
MPC	0.070	0.019	0.008	0.0004	69%	30%	1%	0.028	
MPC-*R + Ph1_100%wt-T	0.068	0.022	0.013	0.0006	62%	36%	2%	0.036	27%
MPC-*R + Ph2_100%wt-T	0.069	0.019	0.010	0.0006	64%	34%	2%	0.030	5%
MPC-*R + Ph3_100%wt-T	0.070	0.031	0.017	0.0008	63%	35%	2%	0.050	75%
MPC-*R + Ph4_100%wt-T	0.069	0.021	0.009	0.0006	68%	30%	2%	0.031	8%
MPC-*R + Ph5_100%wt-T	0.068	0.025	0.010	0.0003	69%	30%	1%	0.036	28%
MPC-*R + Ph6_100%wt-T	0.068	0.028	0.016	0.0006	63%	36%	1%	0.045	57%
MPC-*R + PhX_60%wt-T	0.070	0.024	0.010	0.0003	70%	30%	1%	0.035	24%
MPC-*R + PhT_60%wt-T	0.049	0.016	0.008	0.0002	66%	33%	1%	0.025	-11%
MPC-*R + PhX + T (60%wt) T	0.068	0.022	0.010	0.0003	67%	32%	1%	0.033	17%
MPC-*R + PhT + X (60%wt) T	0.068	0.034	0.012	0.0006	73%	26%	1%	0.047	65%
***R=Ph1_70%wt at Rear surface of the PV device**									

For the final experimental parameter, testing the optimised layer, PhX and PhT with a lower concentration ratio, 60%wt, as single and multiple LDC layers on top of the PV device. The extra layer LDC layer, Ph1_70%wt, was maintained at the rear of the PV device.

Under illumination, when the single LDC layers, PhX and PhT, are attached on top of the PV device the calculated power was found to be 0.070 and 0.049 μW. In these measurements, the only difference found was the PhT, which was lower than the PV device without a layer, this may be caused because of the mixing of phosphors species, Ph1-Ph6 at 10% concentration ratio for each species. As expected, the double LDC layers, (PhX under the PhT and PhT under the PhX), on top of the PV device resulted in the reduced power, 0.068 μW, when compared with the PV device without the LDC layer.

Under dark conditions, the total calculated power 0.025 μW was only low for the single layer of PhT. Thus, the increase in percentage of the total amount of energy converted for each different type of LDC layer arrangement was 24, 17 and 65%, results which were higher than the PV without the LDC layer, (apart from the PhT which decreased -11%). This increase was observed in the Total Energy in the dark which was demonstrated as being higher than the internal capacitance of the MPC PV device. However, these low powers were not enough to power the LED light under light or dark conditions because of the small active area of the PV device, which was much below the minimum amount required for the load.

8.4 Conclusion

This chapter investigated the performance of a-Si, DSSC and MPC PV devices attached to the LDC layers in the photoluminescent decay, under dark conditions. LDC devices have demonstrated the capacity of energy storage after being exposed to light. The I-V characteristics of these PV devices attached to this storage energy device have been examined under dark conditions. The important outcomes of the electrical characterisation are as follows;

I-V characteristics of the silicon-based a-Si PV device attached to the LDC layers showed a significant amount of the total energy conversion of 693.09 μW in dark conditions. As much as 1.07% of the electrical power is being generated, since the photon energy of the LDC layers is transferred to the PV device. This means the energy storage in the down converter layers is generating electrical charges into the PV device under dark conditions. The real application test conducted with this PV, LDC devices and a LED light, showed that it was possible to power the LED for more than 5 minutes.

For the DSSC PV device with the LDC layers attached to it under dark conditions, the electrical powers were found to be weaker due to the size of the active area, and losses were caused by the internal capacitance of the PV device, thus resulting in a poor electrical charge generation into the structure of the PV device. In turn, it became difficult for electrical charges to be extracted from this type of DSSC PV device at this specific size.

The electrical characterisation of the MPC PV device with the LDC layers attached to it, under dark conditions, showed some similarities to the DSSC PV device but more encouraging results were obtained. The amount of power generated or the Total Energy conversion in the dark condition was demonstrated to be higher than the internal capacitance of the MPC PV device. However, these low powers produced for this PV device were not enough to power the LED light under light or dark conditions because of the small active area and the losses caused by the internal capacitance of the PV device. This also resulted in a poor electrical charge generation into the structure of the PV device. Accordingly, it became difficult for electrical charges to be extracted from this type of MPC PV device.

Studies of different types of PV technologies and phosphorescent and capacitor materials demonstrate that, by increasing the size of the PV devices' active area and the number of PV devices connected, these technologies can be combined to contribute to an energy storage solution. By applying a larger PV size combined with a supercapacitor, for example, a 5.5 V/F Panasonic "Gold capacitor" (which specifies a voltage drop at 20 °C from 5.5 V to 3 V in 600 hours ("Panasonic Capacitors (Gold Capacitor)," 2016)), the application could be significantly altered and optimised. However, such studies also show that these technologies may take time to develop greater efficiency; the negative implications of such alterations would also need to be considered. Accordingly, the proven concepts within this research project application indicate that by upscaling the PV device, and by combining phosphorescence with these new types of capacitor, the entire system has the potential to replace batteries. It is hoped that the findings presented here will play a remarkable role in a variety of applications, including buildings and electric vehicles.

CHAPTER 9

CONCLUSIONS AND RECOMMENDATION

9.1 Discussion

This research aimed to enhance PV device efficiency by applying long persistent phosphor species as luminescent material, dispersed in a transparent host polymer layer and considered as a passive approach. Based on various test applications under light and dark conditions and subsequent analysis of the PV devices, it can be concluded that long persistent phosphors are an important method to consider when enhancing PV device capabilities and workability. The results indicate that potential energy photons transfer from the luminescent layers to the PV devices under dark conditions and are capable of powering a LED light for more than 5 minutes. It is by proving that energy converted can be also stored in a capacitor.

The current research explored a variety of new species of long persistent phosphorescent phosphors, which did not exist a few decades ago, and applied them in a host polymer matrix in order to enhance the PV device efficiency. It was revealed that the long persistent phosphors synthesis and characterization processes are still in the development stage, and require more research.

Most of the work published (He et al., 2013; Luo et al., 2019; Que et al., 2016), involved the implantation of the low concentration long persistent phosphors, LPP, into the PV device as a non-passive approach. No one, to date, has studied and developed highly concentrated luminescent layers as a passive approach, with a mixture of various species of LPP. This is the first study that utilises a down-conversion layer of highly concentrated LPP phosphors of various species as an energy storage device to power a PV device and a LED light, for more than 5 minutes.

This research project investigated various types of host materials, LPP phosphors and PV device technologies, in order to combine them to develop a PV device that works in dark conditions.

The combined capabilities of these energy storage devices point to the important difference between phosphorescent phosphors and other techniques presented in the Literature Review, such as organic dyes and quantum dots which also aim to improve the spectral losses of the PV devices. These techniques or concepts obviously concentrate on a better exploitation of the solar spectrum and not on energy storage concepts. However, all of these materials can be applied in the modification of the light spectrum, but only phosphorescent phosphors can store energy on its host structure.

A new ultra-transparent host polymer matrix, Polysiloxane, has been identified which can be used for many applications, such as; characterization of the luminescent species, fluorescent and phosphorescent phosphors, (which may be difficult to synthesise with quartz glass), down-conversion, down-shifting and up-conversion, and PV device technologies. The ultra-transparent host polymer, Polysiloxanes, has demonstrated that it is a good substitute for quartz glass in terms of transmission over with 90%, from the ultraviolet to the infrared spectrum. Different methods of synthesis have been tested, and it proved simple to synthesize the host layer, which does not require expensive fabrication processes.

The stability and aging of the host polymer was investigated, and were found to suit many optical applications, as they are very stable and do not degrade significantly over several months. However, it was found that this polymer has shown a slight reduction of less than 1.5% in transmission in the range of 240-310nm, (which could be caused by the polymerization or degradation of this polymer, over a total of a 65 day period), but does not seem to be a problem for the luminescent phosphor application because the phosphorescent species absorbs a wide range in the UV and re-emits its absorbed energy photons > 400nm.

The optical properties have shown that they are suitable to luminescent layers and for investigations of photoluminescent quantum yield, PLQY, of the phosphor species, (which is insoluble in all known solvents), without damaging its crystallisation. The host matrix, Polysiloxane, were used to fabricate the luminescent layers at various concentration ratios (0.1-100%wt) that were then applied as a passive approach to enhance the PV device efficiency.

Many different types of long persistent phosphors were investigated. However only a few of them were available and acquired from chemical companies to be tested during this investigation. They were found to satisfy the expectations for this project application. Among them, the following can be highlighted: Strontium silicate aluminate, Europium and Dysprosium doped Ph1, ($Sr_{2.90}Eu_{0.03}Dy_{0.07}Al_4SiO_{11}$). Both Strontium aluminate, Europium and Dysprosium doped Ph2 ($Sr_{3.84}Eu_{0.06}Dy_{0.10}Al_{14}O_{25}$) and Ph3 ($Sr_{0.95}Eu_{0.02}Dy_{0.03}Al_2O_4$) have demonstrated high photoluminescent quantum efficiency, Ph1; 0.48%, Ph2; 0.44% and Ph3; 0.62%, among all the phosphorescent species. They all have absorption in the UV range, 200-400nm, and emission peaks centred at the visible spectrum range. Interestingly, the phosphorescent intensity or brightness does not necessarily result in the longest phosphorescence lifetime decay. It was observed that the Ph3 sample ($Sr_{0.95}Eu_{0.02}Dy_{0.03}Al_2O_4$) which has the highest photoluminescent quantum efficiency, resulted in a shorter lifetime decay than the other two phosphorescent phosphors. Thus, this phosphor, (Ph3), appeared to have a more fluorescent characteristic than phosphorescent. The fluorescent phosphors such as the standard reference phosphors from Japan NIMS, have IQE above 0.82% and the closest to this value is Ph3, (within 0.62%), which may explain this observation. On account of long lifetime decay, it was found that the higher the concentration ratio, the longer the decay.

A new method, known as “The Mixed Method”, which is used to measure the quantum efficiency of the long persistent phosphor, has been proposed. This method was used to measure the PLQY of the phosphors and appears to have great potential, by improving upon the existing methods, which tend to use the same instruments to measure the PLQY of the fluorescent materials. To confirm the reproducibility of this method three repeat measurements were made for each sample measured. These results showed an uncertainty of about 0.01. This is also a very important optical parameter for luminescent materials.

The novel luminescent devices, PhX and PhT, containing mixes of various species of LPP phosphors, were conceived, fabricated and tested for this project under illumination and dark conditions, as well as other individual layers composed of single LPP species. These devices resulted in significant advantages over the conventional method to enhance PV device

efficiency. They were tested in many different types of PV device technologies, on the top or at the rear, just by stacking and removing the air bubble between the layer and the PV device surface. This advantage can be seen not just in the characterization process of the luminescent layer, but also during the test performance of the PV device, with and without the layer, to determine gains or losses from a specific application.

Through this luminescent layer on the top surface of the PV device, it was found that low concentration ratio 1%wt under the illumination may increase the PV device efficiency, (by up to 4.1958%). This is due to the conversion of the low energy photons into higher energy photons, at a visible range and trapping light within the layer. Whereas, it can be seen that by applying a high concentration ratio >20%wt of luminescent layers on top of the PV device under the illumination, it has resulted in a significant reduction of the PV device efficiency. This reduction is caused by the highly reflective layer which causes light reflectance or scattering before it reaches the PV device. The highest reflectance level for the LDC layer was reached at 70%wt. However, this inconvenience may be avoided by an using an anti-reflective coating design to reflect the down converted emission back into the PV device, as reported by de la Mora et al.,(2017). This approach was not applied here. The layers were tested as a reflector at the rear of the PV device and its function was to reflect all non-absorbed light and down converted emission back into the PV device, thus enhancing the PV device efficiency.

Under illumination, the I-V characteristic measurement results of the DSSC with the luminescent layers, within a concentration ratio of >60%wt at the rear surface, allows for an increase of up to 4% in the PV device efficiency. On the contrary, when these layers are placed on the top surface of the PV device, the efficiency deteriorated by up to -57%. DSSC PV device has shown that the LDC layers are an excellent option to improve the PV device efficiency, but only when applied at the rear surface of the PV device, under illumination. However, some results have shown that by adding the LDC layer on top of the DSSC PV device it will absorb the UV light, which could help to ensure the long-term stability of the sensitised dyes.

Similar results were found to the MPC PV device under illumination, with these layers placed at the rear surface allowing for an increase of up to 2% in the PV device efficiency. When these

LDC layers are placed on the top surface of the PV device, they can affect the PV device efficiency performance, thus potentially reducing its efficiency by up to -44%.

With the concentration ratio >60%wt, it is emphasised that this measurement is needed to form the basis of energy storage capabilities under dark conditions, after exposure to illumination. The optimum concentrations were found to be 60%wt for application on the top and at the rear of the PV device, particularly for the mixing of the phosphorescent species layers, PhX and PhT, under dark conditions. LDC layers as energy an storage device in dark conditions, with high concentrations, 100%wt, or even better, more than one LDC layer to create a longer afterglow effect. Furthermore, by applying the concentrated layer on top, it reduced the PV efficiency under illumination, but increased the emission time under dark conditions. These higher concentrations of > 80%wt layers at the rear are ideal for the transparent PV devices, which don't contain a reflective coating or metal back layer in their architecture. This is because LDC layers can be used as a reflector simultaneously, along with down converted emission, and thus improve the PV device efficiency in the dark and under an illuminated condition. However, it may compromise the amount of light reaching the LDC layer as less light will pass through a transparent PV device, but this down converted emission energy can still be used to power the PV device.

The investigation of the LDC layers as energy storage devices has shown that the emission of energy photons during the photoluminescent decay can generate electricity by the PV device following exposure to light. The practical test application was used with a systematic approach to analyse the effect of LDC devices combined with different types of PV device technologies; a-Si, DSSC and MPC PV devices, under dark conditions. All different types of LDC devices demonstrated the capacity of energy storage after exposure to light. The I-V characteristics of the PV devices attached to these energy storage devices have been examined under dark conditions, after exposure to light. It was found that the energy from the LDC devices can be transferred, and can generate electrical power into the PV device.

I-V characteristics of the silicon-based a-Si PV device attached to the LDC device showed a significant amount of the total energy conversion of 693.09 μW in dark conditions. As much

as 1.07% of the electric power is being generated, since the photon's energy of the LDC device was transferred into the PV device. The real application test conducted with this PV device combined with the LDC devices and an LED light, showed that it is possible to power the LED for more than 5 minutes using a capacitor.

The same application test, using the DSSC PV device with the LDC device attached to it under dark conditions, after being exposed to illumination, resulted in low power due to the size of the active area and losses caused by the internal capacitance of the PV device. This meant a subsequent poor electrical charge being channelled into the structure of this PV device. In such circumstances it becomes difficult to extract electrical charges from this type of DSSC PV device.

Similar results were found in the electrical characterisation of the MPC PV device with the LDC layers attached to it, after exposure to illumination, under dark conditions. However, these characterisations resulted in better power output performances, which were significantly higher than the DSSC PV device. The amount of power generated, or the total energy converted in the dark condition was demonstrated to be higher than the internal capacitance of the MPC PV device. However, the low power produced for this PV device was not enough to power the LED light under dark conditions because of the small size of the active area, and the losses caused by the internal capacitance of the PV device.

9.2 Contribution to Knowledge

- ✓ An ultra-transparent host polymer matrix was studied for luminescent applications and an optimised method developed to produce a luminescent layer of various concentration ratios, maintaining its thickness.
- ✓ A new standard method was proposed to measure the PLQY of the long persistent phosphor species, which can be dispersed in a host polymer matrix that does not compromise the crystallisation structure of the phosphors.
- ✓ Different species of long persistent phosphors were investigated, and their novel optical properties reported.

These results can be used as reference values for further investigations and analysis of both types of phosphors; fluorescent and phosphorescent species.

- ✓ Optimised LDC devices were fabricated by mixing various types of LPP at high concentration ratio to be used to enhance the PV device performance.
- ✓ Down-conversion mechanism was investigated and successfully applied as a passive approach to enhance the different types of PV device technologies, including Dye-sensitized, Monolithic Perovskite and silicon-based multijunction mini-module amorphous silicon PV devices.
- ✓ The LDC devices fabricated with long persistent phosphors of various species were used as energy storage devices to power a PV device, after being exposed to light, in dark conditions.
- ✓ The amount of energy converted from the LDC devices to the PV device, after being exposed to light, has been characterized in terms of electrical power generated from the PV device, which was able to power a LED light for more than 5 minutes. With minimal adaptation, these combined, developed devices can be used in many other applications.

9.3 Recommendations for Future Work

The main aim of this research project was to investigate different types of long persistent phosphors to enhance the PV device performance under light and dark conditions applied in a small-scale device only. However, studies have shown that it can be upscaled; this is a proven method, in order to improve the PV device performance with the introduction of multiple devices connected in series, or even better, the direct application in larger size devices, (e.g. as in the case of a-Si device, the largest PV device tested).

The optimization of the LDC device with an LPP of higher quantum efficiency (close to a unity or higher) and photoluminescence decay, could result in a better energy storage device, which in turn, could enhance the PV device even more significantly.

Investigation of the synthesis procedure to produce a white-emitting long persistent phosphor, which demonstrated a high PLQY and photoluminescence decay may be an important breakthrough to PV device enhancement. The optimized LDC devices produced PhX and PhT by mixing various phosphors species. This also indicates that mixing different species containing different PLQYs may compromise the application.

The LDC layer could be improved by applying a reflective coating on the surfaces that are not receiving direct light or attached to the PV device. This will enhance the light trapping mechanism inside the layer forcing the energy photons into the PV device, which could result in significant enhancement.

9.4 Outlook

The results presented in this thesis helped to increase the understanding of both phosphorescent and photovoltaic technologies. The materials and methods employed show great potential for use in a wide range of investigations. In this same way, new PV technologies, new bulk materials, new re-engineering designs and systems performance improvement, as well as much-needed work create a more accessible technology, are all required. Above all, the most important need is to review the current conceptions about the environment and how humans are using energy sources in daily life. The main objective of this research project is to investigate new ways to improve the current technologies which are used to generate energy, such as enhancing the efficiency and energy storage of devices. New conceptions and environmentally friendly approaches have been reviewed, not just by generating more energy, but also by consuming less electrical power which is the most important feature, as it will cost less in every sense of the word.

Advances in PV device technologies are contributing to new types of energy products and services across the globe from in-grid to off-grid and offer many potential benefits for economies, societies, and individuals. With this potential, come questions about the impact of energy storage battery technologies on the work functionality and working time of the PV

device system. Building on the insights from this research project, new evidence emerges of an energy storage device facilitated by the application of the long persistent phosphors and capacitors. Drawing from these tests, it may be considered how these devices can work together.

Thus, this research brings together key insights from current investigations and enables new possibilities – from enhancing the PV device capabilities to energy storage devices. Current understanding about the impact of energy storage by the PV systems, (where much of the difficulty and costs are linked to battery devices which are considered as grid storage solutions) is helping restore the balance of renewable energy. However, scientists claim that new types of energy storage technologies are needed urgently to replace the present types of batteries and "if nothing changes, demand will outstrip production within 20 years."(Turcheniuk et al., 2018).

Despite this uncertainty, evidence from this work results in waves of new possibilities (including using phosphorescent materials to power the multijunction amorphous silicon PV devices during the night time by storing electrical energy into a capacitor), and can provide evidence and insights to new approaches for grid storage solutions. Therefore, considering that it is not standard procedure to apply for all types of PV device, (both DSSC and MPC devices utilised in this research indicate there is some incompatibility for this project application due to slow response), this remains a topic which requires special attention. Consequently, the damning effect of these types of energy storage device combinations on PV devices in the dark, using such circuits, has been overlooked until now. This needs to change as it has been clearly demonstrated here that the charging and energy storage within a capacitor, using these means, is an extremely worthwhile exercise.

REFERENCES

A. Ryan, A., O. Senge, M., 2015. How green is green chemistry? Chlorophylls as a bioresource from biorefineries and their commercial potential in medicine and photovoltaics. Photochem. Photobiol. Sci. 14, 638–660. https://doi.org/10.1039/C4PP00435C

Abbott, K. 1998. Critical Realism In Industrial Relations Theory. Current Research In Alves-Mazzotti, A. J. & Gewandsznajder, F. The Method in Science.

Aberle, A.G., Zhang, W., Hoex, B., 2011. Advanced loss analysis method for silicon wafer solar cells. Energy Procedia, Proceedings of the SiliconPV 2011 Conference (1st International Conference on Crystalline Silicon Photovoltaics) 8, 244–249. https://doi.org/10.1016/j.egypro.2011.06.131

Albani, J.R., 2011. Structure and Dynamics of Macromolecules: Absorption and Fluorescence Studies: Absorption and Fluorescence Studies. Elsevier.

Alves-Mazzotti, A. J. & Gewandsznajder, F. 1999. The Method In Science Natural And Social, Quantitative And Qualitative Research. 2. Ed. Thompson Learning.

Amudha, P., Jayakumar, M., Kulandaivelu, G., 2005. Impacts of ambient solar uv (280-400 nm) radiation on three tropical legumes. Journal of Plant Biology 48, 284–291.

ANEEL - Agência Nacional de Energia Elétrica [WWW Document], n.d. URL http://www.aneel.gov.br/aplicacoes/noticias/Output_Noticias.cfm?Identidade=6875&id_area=90.

Ananda, W., 2017, July. External quantum efficiency measurement of solar cell. In 2017 15th International Conference on Quality in Research (QiR): International Symposium on Electrical and Computer Engineering (pp. 450-456). IEEE.

Applications and Use of Integrating Spheres With the LAMBDA 650 and 850 UV/Vis and LAMBDA 950 UV/Vis/NIR Spectrophotometers [WWW Document], n.d. URL https://webcache.googleusercontent.com/search?q=cache:PEq5ZI_LAuQJ:https://www.perkinelmer.com/CMSResources/Images/44-74191APP_LAMBDA650IntegratingSpheres.pdf+&cd=2&hl=en&ct=clnk&gl=us&client=firefox-b.

Bae, J., Kim, YongHo, Kim, H., Kim, YuBae, Jin, J., Bae, B.-S., 2015. Ultraviolet Light Stable and Transparent Sol–Gel Methyl Siloxane Hybrid Material for UV Light-Emitting Diode (UV LED) Encapsulant. ACS Appl. Mater. Interfaces 7, 1035–1039. https://doi.org/10.1021/am507132a

Bagher, A.M., 2014. Introduction to Organic Solar Cells. Sustain. Energy Sustain. Energy 2, 85–90.

Balachandran, P.V., Rondinelli, J.M., 2015. Massive band gap variation in layered oxides through cation ordering. Nat. Commun. 6. https://doi.org/10.1038/ncomms7191

Basic Flux Oxides in Glazes: Tutorial IV (CeramicsWeb) - Meeneecat [WWW Document], n.d. URL https://sites.google.com/site/meeneecat/educational-materials/basic-flux-oxides-in-glazes-ceramicsweb.

Bass, M., Stryland, E.W.V., Williams, D.R., Wolfe, W.L., 1995. Handbook of Optics Volume II Devices, Measurements, and Properties 2nd edition.

Bequerel, E. (1839) Compt. Rendues 9,561–566.

Berberan-Santos, M.N., Bodunov, E.N., Valeur, B., 2005. Mathematical functions for the analysis of luminescence decays with underlying distributions 1. Kohlrausch decay function (stretched exponential). Chem. Phys. 315, 171–182.

Binnemans, K., 2015. Rare earths: essential elements for the transition to a low-carbon economy. Presented at the Proceedings of the Bauxite Residue Valorisation and Best Practices Conference 2015, pp. 291–299.

Bisquert, J., 2003. Chemical capacitance of nanostructured semiconductors: its origin and significance for nanocomposite solar cells. Phys. Chem. Chem. Phys. 5, 5360–5364.

Bol, A.A., Ferwerda, J., Bergwerff, J.A., Meijerink, A., 2002a. Luminescence of nanocrystalline ZnS:Cu2+. J. Lumin. 99, 325–334.

Bol, A.A., Ferwerda, J., Bergwerff, J.A., Meijerink, A., 2002b. Luminescence of nanocrystalline ZnS:Cu2+. J. Lumin. 99, 325–334. https://doi.org/10.1016/S0022-2313(02)00350-2BPOCchapter29.pdf, n.d.

Brian Walsh, 22:40:02 UTC. Judd-Ofelt Theory: Principles and Practices.

Brendel, R., Werner, J.H., Queisser, H.J., 1996. Thermodynamic efficiency limits for semiconductor solar cells with carrier multiplication. Solar Energy Materials and Solar Cells 41–42, 419–425.

Brouwer, A.M., 2011. Standards for photoluminescence quantum yield measurements in solution (IUPAC Technical Report). Pure Appl. Chem. 83.

Brown, M.E., 2001. Introduction to Thermal Analysis: Techniques and Applications. Springer Science & Business Media.

Bünzli, J.-C.G., Chauvin, A.-S., 2014. Chapter 261 - Lanthanides in Solar Energy Conversion, in: Jean-Claude G. Bünzli and Vitalij K. Pecharsky (Ed.), Handbook on the Physics and Chemistry of Rare Earths, Including Actinides. Elsevier, pp. 169–281.

Bünzli, J.-C.G., Pecharsky, V.K., 2013. Handbook on the Physics and Chemistry of Rare Earths. Newnes.

Buxbaum, G., Pfaff, G., 2006. Industrial Inorganic Pigments. John Wiley & Sons.

CAO, X., WEI, T., CHEN, Y., YIN, M., GUO, C., ZHANG, W., 2011. Increased downconversion efficiency and improved near infrared emission by different charge compensations in CaMoO4:Yb3+ powders. J. Rare Earths 29, 1029–1035.

Carson, J.A., 2008. Solar Cell Research Progress. Nova Publishers.

Catherine Tams, C., and Enjalbert, N., 2009. The Use of UV/Vis/NIR Spectroscopy in the Development of Photovoltaic Cells.

Chalcogenide Photovoltaics [WWW Document], 2018.epdf. tips. URL https://epdf.tips/queue/chalcogenide-photovoltaics.html

Chang, C., Li, W., Huang, X., Wang, Z., Chen, X., Qian, X., Guo, R., Ding, Y., Mao, D., 2010. Photoluminescence and afterglow behavior of Eu2+, Dy3+ and Eu3+, Dy3+ in Sr3Al2O6 matrix. J. Lumin. 130, 347–350. https://doi.org/10.1016/j.jlumin.2009.09.016

Chang, C., Mao, D., 2004. Long lasting phosphorescence of Sr4Al14O25:Eu2+, Dy3+ thin films by magnetron sputtering. Thin Solid Films 460, 48–52.

Chang, C., Yuan, Z., Mao, D., 2006. Eu2+ activated long persistent strontium aluminate nano scaled phosphor prepared by precipitation method. J. Alloys Compd. 415, 220–224.

Chemed, C., 2004. Types of Polymers [WWW Document]. URL http://chemed.chem.purdue.edu/genchem/topicreview/bp/1polymer/types.html

Chemical Communications, n.d. Chem. Commun.

Chemistry of Sustainable Energy [WWW Document], n.d. Scribd. URL https://www.scribd.com/doc/305978579/Chemistry-of-Sustainable-Energy (accessed 5.16.16b).

Chen, I.-C., Chen, K.-K., Chen, H.-S., Du, J., Lin, T.-J., Lin, S.-S., Chen, T.-M., Shieh, T.-Y., 2012. Investigations into thermoluminescence and afterglow characterization of strontium aluminates with boron-modification and reductions via sol-gel route. J. Rare Earths 30, 972–978.

Chen, J.-X., Zhang, C.-F., Gao, W.-X., Jin, H.-L., Ding, J.-C., Wu, H.-Y., 2010. B2O3/Al2O3 as a new, highly efficient and reusable heterogeneous catalyst for the selective synthesis of β-enamino ketones and esters under solvent-free conditions. J. Braz. Chem. Soc. 21, 1552–1556.

Chen, S., Zhou, G., Su, F., Zhang, H., Wang, L., Wu, M., Chen, M., Pan, L., Wang, S., 2012. Power conversion efficiency enhancement in silicon solar cell from solution processed transparent upconversion film. Mater. Lett. 77, 17–20.

Chergui, Y., Nehaoua, N., Mekki, D.E., 2011. Comparative Study of Dye-Sensitized Solar Cell Based on ZnO and TiO2 Nanostructures. Sol. Cells - Dye-Sensitized Devices.

Chuang, C.-H.M., Brown, P.R., Bulović, V., Bawendi, M.G., 2014. Improved performance and stability in quantum dot solar cells through band alignment engineering. Nat. Mater. 13, 796–801.

Collavini, S., Völker, S.F., Delgado, J.L., 2015. Understanding the Outstanding Power Conversion Efficiency of Perovskite-Based Solar Cells. Angew. Chem. Int. Ed. 54, 9757–9759.

Conibeer, G., 2007. Third-generation photovoltaics. Mater. Today 10, 42–50.

COP24: UN climate change conference, what's at stake and what you need to know [WWW Document], 2018. UN News. URL https://news.un.org/en/story/2018/11/1026851 (accessed 3.26.19).

Cotfas, D.T., Cotfas, P.A., Machidon, O.M., 2018. Study of Temperature Coefficients for Parameters of Photovoltaic Cells [WWW Document]. Int. J. Photoenergy.

Cristóbal López, A.B., Martí Vega, A., Luque López, A. (Eds.), 2012. Next generation of photovoltaics: new concepts, Springer series in optical sciences. Springer, Heidelberg; London.

Daicho, H., Shinomiya, Y., Enomoto, K., Nakano, A., Sawa, H., Matsuishi, S., Hosono, H., 2018. A novel red-emitting K2Ca(PO4)F:Eu2+ phosphor with a large Stokes shift. Chem. Commun. 54, 884–887.

Daniels, F., Boyd, C.A., Saunders, D.F., 1953. Thermoluminescence as a Research Tool. Science 117, 343–349.

de la Mora, M.B., Amelines-Sarria, O., Monroy, B.M., Hernández-Pérez, C.D., Lugo, J.E., 2017. Materials for downconversion in solar cells: Perspectives and challenges. Sol. Energy Mater. Sol. Cells 165, 59–71.

de Mello, J.C., Wittmann, H.F., Friend, R.H., 1997. An improved experimental determination of external photoluminescence quantum efficiency. Adv. Mater. 9, 230–232.

de Wild, J., Meijerink, A., Rath, J.K., van Sark, W.G.J.H.M., Schropp, R.E.I., 2010a. Towards upconversion for amorphous silicon solar cells. Sol. Energy Mater. Sol. Cells, Inorganic and Nanostructured Photovoltaics 94, 1919–1922.

de Wild, J., Rath, J.K., Meijerink, A., van Sark, W.G.J.H.M., Schropp, R.E.I., 2010b. Enhanced near-infrared response of a-Si:H solar cells with β-NaYF4:Yb3+ (18%), Er3+ (2%) upconversion phosphors. Sol. Energy Mater. Sol. Cells 94, 2395–2398.

Detailed Balance Limit of Efficiency of p-n Junction Solar Cells [WWW Document], n.d. URL about:reader?url=http%3A%2F%2Fscitation.aip.org%2Fcontent%2Faip%2Fjournal%2Fjap%2F32%2F3%2F10.1063%2F1.1736034 (accessed 4.21.16).

Dexter, D.L., 1957. Possibility of Luminescent Quantum Yields Greater than Unity. Phys. Rev. 108, 630–633.

Dharmadasa, I.M., 2012. Advances in Thin-Film Solar Cells. Pan Stanford Publishing, Singapore.

Differential Scanning Calorimeter DSC7000 Series: Hitachi High-Technologies GLOBAL [WWW Document], n.d. URL https://www.hitachi-hightech.com/global/product_detail/?pn=ana-dsc7000x (accessed 1.1.19).

Dong, P., Zhu, Y., Zhang, J., Peng, C., Yan, Z., Li, L., Peng, Z., Ruan, G., Xiao, W., Lin, H., Tour, J.M., Lou, J., 2014. Graphene on Metal Grids as the Transparent Conductive Material for Dye Sensitized Solar Cell. J. Phys. Chem. C 118, 25863–25868.

Dorenbos, P., 2005. Mechanism of Persistent Luminescence in Eu [sup 2+] and Dy [sup 3+] Codoped Aluminate and Silicate Compounds. J. Electrochem. Soc. 152, H107.

Duan, Q., Qin, F., Wang, D., Xu, W., Cheng, J., Zhang, Z., Cao, W., 2011. Quantum cutting mechanism in Tb3+-Yb3+ co-doped oxyfluoride glass. J. Appl. Phys. 110, 113503.

Dulski, T.R., 1996. A Manual for the Chemical Analysis of Metals. ASTM International.

Dutczak, D.A., 2013. Eu2+ activated persistent luminescent materials [WWW Document]. URL http://dspace.library.uu.nl/handle/1874/287422 (accessed 6.22.16).

Dye Sensitized Solar Cells DSSC-DSC [WWW Document], n.d. URL https://www.gamry.com/application-notes/physechem/dssc-dye-sensitized-solar-cells/ (accessed 3.17.19).

Lynn, P.A., 2010. Electricity from sunlight: an introduction to photovoltaics. Wiley, Oxford.

Elleuch, R., Salhi, R., Al-Quraishi, S.I., Deschanvres, J.-L., Maâlej, R., 2014. Efficient antireflective downconversion Er3+ doped ZnO/Si thin film. Phys. Lett. A 378, 1733–1738.

Emery, K.A., 2007. Comment on "Roles of donor and acceptor nanodomains in 6% efficient thermally annealed polymer photovoltaics" [Appl. Phys. Lett. 90, 163511 (2007)]. Appl. Phys. Lett.

Eurostat, 2015. Greenhouse Gas Emissions [WWW Document], n.d. URL https://ec.europa.eu/eurostat/statistics-explained/index.php?title=File:Greenhouse_gas_emissions,_analysis_by_source_sector,_EU-28,_1990_and_2013_(percentage_of_total)_new.png&oldid=271858(accessed 02.25.16).

Evans, R.C., Douglas, P., Winscom, C.J., 2006. Coordination complexes exhibiting room-temperature phosphorescence: Evaluation of their suitability as triplet emitters in organic light emitting diodes. Coord. Chem. Rev. 250, 2093–2126.

Fang, Y.-C., Kao, P.-C., Yang, Y.-C., Chu, S.-Y., 2011. Two-Step Synthesis of SrSi2O2N2: Eu2+ Green Oxynitride Phosphor: Electron-Phonon Coupling and Thermal Quenching Behavior. J. Electrochem. Soc. 158, J246–J249. https://doi.org/10.1149/1.3600349

Fascinating SiliconeTM Chemistry –Silicone Polymerization & Finishing - Dow Corning [WWW Document], n.d. URL http://www.dowcorning.com/content/discover/discoverchem/si-finishing.aspx (accessed 10.1.15).

Feldmann, C., Jüstel, T., Ronda, C. r., Schmidt, P. j., 2003. Inorganic Luminescent Materials: 100 Years of Research and Application. Adv. Funct. Mater. 13, 511–516.

Fischer, M., Georges, J., 1996. Fluorescence quantum yield of rhodamine 6G in ethanol as a function of concentration using thermal lens spectrometry. Chem. Phys. Lett. 260, 115–118. https://doi.org/10.1016/0009-2614(96)00838-X

Fischer, S., Fröhlich, B., Steinkemper, H., Krämer, K.W., Goldschmidt, J.C., 2014. Absolute upconversion quantum yield of β-NaYF4 doped with Er3+ and external quantum efficiency of upconverter solar cell devices under broad-band excitation considering spectral mismatch corrections. Sol. Energy Mater. Sol. Cells 122, 197–207. https://doi.org/10.1016/j.solmat.2013.12.001

FitzGerald, S., 2008. F-3018 PLQY integrating sphere accessory, Methodology.

Formulation of Phosphorescence Mechanisms in Inorganic Solids Based on a New Model of Defect Conglomeration [WWW Document], n.d. URL about:reader?url=http%3A%2F%2Fpubs.acs.org%2Fdoi%2Fabs%2F10.1021%2Fcm052728q (accessed 12.10.15).

French, R.H., Rodríguez-Parada, J.M., Yang, M.K., Derryberry, R.A., Pfeiffenberger, N.T., 2011. Optical properties of polymeric materials for concentrator photovoltaic systems. Sol. Energy Mater. Sol. Cells, Photovoltaics, Solar Energy Materials & Thin Films, IMRC 2009-Cancun 95, 2077–2086.

Fujishima, A., Rao, T.N., Tryk, D.A., 2000. Titanium dioxide photocatalysis. J. Photochem. Photobiol. C Photochem. Rev. 1, 1–21. https://doi.org/10.1016/S1389-5567(00)00002-2

Fundamentals of Phosphors [WWW Document], n.d. Scribd. URL (accessed 10.1.14).

Fukuhara, M., Kuroda, T., Hasegawa, F., 2014. Realizing a supercapacitor in an electrical circuit. Appl. Phys. Lett. 105, 202904. https://doi.org/10.1063/1.4902410

Gainer, C.F., Romanowski, M., 2013. A review of synthetic methods for the production of upconverting lanthanide nanoparticles. J. Innov. Opt. Health Sci. 07, 1330007. https://doi.org/10.1142/S1793545813300073

Galluzzi, F., Scafé, E., 1984. Spectrum shifting of sunlight by luminescent sheets: Performance evaluation of photovoltaic applications. Sol. Energy 33, 501–507.

Georgobiani, A.N., Gutan, V.B., Demin, V.I., Semendyaev, S.V., 2009. Luminescence and Optical-Memory model of SrAl2O4:Eu2+,Dy3+ and Sr4Al14O25:Eu2+,Dy3+. Inorg. Mater. 45, 1289–1294. https://doi.org/10.1134/S0020168509110181

Gesang, T., Fanter, D., Höper, R., Possart, W., Hennemann, O.-D., 1995. Comparative film thickness determination by atomic force microscopy and ellipsometry for ultrathin polymer films. Surf. Interface Anal. 23, 797–808. https://doi.org/10.1002/sia.740231202

Girtan, M. and Mallet, R., 2014. On the electrical properties of transparent electrodes. Proc. Romanian Acad. A, 15(2), pp.146-150.

Girtan, M., 2018. Future solar energy devices. Springer.

Goetzberger, A., Goldschmidt, J.C., Peters, M., Löper, P., 2008. Light trapping, a new approach to spectrum splitting. Sol. Energy Mater. Sol. Cells 92, 1570–1578. https://doi.org/10.1016/j.solmat.2008.07.007

Goldschmidt, J.C., Fischer, S., Löper, P., Krämer, K.W., Biner, D., Hermle, M., Glunz, S.W., 2011. Experimental analysis of upconversion with both coherent monochromatic irradiation and broad spectrum illumination. Sol. Energy Mater. Sol. Cells 95, 1960–1963.

Goodman, N.B., Ley, L., Bullett, D.W., 1983. Valence-band structures of phosphorus allotropes. Phys. Rev. B 27, 7440–7450.

Göpferich, A., 1996. Mechanisms of polymer degradation and erosion. Biomaterials, Polymer Scaffolding and Hard Tissue Engineering 17, 103–114. https://doi.org/10.1016/0142-9612(96)85755-3

Grabolle, M., Spieles, M., Lesnyak, V., Gaponik, N., Eychmüller, A., Resch-Genger, U., 2009. Determination of the Fluorescence Quantum Yield of Quantum Dots: Suitable Procedures and Achievable Uncertainties [WWW Document]. URL http://pubs.acs.org/doi/full/10.1021/ac900308v (accessed 5.30.17).

Grätzel, M., 2003. Dye-sensitized solar cells. J. Photochem. Photobiol. C Photochem. Rev. 4, 145–153. https://doi.org/10.1016/S1389-5567(03)00026-1

Greatly enhanced Dy3+ emission via efficient energy transfer in gadolinium aluminate garnet (Gd3Al5O12) stabilized with Lu3+ - Journal of Materials Chemistry C (RSC Publishing), n.d. J. Mater. Chem. C.

Green, M.A., 1981. Solar cell fill factors: General graph and empirical expressions. Solid-State Electron. 24, 788–789. https://doi.org/10.1016/0038-1101(81)90062-9

Green, M.A., 1982. Solar cells: Operating principles, technology, and system applications.

Green, M.A., 2006. Third Generation Photovoltaics: Advanced Solar Energy Conversion. Springer.

Green, M.A., Hishikawa, Y., Dunlop, E.D., Levi, D.H., Hohl-Ebinger, J., Ho-Baillie, A.W.Y., 2018. Solar cell efficiency tables (version 51). Prog. Photovolt. Res. Appl. 26, 3–12. https://doi.org/10.1002/pip.2978

Green, M.A., Ho-Baillie, A., Snaith, H.J., 2014. The emergence of perovskite solar cells. Nat. Photonics 8, 506–514.

Grimminger, R., 2014. LASER SPECTROSCOPY OF RADICALS CONTAINING GROUP IIIA AND VA ELEMENTS. Theses Diss.--Chem.

Gschneidner, K.A., Eyring, L., Lander, G.H., 2001. Handbook on the Physics and Chemistry of Rare Earths. Elsevier.

Guanming, Q., Yongjie, C., Jingqiang, C., Xiujuan, G., Hui, W., Bo, S., 2007. Synthesis of Long Afterglow Phosphors Doped B SrAl2O4:Eu2+, Dy3+ and Its Luminescent Properties. J. Rare Earths 25, Supplement 1, 86–89.

Guilbault, G.G., 1990. Practical Fluorescence, Second Edition. CRC Press.

Guo, C., Luan, L., Huang, D., Su, Q., Lv, Y., 2007. Study on the stability of phosphor SrAl2O4:Eu2+, Dy3+ in water and method to improve its moisture resistance. Mater. Chem. Phys. 106, 268–272.

Gupta, M.C., Ballato, J., 2006. The Handbook of Photonics, Second Edition. CRC Press.

H. Sargent, E., 2005. Infrared Quantum Dots. Adv. Mater. 17, 515–522.

Hagemann, H., Lovy, D., Yoon, S., Pokrant, S., Gartmann, N., Walfort, B., Bierwagen, J., 2016. Wavelength dependent loading of traps in the persistent phosphor SrAl2O4:Eu2+, Dy3+. J. Lumin. 170, 299–304.

Halme, J., Vahermaa, P., Miettunen, K., Lund, P., 2010. Device Physics of Dye Solar Cells. Advanced Materials 22, E210–E234. https://doi.org/10.1002/adma.201000726

Hamer, F., Hamer, J., 2004. The Potter's Dictionary of Materials and Techniques. University of Pennsylvania Press.

Han, L., Koide, N.C., 2006. Modeling of an equivalent circuit for dye-sensitized solar cells: improvement of efficiency of dye-sensitized solar cells by reducing internal resistance. Comptes Rendus Chim. 9, 645–651.

Han, L., Koide, N., Chiba, Y., Islam, A., Komiya, R., Fuke, N., Fukui, A. and Yamanaka, R., 2005. Improvement of efficiency of dye-sensitized solar cells by reduction of internal resistance. Applied Physics Letters, 86(21), p.213501.

Handbook on the Physics and Chemistry of Rare Earths, Volume 44 - 1st Edition [WWW Document], n.d. URL https://www.elsevier.com/books/handbook-on-the-physics-and-chemistry-of-rare-earths/bunzli/978-0-444-62711-7 (accessed 4.10.18).

Hart, C., 1998. Doing a Literature Review: Releasing the Social Science Research Imagination, 1 edition. ed. SAGE Publications Ltd, London.

Harvey, E.N., Edmund N., 1957. A history of luminescence from the earliest times until 1900. Philadelphia, American Philosophical Society.

Hashmi, S.G., Martineau, D., Dar, M.I., Myllymäki, T.T.T., Sarikka, T., Ulla, V., Zakeeruddin, S.M.,

Grätzel, M., 2017. High performance carbon-based printed perovskite solar cells with humidity assisted thermal treatment. J. Mater. Chem. A 5, 12060–12067. https://doi.org/10.1039/C7TA04132B

He, W., Atabaev, T.S., Kim, H.K., Hwang, Y.-H., 2013a. Enhanced Sunlight Harvesting of Dye-Sensitized Solar Cells Assisted with Long Persistent Phosphor Materials. J. Phys. Chem. C 117, 17894–17900. https://doi.org/10.1021/jp307954n

He, W., Atabaev, T.S., Kim, H.K., Hwang, Y.-H., 2013b. Enhanced Sunlight Harvesting of Dye-Sensitized Solar Cells Assisted with Long Persistent Phosphor Materials. J. Phys. Chem. C 117, 17894–17900.

Hernández-Rodríguez, M.A., Imanieh, M.H., Martín, L.L., Martín, I.R., 2013. Experimental enhancement of the photocurrent in a solar cell using upconversion process in fluoroindate glasses exciting at 1480 nm. Sol. Energy Mater. Sol. Cells 116, 171–175.

Hezel, R., 2003. Novel applications of bifacial solar cells. Prog. Photovolt. Res. Appl. 11, 549–556.

Highly Efficient Hybrid Polymer and Amorphous Silicon Multijunction Solar Cells with Effective Optical Management - Tan - 2016 - Advanced Materials [WWW Document], n.d. URL about:reader?url=http%3A%2F%2Fonlinelibrary.wiley.com%2Fdoi%2F10.1002%2Fadma.201504483%2Ffull (accessed 2.25.16).

H. Ahmed, (2014) "Materials Characterization and Plasmonic Interaction in Enhanced Luminescent Down-Shifting Layers for Photovoltaic Devices", PhD Thesis, Dublin, Dublin Institute of Technology.

Höppe, H.A., 2009. Recent Developments in the Field of Inorganic Phosphors. Angew. Chem. Int. Ed. 48, 3572–3582.

Hosseini, Z., Huang, W.-K., Tsai, C.-M., Chen, T.-M., Taghavinia, N., Diau, E.W.-G., 2013. Enhanced Light Harvesting with a Reflective Luminescent Down-Shifting Layer for Dye-Sensitized Solar Cells [WWW Document]. URL http://pubs.acs.org/doi/abs/10.1021/am401584y (accessed 8.1.16).

Hovel, H.J., Hodgson, R.T., Woodall, J.M., 1979. The effect of fluorescent wavelength shifting on solar cell spectral response. Sol. Energy Mater. 2, 19–29.

How do Photovoltaics Work? - NASA Science [WWW Document], n.d. URL http://science.nasa.gov/science-news/science-at-nasa/2002/solarcells/ (accessed 5.11.16).

Huang, M.N., Ma, Y.Y., Huang, X.Y., Ye, S., Zhang, Q.Y., 2013. The luminescence properties of Bi3+ sensitized Gd2MoO6:RE3+ (RE = Eu or Sm) phosphors for solar spectral conversion. Spectrochim. Acta. A. Mol. Biomol. Spectrosc. 115, 767–771. https://doi.org/10.1016/j.saa.2013.06.111

Huang, Y., Zhang, S., Kim, S.I., Yu, Y.M., Seo, H.J., 2011. Multisite Structure and Luminescence Spectra from 4f65d1 → 4(8S7/2) and 4(6P7/2) → 4(8S7/2) Transitions in Eu2+-Doped NaMgPO4. J. Electrochem. Soc. 159, J23–J28. https://doi.org/10.1149/2.013202jes

Hu, M., Liu, L., Mei, A., Yang, Y., Liu, T., Han, H., 2014. Efficient hole-conductor-free, fully printable mesoscopic perovskite solar cells with a broad light harvester NH2CHNH2PbI3. J. Mater. Chem. A 2, 17115–17121. https://doi.org/10.1039/C4TA03741C

Ireland [WWW Document], n.d., Sigma-Aldrich. URL http://www.sigmaaldrich.com/ireland.html (accessed 4.15.14).

Is a Doctorate in Engineering a Route to Industry Success? > ENGINEERING.com [WWW Document], n.d. URL http://www.engineering.com/Education/EducationArticles/ArticleID/8287/Is-a-Doctorate-in-Engineering-a-Route-to-Industry-Success.aspx (accessed 8.27.14).

J, M. Martinez, 2004. Batteries in PV systems, Wroclaw University of Technology.

J. Snaith, H., 2012. How should you measure your excitonic solar cells? Energy Environ. Sci. 5, 6513–6520. https://doi.org/10.1039/C2EE03429H

Jacoby, M., 2016. The future of low-cost solar cells | May 2, 2016 Issue - Vol. 94 Issue 18 | Chemical & Engineering News [WWW Document]. URL http://cen.acs.org/articles/94/i18/future-low-cost-solar-cells.html (accessed 5.16.16).

Jain, A., Hirata, G.A., Farías, M.H., Castillón, F.F., 2016. Synthesis and characterization of (3-Aminopropyl) trimethoxy-silane (APTMS) functionalized Gd 2 O 3: Eu 3+ red phosphor with enhanced quantum yield. Nanotechnology 27, 065601. https://doi.org/10.1088/0957-4484/27/6/065601

Jia, D., Meltzer, R.S., Yen, W.M., Jia, W., Wang, X., 2002. Green phosphorescence of CaAl2O4:Tb3+, Ce3+ through persistence energy transfer. Appl. Phys. Lett. 80, 1535–1537. https://doi.org/10.1063/1.1456955

Jia, W., Yuan, H., Lu, L., Liu, H., Yen, W.M., 1998. Phosphorescent dynamics in SrAl2O4: Eu2 +, Dy3 + single crystal fibers. J. Lumin., Proceedings of the Eleventh International Conference on Dynamical Processes in Excited States of Solids 76–77, 424–428. https://doi.org/10.1016/S0022-2313(97)00230-5

Jia, Y., Li, H., Zhao, R., Sun, W., Su, Q., Pang, R., Li, C., 2014. Luminescence properties of a new bluish green long-lasting phosphorescence phosphor Ca9Bi(PO4)7:Eu2+,Dy3+. Opt. Mater., OPTMAT_IWPPP 2013 in Guangzhou 36, 1781–1786. https://doi.org/10.1016/j.optmat.2014.04.006

Jin, T., Inoue, S., Machida, K., Adachi, G., 1997. Photovoltaic Cell Characteristics of Hybrid Silicon Devices with Lanthanide Complex Phosphor-Coating Film. J. Electrochem. Soc. 144, 4054–4058. https://doi.org/10.1149/1.1838135

Johnson, I., Davidson, M.W., 2012. Olympus Microscopy Resource Center | Jablonski Energy Diagram - Java Tutorial [WWW Document]. Natl. High Magn. Field Lab. 1800 East Paul Dirac Dr Fla. State Univ. Tallahass. Fla. 32310. URL http://www.olympusmicro.com/primer/java/jablonski/jabintro/ (accessed 10.1.14).

Kaldellis, J.K., Zafirakis, D., Kondili, E., 2010. Energy pay-back period analysis of stand-alone photovoltaic systems. Renew. Energy, Special Section: IST National Conference 2009 35, 1444–1454. https://doi.org/10.1016/j.renene.2009.12.016

Kapur, V.K., Meeting, E.S., 1999. Photovoltaics for the 21st Century: Proceedings of the International Symposium. The Electrochemical Society.

Kasha, M., 1947. Phosphorescence and the Rle of the Triplet State in the Electronic Excitation of Complex Molecules. Chem. Rev. 41, 401–419. https://doi.org/10.1021/cr60129a015

Kawano, Katsuya, Hashimoto, N., Nakata, R., 1997. Effects on Solar Cell Efficiency of Fluorescence of Rare-Earth Ions. Mater. Sci. Forum 239–241, 311–314. https://doi.org/10.4028/www.scientific.net/MSF.239-241.311

Kawano, Katsuyasu, Arai, K., Yamada, H., Hashimoto, N., Nakata, R., 1997. Application of rare-earth complexes for photovoltaic precursors. Sol. Energy Mater. Sol. Cells 48, 35–41. https://doi.org/10.1016/S0927-0248(97)00066-4

Kennedy, M. et al (2010). Solar Cell Efficiency Enhancement Through Down-Shifting and Up-Converting Layers: the Ephocell Project: Luminescent Downshifting Quantum Yield Measurements. 25th European Photovoltaic Solar Energy Conference and Exhibition, Valencia, Spain, 6-9 September.

Khmil, D.N., Kamuz, A.M., Oleksenko, P.F., Kamuz, V.G., Aleksenko, N.G., Kamuz, O.A., 2015. Determination of the spectral dependence for the absorption coefficient of phosphor inorganic microparticles. Semicond. Phys. Quantum Electron. Optoelectron. 18, 334–340. https://doi.org/10.15407/spqeo18.03.334

Kishore, J., Thiyagarajan, S., Gunanathan, C., 2019. Ruthenium (II)-catalysed direct synthesis of ketazines using secondary alcohols. Chem. Commun. https://doi.org/10.1039/C9CC01383K

Kitai, A., 2008. Luminescent Materials and Applications. John Wiley & Sons.

Klampaftis, E., Ross, D., McIntosh, K.R., Richards, B.S., 2009. Enhancing the performance of solar cells via luminescent down-shifting of the incident spectrum: A review. Sol. Energy Mater. Sol. Cells 93, 1182–1194. https://doi.org/10.1016/j.solmat.2009.02.020

Kong, J., Lee, J., Kim, G., Kang, H., Choi, Y., Lee, K., 2012. Building mechanism for a high open-circuit voltage in an all-solution-processed tandem polymer solar cell. Phys. Chem. Chem. Phys. 14, 10547–10555. https://doi.org/10.1039/C2CP41501A

Krygowski, T.W., 1998. A novel simultaneous diffusion technology for low-cost, high-efficiency silicon solar cells. ProQuest Diss. Theses Thesis PhD--Ga. Inst. Technol. 1998 Publ. Number AAI9837768 ISBN 9780591914337 Source Diss. Abstr. Int. Vol. 59-06 Sect. B Page 2944 316 P.

Lahoz, F., Pérez-Rodríguez, C., Hernández, S.E., Martín, I.R., Lavín, V., Rodríguez-Mendoza, U.R., 2011. Upconversion mechanisms in rare-earth doped glasses to improve the efficiency of silicon solar cells. Sol. Energy Mater. Sol. Cells 95, 1671–1677. https://doi.org/10.1016/j.solmat.2011.01.027

Lai, H., Wang, Y., Du, G., Li, W., Han, W., 2014. Dual functional YVO4:Eu3+, Bi3+@SiO2 submicron-sized core–shell particles for dye-sensitized solar cells: Light scattering and downconversion. Ceram. Int. 40, 6103–6108. https://doi.org/10.1016/j.ceramint.2013.11.061

Lakowicz, J.R., 2011. Principles of Fluorescence Spectroscopy, 3rd edition. ed. Springer, New York.

Leboeuf, C., Ossenbrink, H.A., 1991. PV module power output: sensitivity and uncertainty in non-STC measurements, in: The Conference Record of the Twenty-Second IEEE Photovoltaic Specialists Conference - 1991. Presented at the The Conference Record of the Twenty-Second IEEE Photovoltaic Specialists Conference - 1991, pp. 614–619 vol.1. https://doi.org/10.1109/PVSC.1991.169284

Leow, S.W., 2014. Low-Cost Photovoltaics: Luminescent Solar Concentrators And Colloidal Quantum Dot Solar Cells. eScholarship.

Li, C., Song, Z., Li, Y., Lou, K., Qiu, J., Yang, Z., Yin, Z., Wang, X., Wang, Q., Wan, R., 2013. Enhanced NIR downconversion luminescence by precipitating nano Ca5(PO4)3F crystals in Eu2+–Yb3+ co-doped glass. Spectrochim. Acta. A. Mol. Biomol. Spectrosc. 114, 575–578. https://doi.org/10.1016/j.saa.2013.05.074

Lian, H., Hou, Z., Shang, M., Geng, D., Zhang, Y., Lin, J., 2013. Rare earth ions doped phosphors for improving efficiencies of solar cells. Energy 57, 270–283. https://doi.org/10.1016/j.energy.2013.05.019

Liu, B., Shi, C., Yin, M., Dong, L., Xiao, Z., 2005. The trap states in the Sr2MgSi2O7 and (Sr,Ca)MgSi2O7 long afterglow phosphor activated by Eu2+ and Dy3+. J. Alloys Compd. 387, 65–69. https://doi.org/10.1016/j.jallcom.2004.06.061

Liu, G., Jacquier, B., 2006. Spectroscopic Properties of Rare Earths in Optical Materials. Springer Science & Business Media.

Liu, J., Yao, Q., Li, Y., 2006. Effects of downconversion luminescent film in dye-sensitized solar cells. Appl. Phys. Lett. 88, 173119. https://doi.org/10.1063/1.2198825

Liu, T., Xiong, Y., Mei, A., Hu, Y., Rong, Y., Xu, M., Wang, Z., Lou, L., Du, D., Zheng, S., Long, X., Xiao, S., Yang, S., Han, H., 2019. Spacer layer design for efficient fully printable mesoscopic perovskite solar cells. RSC Adv. 9, 29840–29846. https://doi.org/10.1039/C9RA05357C

Liu, Z., Li, J., Yang, L., Chen, Q., Chu, Y., Dai, N., 2014. Efficient near-infrared quantum cutting in Ce3+–Yb3+ codoped glass for solar photovoltaic. Sol. Energy Mater. Sol. Cells 122, 46–50. https://doi.org/10.1016/j.solmat.2013.10.030

Long Afterglow Phosphors [WWW Document], n.d. PowerShow. URL http://www.powershow.com/view/b77a6-ZWIxY/Long_Afterglow_Phosphors_powerpoint_ppt_presentation (accessed 4.8.14).

Lu, Y., Li, Y., Xiong, Y., Yin, Q., 2004. SrAl2O4: Eu2+, Dy3+ phosphors derived from a new sol-gel route. Microelectron. J. 35, 379–382. https://doi.org/10.1016/S0026-2692(03)00250-7

Luitel, H.N., 2010. Preparation and Properties of Long Persistent Sr_4Al_14O_25 Phosphors Activated by Rare Earth Metal Ions.

Luitel, H.N., Watari, T., Chand, R., Torikai, T., Yada, M., 2013. Giant Improvement on the Afterglow of Sr4Al14O25:Eu<sup><b>2. J. Mater. 2013, e613090. https://doi.org/10.1155/2013/613090

Luminescent Down Shifting [WWW Document], n.d. URL http://siser.eps.hw.ac.uk/research/next-generation/luminescent-down-shifting (accessed 8.21.15).

Luo, X., Ahn, J.Y., Kim, S.H., 2019. Aerosol synthesis and luminescent properties of CaAl2O4:Eu2+, Nd3+ down-conversion phosphor particles for enhanced light harvesting of

dye-sensitized solar cells. Sol. Energy 178, 173–180. https://doi.org/10.1016/j.solener.2018.12.029

Luque, A., Hegedus, S., 2003. Handbook of Photovoltaic Science and Engineering. Wiley.

Lynn, P.A., 2010. Electricity from sunlight: an introduction to photovoltaics. Wiley, Oxford.

Ma, Y., Li, H., Yuan, J., 2016. In-situ solution chemical reaction deposition of Bi2S3 quantum dots on mesoscopic TiO2 films for application in quantum-dot-sensitized solar cells. Integr. Ferroelectr. 169, 42–49. https://doi.org/10.1080/10584587.2016.1162610

Malta, O.L., Brito, H.F., Menezes, J.F.S., Gonçalves e Silva, F.R., de Mello Donegá, C., Alves, S., 1998. Experimental and theoretical emission quantum yield in the compound Eu(thenoyltrifluoroacetonate)3.2(dibenzyl sulfoxide). Chem. Phys. Lett. 282, 233–238. https://doi.org/10.1016/S0009-2614(97)01283-9

Marchionna, S., Meinardi, F., Acciarri, M., Binetti, S., Papagni, A., Pizzini, S., Malatesta, V., Tubino, R., 2006. Photovoltaic quantum efficiency enhancement by light harvesting of organo-lanthanide complexes. J. Lumin. 118, 325–329. https://doi.org/10.1016/j.jlumin.2005.09.010

Markham, J.P.J., Lo, S.-C., Magennis, S.W., Burn, P.L., Samuel, I.D.W., 2002. High-efficiency green phosphorescence from spin-coated single-layer dendrimer light-emitting diodes. Appl. Phys. Lett. 80, 2645–2647. https://doi.org/10.1063/1.1469218

Martinez, J., 2011. BATTERIES IN PV SYSTEMS [WWW Document]. URL http://e-archivo.uc3m.es/bitstream/handle/10016/12628/PFC_Javier_Mohedano_Martinez.pdf?sequence=1 (accessed 9.7.14).

Martins, F.R., Pereira, E.B., Abreu, S.L., 2007. Satellite-derived solar resource maps for Brazil under SWERA project. Sol. Energy 81, 517–528. https://doi.org/10.1016/j.solener.2006.07.009

Maruyama, T., Enomoto, A., Shirasawa, K., 2000. Solar cell module colored with fluorescent plate. Sol. Energy Mater. Sol. Cells 64, 269–278. https://doi.org/10.1016/S0927-0248(00)00227-0

Matsuzawa, T., Aoki, Y., Takeuchi, N., Murayama, Y., 1996. A New Long Phosphorescent Phosphor with High Brightness, SrAl2 O 4: Eu2 +, Dy3 +. J. Electrochem. Soc. 143, 2670–2673. https://doi.org/10.1149/1.1837067

McDonald, S.A., Konstantatos, G., Zhang, S., Cyr, P.W., Klem, E.J.D., Levina, L., Sargent, E.H., 2005. Solution-processed PbS quantum dot infrared photodetectors and photovoltaics. Nat. Mater. 4, 138–142. https://doi.org/10.1038/nmat1299

McEvoy, A., Markvart, Tom, Castaner, Luis, Markvart, T., Castaner, L., 2003. Practical Handbook of Photovoltaics: Fundamentals and Applications. Elsevier.

Meijeirnk, A., 2011. Lanthanide Ions as Photon Managers for Solar Cells. Mater. Matters 6(4), p.113.

Metzdorf, J., 1987. Calibration of solar cells. 1: The differential spectral responsivity method. Appl. Opt. 26, 1701–1708. https://doi.org/10.1364/AO.26.001701

Minnaert, B., Veelaert, P., 2014. A Proposal for Typical Artificial Light Sources for the Characterization of Indoor Photovoltaic Applications. Energies 7, 1500–1516. https://doi.org/10.3390/en7031500

Mirershadi, S., Ahmadi-Kandjani, S., 2015. Efficient thin luminescent solar concentrator based on organometal halide perovskite. Dyes Pigments 120, 15–21. https://doi.org/10.1016/j.dyepig.2015.03.035

Molar mass of CO2 - Chemistry Online Education [WWW Document], n.d. URL http://www.webqc.org/mmcalc.php (accessed 6.10.14).

Muffler, H.-J., Bär, M., Lauermann, I., Rahne, K., Schröder, M., Lux-Steiner, M.C., Fischer, C.-H., Niesen, T.P., Karg, F., 2006. Colloid attachment by ILGAR-layers: Creating fluorescing layers to increase quantum efficiency of solar cells. Sol. Energy Mater. Sol. Cells, 14th International Photovoltaic Science and Engineering Conference14th International Photovoltaic Science and Engineering Conference 90, 3143–3150. https://doi.org/10.1016/j.solmat.2006.06.034

Mülhaupt, R., 2004. Hermann Staudinger and the Origin of Macromolecular Chemistry. Angew. Chem. Int. Ed. 43, 1054–1063. https://doi.org/10.1002/anie.200330070

Nakazawa, E., Murazaki, Y., Saito, S., 2006. Mechanism of the persistent phosphorescence in Sr4Al14O25:Eu and SrAl2O4:Eu codoped with rare earth ions. J. Appl. Phys. 100, 113113. https://doi.org/10.1063/1.2397284

Noel, N.K., Stranks, S.D., Abate, A., Wehrenfennig, C., Guarnera, S., Haghighirad, A.-A., Sadhanala, A., Eperon, G.E., Pathak, S.K., Johnston, M.B., Petrozza, A., Herz, L.M., Snaith, H.J., 2014. Lead-free organic–inorganic tin halide perovskites for photovoltaic applications. Energy Environ. Sci. 7, 3061–3068. https://doi.org/10.1039/C4EE01076K

NREL, 2010. Quantum Dots Promise to Significantly Boost Photovoltaic Efficiencies., Energy Lab., NREL is a national laboratory of the U.S. Department of Energy, Office of Energy Efficiency and Renewable Energy, operated by the Alliance for Sustainable Energy, LLC. [Web WWW Document], n.d. URL https://www.nrel.gov/docs/fy13osti/59015.pdf (accessed 07.18.14).

NREL, 2016. Silicon Materials and Devices., historical information [WWW Document], n.d. URL http://www.nrel.gov/pv/silicon_materials_devices.html (accessed 11.22.16).

NREL (Reported Best Research Cell Efficiencies) [WWW Document], 2018. URL https://www.nrel.gov/pv/cell-efficiency.html (accessed 12.15.18).

O'Flynn, K.P., Twomey, B., Breen, A., Dowling, D.P., Stanton, K.T., 2011. Microwave-assisted rapid discharge sintering of a bioactive glass–ceramic. J. Mater. Sci. Mater. Med. 22, 1625–1631. https://doi.org/10.1007/s10856-011-4339-y

O'Hara, P.B., St. Peter, W., Engelson, C., 2005. Turning on the Light. J. Chem. Educ. 82, 48A. https://doi.org/10.1021/ed082p48A

Obukuro, Y., Matsushima, S., Nakamura, H., Arai, M., Yamada, H., Xu, C.-N., 2014. Electronic structure of Eu2+-doped SrAl2O4 using modified Becke-Johnson exchange potential. Solid State Commun. 186, 46–49. https://doi.org/10.1016/j.ssc.2014.01.026

Omar, M.A., 1975. Elementary solid state physics: principles and applications, Addison-Wesley series in solid state sciences. Addison-Wesley Pub. Co, Reading, Mass.

Pan, A.C., Zanesco, I., Moehlecke, A., 2014. Industrial Bifacial Silicon Solar Cells with Up-converter and PbS Quantum Dots. Energy Procedia, Proceedings of E-MRS Spring Meeting 2013 Symposium D Advanced Inorganic Materials and Structures for Photovoltaics 27-31 May 2013, Strasbourg, France 44, 160–166. https://doi.org/10.1016/j.egypro.2013.12.023

Panasonic Capacitors (Gold Capacitor) [WWW Document], 2016. URL https://industrial.panasonic.com/sa/ds/library/EDLC_TechnicalGuide (accessed 10.10.19).

Patent US5665175 - Semiconductors - Google Patents [WWW Document], n.d. URL http://www.google.com/patents/US5665175 (accessed 8.19.14).

Patnaik, P., 2002. Handbook of Inorganic Chemicals, 1 edition. ed. McGraw-Hill Professional, New York.

Pengyue, Z., Zhanglian, H., Huaxiang, S., Zhenxiu, X., Xianping, F., 2006. Luminescence Characterization of Mg Doped Y2O2S:Ti Long Afterglow Phosphor. J. Rare Earths 24, 115–118. https://doi.org/10.1016/S1002-0721(07)60337-8

Petrova-Koch, V., 2009. Milestones of Solar Conversion and Photovoltaics. Springer Berlin Heidelberg.

Phosphors | Yuji International [WWW Document], n.d. URL https://www.yujiintl.com/nims-standard-reference-phosphor (accessed 1.1.19).

Phosphorus» historical information [Web Elements Periodic Table] [WWW Document], n.d. URL https://www.webelements.com/phosphorus/history.html (accessed 4.22.16).

Photoluminescence Spectroscopy [WWW Document], n.d. chemwiki.ucdavis.edu. URL http://chemwiki.ucdavis.edu/Analytical_Chemistry/Analytical_Chemistry_2.0/10_Spectroscopic_Methods/10F%3A_Photoluminescence_Spectroscopy (accessed 3.2.15).

Photovoltaic Thermal System Achieves 86% Efficiency > ENGINEERING.com [WWW Document], n.d. URL http://www.engineering.com/ElectronicsDesign/ElectronicsDesignArticles/ArticleID/6123/Photovoltaic-Thermal-System-Achieves-86-Efficiency.aspx (accessed 8.7.13).

Piatkevich, K.D., Malashkevich, V.N., Morozova, K.S., Nemkovich, N.A., Almo, S.C., Verkhusha, V.V., 2013. Extended Stokes Shift in Fluorescent Proteins: Chromophore–Protein Interactions in a Near-Infrared TagRFP675 Variant. Sci. Rep. 3. https://doi.org/10.1038/srep01847

Piper, W.W., DeLuca, J.A., Ham, F.S., 1974. Cascade fluorescent decay in Pr3+-doped fluorides: Achievement of a quantum yield greater than unity for emission of visible light. J. Lumin. 8, 344–348. https://doi.org/10.1016/0022-2313(74)90007-6

Pisarski, W.A., Żur, L., Sołtys, M., Pisarska, J., 2013. Terbium-terbium interactions in lead phosphate glasses. J. Appl. Phys. 113, 143504. https://doi.org/10.1063/1.4799592

Poortmans, J., Arkhipov, V., 2006. Thin Film Solar Cells: Fabrication, Characterization and Applications. John Wiley & Sons.

Porrès, L., Holland, A., Pålsson, L.-O., Monkman, A.P., Kemp, C., Beeby, A., 2006. Absolute Measurements of Photoluminescence Quantum Yields of Solutions Using an Integrating Sphere. J. Fluoresc. 16, 267–273. https://doi.org/10.1007/s10895-005-0054-8

Polysiloxanes - by Lachelle Sussman [WWW Document], n.d. URL http://wwwcourses.sens.buffalo.edu/ce435/Polysiloxanes/ (accessed 9.28.19).

Projeto Ockham - Ciência e pensamento crítico [WWW Document], n.d. URL http://www.projetoockham.org/ferramentas_metodo_1.html (accessed 5.29.14).

PVEducation [WWW Document], n.d. URL https://www.pveducation.org/pvcdrom/solar-cell-operation (accessed 3.14.19).

pv-tools: LOANA system: methods: IQE measurement [WWW Document], n.d. URL http://www.pv-tools.de/products/loana-system/methods/internal-quantum-efficiency.html (accessed 3.18.19).

Qarony, W., Hossain, M.I., Hossain, M.K., Uddin, M.J., Haque, A., Saad, A.R., Tsang, Y.H., 2017. Efficient amorphous silicon solar cells: characterization, optimization, and optical loss analysis. Results Phys. 7, 4287–4293. https://doi.org/10.1016/j.rinp.2017.09.030

Qian, Y., Wang, B., Wang, R., Gao, S., Niu, Y., 2014. Upconversion for enlarging solar spectrum response in near-stoichiometric and congruent Er:LiNbO3 crystals. Opt. Mater. 36, 941–944. https://doi.org/10.1016/j.optmat.2013.12.041

Que, M., Que, W., Yin, X., Shao, J., 2016. Enhanced sunlight harvesting of dye-sensitized solar cells through the insertion of a (Sr, Ba, Eu)2SiO4-TiO2 composite layer. Mater. Res. Bull. 83, 19–23. https://doi.org/10.1016/j.materresbull.2016.05.020

R. K Gartia, N.C., 2014. Thermoluminescence of Persistent Luminescent Materials. Defect Diffus. Forum 357, 171–191. https://doi.org/10.4028/www.scientific.net/DDF.357.171

Raugei, M., Frankl, P., 2009. Life cycle impacts and costs of photovoltaic systems: Current state of the art and future outlooks. Energy, WESC 2006 6th World Energy System Conference Advances in Energy Studies 5th workshop on Advances, Innovation and Visions in Energy and Energy-related Environmental and Socio-Economic Issues 34, 392–399. https://doi.org/10.1016/j.energy.2009.01.001

Richard, G. Jones, 1995. Silicon-Containing Polymers Edited by Richard G. Jones (University of Kent at Canterbury). The Royal Society of Chemistry: Cambridge, 1995. xiii + 197 pp. $88.00. ISBN 0-85404-745-X. [WWW Document]. URL http://pubs.acs.org/doi/abs/10.1021/ja965613j (accessed 6.23.16).

Richards, B. s., McIntosh, K. r., 2007. Overcoming the poor short wavelength spectral response of CdS/CdTe photovoltaic modules via luminescence down-shifting: ray-tracing simulations. Prog. Photovolt. Res. Appl. 15, 27–34. https://doi.org/10.1002/pip.723

Richards, B.S., 2006a. Enhancing the performance of silicon solar cells via the application of passive luminescence conversion layers. Sol. Energy Mater. Sol. Cells, Selected Papers from the Solar Cells and Solar Energy Materials Symposium -IMRC 2005XIV International Materials Research Congress 90, 2329–2337. https://doi.org/10.1016/j.solmat.2006.03.035

Richards, B.S., 2006b. Luminescent layers for enhanced silicon solar cell performance: Down-conversion. Sol. Energy Mater. Sol. Cells 90, 1189–1207. https://doi.org/10.1016/j.solmat.2005.07.001

Rieger, B., Grübel, M., Heidsieck, S. u. h., 2016. 23 - Polysilanes, Polycarbosilanes, Dioxadisilacyclohexane, and Polysiloxanes. Efficient Methods for Preparing Silicon Compounds 275–293. https://doi.org/10.1016/B978-0-12-803530-6.00023-8

Roberts, J.D., Caserio, M.C., 1977. Basic Principles of Organic Chemistry, second edition. W. A. Benjamin, Inc., Menlo Park, CA.

Ronda, C.R., 2008. Luminescence: From Theory to Applications. John Wiley & Sons.

Ronda, C.R., Jüstel, T., Nikol, H., 1998. Rare earth phosphors: fundamentals and applications. J. Alloys Compd. 275–277, 669–676. https://doi.org/10.1016/S0925-8388(98)00416-2

Ronda, C.R., Shea, L.E., Srivastava, A.M., 2000. Physics and Chemistry of Luminescent Materials: Proceedings of the Eighth International Symposium. The Electrochemical Society.

Ronda, Cees R., 2007. Emission and Excitation Mechanisms of Phosphors, in: Ronda, C. (Ed.), Luminescence. Wiley-VCH Verlag GmbH & Co. KGaA, pp. 1–34.

Ronda, Cornelis R. (Ed.), 2007. Luminescence: From Theory to Applications, 1 edition. ed. Wiley-VCH, Weinheim.

Ropp, R.C., 2012. Encyclopedia of the Alkaline Earth Compounds. Newnes.

Rüdiger, M., Fischer, S., Frank, J., Ivaturi, A., Richards, B.S., Krämer, K.W., Hermle, M., Goldschmidt, J.C., 2014. Bifacial n-type silicon solar cells for upconversion applications. Sol. Energy Mater. Sol. Cells 128, 57–68. https://doi.org/10.1016/j.solmat.2014.05.014

Rühle, S., Shalom, M., Zaban, A., 2010. Quantum-Dot-Sensitized Solar Cells. ChemPhysChem 11, 2290–2304. https://doi.org/10.1002/cphc.201000069

Ruiz-González, M.L., González-Calbet, J.M., Vallet-Regí, M., Cordoncillo, E., Escribano, P., Carda, J.B., Marchal, M., 2002. Planar defects in a precursor for phosphor materials: SrAl2 – xBxO4 (x < 0.2). J. Mater. Chem. 12, 1128–1131. https://doi.org/10.1039/b110910n

Sark, W.G.J.H.M. van, Meijerink, A., Schropp, R.E.I., Roosmalen, J.A.M. van, Lysen, E.H., n.d. Modeling improvement of spectral response of solar cells by deployment of spectral converters containing semiconductor nanocrystals. Semiconductors 38, 962–969. https://doi.org/10.1134/1.1787120

Sauer, M., Hofkens, J., Enderlein, J., 2010. Handbook of Fluorescence Spectroscopy and Imaging: From Ensemble to Single Molecules. John Wiley & Sons.

Scheer, R., Schock, H.-W., 2011. Chalcogenide Photovoltaics: Physics, Technologies, and Thin Film Devices. John Wiley & Sons.

Scherg-Kurmes, H., Körner, S., Ring, S., Klaus, M., Korte, L., Ruske, F., Schlatmann, R., Rech, B., Szyszka, B., 2015. High mobility In2O3:H as contact layer for a-Si:H/c-Si heterojunction and µc-

Si:H thin film solar cells. Thin Solid Films, Transparent Conductive Materials, TCM Series (2014) 594, Part B, 316–322. https://doi.org/10.1016/j.tsf.2015.03.022

Schultz, O., Mette, A., Hermle, M., Glunz, S.W., 2008. Thermal oxidation for crystalline silicon solar cells exceeding 19% efficiency applying industrially feasible process technology. Prog. Photovolt. Res. Appl. 16, 317–324. https://doi.org/10.1002/pip.814

Secula, M.S., 2010. Phosphorescent composites based on polyethyleneterephtalate [WWW Document]. URL http://www.academia.edu/3322609/Phosphorescent_composites_based_on_polyethyleneterephtalate (accessed 10.2.14).

Shafia, E., Bodaghi, M., Esposito, S., Aghaei, A., 2014. A critical role of pH in the combustion synthesis of nano-sized SrAl2O4:Eu2+, Dy3+ phosphor. Ceram. Int. 40, 4697–4706. https://doi.org/10.1016/j.ceramint.2013.09.011

Shalav, A., Richards, B.S., Green, M.A., 2007. Luminescent layers for enhanced silicon solar cell performance: Up-conversion. Sol. Energy Mater. Sol. Cells 91, 829–842. https://doi.org/10.1016/j.solmat.2007.02.007

Shalav, A., Richards, B.S., Trupke, T., Krämer, K.W., Güdel, H.U., 2005. Application of NaYF4:Er3+ up-converting phosphors for enhanced near-infrared silicon solar cell response. Appl. Phys. Lett. 86, 013505. https://doi.org/10.1063/1.1844592

Shanker, V., Haranath, D., Swati, G., 2015. Persistence Mechanisms and Applications of Long Afterglow Phosphors. Defect Diffus. Forum 361, 69–94. https://doi.org/10.4028/www.scientific.net/DDF.361.69

Shionoya, S., Yen, W.M., 1998. Phosphor Handbook. CRC Press. Silicon-Based Polymer Science, 1989.

Silicon-based Polymer Science: A Comprehensive Resource Advances in Chemistry Series - AbeBooks [WWW Document], n.d. URL http://www.abebooks.com/book-search/isbn/0841215464/ (accessed 6.23.16).

Singh, V.P., Rai, S.B., Mishra, H., Rath, C., 2014. Stabilization of high temperature hexagonal phase of SrAl2O4 at room temperature: role of ZnO. Dalton Trans. 43, 5309–5316. https://doi.org/10.1039/C3DT52869C

Singhal, 2009. The Pearson Guide To Inorganic Chemistry For The Iit Jee. Pearson Education India.

Slooff, L.H., Kinderman, R., Burgers, A.R., Bakker, N.J., van Roosmalen, J.A.M., Büchtemann, A., Danz, R., Schleusener, M., 2006. Efficiency Enhancement of Solar Cells by Application of a Polymer Coating Containing a Luminescent Dye. J. Sol. Energy Eng. 129, 272–276. https://doi.org/10.1115/1.2735347

Smets, B., Rutten, J., Hoeks, G., Verlijsdonk, J., 1989. 2SrO · 3Al2 O 3 : Eu2 + and 1.29 (Ba , Ca) O , 6Al2 O 3 : Eu2 + Two New Blue-Emitting Phosphors. J. Electrochem. Soc. 136, 2119–2123. https://doi.org/10.1149/1.2097210

Smets, B.M.J., 1987. Phosphors based on rare-earths, a new era in fluorescent lighting. Mater. Chem. Phys. 16, 283–299. https://doi.org/10.1016/0254-0584(87)90103-9

Smooth-on, 2015. Solaris_TB.pdf [WWW Document]. URL https://www.smooth-on.com/tb/files/Solaris_TB.pdf (accessed 6.29.16).

Snaith, H.J., 2012. How should you measure your excitonic solar cells? Energy Environ. Sci. 5, 6513–6520. https://doi.org/10.1039/c2ee03429h

Sohn, K.-S., Park, D.H., Kim, J.S., 2005. Luminescence of Pulsed-Laser-Deposited SrAl[sub 2]O[sub 4]:Eu,Dy Thin Film and Its Role as a Stress Indicator. J. Electrochem. Soc. 152, H161. https://doi.org/10.1149/1.2012947

Sommerdijk, J.L., Bril, A., de Jager, A.W., 1974. Two photon luminescence with ultraviolet excitation of trivalent praseodymium. J. Lumin. 8, 341–343. https://doi.org/10.1016/0022-2313(74)90006-4

Song, M.Y., Chaudhari, K.N., Park, J., Yang, D.S., Kim, J.H., Kim, M.S., Lim, K., Ko, J. and Yu, J.S., 2012. High efficient Pt counter electrode prepared by homogeneous deposition method for dye-sensitized solar cell. Applied energy, 100, pp.132-137.

Spellman, F.R., Bieber, R.M., 2011. The Science of Renewable Energy, 1 edition. ed. CRC Press, Boca Raton, FL.

Spitzer, M.B., Jenssen, H.P., Cassanho, A., 2013. An approach to downconversion solar cells. Sol. Energy Mater. Sol. Cells, Selected publications from the 22nd Space Photovoltaic Research and Technology (SPRAT) Conference 108, 241–245. https://doi.org/10.1016/j.solmat.2012.08.011

Stanley, C., Mojiri, A., Rosengarten, G., 2016. Spectral light management for solar energy conversion systems. Nanophotonics 5, 161–179. https://doi.org/10.1515/nanoph-2016-0035

Sun, H., Pan, L., Piao, X., Sun, Z., 2013. Long afterglow SrAl2O4:Eu,Dy phosphors for CdS quantum dot-sensitized solar cells with enhanced photovoltaic performance. J. Mater. Chem. A 1, 6388–6392. https://doi.org/10.1039/C3TA10596B

Sun, H., Pan, L., Piao, X., Sun, Z., 2014a. Enhanced performance of cadmium selenide quantum dot-sensitized solar cells by incorporating long afterglow europium, dysprosium co-doped strontium aluminate phosphors. J. Colloid Interface Sci. 416, 81–85. https://doi.org/10.1016/j.jcis.2013.10.050

Sun, H., Pan, L., Zhu, G., Piao, X., Zhang, L., Sun, Z., 2014b. Long afterglow Sr4Al14O25: Eu, Dy phosphors as both scattering and down converting layer for CdS quantum dot-sensitized solar cells. Dalton Trans. https://doi.org/10.1039/C4DT01276C

Sun, X.-Y., Sun, X.-D., Li, X.-G., Wang, Z.-Q., He, J., Wang, B.-S., 2014. Performance and building integration of all-ceramic solar collectors. Energy Build. 75, 176–180. https://doi.org/10.1016/j.enbuild.2014.01.045

Suriyamurthy, N., Panigrahi, B.S., 2008. Effects of non-stoichiometry and substitution on photoluminescence and afterglow luminescence of Sr4Al14O25:Eu2+, Dy3+ phosphor. J. Lumin. 128, 1809–1814. https://doi.org/10.1016/j.jlumin.2008.05.001

Švrček, V., Slaoui, A., Muller, J.-C., 2004. Silicon nanocrystals as light converter for solar cells. Thin Solid Films, Proceedings of Symposium D on Thin Film and Nano-Structured Materials for Photovoltaics, of the E-MRS 2003 Spring Conference 451–452, 384–388. https://doi.org/10.1016/j.tsf.2003.10.133

Sweeney, A., 2013. Light reflectance of concrete (PhD Thesis). Trinity College (Dublin, Ireland). Department of Civil, Structural and Environmental Engineering.

Swinehart, D.F., 1962. The Beer-Lambert Law. J. Chem. Educ. 39, 333. https://doi.org/10.1021/ed039p333

Tahhan, A., Dehouche, Z., Fern, G.R., Haverkamp, E., 2015. Photovoltaic cells energy performance enhancement with down-converting photoluminescence phosphors. Int. J. Energy Res. 39, 1616–1622. https://doi.org/10.1002/er.3358

Tamatani, M., 1974. Fluorescence in 2+$ and Mn2+$. Jpn. J. Appl. Phys. 13, 950–956. https://doi.org/10.7567/JJAP.13.950

Technologies, C. on D. in D., Review, S.C. on T.I.-G., Evaluate &., Sciences, D. on E. and P., Council, N.R., 2010. Seeing Photons: Progress and Limits of Visible and Infrared Sensor Arrays. National Academies Press.

The Use of UV/Vis/NIR Spectroscopy in the Development of Photovoltaic Cells, [WWW Document], n.d. URL https://www.perkinelmer.com/pdfs/downloads/APPUseofUVVisNIRinDevelopmentPV.pdf (accessed 7.15.15).

Buenhombre, M. and Luis, J., 2005. Thermal analysis of inorganic materials. Escuela Politécnica Superior da Coruña Mendizábal s/n, 15403 Ferrol, Spain.

Frost, Ray L. and Martens, Wayde N. and Hales, Matthew C. (2009) Thermogravimetric analysis of selected group II carbonate minerals – implication for the geosequestration of greenhouse gases. Journal of Thermal Analysis and Calorimetry, 95(3). pp. 999-1005.

Thermoluminescence of γ-irradiated SrAl2O4:Dy.: EBSCOhost [WWW Document], n.d. URL http://library.ucd.ie:50080/ebsco-w-b/ehost/pdfviewer/pdfviewer?sid=5cfe278e-6000-4ba8-a5b9-db3ee5e9e434%40sessionmgr112&vid=2&hid=108 (accessed 4.14.14).

TPX® Characteristics - Polymers - Research Materials - Goodfellow [WWW Document], n.d. URL http://www.goodfellow.com/larger-quantities/polymers/tpx-characteristics/ (accessed 3.27.19).

Trupke, T., Green, M.A., Würfel, P., 2002. Improving solar cell efficiencies by up-conversion of sub-band-gap light. J. Appl. Phys. 92, 4117–4122. https://doi.org/10.1063/1.1505677

Trupke, T., Shalav, A., Richards, B.S., Würfel, P., Green, M.A., 2006. Efficiency enhancement of solar cells by luminescent up-conversion of sunlight. Sol. Energy Mater. Sol. Cells, 14th International Photovoltaic Science and Engineering Conference14th International Photovoltaic Science and Engineering Conference 90, 3327–3338. https://doi.org/10.1016/j.solmat.2005.09.021

Tsai, C.-Y., Lin, J.-W., Huang, Y.-P., Huang, Y.-C., 2014. Modeling and Assessment of Long Afterglow Decay Curves [WWW Document]. Sci. World J. https://doi.org/10.1155/2014/102524

Tu, Y., Zhou, L., Jin, Y.Z., Gao, C., Ye, Z.Z., Yang, Y.F., Wang, Q.L., 2010. Transparent and flexible thin films of ZnO-polystyrene nanocomposite for UV-shielding applications. J. Mater. Chem. 20, 1594. https://doi.org/10.1039/b914156a

Turcheniuk, K., Bondarev, D., Singhal, V., Yushin, G., 2018. Ten years left to redesign lithium-ion batteries. Nature 559, 467–470. https://doi.org/10.1038/d41586-018-05752-3

Tydex, 2016. THz Materials [WWW Document]. Opt. Spectrosc. Prod. URL http://www.tydexoptics.com/products/thz_optics/thz_materials/ (accessed 6.29.16).

Ueda, J., Tanabe, S., 2011. Broadband near ultra violet sensitization of 1 μm luminescence in Yb3+-doped CeO2 crystal. J. Appl. Phys. 110, 073104. https://doi.org/10.1063/1.3642984

UNFCCC, 2013, n.d. United Nations Framework Convention on Climate Change [WWW Document]. URL http://unfccc.int/2860.php (accessed 5.27.13).

Valeur, B., Berberan-Santos, M.N., 2013. Molecular Fluorescence: Principles and Applications. John Wiley & Sons.

Vergeer, P., Vlugt, T.J.H., Kox, M.H.F., Hertog, M.I. den, Eerden, J.P.J.M. van der, Meijerink, A., 2005. Quantum cutting by cooperative energy transfer in Yb x Y 1− x PO 4: Tb 3+. Phys. Rev. B 71, 014119. https://doi.org/10.1103/PhysRevB.71.014119

Viana, T.S., Rüther, R., Martins, F.R., Pereira, E.B., 2011. Assessing the potential of concentrating solar photovoltaic generation in Brazil with satellite-derived direct normal irradiation. Sol. Energy 85, 486–495. https://doi.org/10.1016/j.solener.2010.12.015

Vinogradov, S.A., Wilson, D.F., 1994. Phosphorescence lifetime analysis with a quadratic programming algorithm for determining quencher distributions in heterogeneous systems. Biophys. J. 67, 2048–2059. https://doi.org/10.1016/S0006-3495(94)80688-5

Wang, C., Xuan, T., Liu, J., Li, H., Sun, Z., 2014. Long Afterglow SrAl2O4:Eu2+,Dy3+ Phosphors as Luminescent Down-Shifting Layer for Crystalline Silicon Solar Cells. Int. J. Appl. Ceram. Technol. n/a-n/a. https://doi.org/10.1111/ijac.12281

Wang, H.M., Li, G.R., Yuan, X.T., Zhang, X.Y., Zhao, Y.T., Wang, J.J., Gu, K.X., Zhang, H., Xu, X.J., 2012. Effects of B₂O₃ Flux on the Synthesis and Microstructure of Aluminum Metal Matrix Composites. Appl. Mech. Mater. 217–219, 31–34. https://doi.org/10.4028/www.scientific.net/AMM.217-219.31

Wegh, null, Donker, null, Oskam, null, Meijerink, null, 1999. Visible quantum cutting in LiGdF4:Eu3+ through downconversion. Science 283, 663–666.

Wenhui Huang, M.Y., 2006. Strontium Isotope Composition and Characteristic Analysis of Cambrian-Ordovician Carbonate in the Region of Tazhong, Tarim Basin. J. China Univ. Geosci. - J CHINA UNIV GEOSCI 17, 246–257. https://doi.org/10.1016/S1002-0705(06)60034-4

Werner, J.H., Kolodinski, S., Queisser, H.J., 1994. Novel optimization principles and efficiency limits for semiconductor solar cells. Phys. Rev. Lett. 72, 3851–3854. https://doi.org/10.1103/PhysRevLett.72.3851

What Is the Lifespan of a Solar Panel? > ENGINEERING.com [WWW Document], n.d. URL http://www.engineering.com/ElectronicsDesign/ElectronicsDesignArticles/ArticleID/7475/What-Is-the-Lifespan-of-a-Solar-Panel.aspx (accessed 4.23.14).

VALEUR, B. (2001). Molecular fluorescence: principles and applications. New York, Wiley-VCH. https://doi.org/10.1002/3527600248

World's Largest Solar-Powered Boat > ENGINEERING.com [WWW Document], n.d. URL http://www.engineering.com/ElectronicsDesign/ElectronicsDesignArticles/ArticleID/6056/Worlds-Largest-Solar-Powered-Boat.aspx#at_pco=smlwn-1.0&at_si=53bd7496ffc98adc&at_ab=per-3&at_pos=0&at_tot=1 (accessed 7.9.14).

Würth, C., González, M.G., Niessner, R., Panne, U., Haisch, C., Genger, U.R., 2012. Determination of the absolute fluorescence quantum yield of rhodamine 6G with optical and photoacoustic methods – Providing the basis for fluorescence quantum yield standards. Talanta 90, 30–37. https://doi.org/10.1016/j.talanta.2011.12.051

Xie, R.-J., Li, Y.Q., Hirosaki, N., Yamamoto, H., 2016. Nitride Phosphors and Solid-State Lighting. CRC Press.

Xue, Z., Deng, S., Liu, Y., Lei, B., Xiao, Y., Zheng, M., 2013. Synthesis and luminescence properties of SrAl2O4:Eu2+, Dy3+ hollow microspheres via a solvothermal co-precipitation method. J. Rare Earths 31, 241–246. https://doi.org/10.1016/S1002-0721(12)60265-8

Yamada, N., Kim, O.N., Tokimitsu, T., Nakai, Y., Masuda, H., 2011. Optimization of anti-reflection moth-eye structures for use in crystalline silicon solar cells. Prog. Photovolt. Res. Appl. 19, 134–140. https://doi.org/10.1002/pip.994

Yang, C.-Y., Som, S., Das, S., Lu, C.-H., 2017. Synthesis of Sr2Si5N8:Ce3+ phosphors for white LEDs via efficient chemical vapor deposition. Sci. Rep. 7, 45832. https://doi.org/10.1038/srep45832

Yang, R.-Y., Chen, H.-Y., Lai, F.-D., 2012. Performance Degradation of Dye-Sensitized Solar Cells Induced by Electrolytes [WWW Document]. Adv. Mater. Sci. Eng. https://doi.org/10.1155/2012/902146

Yaroslav, n.d. Computer program PARAV for calculating optical constants of thin films and bulk materials: Case study of amorphous semiconductors. URL http://www.chalcogenide.org/computer-program-parav-for-calculating-optical-constants-of-thin-films-and-bulk-materials-case-study-of-amorphous-semiconductors/ (accessed 1.18.19).

Yen, W.M., Yamamoto, H., 2007. Phosphor Handbook, Second Edition. ed. CRC Press, United States of America.

Yeon, D.H., Mohanty, B.C., Lee, S.M., Cho, Y.S., 2015. Effect of band-aligned double absorber layers on photovoltaic characteristics of chemical bath deposited PbS/CdS thin film solar cells. Sci. Rep. 5. https://doi.org/10.1038/srep14353

Yoshida, S., Mitsubishi Electric Corp, 1991. Tandem solar cell. U.S. Patent 5,009,719.

You, Y., Young Park, S., 2009. Phosphorescent iridium(iii) complexes: toward high phosphorescence quantum efficiency through ligand control. Dalton Trans. 0, 1267–1282. https://doi.org/10.1039/B812281D

Yu, D.C., Ye, S., Peng, M.Y., Zhang, Q.Y., Qiu, J.R., Wang, J., Wondraczek, L., 2011. Efficient near-infrared downconversion in GdVO4:Dy3+ phosphors for enhancing the photo-response of solar cells. Sol. Energy Mater. Sol. Cells 95, 1590–1593. https://doi.org/10.1016/j.solmat.2011.01.004

Yuji Phosphors | Yuji International, Japan National Institute for Materials Science, NIMS-standard-reference-phosphor, [WWW Document], n.d. URL https://www.yujiintl.com/nims-standard-reference-phosphor (accessed 06.21.17).

Zeigler, J.M., Fearon, F.W.G., 1990. Silicon-based polymer science a comprehensive resource. - Version details [WWW Document]. Trove. URL http://trove.nla.gov.au/version/39098466 (accessed 6.23.16).

Zhang, S., Yang, X., Qin, C., Numata, Y., Han, L., 2014. Interfacial engineering for dye-sensitized solar cells. J. Mater. Chem. A 2, 5167–5177. https://doi.org/10.1039/C3TA14392A

Zhang, X., Cao, Z., Bai, Z., Li, L., Zhao, Z., Du, J., 2000. Photoluminescence measurement of SrAl2O4:Eu2+, Dy3+ incorporated in glass frits. pp. 209–212. https://doi.org/10.1117/12.402621

Znajdek, K., Szczecińska, N., Sibiński, M., Wiosna-Sałyga, G., Przymęcki, K., 2018. Luminescent layers based on rare earth elements for thin-film flexible solar cells applications. Optik 165, 200–209. https://doi.org/10.1016/j.ijleo.2018.03.072

APPENDICES

APPENDIX A: SOLARIS SILICON PRODUCT SPECIFICATIONS

TECHNICAL OVERVIEW	
Mix Ratio: 1A : 1B by volume or weight	
Mixed Viscosity, cps: 1,200	(ASTM D-2393)
Specific Gravity, g/cc: 0.99	(ASTM D-1475)
Specific Volume, cu. in./lb.: 28.1	(ASTM D-1475)
Pot Life: 240 minutes (73°F/23°C)	(ASTM D-2471)
Cure time: 24 hrs (73°F/23°C)	
Color: Clear	
Shore A Hardness: 15	(ASTM D-2240)
Tensile Strength, psi: 180	(ASTM D-412)
100% Modulus, psi: 25	(ASTM D-412)
Elongation @ Break: 290%	(ASTM D-412)
Die B Tear Strength, pli: N/A	(ASTM D-624)
Shrinkage, in./in.: < .001	(ASTM D-2566)
Useful Temp. Range: -149°F to 400°F (-100°C to 205° C)	
Dielectric Strength, volts/mil: 366	(ASTM D-149)
Dielectric Constant, 100 Hz: 2.78	(ASTM D-150)
Dissipation Factor, 100 Hz: 0.00	(ASTM D-150)
Volume Resistivity, ohms-cm: 3.16E+15	(ASTM D-257)
Thermal Conductivity: 0.18	(ASTM D-1461)
Refractive Index: 1.41 nm	(ASTM D-1218)
* All values measured after 7 days at 73°F/23°C	

Source: https://www.smooth-on.com/product-line/solaris/

APPENDIX B: JAPAN NIMS STANDARD REFERENCE PHOSPHORS

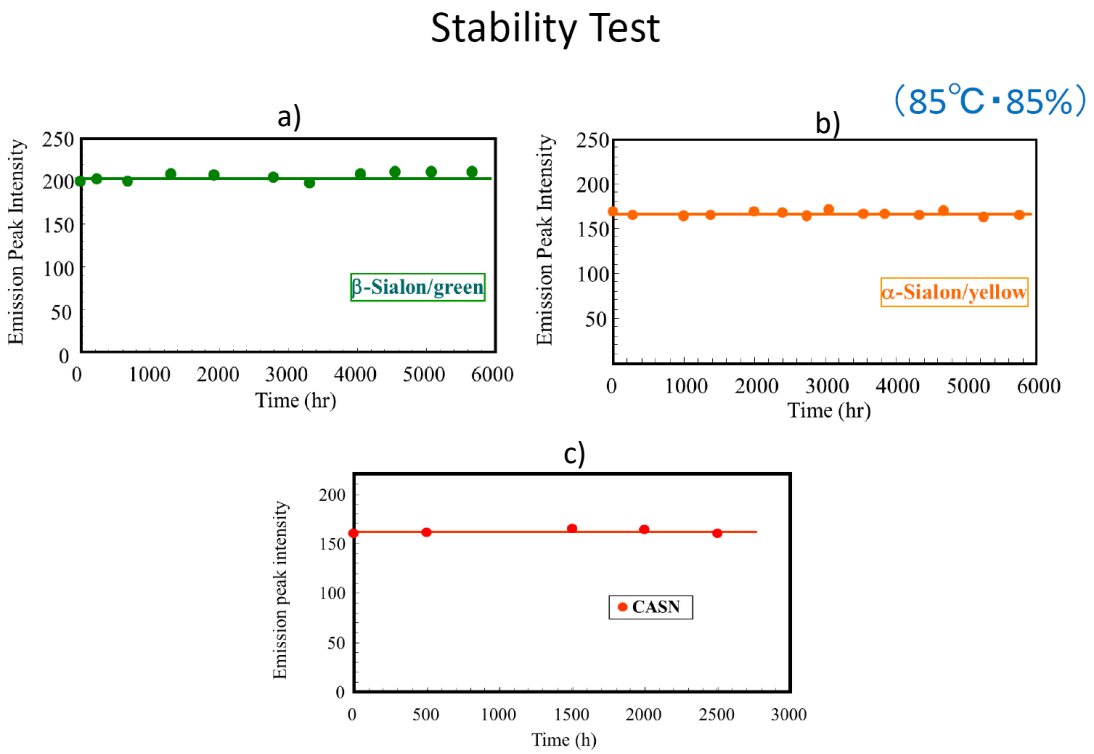

Figure 9.1. Stability test of the standard reference phosphors from Japan NIMS. (a) PhNIMS-G. (B) PhNIMS-O. (a) PhNIMS-R.

APPENDIX C: SOFTWARE USED TO ANALYSE THE OPTICAL PROPERTIES OF THE LUMINESCENT LAYER

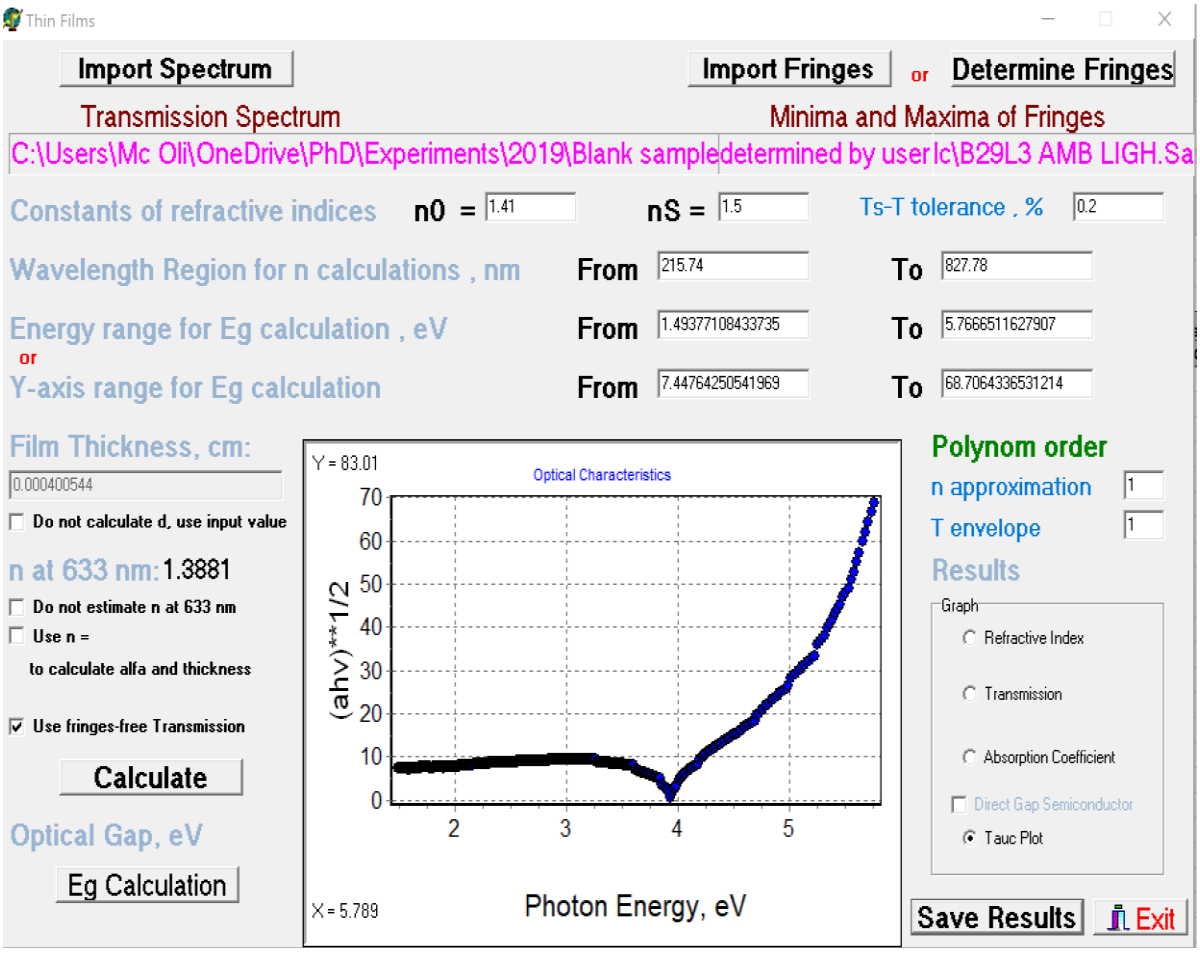

Figure 9.2. Software used PARAV-V2.0: http://www.chalcogenide.org/category/software/

APPENDIX D: SPECTROPHOTOMETRIC AND SPECTROFLUORIMETRIC STUDY OF LUMINESCENCE LAYERS PH2-PH6

Spectrophotometric Study of Luminescent Layers – Ph2

The spectroscopy measurements of the transmission, reflectance and absorptance spectra of the luminescent layer of the various layers that were produced using the Phosphorescent Phosphor Ph2, (see Table 3.2), at various concentrations (1-80%wt) shown in Figure 9.3.

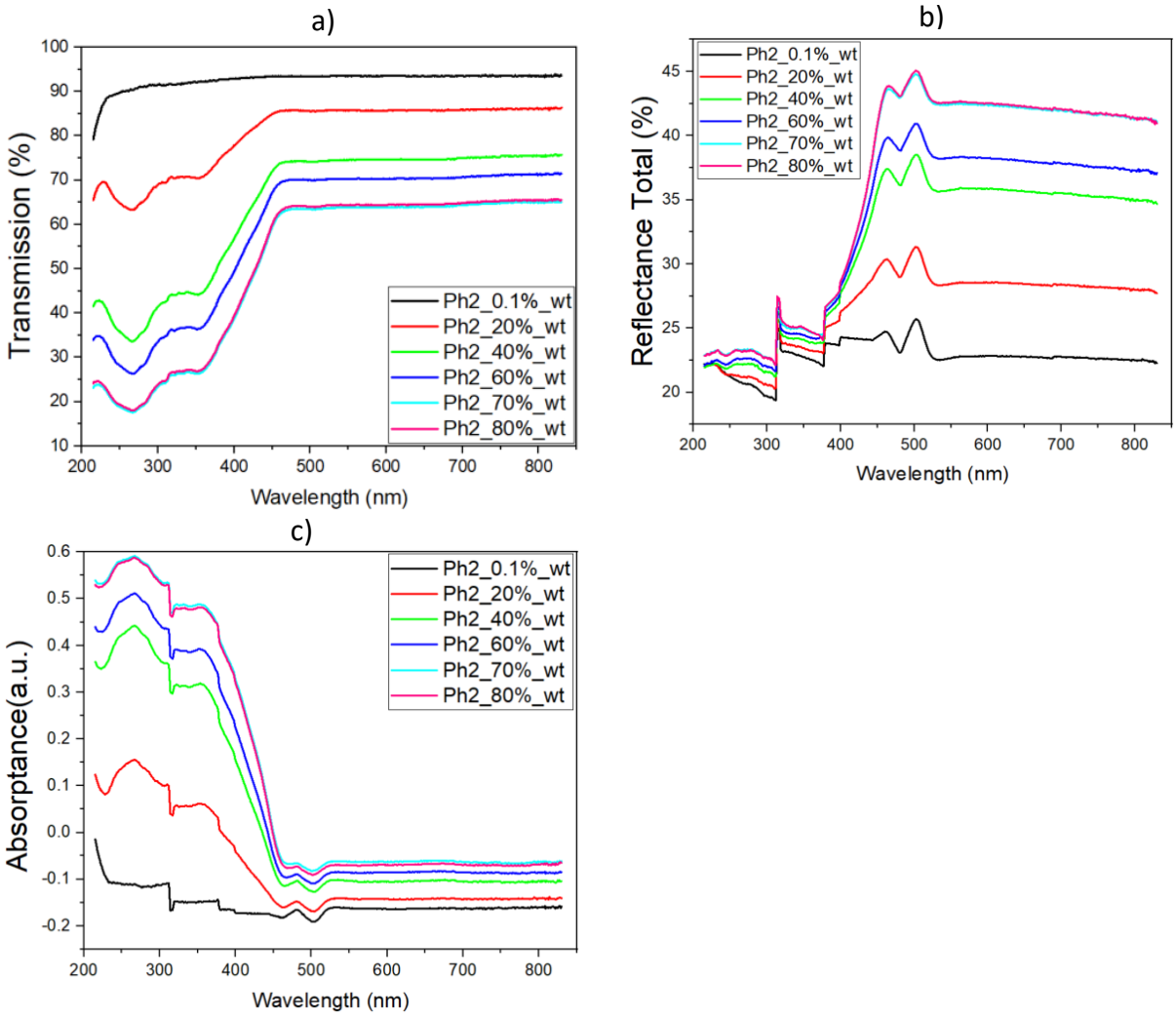

Figure 9.3. Optical (a) total transmission, (b) reflectance total and (c) absorptance spectra of Ph2 luminescent layers at various concentration ratios; 0.1-80%wt.

Spectrofluorimetric Study of Luminescent Layers – Ph2

Figure 9.4 shows the photoluminescent emission and excitation spectra of Ph2 luminescent layer at different excitation wavelengths from 260 nm to 455 nm. The strongest emission spectrum was obtained at 375 nm with an emission centred at 495 nm.

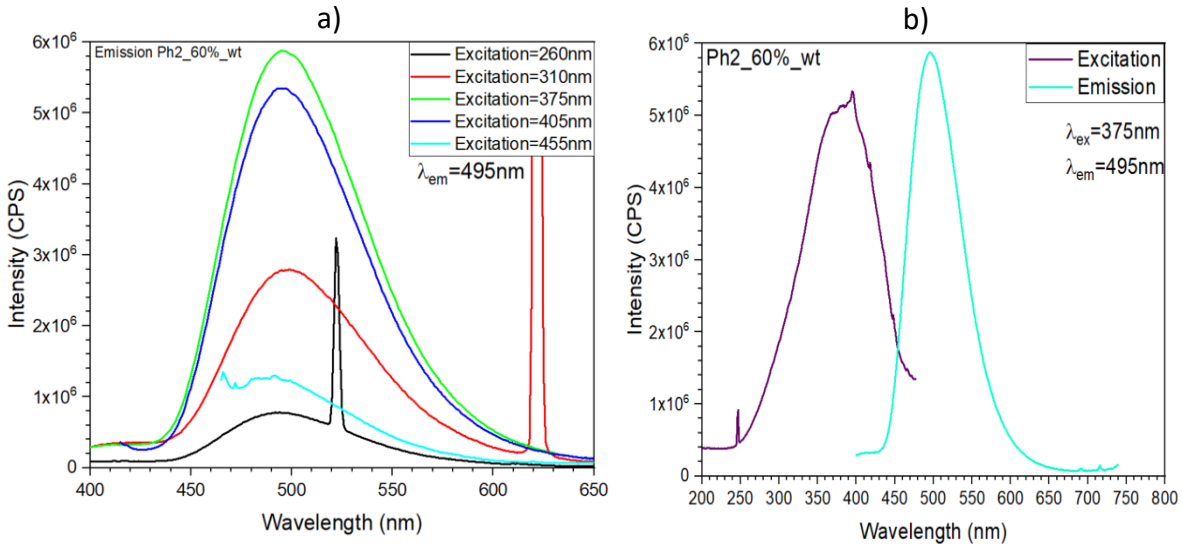

Figure 9.4. a) Emission spectra of Ph2 luminescent layer at 60%wt concentration ratio. (b) The Excitation and emission spectra of Ph2 luminescent layer at 60%wt concentration ratio.

Spectrophotometric Study of Luminescent Layers – Ph3

The spectroscopy measurements of the transmission, reflectance and absorptance spectra of the luminescent layer of the various layers that were produced using the Phosphorescent Phosphor Ph3, (see Table 3.3), at various concentrations (1-80%wt) shown in Figure 9.5.

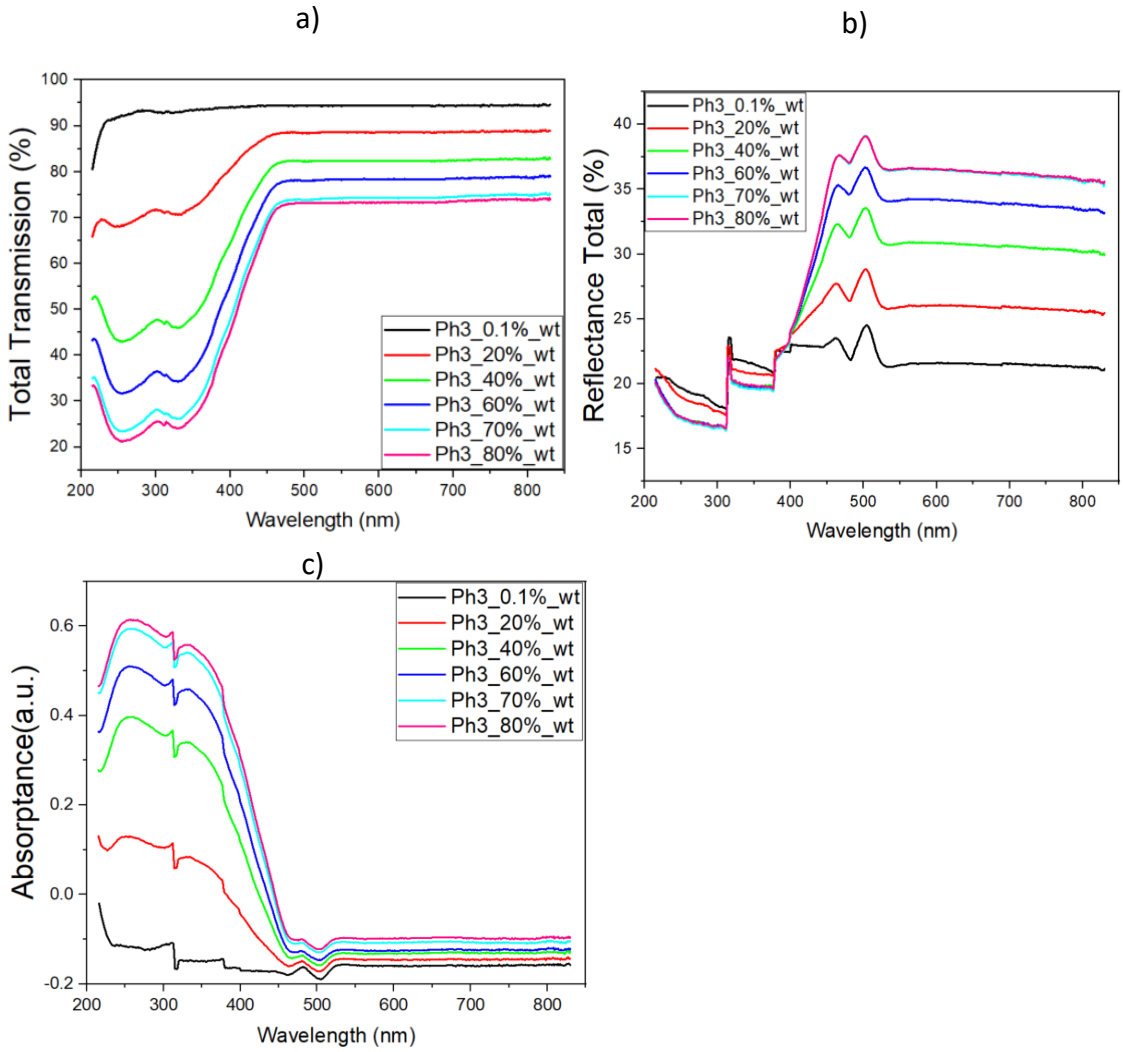

Figure 9.5. Optical (a) total transmission, (b) reflectance total and (c) absorptance spectra of Ph3 luminescent layers at various concentration ratios; 0.1-80%wt.

Spectrofluorimetric Study of Luminescent Layers – Ph3

Figure 9.6 show the photoluminescent emission and excitation spectra of Ph3 luminescent layer at different excitation wavelengths from 310 nm to 455 nm. The strongest emission spectrum was obtained at 375 nm with an emission centred at 520 nm.

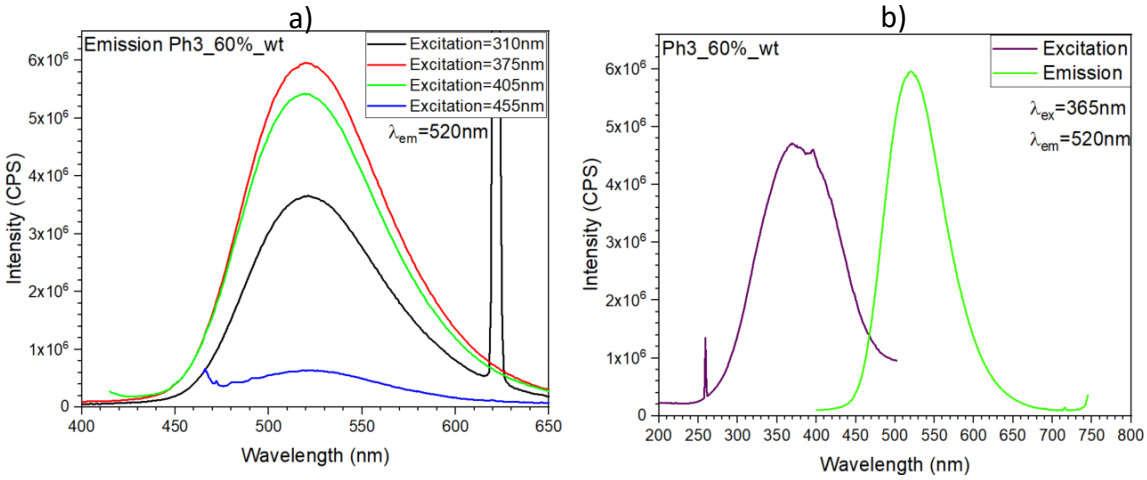

Figure 9.6. (a) Emission spectra of Ph3 luminescent layer at 60%wt concentration ratio. (b) The Excitation and emission spectra of Ph3 luminescent layer at 60%wt concentration ratio.

Spectrophotometric Study of Luminescent Layers - Ph4, Ph5 and Ph6

The spectroscopy measurements of the transmission, reflectance and absorptance spectra of the luminescent layer of the various layers that were produced using the Phosphorescent Phosphor Ph4, Ph5 and Ph6, (see Table 3.2), at 60%wt concentrations shown in Figure 9.7.

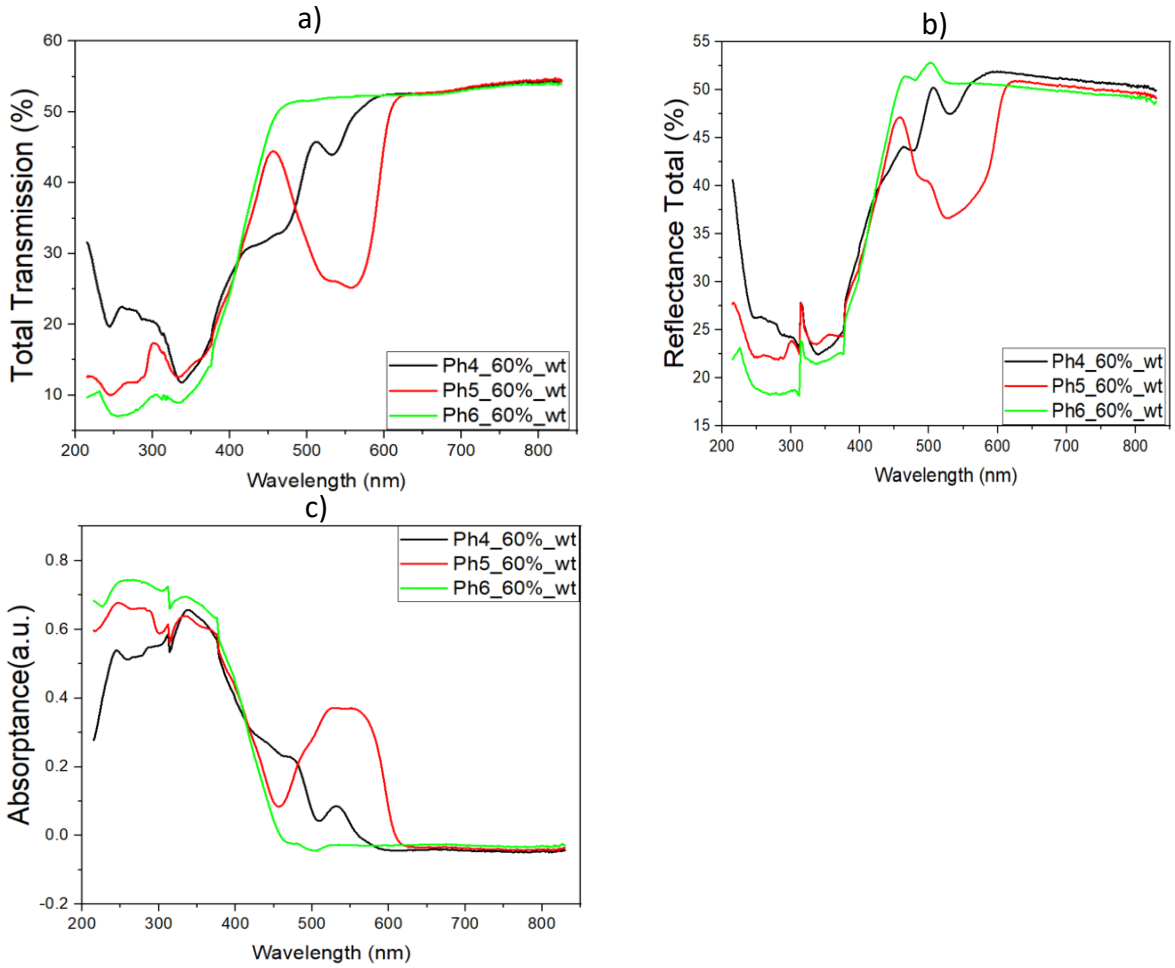

Figure 9.7. (a) Total transmission spectra of Ph4, Ph5 and Ph6 of the luminescent layers at 60%wt concentration ratio. (b) Reflectance total spectra of Ph4, Ph5 and Ph6 of the luminescent layers at 60%wt concentration ratio. (c) Absorptance spectra of Ph4, Ph5 and Ph6 of the luminescent layers at 60%wt concentration ratio.

Spectrofluorimetric Study of Luminescent Layers - Ph4, Ph5 and Ph6

Figure 9.8 shows the photoluminescent emission and excitation spectra of Ph4 at different excitation wavelengths from 260 nm to 455 nm. The strongest emission spectrum was obtained at 375 nm with an emission centred at 495 nm. It be observed that fluorescence emission spectra strongest emission spectrum was obtained at 455 nm with an emission centred at 579 nm.

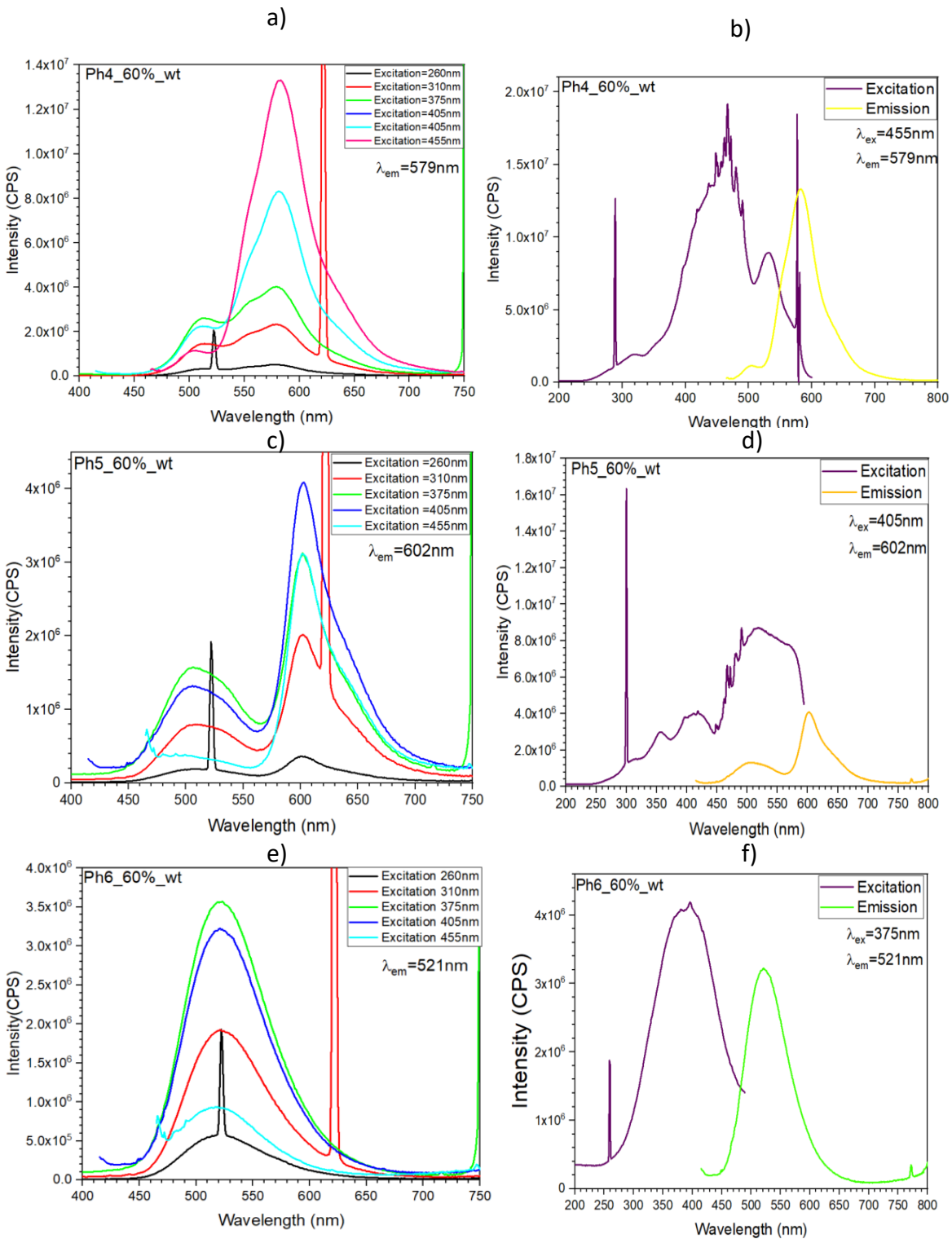

Figure 9.8. (a) Emission spectra of Ph4 of the luminescent layer at 60%wt concentration ratio. (b) Excitation and emission spectra of Ph4 of the luminescent layer at 60%wt concentration ratio. (c) Emission spectra of Ph5 of the luminescent layer at 60%wt concentration ratio. (d) Excitation and emission spectra of Ph5 of the luminescent layer at 60%wt concentration ratio. (e) Emission spectra of Ph6 of the luminescent layer at 60%wt concentration ratio. (f) Excitation and emission spectra of Ph6 of the luminescent layer at 60%wt concentration ratio.